UNIVERSITY OF SÃO PAULO
SÃO CARLOS SCHOOL OF ENGINEERING
DEPARTMENT OF GEOTECHNICAL ENGINEERING

YARA BARBOSA FRANCO

Geosynthetic Reinforced Soil Retaining Walls with Cohesive Backfills

Muros de Solo Reforçado com Geossintéticos com Solos Coesivos

São Carlos - SP
2023

YARA BARBOSA FRANCO

Geosynthetic Reinforced Soil Retaining Walls with Cohesive Backfills

Corrected version (Original version is available at São Carlos School of Engineering)

Supervisor: Prof. Dr. Jefferson Lins da Silva

Co-Supervisor: Prof. Dr. Stefano Utili

Ph. D. Thesis presented to the Graduate Program in Geotechnical Engineering at São Carlos School of Engineering, University of São Paulo, Brazil to obtain the degree of Doctor of Science.

São Carlos - SP
2023

Ficha catalográfica elaborada pela Biblioteca Prof. Dr. Sérgio Rodrigues Fontes da EESC/USP com os dados inseridos pelo(a) autor(a).

B238g

Barbosa Franco, Yara
Geosynthetic Reinforced Soil Retaining Walls with Cohesive Backfills / Yara Barbosa Franco; orientador Jefferson Lins da Silva; coorientador Stefano Utili. São Carlos, 2023.

Tese (Doutorado) - Programa de Pós-Graduação e Área de Concentração em Geotecnia -- Escola de Engenharia de São Carlos da Universidade de São Paulo, 2023.

1. Reinforced soil. 2. Cohesive soil. 3. Geosynthetics. 4. Limit analysis. 5. Reduced model. I. Título.

Eduardo Graziosi Silva - CRB - 8/8907

FOLHA DE JULGAMENTO

Candidata: Engenheira **YARA BARBOSA FRANCO**.

Título da tese: "Geosynthetic Reinforced Soil Retaining Walls with Cohesive Backfills".

Data da defesa: 19/10/2023.

Comissão Julgadora	Resultado
Prof. Associado Jefferson Lins da Silva (Orientador) (EESC-USP)	Aprovada
Profa. Dra. Margarida João Fernandes de Pinho Lopes (Universidade de Aveiro / Portugal)	APROVADA
Dr. Carlos Vinicius dos Santos Benjamim (ENG Consultoria)	APROVADA
Prof. Dr. Heraldo Nunes Pitanga (Universidade Federal de Juiz de Fora)	APROVADA
Prof. Dr. Ennio Marques Palmeira (Universidade de Brasília)	APROVADA

Coordenadora do Programa de Pós-Graduação em Geotecnia:
Profa. Assoc. **Cristina de Hollanda Cavalcanti Tsuha**

Presidente da Comissão de Pós-Graduação:
Prof. Titular **Carlos De Marqui Junior**

Acknowledgements

To my mother Zélia, who throughout life has never spared any effort so that I could fulfil my dreams and get this far, always supporting and motivating me.

To my sister Sarah, my best friend, for always believing in me and encouraging me to face new challenges and get out of my comfort zone.

To my husband Heider, for his constant support and encouragement during the preparation of this work and during the difficult periods when I was overloaded, always being the person who put me up and brightened my day.

To Prof. Jefferson Lins for his guidance, friendship and support during all stages of this work, providing all the necessary resources for the experimental stage of this research and for believing in me unconditionally, encouraging me to always seek more and actively supporting my exchange in England.

To the Geosynthetics Laboratory technician Clever Valentin for all the support, without which the development of this work would not be possible.

To the Geotechnical Department technicians, especially Oscar Neto and Zé Luis, for their help in the laboratory activities related to the characterization and strength tests of the soils tested.

To Ivan Genera for always accepting a challenge and building and making possible most of the pieces and instrumentation used in this research.

To Mi and his colleagues for helping me construct the model wall, doing the heavy work that I would not be able to do on my own.

To the trainees of the Geosynthetics Laboratory, especially Vinícius, for always being willing to help, having been essential during the monitoring of the test wall.

To the fellow masters and PhD students of the Geosynthetics Lab for the exchange of knowledge and help whenever I needed it.

To the companies Huesker and Maccaferri, for supplying geosynthetic materials to be evaluated for use in this research.

To Danilo, from Formatto, for supplying the airbags used in the experimental stage of this research and for all the effort to find a better solution for the application proposed in the study.

To Prof. Valéria Guimarães, for the support and to make possible my exchange in England during the doctorate.

To Prof. Stefano Utili, for his constant guidance during my exchange in England, for the trust deposited since the beginning, for the financial help given to make possible my exchange and for all the technical discussions and questionings that greatly contributed to my formation and to the development of this thesis.

To Prof. Mohamed Rouainia, for all the support in my learning about PLAXIS and numerical analysis.

To my co-workers at ANM, for all the encouragement and positive energy during the final stage of writing this thesis.

To Maristela, Neiva and Álvaro, for all the support given at the geotechnical department office.

To the Structures Department of EESC/USP, for the loan of most of the data acquisition equipment used in the experimental stage of this research.

To the technician Luiz Vareda, from the Structures Department of EESC/USP, for all the help given about instrumentation.

To Bianca Melo, for being a channel of light in my life and bringing yoga to keep me focused on the present and control my anxiety in moments of great overload.

To the National Council for Scientific and Technological Development, CNPq, for granting the scholarship.

Abstract

FRANCO, Y.B. **Geosynthetic Reinforced Soil Retaining Walls with Cohesive Backfills**. 2023. 317p. Tese (Doutorado) - São Carlos, 2023.

Where granular materials are not easily available, local cohesive soils are increasingly employed in geosynthetic reinforced soil walls as a cheap and sustainable option. Conventional design methods do not yet account for the beneficial effect of cohesion in reducing the amount of required reinforcement. Similarly, the contribution of the face to stability is rarely accounted for, despite plenty of experimental evidence in its favour. This thesis evaluated the influence of soil cohesion and a structural facing on the stability of reinforced soil walls by using two approaches: the first was a semi-analytical approach while the second one an experimental approach.

The semi-analytical method employed is based on limit analysis for the design of reinforced soil walls in frictional–cohesive backfills accounting for the wall contribution. A parametric analysis was conducted to evaluate the effect of soil cohesion and friction angle, facing batter, block width, location of the reaction force acting on the face, facing–backfill interface friction, facing–foundation interface friction and reinforcement length. Dimensionless design charts providing the required amount of reinforcement for lengths recommended in design standards are provided for both uniform and linearly increasing reinforcement distributions. It emerges that accounting for the presence of cohesion and the facing element can lead to significant savings in the overall level of reinforcement, and that tension cracks can be particularly detrimental to wall stability for highly cohesive soils so they cannot be overlooked in the design.

The second part of the study comprised the construction, testing and analysis of a 1.47 m high reinforced soil wall model, constructed with a frictional-cohesive soil and a modular block wall facing at LabGsy Laboratory, in São Carlos-SP, Brazil. The model wall was constructed using a dry-stacked column of masonry concrete blocks with a fully restrained toe, with an intended eight-degree facing batter. The backfill soil used was a cohesive-frictional backfill, classified as a sandy-clay. The reinforcement material comprised of 5 layers of relatively weak polyester (PET) knitted geogrid, modified to reduce its stiffness by cutting out some longitudinal ribs. Once constructed the wall was incrementally surcharged to maximum pressure of 150 kPa, limited by airbag capacity. The wall was heavily instrumented to monitor displacements at the facing, surface soil settlements, foundation earth pressures, vertical and horizontal toe loads, and displacements and strains in the soil reinforcement layers.

It was presented the materials, methods, instrumentation design and construction and test box adaptations needed to surcharging the wall model up to 150 kPa. The small magnitude of wall facing deflections measured during construction and surcharging seems to indicate the the model wall was possibility under working stress conditions throughout the entire physical test, far from reaching failure. This could be attributed to the overconsolidated state of the backfill soil due to compaction effort, to the beneficial effect of cohesion on reinforced soil wall behaviour and to the influence of the restrained wall toe to carry part of the load. This indicates that reinforced soil walls built with cohesive soil can perform well since its drainage can be guaranteed. It is expected that the contributions regarding the studies proposed herein can be a step forward in the understanding of the behaviour of GRS-RW with cohesive soils.

Finally, it was developed a series of python scripts to conduct automated numerical analysis in Plaxis 2D by using remote scripting, with the intention of laying the basis for a future numerical study involving automated parametric analysis of reinforced soil walls.

Keywords: Reinforced soil. Cohesive soil. Geosynthetics. Limit analysis. Reduced model. Facing.

Resumo

FRANCO, Y.B. **Muros de Solo Reforçado com Geossintéticos com Solos Coesivos**. 2023. 317p. Tese (Doutorado), São Carlos, 2023.

Quando os materiais granulares não estão facilmente disponíveis, os solos coesivos locais são cada vez mais empregados em muros de solo reforçado com geossintéticos como uma opção barata e sustentável. Os métodos convencionais de projeto ainda não levam em conta o efeito benéfico da coesão na redução da quantidade de reforço necessária. Da mesma forma, a contribuição da face para a estabilidade raramente é considerada, apesar de evidências experimentais significativas a seu favor. Esta tese avaliou a influência da coesão do solo e de uma face estrutural na estabilidade de muros de solo reforçado usando duas abordagens: uma abordagem semi-analítica e uma abordagem experimental.

O método semi-analítico empregado baseia-se na análise limite para o dimensionamento de muros de solo reforçado em solos coesivos friccionais, levando em conta a contribuição da face do muro. Uma análise paramétrica foi conduzida para avaliar o efeito da coesão do solo e do ângulo de atrito, da inclinação da face, da largura do bloco da face, da localização da força de reação que atua na face, do atrito da interface face-aterro, do atrito da interface face-fundação e do comprimento do reforço. Os ábacos de dimensionamento, adimensionais, fornecem a quantidade necessária de reforço para os comprimentos recomendados nos padrões de projeto e são apresentados para distribuições de reforço uniformes e linearmente crescentes. Conclui-se que a consideração da presença de coesão e do elemento de face na estabilidade do sistema pode levar a uma economia significativa no nível geral de reforço, e que as trincas de tração podem ser particularmente prejudiciais à estabilidade do muro reforçado em solos altamente coesivos, de modo que não podem ser negligenciadas no projeto.

A segunda parte da tese compreendeu a construção, o teste e a análise de um modelo reduzido de solo reforçado de 1,47 m de altura, construído com um solo friccional-coesivo e uma face de blocos de concreto modulares no Laboratório LabGsy, em São Carlos-SP, Brasil. O modelo foi construído usando uma coluna de blocos de concreto empilhados com o pé totalmente restringido, com uma inclinação pretendida de face de oito graus. O solo utilizado foi um material coesivo-friccional, classificado como argilo-arenoso. O material de reforço era composto por 5 camadas de geogrelha tecida de poliéster (PET) relativamente fraca, modificada para reduzir sua rigidez por meio do corte de alguns membros longitudinais. Depois de construído, o muro foi carregado de forma incremental até a pressão máxima de 150 kPa, limitada pela capacidade do airbag. O muro foi instrumentado amplamente para monitorar os deslocamentos na face, os recalques do solo na superfície, as tensões na fundação, as cargas verticais e horizontais no pé do muro e os deslocamentos e deformações nas camadas de reforço geossintético.

Foram apresentados os materiais, os métodos, o projeto e a construção da instrumentação e as adaptações da caixa de teste necessárias para sobrecarregar o modelo de muro reforçado até 150 kPa. A pequena magnitude dos deslocamentos da face do muro medida durante a construção e a fase de carregamento parece indicar que a muro estava em condições de serviço durante todo o ensaio, longe de atingir a falha. Tal observação pode ser atribuída ao estado sobreadensado do solo devido ao esforço de compactação, ao efeito benéfico da coesão no comportamento do muro de solo reforçado e à influência do pé do muro restringido para suportar parte da carga. Isso indica que os muros de solo reforçado construídos com solo coesivo podem ter bom desempenho, desde que sua drenagem possa ser garantida. Espera-se que as contribuições relativas aos estudos aqui propostos possam ser um passo adiante na compreensão do comportamento de muros de solo reforçado com geossintéticos com solos coesivos.

Finalmente, foi desenvolvida uma série de scripts em python para realizar análises numéricas automatizadas no Plaxis 2D utilizando scripts remotos, com a intenção de lançar as bases para um futuro estudo numérico envolvendo análises paramétricas automatizadas de muros de solo reforçado.

Palavras-chave: Solo reforçado. Solo coesivo. Geossintéticos. Análise limite. Modelo reduzido. Faceamento.

List of Figures

Nomenclature

c	cohesion
θ	generic angle of the log-spiral part of the failure surface
θ_0	angle between line P-A and the horizontal
r	generic radius for the log-spiral slip surface (C-D)
r_0	distance from point P to the wall toe
$\dot{D}$	total energy dissipation rate
$\dot{W}$	total external work rate
$\dot{D}_r$	energy dissipation rate within the reinforcement
$\dot{D}_s$	energy dissipation rate within the soil
$\dot{W}_s$	external work rate done by the soil weigh
ϕ	soil internal friction angle
$\dot{W}_q$	external work rate done by the surcharge load
$\dot{W}_w$	external work rate done by the pore water pressure
$\dot{W}_f$	external work rate done by the facing element
$f_1, f_2, f_3 ... f_6$	functions to calculate the external work rate made by soil weight
f_w	function to evaluate the external work rate done by the pore water pressure
θ_h	angle between line P-D and the horizontal
θ_C	angle between line P-C and the horizontal
P_f	reaction force acting on the facing element
g_1	function for the dissipated energy rate made by the soil along the log-spiral slip surface (C-D)
g_2	function for the dissipated energy rate made by the reinforcement along B-C and C-D
θ_h	angle between line P-D and the horizontal

f_7	non-dimensional function to calculate the external work rate done by facing element
D	vertical distance between the wall force location and the wall toe
β	wall facing batter
K_t	average tensile strength of a uniformly distributed reinforcement
δ_{base}	interface friction angle between the wall facing and the foudation soil
G_f	wall facing self-weight
K	generic average tensile strength of reinforcement
N	number of geosynthetic layers
$P_{f,s}$	shear component of the reaction force acting on the wall facing
N_b	number of facing blocks
T	tensile strength of a reinforcement layer
H	wall height
γ_b	facing block unit weight
w_b	block width (toe to heel)
y	vertical upward coordinate departing from the slope toe
δ	interface friction angle between the wall face and the retained soil
h_b	block height
δ_h	interface friction angle between the facing and the retained soil in respect to the horizontal
L	total length of the reinforcement layers
$L_{e(i)}$	effective length of reinforcement layer i resisting pull- out failure
$\theta_{(i)}$	angle related to the intersection of the failure surface with the i-layer
$L_{a(i)}$	active length of reinforcement layer i
$L_{c(i)}$	length of reinforcement layer i as illustrated in Fig. 2

$z^*_{(i)}$	overburden depth of reinforcement layer i which for gentle slopes can be less than zi
$z_{(i)}$	depth of reinforcement layer i below the wall crest
f_b	bond coefficient between the soil and geosynthetic-reinforcement
$\sum_{rupture}$	summation of layers failing in tensile rupture
R_h	horizontal force acting at the wall toe
$\sum_{pullout}$	summation of layers failing by pullout
ψ	ratio between the horizontal force on the wall toe and the total force carried by all reinforcement layers
R_v	normal force acting at the base of the facing
δ_{bb}	Interface friction angle between the wall facing blocks
$\dot{\theta}$	angular velocity of the sliding soil mass
$\dot{W}_1, \dot{W}_2 ... \dot{W}_6$	external work rates for different regions
γ	soil unit weight
λ	dimensioneless term larger than 1 representing the position of the reaction force at the wall
Ω	height factor for failure mechanisms emerging at the wall facing
i	denotes ith layer of reinforcement
i_{block}	identification of the block immediately above the inter-block interface intersected by the failure mechanism
l_1, l_2	lengths defined in Fig. 2
N'	Number of reinforcement layers above the exit point of the failure surface at the wall facing
$P_{f,h}$	horizontal component of the reaction force acting on the wall facing
r_u	pore pressure coefficient
T_p	pullout force
w_{sb}	horizontal setback at the block
z_c	crack depth

Contents

1 Introduction

1.1 Initial considerations

From the pioneering work of the French architect and engineer Henri Vidal in the mid-1960s, who introduced Reinforced Earth (VIDAL, 1966), the technique of soil reinforcement has evolved. The range of materials used to reinforce the soil mass increased, and in the 1970s early applications of geosynthetic material were made with geotextiles. Geogrid material started to be used in reinforced soil structures around the 1980s, and after this period the choice by this geosynthetic material significantly increased (BERG; CHRISTOPHER; SAMTANI, 2009a). Geogrids presents higher stiffness and tensile strength when compared to non-woven geotextiles (SCHLOSSER; DELAGE, 1987). The popularity of reinforced soil solution is based on the simplicity of the design and construction, low cost when compared to conventional retaining walls, and the ability to accommodate deformations. Koerner and Koerner (2013) estimated a number around of 150000 of existent mechanically stabilized earth structures worldwide at the time of their study, either with metallic or polymeric reinforcement.

In the last decades, the use of Geosynthetic Reinforced Soil Retaining Walls (GRS-RW) has increased for application in highways, bridge abutments, railways and other infrastructure projects due to its technical and economic advantages. Following this, studies to improve the understanding of the mechanisms related to the structure behaviour and to develop better design methodologies experienced a sharp increase since the late '90s. However, due to the complexity of such structures, the emergence of new geosynthetic material and the use of non-conventional types of soil, there are still questions to be answered regarding the behaviour of GRS-RW. In fact, observations of real structures performance have frequently demonstrated the conservatism in the design, indicating the need to further research in the area to improve this understanding.

The majority of studies on reinforced structures deals with granular soil, ideal material to be used in such structures due to its better drainage capacity and strength. However, the abundance of cohesive lateritic soils in Brazil, which usually presents high shear strength and low compressibility, favours the use of such materials for reinforced soil walls, despite its poor drainage capacity. In practice, this type of soil is used without any specific design guidelines and without much knowledge about the mechanisms involved in structure response.

This research aims to investigate the behaviour of reinforced soil walls with frictional-cohesive soils while accounting for the influence of the facing wall on system's stability by two approaches: experimental and analytical. The proposed study involves areas of great interest for the international community in geotechnical engineering, that is, the improvement in the design of GRS-RW, the use of frictional-cohesive soils for such structures (abundant in areas of tropical climate) and the evaluation of the effect of the facing wall on system's behaviour. Therefore, the contribution regarding the studies proposed herein is believed to have a significant impact on the research area.

To the best of our knowledge, this is the first time that both the facing element and backfill cohesion, while considering the presence of tension cracks, are accounted for in the design of reinforced walls. Furthermore, this is one of few reduced-scale 1-g model reinforced soil-wall constructed with cohesive soil and a structural wall facing.

1.2 Objectives and work plan

The main goal of this research is to expand the knowledge on the behaviour of reinforced soil-walls with cohesive soils and on the influence of the facing wall on system stability. To this end a series of specific objectives were defined and are summarized as follows:

1. Extension of a semi-analytical method, based on limit analysis, for the design of reinforced soil walls with cohesive backfill while accounting for the stabilizing effect of the wall facing (extension of the work of Abd and Utili (2017)). This is achieved by explicitly accounting for the facing weight to estimate toe load capacity;

2. Implementation of a novel solution scheme to evaluate all possible combinations of internal failure mechanisms (soil shear failure with reinforcement rupture and pullout) and a prescribed reinforcement length, including failure mechanisms emerging at the wall facing;

3. Application of the semi-analytical model proposed to produce dimensionless design charts that accounts for soil cohesion, soil tension cracks and wall facing effect on system stability;

4. Development of a test methodology to construct and surcharge a reduced-scale GRS-RW at LabGsy Laboratory, comprising of implementation of test box customizations, instrumentation plan design, construction (when applicable) and installation, and toe system design, manufacturing and installation;

5. Construction and monitoring of a reduced-scale GRS-RW with cohesive soil and a block wall facing with a restrained wall toe;

6. Compilation and treatment of measured data to produce graphic results of wall behaviour during construction and surcharging and discussion of test results;

7. Develop a series of python scripts to conduct automated numerical analysis in Plaxis 2D by using remote scripting, with the intention of laying the basis for a future numerical study involving automated parametric analysis of reinforced soil walls.

The model wall was constructed at 1/4 scale, with 1.47 m high by 1.42 m wide. The cohesive soil backfill retained extended 1.8 m behind the facing. The facing was comprised of a stack of reduced-scale solid concrete blocks and was attached to five horizontal layers of a polyester geogrid reinforcement having a length of 100 cm. Surcharging of the model wall was achieved by a surcharging system comprised of two airbags. Measurements such as facing displacements, foundation pressure, reinforcement displacement and strains and toe loads were continuously recorded during wall construction and surcharging.

1.3 Thesis Organisation

This thesis is divided into seven chapters, which are briefly summarised as follows.

Chapter 1 provides a brief introduction and a statement of the objectives and work plan in this research.

Chapter 2 provides a review of the relevant literature and background material on the design methods available for reinforced soil walls design and previous experimental studies undertaken in the field, which supports the need for the research undertaken herein.

Chapter 3 comprises the extension of a semi-analytical method based on the upper bound theorem of limit analysis to design geosynthetic reinforced backfills in cohesive soils accounting for the stabilizing effect of facing elements and the presence of tension cracks in the backfill soil.

Chapter 4 comprises the results obtained by using the semi-analytical methods presented in Chapter 3, showing dimensionless design charts providing the amount of reinforcement needed as a function of cohesion, tension cracks, reinforcement length, angle of shearing resistance, facing batter and facing dimensions.

Chapter 5 comprises a detailed description of the experimental program, including test methodology, test program, test facility, materials and instrumentation used and the construction and surcharging of the model wall.

Chapter 6 presents the measured results from the physical test monitoring during construction and surcharging and a discussion on data reliability and wall behaviour.

Chapter 7 gives a summary of the results, main conclusions of the thesis and recommendations for future work.

2 Background

2.1 Design of Geosynthetic Reinforced Soil Retaining Walls (GRS-RW)

In the design of conventional retaining structures, the wall is usually treated as a cantilever structure supported at its base (TATSUOKA et al., 1998). Its function is to resist the horizontal thrust imposed by the unreinforced backfill soil, usually considered as the active earth pressure. Therefore, the structural element is designed to resist large internal moment and the designer should verify stability against sliding along the wall's base, overturning and foundation bearing capacity to guarantee the stability of the system. For reinforced soil retaining walls, the reinforcement layers are responsible to maintain stability, by retaining the backfill soil thanks to the tensile force developed through the interaction between the soil and the reinforcement. Thus, in theory, the facing system has no structural function. However, as it will be discussed later, facing rigidity along with toe restraint can contribute to wall stability.

The reinforcement element restrains soil deformations by developing tensile force, which results in a larger strength of the system. The soil and soil-reinforcement interface strength are both, by nature, frictional (when considering granular soils) and therefore, they are a function of normal effective stress distribution (LEE; ADAMS; VAGNERON, 1973). This distribution, in its turn, is a function of various factors, such as overburden stress, drainage, type of materials, etc.

Conventional design of reinforced soil structures is usually done in the ultimate limit state. It treats the verification of external stability, similarly to conventional retaining structures (overturning, sliding, and foundation bearing capacity), and of internal stability. In the internal stability analysis, potential failure surfaces in the reinforced zone are evaluated, being considered reinforcement rupture and pullout. Maximum tensile loads in the reinforcements (T_{max}) are estimated and its spacing and length determined. Verifications regarding the failure of the facing or connection should also be performed (MIRMORADI; EHRLICH, 2015b).

The most used design methods are based on Limit Equilibrium (LE), not explicitly considering soil deformations and soil-reinforcement interaction, and neither the type of construction (CLAYBOURN; WU, 1993; KARPURAPU; BATHURST, 1995; ZORNBERG; SITAR; MITCHELL, 1998a,b; LESHCHINSKY; VULOVA, 2001). Since it considers only the ultimate limit state of the structure, the tensile strength and pullout resistance of the reinforcement are the parameters of interest, without considerations regarding reinforcement stiffness.

The reinforced backfill is divided into two parts, active and passive zones. In the active zone, the geosynthetic should resist the tensile loads without rupture, while in the passive zone it should have sufficient length to avoid pullout. Maximum reinforcement loads are assumed to occur in the intersection of the potential failure surface with each reinforcement layer. The works of Jewell, Paine, and Woods (1984), Leshchinsky and Perry (1989), Leshchinsky and Boedeker (1989), Mitchell, Villet, and Board (1987), Jewell (1991) and Leshchinsky, Ling, and Hanks (1995) present design methodologies based on LE analysis. They differ in the assumed failure surface (linear, bilinear, logarithmic spiral, circular), reinforcement rotation allowance, range of facing batter, consideration of surcharge and of cohesive contribution. Current standards in North America such as FHWA (BERG; CHRISTOPHER; SAMTANI, 2009b) and AASHTO (2002) recommend the use of the Simplified Method (Simplified Coherent Gravity Method) for geosynthetic reinforced soil walls, which is based on the tieback wedge analysis.

According to Holtz and Lee (2002b), the tieback wedge analysis (LE method) is one of the oldest and most common methods to design reinforced soil structures (Figure 2.1). It considers classical earth pressure theory and treats the reinforcements as "tiebacks" extending beyond the assumed Rankine failure surface. The soil shear strength is assumed to be totally mobilized simultaneously in all points of the failure surface and the structure is at incipient collapse. The reinforcement is also assumed to be at peak load capacity. However, as stated by Allen and Bathurst (2013; 2015), peak reinforcement strength requires strain levels larger than those associated with soil failure, which makes simultaneously peak mobilization of the reinforcement unlike to occur.

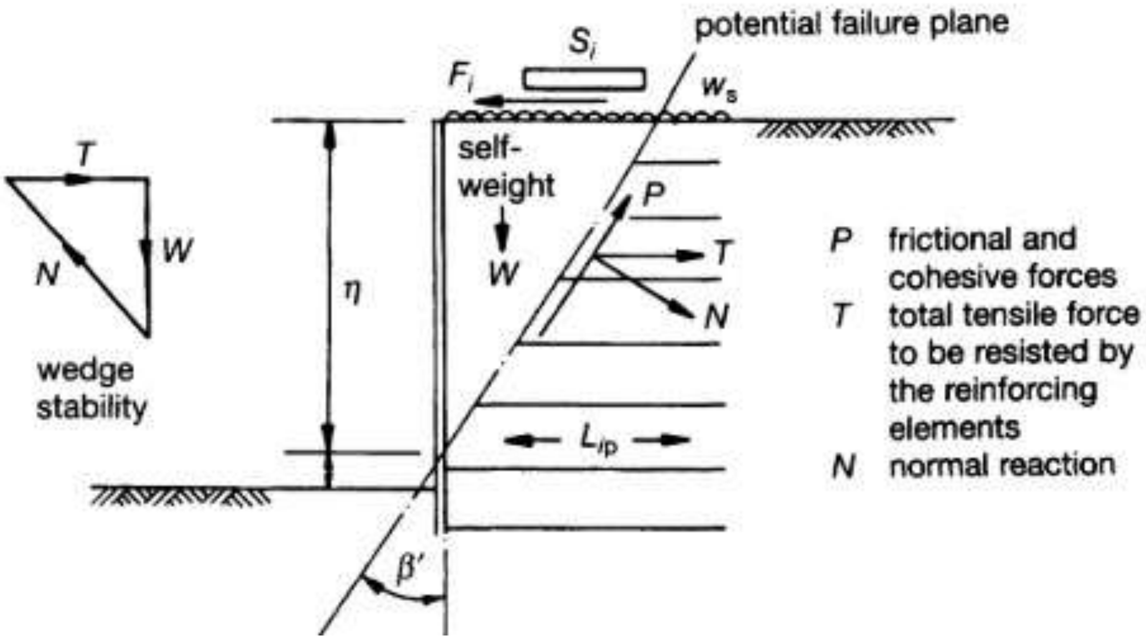

Figure 2.1: Tie-back analysis- wedge stability (JONES, 1996)

Assuming a given earth pressure distribution, usually an active condition K_a (JONES, 1996), the geosynthetic is responsible to resist the earth pressure distributed in its tributary area (local equilibrium). The maximum reinforcement loads are predicted at the bottom of the wall (calculated by Eq. 2.1) which is usually not the case in real structures. According to Holtz and Lee (2002b) the tieback wedge analysis tends to overestimate the earth pressure distribution and is unable to predict tensile stresses accurately in the geosynthetic and face deformations under working stresses condition.

$$T_{max,i} = K_a S_{v,i} \left(\gamma z_i + q\right) \tag{2.1}$$

where $T_{max,i}$is the maximum mobilized tension in the reinforcement, z_i is the depth of the reinforcement from the wall crest, $S_{v,i}$ is the vertical reinforcement spacing, q is the surcharge pressure, and K_a is the active earth pressure coefficient.

Alternative reinforcement tension distributions are presented by Zornberg, Sitar, and Mitchell (1998b), as shown in Figure 2.2. Allen and Bathurst (2002) presented distribution of reinforcement loads estimated from strain measurements of full-scale field walls and they showed that the load distribution is not triangular as conventionally assumed, but rather it has a trapezoidal shape (Figure 2.3). Huang et al. (2010), investigating the influence of toe restraint with finite-difference analysis (FLAC), have shown that the load distribution becomes more triangular when decreasing toe restraint, for uniform reinforcement spacing and type. However, the correspondent toe stiffness was significantly lower than those deduced from experimental measurements. The differences in the assumed and actual load distributions have been considered by the authors as a significant cause for the poor correlation between measured and predicted loads in GRS-RW.

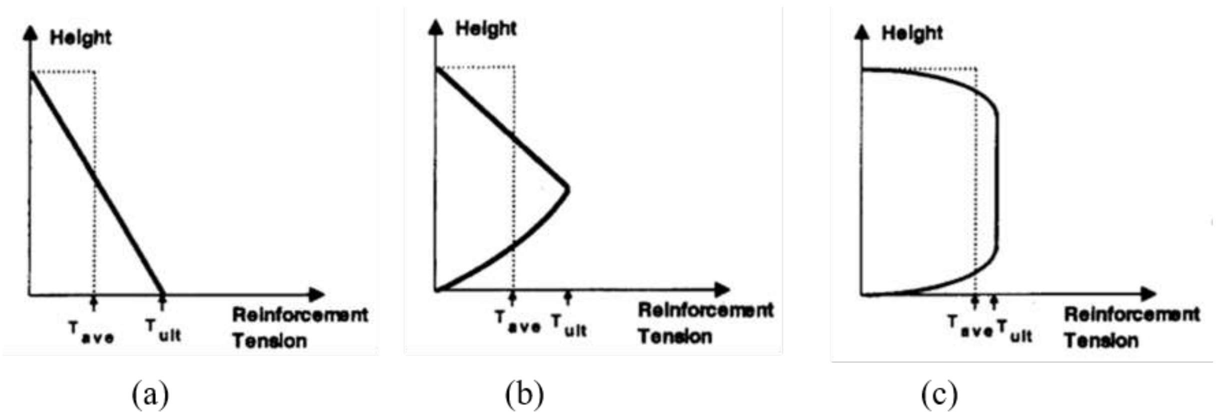

Figure 2.2: Estimated reinforcement tension distribution (a) Linear, conventionally assumed; (b) when first layer reaches Tult; (c) at failure (ZORNBERG; SITAR; MITCHELL, 1998b).

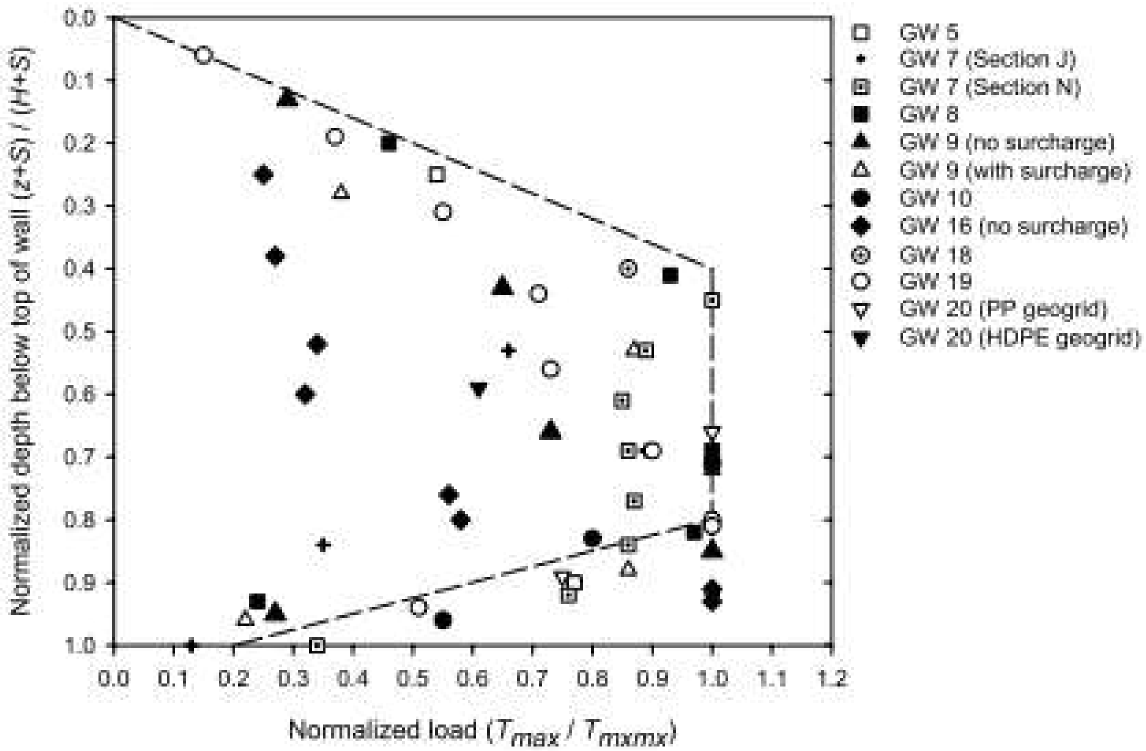

Figure 2.3: Normalized load estimated from strain measurements as a function of normalized depth below wall top (ALLEN; BATHURST, 2002).

Zornberg, Sitar, and Mitchell (1998a), evaluating reinforced soil slopes with granular backfill in the centrifuge environment, showed that LE analysis was able to adequately predict structure behaviour at collapse state. Regarding the service condition, Bathurst and Simac (1991) presented typical results of large-scale GRS-RW with an incremental panel wall reinforced with geogrids, constructed under laboratory conditions (3.6-m high). They compared the results correspondent to service and ultimate conditions and showed that the strain patterns in the geogrids significantly differ between the two states. This observation indicates that mechanisms of load development and distribution in GRS-RW are not the same for ultimate limit state and working stress conditions (ALLEN; BATHURST, 2002).

Given the limitations of the LE based methods, different authors believe that the conventionally used design methods are conservative (RESL, 1990; BATHURST; SIMAC, 1991; ROWE; HO, 1992; KARPURAPU; BATHURST, 1995; LESHCHINSKY, 2001; BATHURST et al., 2002; BATHURST, ALLEN; WALTERS, 2005; BENJAMIM; BUENO; ZORNBERG, 2007; HUANG et al., 2010). Rowe and Ho (1992) attribute as one source of this conservatism the disregard of the interaction between the different elements of a reinforced soil structure (backfill soil, reinforcement, facing, wall toe and foundation). At working stress state, stresses are not fully mobilized in each structure component, and therefore the load distribution depends on the relative stiffness of each component, with the stiffest components attracting more load (ALLEN; BATHURST, 2002, 2013). By disregarding the effect of reinforcement stiffness, for example, conventional design methods predict the same reinforcement loads for identical walls varying only on the geosynthetic stiffness. This is obviously far from reality.

Working stress design methods have been developed in the past years in an attempt to better predict reinforced soil structures behaviour at service limit state.

Ehrlich and Mitchell (1994) presented an analytical procedure for the internal design of vertical reinforced soil walls under service state that explicitly considers the soil stress-strain response (non-linear elastic hyperbolic constitutive model), the influence of reinforcement stiffness and soil compaction. By an iterative process, it is possible to obtain the required reinforcement strength, length, and spacing. However, predictions of wall deformation are not contemplated in the method, and the effects of facing stiffness and inclination, and toe restraint are not considered. According to Ehrlich and Mitchell (1994), the method predictions showed good agreement with measured data from full-scale walls. The consideration of compaction induced stresses was a novelty of the method, and, as stated by the authors, it can significantly influence reinforcement tension at shallow depths.

Mirmoradi and Ehrlich (2015a), recognizing the importance of compaction, proposed a simpler analytical procedure for its accountability in any conventional design method. Nonetheless, if used in the formulation of conventional methods (LE based) this procedure includes an additional component that tends to increase the estimated maximum reinforcement load, which furthers the conservativeness of methods already seen as over-conservative.

A simplification of the original method of Ehrlich and Mitchell (1994) was proposed by Ehrlich and Mirmoradi (2016). The modifications relate to the calculation of maximum reinforcement loads (no need for iteration) and the consideration of facing batter (not available in the original method). Also, unlike the original method, in which soil cohesion could be considered, the authors chose to simplify the new method for only cohesionless backfill soil. Good agreement was found between the two methods. Facing stiffness and toe restraint are still not considered in this updated method.

The K-Stiffness method, originally proposed by Allen et al. (2003) and Bathurst, Allen, and Walters (2005), is an empirical method based on field measurements of full-scale field and laboratory structures with granular backfill soil. It considers the effects of reinforcement stiffness, facing stiffness and batter, and soil strength. Reinforcement maximum loads are calculated from Eq. 2.2. Auxiliary equations are found in the original reference (ALLEN et al., 2003).

$$T_{max,i} = S_{v,i}\sigma_h D_{t,max}\Phi \tag{2.2}$$

where $T_{max,i}$is the maximum mobilized tension in the reinforcement, $S_{v,i}$ is the vertical reinforcement spacing (tributary area), σ_h is the lateral earth pressure acting over the reinforcement tributary area, and $D_{t,max}$ is the load distribution factor that modifies the reinforcement load based on layer location, and Φ is the influence factor that is the product of factors that account for the effects of local and global reinforcement stiffness, facing stiffness, and face batter.

Although not explicitly considering the toe restraint (not calibrated for it), Huang et al. (2010) concluded that the K-Stiffness method implicitly takes it into account since the good agreement between the methods prediction and numerical results was a function of toe stiffness input. The lowest toe restrains resulted in the most divergent results between reinforcement load predictions and numerical results.

Miyata and Bathurst (2007) have extended the original K-Stiffness method for the case of c-ϕ backfill soils, by adding a cohesion influence factor (Φ_c). Shortly after, Bathurst et al. (2008) presented a refinement of the method with new full-scale walls (mostly Japanese walls) added to the database. A small adjustment was made in the coefficient term related to the wall facing stiffness (Φ_{fs}) and consideration of cohesive contribution was sustained. However, the method calibration dataset still lacks model walls with varied facing batters and a wider range of facing types, which limits the method comprehensiveness (BATHURST et al., 2008).

Good agreement between the K-Stiffness method and measurement reinforcement loads from GRS walls have been reported by Bathurst et al. (2009) and Miyata, Bathurst, and Miyatake (2015). Recently, Allen and Bathurst (2015), recognizing the need for further improvement, updated the method and called it the Simplified Stiffness Method. The database was amplified to better address facing batter, reinforcement stiffness range of values, the effect of surcharge heights greater than 1 m, and the effect of wall height. The foundation of the case studies walls ranged from soft to firm conditions. According to the authors it resulted in more accurate predictions of reinforcement loads on average.

As pointed out by Bathurst, Allen, and Huang (2010) and Ehrlich and Mirmoradi (2016), the applicability of the K-Stiffness methods and its refinements is limited to the range of walls database that the method was based on. Therefore, when applied for different wall conditions it can under-predict reinforcement loads, being unsafe to be used in design (RICCIO; EHRLICH; DIAS, 2014; MIRMORADI; EHRLICH, 2015a).

Another type of method that can be used to determine the length and tensile strength needed for the reinforcements in geosynthetic reinforced soil walls and slopes is based on the upper bound limit analysis, an ultimate limit state method. Previous studies such as Abd and Utili (2017), Li and Young (2018), Michalowski and Zhao (1995), Zhao (1996), Michalowski (1997, 1998) have addressed internal stability of reinforced soil walls or slopes via limit analysis.

Abd and Utili (2017) investigated the stability of geosynthetic reinforced slopes without any retaining structure (facing batter ranging from 40° to 90°). In their work, the authors proposed a new semi-analytical method, based on limit analysis, for the design of geo-reinforced slopes with cohesive backfills, considering the presence of cracks that can reduce the stability of the system. Two types of cracks were considered: 'pre-existing' cracks (prior to the formation of a failure mechanism) and 'formation' cracks, due to the slope failure mechanism. The authors considered a rotational failure mechanism with a vertical crack as shown in Figure 2.4. To calculate the minimum amount of reinforcement it was considered a rupture failure, while for determination of reinforcement length rupture and pullout were assumed. Also, two reinforcement distributions were considered: uniform distribution (UD) and linear increasing distribution (LID) (Figure 2.5).

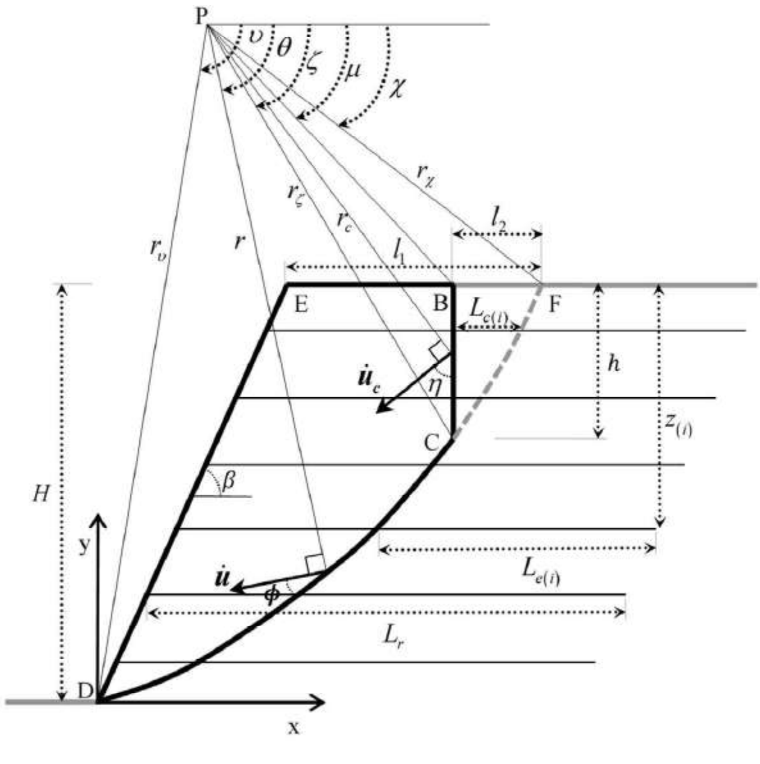

Figure 2.4: Rotational failure mechanism in a reinforced slope with a crack (B-C). (Source: Abd and Utili (2017)).

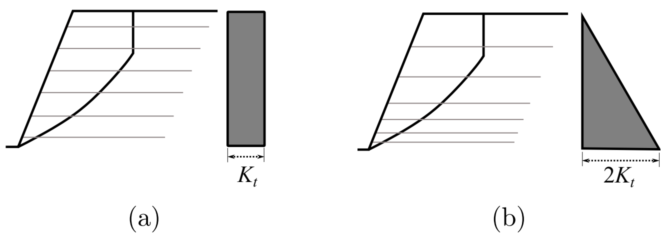

Figure 2.5: Geosynthetic-reinforcement layouts (a) Uniform distribution, and (b) Linearly increasing distribution with depth.

From energy balance, Abd and Utili (2017) arrived in the following objective function to be optimised to determine the required reinforcement:

$$\frac{K_t}{\gamma H} = f\left(\chi, \upsilon, \xi, \beta, r_u, \varphi, c/\gamma H, t\right) \tag{2.3}$$

where, K_t is the average tensile strength of a uniformly distributed reinforcement; γ is the unit weight of the soil; H is the slope height; χ, υ and ξ are angles given in Figure 2.4; β is the slope face inclination; r_u is the pore pressure coefficient; φ is the soil angle of shearing resistance; c is the soil cohesion; and t is a dimensionless coefficient representing the soil tensile strength.

The method validation was made by numerical analysis and is reproduced in Figure 2.6. Other design charts are provided in the reference work (ABD; UTILI, 2017) . It was shown that accounting for the presence of cohesion can lead to significant savings.

In fact, the consideration of cohesion in the design of GRS-RW can have a beneficial effect, reducing the amount of required reinforcement while maintaining a desirable level of safety for the structure. Vahedifard et al. (2014) used limit equilibrium to investigate the effect of cohesion on GRS-RW and concluded that the impact on the design seismic active earth pressure coefficient is significant. However, the authors recommended caution when using cohesion in design, "given the significant uncertainties associated with the determination of cohesion and apparent cohesion in partially saturated soils".

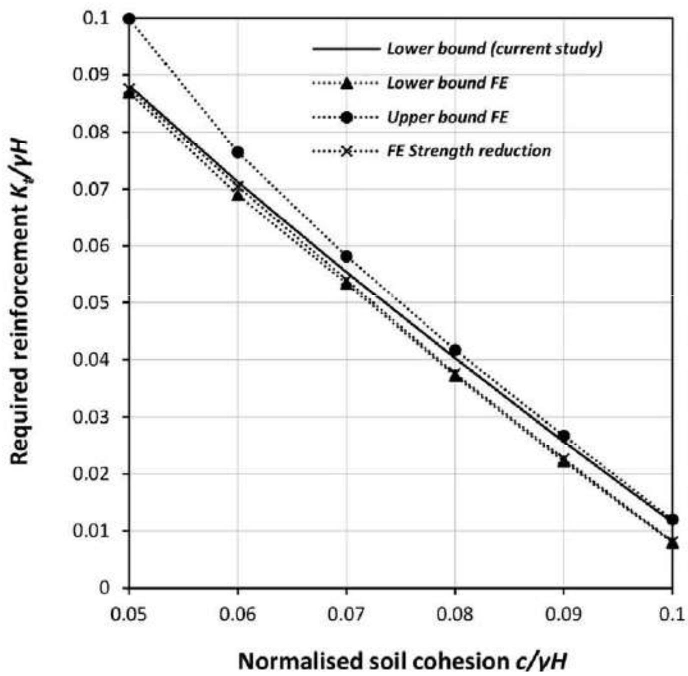

Figure 2.6: Comparison between the analytical lower bounds of required reinforcement and finite element analyses results. (Source: Abd and Utili (2017)).

Recently, some researches have evaluated the active earth pressures for retaining structures with cohesive backfills. Vahedifard et al. (2015) studied the effect of tension cracks and unsaturated conditions based on limit equilibrium analysis for the evaluation of external stability of retaining structures (Figure 2.7). By moment equilibrium and iterative analysis, it was possible to obtain the maximum lateral earth thrust on the retaining wall that satisfied the limit equilibrium state. Li and Yang (2018) studied the effect of tension cracks and of unsaturated conditions for retaining structures based on the kinematic approach of limit analysis (work-energy balance), a similar approach as the adopted by Abd and Utili (2017), however, considering a retaining structure without reinforcement (Figure 2.8). Other studies evaluating the impact of cohesion on seismic stability analysis (VAHEDIFARD et al., 2014) and the impact of tensile strength cut-off on the active earth pressure (LI; YANG, 2019) were also carried on. However, these studies have focused on the external stability of retaining structures and no considerations about internal stability for geosynthetic reinforced soil walls have been addressed, which is one goal of the present work.

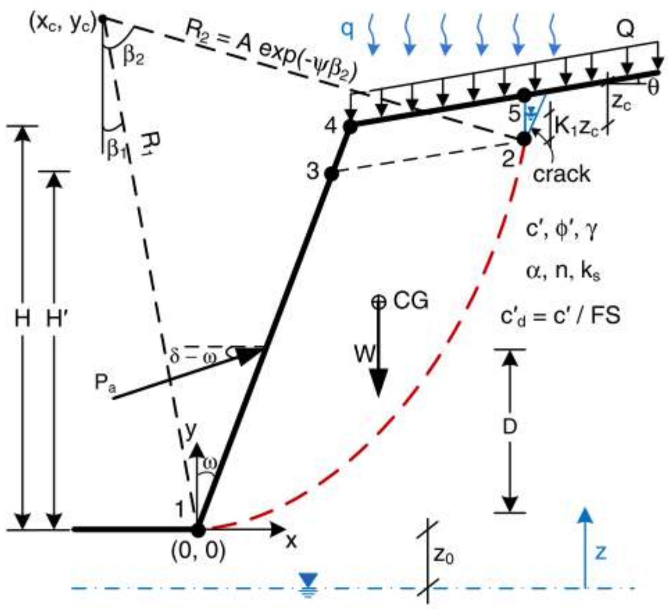

Figure 2.7: Failure mechanism adopted by Vahedifard et al. (2015) for an unsaturated retaining structure. for an unsaturated retaining structure (source: Vahedifard et al. (2015)).

This research proposal aims to extend the formulation of Abd and Utili (2017) for the case of GRS-RW, where there is the presence of a retaining structure (lateral earth thrust on the retaining wall should be considered). This is an area of a growing interest of the scientific community.

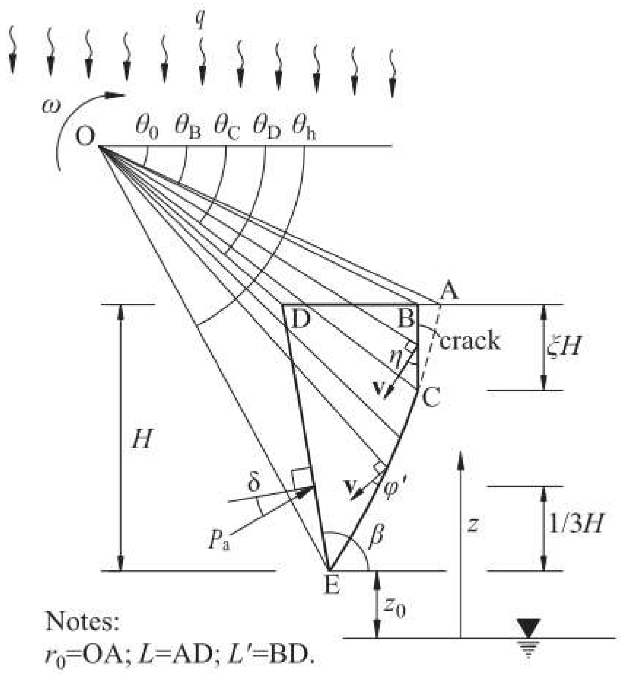

Figure 2.8: Schematic diagram of rotational failure mechanism with a vertical crack adopted by Li and Yang (2018) (source: Li and Yang (2018)).

2.2 Influence of the wall facing on GRS-RW stability

The facing element in reinforced soil structures traditionally has a function of aesthetics and protection against backfill erosion. Varied facing types are available, such as segmental precast concrete panels, dry cast modular block wall units, welded wire mesh, gabion facing, and geosynthetic facing. These facing elements are accounted for when performing numerical analysis of reinforced soil wall systems with the use of Finite Element Method (FEM) or Finite Difference Method (FDM). However, conventional design methodologies, here taken as methods based on Limit Equilibrium and analytical methods, ignore the potential contribution of the face to system's performance ((BERG; CHRISTOPHER; SAMTANI, 2009a); NCMA, (2010); AASHTO, (2017)). Nonetheless, plenty of works have recognized that a hard facing element associated with toe restraint may contribute to structure's stability.

To evaluate the influence of the facing type on wall behaviour, large-scale tests (3.6-m height) were performed by Bathurst (1993), with an incremental panel and a full-height facing, and by Bathurst et al. (2006), with a dry-stacked modular concrete block facing and a wrapped-face. The reinforced soil wall models were backfilled with sand material and loaded in stages up to failure. Ehrlich and Mirmoradi (2013) evaluated the effects of facing stiffness and toe resistance with block and wrapped facing types and sand as the backfill material. The reduced 1.5-m height models were surcharged in stages up to 100 kPa and the wall behaviours evaluated in function of facing properties. In other studies, the influence of toe restraint was evaluated in centrifuge tests with reinforced sand

(ZHANG; CHEN; YU, 2019) and the facing contribution to seismic response was studied in reduced-scale tests under cyclic loading (shaking table test) (EL-EMAM; BATHURST, 2005).

Numerical studies with Finite Element (FEM) and Finite Difference (FDM) methods were conducted mainly for working stress conditions, without surcharge loading, and with sand as backfill material. Parametric analyses were performed to evaluate the influence of different parameters, such as the influence of the wall facing parameters. Ho and Rowe (1996) evaluated, among other factors, the effect of toe restraint in reinforcement loads with continuous full panel facing, showing that for shorter walls the toe attracts a larger portion of the load, thus reducing the reinforcement load. The effect of modular block facing properties on wall behaviour was studied by Ling and Leshchinsky (2003), who shown that the block width impacted wall displacements, geosynthetic loads and lateral earth pressures at the facing, while varying the interface friction between blocks had negligible effect on wall behaviour. Huang et al. (2010) focused on the studied of the influence of toe restraint on the behaviour of reinforced soil with modular block facing by varying the horizontal toe stiffness. They found that the wall toe can significantly contribute to the stability of the structure under working stress conditions. Similarly, Mirmoradi and Ehrlich (2015b) investigated the influence of facing stiffness and two different toe conditions: free-base and fixed-base. They showed that the combined effect of those factors can have a significant influence on reinforcement load, specially in the layers close to the bottom of the wall. .

Nonetheless, studies that aim to quantify and incorporate the facing contribution explicitly in the design are scant. Previous studies were conducted in the framework of limit equilibrium (ISMEIK; GULER, 1998; LESHCHINSKY; LING; HANKS, 1995; LESHCHINSKY; ZHU; MEEHAN, 2010; LESHCHINSKY; LESHCHINSKY; LESHCHINSKY, 2017) and of analytical methods (XIE; LESHCHINSKY; YANG, 2016), but they were all restricted to cohesionless soils. Some recent studies have been focusing on improving the selection of reinforcement layout, through optimization techniques (GONZÁLEZ-CASTEJÓN; SMITH, 2021) or through visual tools such as safety maps with consideration of the facing (LESHCHINSKY; LESHCHINSKY; LESHCHINSKY, 2017), however without accounting for the impact of cohesion and tension cracks to the wall's stability.

2.3 Influence of soil cohesion on GRS-RW stability

The conservative assumption of neglecting cohesion in design is due to the fact that geosynthetics were initially conceived for cohesionless granular soils and that the first design guidelines published for geosynthetic reinforced earth structures disregard the beneficial effect of cohesion e.g. AASHTO and Jewell (1996). However, the recent editions of AASHTO LRFD *bridge design specifications* (AASHTO, (2012), (2017)) allow for the inclusion of cohesion in the seismic design of geo-reinforced slopes although unfortunately no formulae are provided for this purpose. The AASHTO revisit was prompted by the work of Anderson et al. (2008) which, for example, shows that an amount of cohesion as much as 10 kPa can reduce the thrust against an earth structure of up to 50-75% for typical design conditions. In light of these findings, Vahedifard et al. (2014) have investigated the beneficial effect of cohesion on geosynthetic reinforced earth structures based on limit equilibrium concluding that 'the results clearly demonstrate the significant impact of cohesion on the K_{ae} value' (K_{ae} being an approximate estimate of the design seismic active earth pressure coefficient). Indeed, experimental studies such as the works of Gregg (2008) and Riccio, Ehrlich, and Dias (2014) have shown the beneficial effect of soil cohesion on wall behavior.

Cohesive soils manifest limited, if not negligible, tensile strength so they are subject to the formation of cracks (THUSYANTHAN et al., 2007; PORBAHA; GOODINGS, 1997). Tension cracks forming in geo-reinforced slopes have been reported in experiments in the geotechnical centrifuge (PORBAHA; GOODINGS, 1997; SUAH; GOODINGS, 2001) and in post-earthquake field observations (LING; LESHCHINSKY; CHOU, 2001). Moreover, Baker (1981), Michalowski (2013), Utili (2013) and Utili and Abd (2016) investigating the stability of uniform cohesive frictional (c-ϕ) slopes concluded that when the presence of cracks is neglected, slope stability may be significantly overestimated. The same conclusions were reached by Abd and Utili (2017) for the case of c-ϕ geo-reinforced slopes. Therefore, the presence of tension cracks must be accounted for to achieve a safe design. Porbaha et al. (2000) and Chen et al. (2018) evaluated the case of cohesive soil retaining structures, disregarding the presence of facing elements and tension cracks, whereas Chehade et al. (2019) accounted for tension cracks but not the facing contribution.

In the context of Brasil, important and pioneering researches in the country were conducted using non-conventional fills for reinforced soil slopes and walls. Benjamim (2006) constructed 8 large-scale field walls of 4-m high reinforced with woven and non-woven geotextile and three types of soils: sand, silty sand and a silty clay. Portelinha (2012) evaluated the influence of saturation on the behaviour of reinforced soil walls reinforced with non-woven geotextiles and using a frictional-cohesive soil. Santos (2011) conducted an experimental program to evaluate the behaviour of reinforced walls constructed with recycled construction and demolition waste (RCD-R) and fine soil. A total of 2 field model walls and 1 laboratory model wall with 3,60-m high, using different types of reinforcement.

2.4 Upper bound Limit Analysis

2.4.1 Derivation of the semi-analytical solution

Abd and Utili (2017) added the effect of cohesion and the presence of tension cracks in the formulation presented by Michalowski (1997) for cohesionless soils. However, their study was restricted to reinforced soil slopes, with no facing element. In the formulation here presented the presence of a retaining wall is added.

The assumed failure surface is described by the following log-spiral expression:

$$r = r_0 \exp\left[\tan\phi\,(\theta - \theta_0)\right] \tag{2.4}$$

where θ and θ_0 are the angles made by r and r_0 respectively with the horizontal, r is the distance between the spiral centre (point P in Figure 2.4) and a generic point on the log-spiral slip surface, and r_0 is the length of line PA.

The energy balance equation is given by:

$$\dot{D} = \dot{W} \tag{2.5}$$

where $\dot{D}$ is the internal energy dissipation rate and $\dot{W}$ is the external work rate.

In the following, we first examine the case of failure of all reinforcements, which implies that the geosynthetic length is sufficiently long to develop the load correspondent to its tensile strength. In the sequence, we evaluate the case of a fixed reinforcement, based on minimal length recommendations of various design standards (BERG; CHRISTOPHER; SAMTANI, 2009a); NCMA, (2010), BSI, (2010);AASHTO, (2017), with a combined mode of failure (pullout and tensile failure). This second approach, with a predefined length, may lead to larger values for the required reinforcement strength than the one obtained with the failure of all layers. Nonetheless, it allows the designer to evaluate whether the cost savings achieved by shortening the reinforcement length would be sufficient to offset the needed increase in strength. It is worth noting that the bulk of the cost savings in a reinforced soil wall with cohesive soils is associated with reduced excavation of wall footprint and the use of the local and less expensive fill material. Since the reinforcement length directly affects the volume of reinforced soil fill its reduction may have a significant impact on the final cost of the solution.

2.4.2 Required Reinforcement Strength

Limit analysis formulation considers the wall at imminent collapse with the soil-reinforcement system behaving as a rigid-perfectly plastic body. The load in each reinforcement layer is assumed to reach its tensile strength, given a sufficient length is provided.

For a general case, internal energy dissipation comes from the reinforcement ($\dot{D}_r$) and the soil ($\dot{D}_s$) along the crack (B-C in Figure 3.4) and along the log-spiral failure surface (C-D in Figure 3.4), since the homogeneous soil mass is assumed rigid. For a cohesionless soil the latter term is null. The external work is done by the soil-self weight ($\dot{W}_s$), any pore water pressure in the ground ($\dot{W}_w$), the surcharge load ($\dot{W}_q$) and the wall facing contribution ($\dot{W}_f$). Surcharge load, in this work, is not considered but it can be added in the formulation by derivating f_q in Eq. 2.11. For the case of open cracks, Eq. 2.5 can be re-written as:

$$\dot{D}_{r(B-C)} + \dot{D}_{s(C-D)} + \dot{D}_{r(C-D)} = \dot{W}_s + \dot{W}_w + \dot{W}_q + \dot{W}_f \tag{2.6}$$

where:

$$\begin{aligned} \dot{D}_{s(C-D)} &= c\dot{\theta}r_0^2 \exp\left[2\tan\phi\left(\theta_C - \theta_0\right)\right] \frac{\exp\left[2\tan\phi\left(\theta_h - \theta_C\right) - 1\right]}{2\tan\phi} \\ &= c\dot{\theta}r_0^2 g_1\left(\theta_0, \theta_h, \theta_C, \phi\right) \end{aligned} \tag{2.7}$$

$$\begin{aligned} \dot{D}_{r(B-D)} &= \dot{D}_{r(B-C)} + \dot{D}_{r(C-D)} = \frac{1}{2}K_t\dot{\theta}r_{_0}^2 \left\{\exp\left[2\tan\phi\left(\theta_h - \theta_0\right)\right]\sin^2\theta_h - \sin^2\theta_0\right\} \\ &= K_t\dot{\theta}r_0^2 g_2\left(\theta_0, \theta_h, \theta_C, \phi\right) \end{aligned} \tag{2.8}$$

$$\begin{aligned} \dot{W}_s &= \dot{W}_1 - \dot{W}_2 - \dot{W}_3 - \left(\dot{W}_4 - \dot{W}_5 - \dot{W}_6\right) \\ &= \gamma\dot{\theta}r_0^3\left(f_1 - f_2 - f_3 - f_4 + f_5 + f_6\right) \end{aligned} \tag{2.9}$$

$$\dot{W}_w = \gamma\dot{\theta}r_0^3 r_u f_w \tag{2.10}$$

$$\dot{W}_q = q\dot{\theta}r_0^2 f_q \tag{2.11}$$

Equation 2.8 is related to the case of uniform distribution of reinforcement (UD). The correspondent expressions for the case of linear distribution (LID) are reported in Appendix A. Abd and Utili (2017) have shown that $\dot{D}_{r(A-C)} = \dot{D}_{r(B-C)}$ and therefore energy dissipated by the reinforcement can be expressed solely by Eq. 2.8. In this paper it is advocated that crack formation, unlike the ductile formation of the log-spiral D-C, is a brittle phenomenon, therefore energy dissipated by crack formation should not be accounted in LA so $\dot{D}_{s(B-C)} = 0$.

The terms $f_1, f_2, f_3, f_4, f_5, f_6$, and f_w are non-dimensional functions dependent on the failure surface geometry $(\theta_0, \theta_h, \theta_C, \beta)$, γ is the soil unit weight, $\dot{\theta}$ is the angular velocity of the sliding soil mass and ϕ is the soil internal friction angle. Their analytical expressions are reported in Appendix B of this paper, previously presented by Chen (1975).

The work rate done by the reaction force acting on the facing element (P_f) is calculated as a dot product of this force and the velocity at its point of action, which can be expressed as:

$$\dot{W}_f = -\dot{\theta} r_0 P_f f_7 \tag{2.12}$$

2.5 Model scaling laws

When trying to study the behaviour of a field-sized structure (prototype) by means of a reduced scale model at laboratory environment it is important to base the design of the model wall, as much as possible, by applying scaling laws deduced from dimensional analysis to material and geometry parameters, so the model behaviour becomes similar to the prototype one in terms of stresses and strains. In the field of experimental geotechnics this is particularly difficult, since meeting the scaling requirements for all the materials at the same time is not feasible (VISWANADHAM; KÖNIG, 2004), being particularly harder to satisfy similitude requirements for 1g (single gravity) modelling according to Wood (2004). For example, a full scaling of a GRS-RW would require meeting the scaling factors for soil particle size, strength and deformation parameters, geogrid aperture size, strength and stiffness, facing strength, geometry and stiffness, etc. In addition, soils usually exhibit stress dependent behaviour, which makes it harder to project the prototype behaviour by means of a reduced scale model, due to the low confining stresses that occur in this latter case. Therefore, it is common to comply with the main scaling factors that are believed to control the structure's behaviour, arguing that the remaining requirements are of second order importance (WOOD, 2004).

Despite the limitations of 1g modelling Wood (2004) presents some advantages of this type of investigation:

1. Easy to define and control boundary conditions, providing a reliable data set to be used in numerical modelling validation and parametric analysis and back analysis;

2. Possible to construct large models, function of laboratory spacing and equipment availability, that reduces the negative effects associated with small models;

3. Sufficient space available for instrumentation of the model, which facilitates its control and observation with smaller soil disturbance due to instrument placement, when compared to centrifuge modelling.

According to Viswanadham and König (2004) very few studies attempted to consider similitude requirements for geosynthetic materials in 1g reduced model tests of reinforced soil structures, which the authors attributed to the initial interest in understanding the behaviour qualitatively. The same is noticed regarding the modelling of facing blocks.

Scaling factors to model geosynthetic material are given by the authors, being emphasized by the importance of 'scaling-down the geosynthetic even for 1g model studies'. Factors for geometry and soil parameters are given by Iai (1989) and further discussed and detailed by Wood (2004). The factors of interest for the present research are summarized in Table 2.1, assuming the same soil for the model and the prototype wall.

Parameter	Symbol	Scale factor (1g model)
Scale	λ^*	-
Wall height (m)	H	$1/\lambda$
Gravity	g	**1**
Soil unit weight (kN/m³)	γ	**1**
Friction angle (deg)	φ	**1**
Cohesion (kPa)	c	$1/\lambda$
Normalized cohesion	$c/\gamma H$	**1**
Soil strain	ε_s	1
Soil particle size	D_{50}	$1/\lambda$
Reinforcement dimensions (longitudinal and transversal apertures and rib thickness) (mm)	S_l, S_t, T_l, T_t	$1/\lambda$
Cross-section area of rib (m^2)	A_r	$1/\lambda^2$
Cross-section area of rib/unit length (m^2)	A'_r	$1/\lambda$
Reinforcement peak tensile strength (kN/m)	T_{ult}	$1/\lambda^2$
Reinforcement stiffness at 5% strain (kN/m)	$J_{5\%}$	$1/\lambda^2$
Pull-out force (kN/m)	T_p	$1/\lambda^3$
Bond stress (kN/m^2)	τ_b	$1/\lambda$
Soil-geosynthetic friction angle (deg)	φ_{sg}	1
Facing block width – toe to heel (cm)	w_b	$1/\lambda$
Normalized block width	w_b/H	**1**
Facing block height (cm)	h_b	$1/\lambda$
Facing block depth (cm)	d_b	$1/\lambda$

Table 2.1: Scaling factors of interest recommended in the literature and used (in bold) in this research for 1g models (after Iai (1989) and Viswanadham and König (2004).

3 Design of reinforced cohesive soil walls accounting for wall facing contribution to stability

3.1 Assumptions made in the analytical method

There are two main approaches to investigate the stability of geosynthetics-reinforced structures: one where the local equations of equilibrium for an equivalent continuum formed by ground and reinforcement together are derived via homogenization techniques (e.g. Buhan et al. (1989); Sawicki (1983)), called continuum approach by Michalowski and Zhao (1995), and another one, to be used here, where ground and geo-reinforcement are considered as two separate structural components, called structural approach (MICHALOWSKI; ZHAO, 1995).

In this thesis the structural approach will be employed together with the kinematic (upper bound) method of limit analysis (LA) assuming a rigid rotational mechanism to obtain lower bounds on the required level of reinforcement. This means the calculated levels of reinforcement are smaller than the values required to avoid collapse. However, numerical analyses run by Abd and Utili (2017) for the case of geo-reinforced slopes in c–ϕ soils without facing elements show that the lower bounds on the reinforcement strength found by assuming a rigid rotational mechanism as here are very close to upper bounds obtained by numerical Finite Element Limit Analysis (FELA) (SLOAN, 2013) with the static method, with the difference between them being lower than 14% for any value of cohesion considered. Hence, true collapse values were determined with an accuracy of ±7% by taking the average of the two bounds. Also, finite element displacement-based analyses with strength reduction technique (FESR) were performed by Abd and Utili (2017), assuming the validity of the normality rule consistent with the theory of limit analysis. These provided values of reinforcement very close to the lower bounds found by the kinematic method of LA assuming a rigid rotational mechanism.

Note that LA assumes a simplified constitutive behaviour for both ground and reinforcement, i.e. rigid-perfectly plastic, and the validity of the normality rule, i.e. associated plastic flow, which at rigour does not hold true for most soils. We acknowledge that for a drained stability analysis involving soils with high friction angles, the use of an associated flow rule predicts excessive dilation during shear failure, and raises the question of whether the bound theorems will provide realistic estimates of the limit load. Already in the pioneering investigation of this issue, Davis (1968) argued that the flow rule will not have a major influence on the limit load for frictional soils unless the problem is strongly constrained in a kinematic sense. A precise definition of the degree of kinematic

This chapter has been published in Géotechnique (see Franco, Utili, and Silva (2023)) constraint is elusive, but our problem is not strongly constrained, since it involves a freely deforming upper ground surface and a semi-infinite domain. For these cases, Davis (1968) conjectured that it is reasonable to assume that the bound theorems will give acceptable estimates of the true limit load. More recently, Muraro, Madaschi, and Gajo (2015) performed displacement based FEM analyses of the active thrust upon retaining walls showing *"soil dilatancy has negligible effects on the stability of the wall"*. Also Potts and Fourie (1986) found that the dilation angle bears very little influence on soil pressure for a retaining wall with a horizontal ground surface.

In the stability charts produced in the literature for slopes in cohesive soils two scenarios of tension cracks have been considered so far: cracks pre-existing shear failure (UTILI, 2013) and cracks forming simultaneously with the shear failure surface (MICHALOWSKI, 2013). Here cracks are assumed to pre-exist the formation of the shear log-spiral failure since there is experimental evidence showing that crack formation in cohesive soils is a brittle phenomenon (e.g. Thusyanthan et al. (2007)) unlike the log-spiral part of the slope failure mechanism where failure is in shear and ductile. This implies that stress redistribution can be assumed only along the log-spiral part of the mechanism with the crack to be assumed opened by the time the progressive ductile failure along the log-spiral part of the mechanism reaches the crack. Therefore, in the energy balance equation employed for the derivation of the analytical solution (see section 4) we assumed no energy is dissipated by crack formation.

The assumption of open crack implies the solution is independent of the amount of soil tensile strength. Of course, the depth of tension cracks is dependent on the amount of soil tensile strength and of the tensile stresses arising in the backfill, with crack depth being dictated by the extent of the region where tensile stresses exceed soil tensile strength. This means one would expect the ground tensile strength to be related to the depth of the tension cracks and so in turn to the amount of reinforcement prescribed by the solution. But the very onset of a crack changes the stress distribution so that complex FEM numerical modelling and constitutive equations are required to mimic crack propagation to find out the link between crack depth and ground tensile strength. Here, consistently with the Limit Analysis kinematic approach, the crack is a geometric boundary condition for the failure mechanism considered. Among all the potential failure mechanisms, with each potential mechanism involving a crack of a specific depth and location, the critical failure mechanism is found as a worst case scenario, i.e. the mechanism giving rise to the lowest stability factor. So the crack (depth and location) that has the most adverse effect on stability is found as a result. This assumption errs on the safe side since the actual crack depth may be less than the depth of the crack associated to the worst case scenario depending on the actual distribution of tensile stresses in the backfill and ground tensile strength.

The amount of cohesion that can be relied upon in the design of backfills made of c-ϕ

soils depends on several factors that vary over time, to name a few: the ground moisture content, the level of the phreatic line in the structure, the intended design lifetime for the reinforced wall since this has implications on the weather induced deterioration the soil strength is likely to experience over time, etc. Several publications deal with the choice of the values for c for clay soils with the use of peak strength, residual strength, operational strength (POTTS; KOVACEVIC; VAUGHAN, 1997), and critical state strength advocated depending on the geotechnical problem tackled. The choice of the value for cohesion is outside the scope of this thesis. Take and Bolton (2011) provide a good coverage of the literature with regard to such a choice for clay slopes. Here, it is enough to recall that the designer must be careful to design the reinforcement considering the worst case scenario in terms of hydraulic conditions that can occur over the entire lifetime of the structure and adopting a cautious approach.

It is important to note that even in case of soils possessing no true cohesion, i.e. exhibiting zero shear strength at zero confinement, their shear strength can still be suitably described by the failure criterion here adopted (see Figure 3.1). In this case c is to be interpreted as an apparent cohesion with the strength envelope intercepting the τ axis at the origin. From a mathematical point of view the presence of this apparent cohesion means that the straight part of the failure criterion is above the line and therefore reinforcement can be saved.

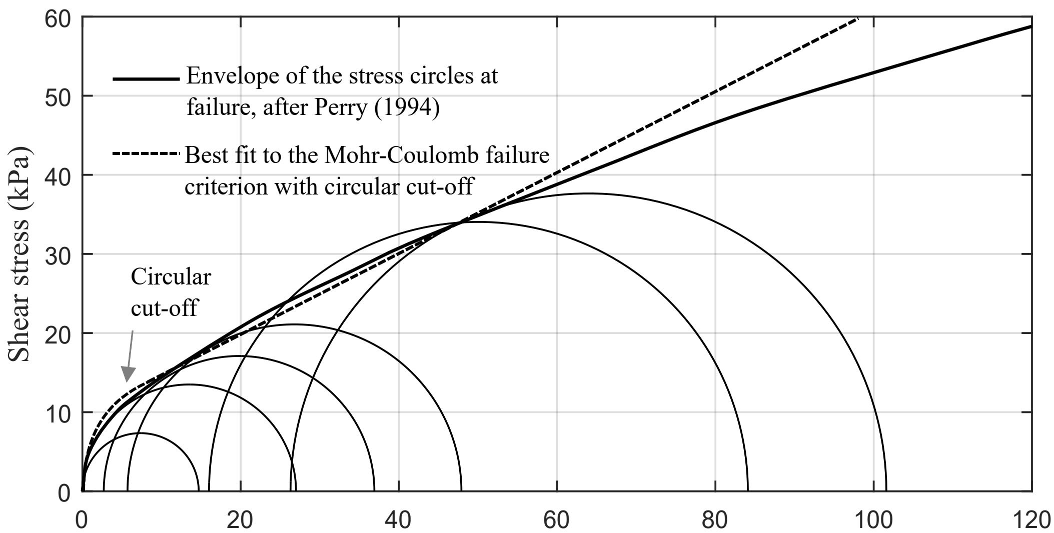

Figure 3.1: Shear strength of London clay achieved from drained compressive triaxial tests at low stresses: non linear envelope (solid curve) of the stress circles at failure (after (PERRY, 1994)); linear c-ϕ best fit with tension cut-off (dashed curve).

3.2 Problem description

According to Bathurst, Simac, and Berg (1993) typical facing batters, β, are in the range of 75° to 87° for geosynthetic reinforced structures. Therefore, in this work we considered uniform $c - \phi$ reinforced soil walls with facing batters between 70° and 90°. A homogeneous soil without external surcharge is here assumed for sake of simplicity. However, an external surcharge can be straightforwardly added in the calculations.

Two reinforcement distributions were considered:

1. A uniform distribution (UD): reinforcement layers of equal strength equally spaced (Figure 3.2a);

2. A linearly increasing distribution (LID): reinforcement layers with decreasing vertical spacing and increasing strength over depth (Figure 3.2b).

The expressions for the reinforcement strength distribution over depth for the UD and LID cases, respectively, are:

$$K_t = \frac{NT}{H} \tag{3.1}$$

$$K = 2K_t \frac{(H - y)}{H} \tag{3.2}$$

where K_t is the average strength of reinforcement in the reinforced soil wall, K is the local reinforcement strength for LID distribution, N is the number of reinforcement layers, T is the strength of a single layer at yielding point, H is the wall height and y is the vertical upward coordinate departing from the wall toe.

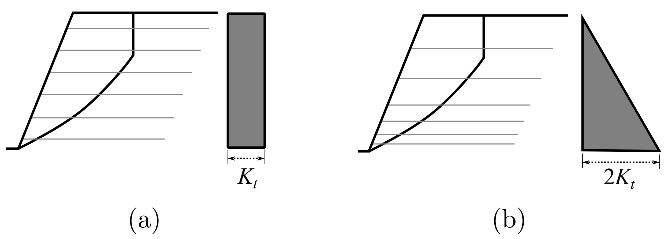

Figure 3.2: Geosynthetic-reinforcement layouts (a) Uniform distribution, and (b) Linearly increasing distribution with depth.

A log-spiral failure mechanism with a vertical tension crack is here assumed, a kinematically admissible failure surface in limit analysis (Figure 3.3). In this mechanism, all deformations occur along the log-spiral D-C, with no energy dissipation accounted for the brittle opening of the tension crack B-C.

In this thesis tensile failure and combined failure are evaluated. The former assumes that all layers fail in tensile rupture and that the reinforcement length is sufficiently long to mobilize its tensile strength. In the combined failure, some layers fail in tensile rupture while others by pullout, including also the possibility of compound failure (some layers are bypassed by the failure surface). A third possible failure mechanism is direct sliding over one reinforcement layer (MICHALOWSKI, 1997), but this is not addressed in this study.

Two types of wall facing are here considered, a continuous facing and a modular stacked block facing. The way we treat the direction of the resultant force acting at the wall differentiates them. For the continuous facing, we adopted the direction used for conventional retained structures, with the resultant reaction force inclined at an angle δ with the perpendicular to the facing batter, where δ is the interface friction angle between the continuous face and the retained soil (Figure 3.4a). This facing system is representative of the widely used full-height rigid facing in Japan (TATSUOKA et al., 1998). For the second facing, with discrete blocks, we assumed a modified direction for the resultant (Figure 3.4b) that accounts only for the friction at the vertical interfaces between blocks and the retained soil (LESHCHINSKY et al., 2012; VAHEDIFARD et al., 2014; XIE; LESHCHINSKY; YANG, 2016).

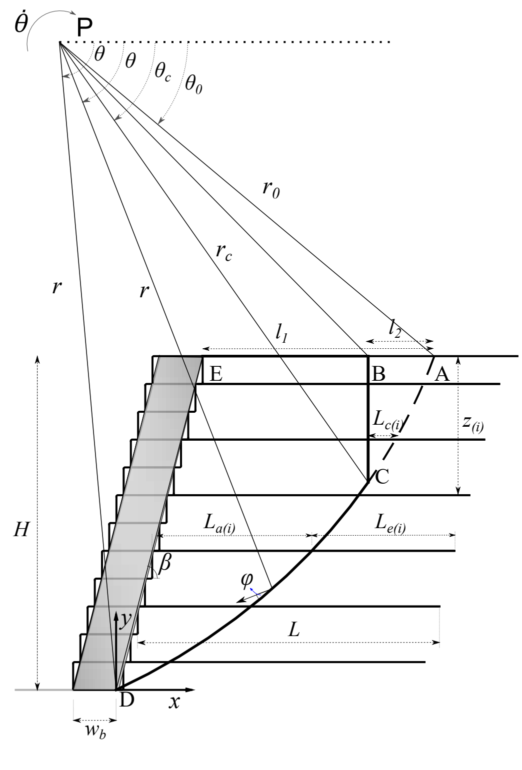

Figure 3.3: Rotational failure mechanism in a reinforced soil wall with a vertical crack and notations. Two types of wall facing considered: modular block facing and full-height rigid facing (in grey).

3.3 Derivation of the semi-analytical solution

Abd and Utili (2017) added the effect of cohesion and the presence of tension cracks in the formulation presented by Michalowski (1997) for cohesionless soils. However, their study was restricted to reinforced soil slopes, with no facing element. In the formulation here presented the presence of a retaining wall is added.

The assumed failure surface is described by the following log-spiral expression:

$$r = r_0 \exp\left[\tan\phi\left(\theta - \theta_0\right)\right] \tag{3.3}$$

where θ and θ_0 are the angles made by r and r_0, respectively, with the horizontal, r is the distance between the spiral centre (point P) and a generic point on the log-spiral slip surface, and r_0 is the length of line PA in Figure 3.3.

The energy balance equation is given by:

$$\dot{D} = \dot{W} \tag{3.4}$$

where $\dot{D}$ is the internal energy dissipation rate and $\dot{W}$ is the external work rate.

In the following, we first examine the case of failure of all reinforcements, which implies that the geosynthetic length is sufficiently long to develop the load correspondent to its tensile strength. In the sequence, we evaluate the case of a fixed reinforcement, based on minimal length recommendations of various references and design standards (BERG; CHRISTOPHER; SAMTANI, 2009; NCMA, 2010, BSI, 2010; AASHTO, 2017), with a combined mode of failure (pullout and tensile failure). This second approach, with a predefined length, may lead to larger values for the required reinforcement strength than the one obtained with the failure of all layers. Nonetheless, it allows the designer to evaluate whether the cost savings achieved by shortening the reinforcement length would be sufficient to offset the needed increase in strength. Since the reinforcement length directly affects the volume of soil backfill, its reduction may have a significant impact on the overall cost of the structure. In fact, the main cost savings that can be realized by employing cohesive soils as backfill are due to reduced backfill volume and the use of local less expensive materials.

3.3.1 Required Reinforcement Strengthre

LA formulation considers the wall at imminent collapse with the soil-reinforcement system behaving as a rigid-perfectly plastic body. Each reinforcement layer is assumed to be at yield assuming a sufficient anchorage length is provided.

For a general case, internal energy dissipation comes from the reinforcement ($\dot{D}_r$) and the soil ($\dot{D}_s$) along the crack (B-C in Figure 3.3) and along the log-spiral failure surface (C-D in Figure 3.3), since the homogeneous soil mass is assumed rigid. For a cohesionless soil the latter term is null. The external work is done by the soil self-weight ($\dot{W}_s$), any pore water pressure in the ground ($\dot{W}_w$) and the wall facing contribution ($\dot{W}_f$). The term $\dot{W}_s$ is calculated as the work of block E-D-A minus the work of block B-C-A (Figure 3.3). The work of block E-D-A and of block B-C-A are calculated by the algebraic summation of the work of blocks P-D-A, P-E-A and P-D-E (CHEN, 1975) and of blocks P-C-A, P-B-A and P-C-B (UTILI, 2013; UTILI; NOVA, 2007), respectively. Therefore, for the case of open cracks, Eq. 3.4 can be re-written as:

$$\dot{D}_{r(B-C)} + \dot{D}_{s(C-D)} + \dot{D}_{r(C-D)} = \dot{W}_s + \dot{W}_w + \dot{W}_f \tag{3.5}$$

where:

$$\begin{aligned}\dot{D}_{s(C-D)} &= c\dot{\theta}r_0^2 \exp\left[2\tan\phi\left(\theta_C-\theta_0\right)\right] \frac{\exp\left[2\tan\phi\left(\theta_h-\theta_C\right)-1\right]}{2\tan\phi} \\ &= c\dot{\theta}r_0^2 g_s\left(\theta_0,\theta_h,\theta_C,\phi\right)\end{aligned} \tag{3.6}$$

$$\begin{aligned}\dot{D}_{r(B-D)} = \dot{D}_{r(B-C)} + \dot{D}_{r(C-D)} &= \frac{1}{2}K_t\dot{\theta}r_0^2\left\{\exp\left[2\tan\phi\left(\theta_h-\theta_0\right)\right]\sin^2\theta_h - \sin^2\theta_0\right\} \\ &= K_t\dot{\theta}r_0^2 g_r\left(\theta_0,\theta_h,\phi\right)\end{aligned} \tag{3.7}$$

$$\begin{aligned}\dot{W}_s &= \dot{W}_1 - \dot{W}_2 - \dot{W}_3 - \left(\dot{W}_4 - \dot{W}_5 - \dot{W}_6\right) \\ &= \gamma\dot{\theta}r_0^3\left(f_1 - f_2 - f_3 - f_4 + f_5 + f_6\right)\end{aligned} \tag{3.8}$$

$$\dot{W}_w = \gamma\dot{\theta}r_0^3 r_u f_w \tag{3.9}$$

Equation 3.7 is related to the case of uniform distribution of reinforcement (UD). The correspondent expressions for the case of linear distribution (LID) are reported in Appendix A. Abd and Utili (2017) have shown that $\dot{D}_{r(A-C)} = \dot{D}_{r(B-C)}$ and therefore energy dissipated by the reinforcement can be expressed solely by Eq. 3.7. In this thesis it is advocated that crack formation, unlike the ductile formation of the log-spiral D-C, is a brittle phenomenon, therefore energy dissipated by crack formation should not be accounted in LA so $\dot{D}_{s(B-C)} = 0$.

The terms $f_1, f_2, f_3, f_4, f_5, f_6$ and f_w are non-dimensional functions dependent on the failure surface geometry $(\theta_0, \theta_h, \theta_C, \beta)$, γ is the soil unit weight, $\dot{\theta}$ is the angular velocity of the sliding soil mass and ϕ is the soil internal friction angle. Their analytical expressions are reported in Appendix B of this paper.

The work rate done by the reaction force acting on the facing element (P_f) is calculated as a dot product of this force and the velocity at its point of action, which can be expressed as:

$$\dot{W}_f = -\dot{\theta} r_0 P_f f_7 \tag{3.10}$$

where f_7 is a non-dimensional function provided by Li and Yang (2019) for the conventional direction of the thrust (Figure 3.4a) and by Xie, Leshchinsky, and Yang (2016) for the modified direction (Figure 3.4b). Their full expressions are reported in Appendix B.

Note that P_f is negative since it acts to stabilize the system. The positive effect for stability of adhesive forces at the interface soil-wall is neglected and therefore in its respect the present analyses are conservative. Since the focus of this thesis is to evaluate the contribution of the facing element and soil cohesion on structure's stability we chose to treat conservatively other assumptions such as adhesion.

By isolating the facing element in Figure 3.3 and calculating its rigid body equilibrium, P_f can be determined (Figure 3.4). Note that the horizontal force acting at the wall toe may be composed by passive resistance mobilized in front of the embedded face and friction force between the base of the first block and the foundation soil. However, American public and private design guidelines such as AASHTO LRFD *bridge design specification* (AASHTO, 2017) and NCMA *design manual for segmental retaining walls* NCMA, (2010) do not recommend counting on the passive earth pressures for the stability of unreinforced and reinforced soil structures, since it is hard to guarantee it for all the service life of the structure. Similarly, British standard BS 8006 *code of practice for strengthened/reinforced soils and other fills* BSI, (2010) recommends to neglect passive earth pressures acting on the wall toe for external stability calculations. Hence, here only the frictional contribution was considered, consistently with Leshchinsky, Zhu, and Meehan (2010).

Leshchinsky et al. (2012) argue that interface friction mobilization between the horizontal setbacks of the blocks (w_{sb} in Figure 3.4b) and the soil is likely to be partial so it cannot be relied upon. Assuming full mobilization would imply a questionable upward normal force acting along the horizontal interface. Therefore, as in Leshchinsky (2012), the forces exchanged under the block setbacks are ignored and only the interface friction at the vertical block faces is assumed in contact with the fill. This assumption is appropriate for the case of inclined segmental block facing. In this case, the resultant reaction force assumes the direction depicted in Figure 3.4b, inclined at an angle δ with the horizontal. This direction is here identified, as in Vahedifard et al. (2014), as modified direction and has been adopted previously by Xie, Leshchinsky, and Yang (2016) and Vahedifard et al. (2014) for the case of reinforced soil walls with segmental blocks. The so-called conventional direction by Vahedifard et al. (2014), shown in Figure 3.4a, refers to the usual direction adopted for stability problems of conventional retaining structures, with a continuum facing.

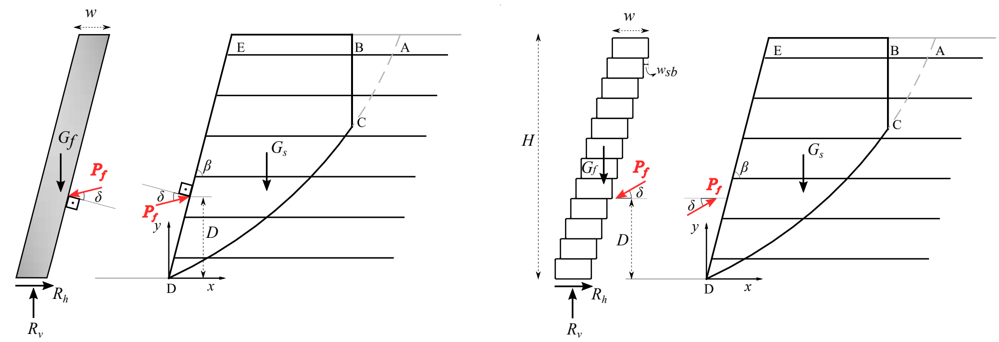

Figure 3.4: Free-body diagram of the facing element (a) conventional direction; (b) modified direction.

P_f in Figure 3.4, carried by the facing element, is the net force between the active earth pressure and the reinforcement connection loads acting at the back face of the wall. The location of P_f, given by D in Figure 3.4, may depend on some factors such as the toe restraint condition and wall height. Indeed, the effect of toe restraint is more significant for shorter walls, for which the dimensions of the blocks relative to the wall height can have a significant influence on wall stability (LESHCHINSKY, 2007). For higher structures, the toe restraint influence usually is limited to the lower section of the wall (HOLTZ; LEE, 2002a; MIRMORADI; EHRLICH, 2015b).

Considering an interface friction angle between the face and wall base (usually a levelling pad) or between the levelling pad and the foundation soil (whichever is smaller) equal to δ_{base} and an interface friction angle δ between the reinforced soil and the back of the wall, from the rigid body equilibrium of the facing, P_f is expressed as (conventional direction):

$$P_f = \frac{G_f \tan \delta_{base}}{\cos(\delta + \beta - \pi/2) - \sin(\delta + \beta - \pi/2) \tan \delta_{base}} \tag{3.11}$$

where G_f is the face self-weight.

For the modified direction (case of stacked blocks), P_f is given by:

$$P_f = \frac{G_f \tan \delta_{base}}{\cos \delta - \sin \delta \tan \delta_{base}} \tag{3.12}$$

In the latter case, the force that should be sustained by the facing element is independent of the facing batter β.

Downdrag forces contribute to the stability of the system by summing up to the facing weight and composing the normal force acting at the wall base. However, design such as NCMA (2010) suggest ignoring the downdrag forces ($P_f \sin\delta$ in Figure 3.4), due to the difficulty of compaction near the face and the unpredictability of the normal force acting at the vertical segments of the blocks (LESHCHINSKY; ZHU; MEEHAN, 2010). Disregarding downdrag forces, to be conservative, leads to simpler expressions for Eq. 3.11 and Eq. 3.12:

$$P_f = \frac{G_f \tan\delta_{base}}{\cos(\delta + \beta - \pi/2)} \tag{3.13}$$

$$P_f = \frac{G_f \tan\delta_{base}}{\cos\delta} \tag{3.14}$$

Note that downdrag forces may also arise from the hanging of reinforcement layers at the facing connections, that occurs when the reinforced soil settles more than the facing element. These are difficult to predict but can provide a significant contribution to wall's stability, especially for full-height rigid facing with high connection strengths (LESHCHINSKY; ZHU; MEEHAN, 2010; DAMIANS et al., 2013).

The face self-weight, per meter of wall, is calculated as the sum of the weight of all blocks, for the stacked block facing case:

$$G_f = N_b h_b \gamma_b w_b = H \gamma_b w_b \tag{3.15}$$

where N_b, γ_b, w_b and h_b are the total number of blocks, the block unit weight and the block width (toe to heel) and height, respectively. H is the wall height. The wall height comes assuming the full height of the dry-stacked block contributing to toe load capacity.

For facing batters $\beta < 82°$, the hinge height approach is recommended in some design manuals (BERG; CHRISTOPHER; SAMTANI, 2009a; AASHTO, 2017) to estimate the normal stress transmitted between dry-stacked block facing units, limiting the maximum design weight of the units that can be transferred to the wall base. This value is used to estimate the connection strength of the reinforcement-facing connection, when the connection is frictional. However, studies considering an unyielding foundation have shown that this is an overly conservative assumption, since downdrag forces at the interface between the soil and the face result in vertical toe loads higher than the facing self-weight (BATHURST; WALTERS, 2000; HATAMI; BATHURST, 2005). This has prompted the 3rd edition of NCMA design manual (NCMA, 2010) to remove the consideration of the hinge height entirely, even for facing batters up to 70°. For this reason, the full height of the wall is here used to estimate the toe capacity.

Defining the angle of P_f with respect to the horizontal as $\delta_h = \delta + \beta - \pi/2$ for the conventional force direction and $\delta_h = \delta$ for the modified force direction and substituting Eq. (3.15) into Eq. (3.11) or into Eq. 3.12, the following expression is obtained (normalized by γH^2):

$$\frac{P_f}{\gamma H^2} = \frac{(\gamma_b/\gamma)\,(w_b/H)\tan\delta_{base}}{\cos\delta_h - \sin\delta_h \tan\delta_{base}} \tag{3.16}$$

By substituting the energy rate contributions calculated through Eq. (3.6) to Eq. (3.10) into Eq. (3.5) it is possible to obtain the objective function to be optimized to determine the minimum level of reinforcement required (lower bound) when a sufficient reinforcement length is assumed (all layers fail in tensile rupture), while accounting for the facing and cohesion contributions:

$$\frac{K_t}{\gamma H} = \frac{(f_1 - f_2 - f_3 - f_4 + f_5 + f_6 + r_u f_w)}{\left(\frac{H}{r_0}\right)(g_r)} - \left(\frac{c}{\gamma H}\right)\left(\frac{g_s}{g_r}\right) - \left(\frac{H}{r_0}\right)\frac{P_f}{\gamma H^2}\frac{f_7}{(g_r)} \tag{3.17}$$

$$\frac{K_t}{\gamma H} = f\left(\theta_0, \theta_h, \theta_C, \beta, r_u, \phi, c/\gamma H, \delta, D, w_b/H, \delta_{base}\right)$$

3.3.2 Length of reinforcement

The minimum length of reinforcement is calculated by considering a combined failure mechanism, involving pullout of some layers and rupture of others. Compound failure mechanisms in which the failure surface extends into the unreinforced soil zone are taken into account as well. In these cases, the remaining crossed layers can fail by pullout, by tension or a combination of both.

Assuming layers of equal length, the normalized length of reinforcement (L/H) is given by :

$$\frac{L}{H} = \frac{L_{e(i)}}{H} + \left(\frac{L_{a(i)}}{H} - \frac{L_{c(i)}}{H}\right) \tag{3.18}$$

where $L_{e(i)}/H$ is the effective (or anchorage) length of reinforcement layer i yet to be calculated, $\theta_{(i)}$ the angle related to the intersection between the failure surface and layer i, $L_{a(i)}/H$ the reinforcement length of layer i in the active zone up to the failure surface, and $L_{c(i)}/H$ part of the anchorage length of the reinforcement spared because of the crack (see Figure 3.3).

Trigonometry dictates that:

$$\frac{L_{a(i)}}{H} = -\left(\cos\theta_h + \sin\theta_h \cot\beta\right) \frac{r_0}{H} \exp\left[\tan\phi\left(\theta_h - \theta_0\right)\right] + \\ + \left(\cos\theta_{(i)} + \sin\theta_{(i)} \cot\beta\right) \frac{r_0}{H} \exp\left[\tan\phi\left(\theta_{(i)} - \theta_0\right)\right] \tag{3.19}$$

For reinforcement layers crossing the crack, $L_{c(i)}/H$ is calculated by:

$$\frac{L_{c(i)}}{H} = \frac{r_0}{H}\left\{\exp\left[\tan\phi\left(\theta_{(i)} - \theta_0\right)\right]\cos\theta_{(i)} - \exp\left[\tan\phi\left(\theta_C - \theta_0\right)\right]\cos\theta_C\right\} \tag{3.20}$$

whereas for any reinforcement below the crack tip $L_{c(i)} = 0$.

$L_{e(i)}/H$ is determined from the following expression (extension of the formulation of Michalowski (1997) to account for cohesion and the facing):

$$\frac{K_t}{\gamma H} = \frac{\left(\frac{r_0}{H}\right)^2 \left(f_1 - f_2 - f_3 - f_4 + f_5 + f_6 + r_u f_w\right) - \left(\frac{r_0}{H}\right)\left(\frac{c}{\gamma H}\right)\left(g_s\right)}{\frac{1}{N}\sum_{rupture}\left(\sin\theta_0 + \frac{z_{(i)}}{r_0}\right)} + \\ + \frac{-\frac{P_f}{\gamma H^2} f_7 - 2 f_b \tan\phi\left(1 - r_u\right)\sum_{pullout}\left[\frac{z^*_{(i)}}{H}\frac{L_{e(i)}}{H}\left(\sin\theta_0 + \frac{z_{(i)}}{r_0}\right)\right]}{\frac{1}{N}\sum_{rupture}\left(\sin\theta_0 + \frac{z_{(i)}}{r_0}\right)} \tag{3.21}$$

where $z^*_{(i)}$ is the overburden depth or reinforcement layer i, which for gentle slopes can be less than the depth $z_{(i)}$ (JEWELL, 1990), not the case of the walls evaluated herein. f_b is the bond coefficient between the soil and reinforcement, and N is the number of geosynthetic layers. $\sum_{rupture}$ refers to the summation of layers failing in tensile rupture, whereas $\sum_{pullout}$ to the summation of layers failing by pullout.

In Eq. 3.21, the adhesion between the soil and reinforcement was neglected. Thus, only the interface friction, in the form of the parameter f_b, was considered for the calculation of the pullout force.

To find the minimum required reinforcement length Michalowski (1997) adopted the criteria that the most adverse combined failure mechanism makes a required reinforcement value no larger than the one calculated in Eq. 3.17, in which all the layers fail in tension. In this way, according to the author, the reinforcement would be used economically (being fully utilized). This is achieved by imposing the value $K_t/\gamma H$ calculated in Eq. 3.17 into Eq.3.21. Michalowski (1997) study focused only on cohesionless soils. However, for cohesive soils with low friction angles this approach results in excessively long and unpractical reinforcement lengths. For this reason, in the present study, the approach previously adopted by Chehade et al. (2019; 2020) is employed: the case of a predefined reinforcement length with a combined mode of failure (pullout and tensile failure). The approach used herein may lead to larger values for the required reinforcement strength.

However, it allows the designer to evaluate if by shortening the reinforcement the structure cost savings would be sufficient to offset the increase of the required strength. Note that reinforcement length affects the costs of a reinforced soil structure more than the geosynthetic strength, since it is directly related to the volume of reinforced fill material.

Equation 3.21 can be re-written by substituting $L_{e(i)}/H$ given in Eq. 3.18 and thus expliciting L/H:

$$\frac{K_t}{\gamma H} = \frac{\left(\frac{r_0}{H}\right)^2 (f_1 - f_2 - f_3 - f_4 + f_5 + f_6 + r_u f_w) - \left(\frac{r_0}{H}\right)\left(\frac{c}{\gamma H}\right)(g_s)}{\frac{1}{N}\sum_{rupture}\left(\sin\theta_0 + \frac{z_{(i)}}{r_0}\right)} + \\ + \frac{-\frac{P_f}{\gamma H^2} f_7 - 2 f_b \tan\phi\,(1 - r_u)\,(C_1 L/H - C_2)}{\frac{1}{N}\sum_{rupture}\left(\sin\theta_0 + \frac{z_{(i)}}{r_0}\right)} \tag{3.22}$$

$$\frac{K_t}{\gamma H} = f\left(\theta_0, \theta_h, \theta_C, \beta, r_u, \phi, c/\gamma H, \delta, D, w_b/H, \delta_{base}, L/H, f_b, N\right)$$

where:

$$C_1 = \sum_{pullout}\left[\frac{z^*_{(i)}}{H}\left(\sin\theta_0 + \frac{z_{(i)}}{r_0}\right)\right] \tag{3.23}$$

$$C_2 = \sum_{pullout}\left[\frac{z^*_{(i)}}{H}\left(\frac{L_{a(i)}}{H} - \frac{L_{c(i)}}{H}\right)\left(\sin\theta_0 + \frac{z_{(i)}}{r_0}\right)\right] \tag{3.24}$$

It is worth mentioning that the required reinforcement in Eq. 3.22 is not a strict lower bound because the pullout force calculation is only an approximation, since it is necessary to assume a distribution of normal stresses (overburden stresses) acting on the reinforcement. However, as stated by Michalowski (1997), it gives a reasonable estimate. Also, from Eq. 3.22 it follows that now the required reinforcement is dependent on the number of reinforcement layers (N) chosen.

3.3.3 Modes of failure

A rotational failure mechanism consisting of a log-spiral passing through the wall toe is assumed and a search for the most critical failure surface (lower bound on the required reinforcement) is performed over θ_0, θ_h and θ_c. Several cracks may develop over time in a geo-reinforced wall wherever the soil tensile strength is exceeded. Among these cracks the failure mechanism will always engage the one crack that has the most adverse effect on stability. θ_c identifies the geometry of the crack. Maximisation of the function in Eq. 3.21 with respect to θ_0, θ_h and θ_c implies that the most adverse failure mechanism for the wall is found together with the crack most adverse to the stability of the structure. Note that it is unlikely that the most adverse crack will ever be present, but instead various less critical cracks will form in the reinforced soil over time. However, assuming the existence of the most adverse crack implies that the very worst case scenario in terms of tensile cracks is assumed which is a desirable choice for a conservative design.

For a predefined reinforcement length L/H five failure modes are considered, as shown in Figure 3.5. For a given L/H and a potential failure surface (a given set of θ_0, θ_h and θ_c) it is possible to verify the number of reinforcement layers been bypassed and crossed by calculating the anchorage length L_e/H (substitution of Eq. 3.19 and Eq. 3.20 in Eq. 3.18). If $L_{e(i)}/H < 0$ the evaluated failure surface bypasses the considered layer.

Here a novel solution scheme was implemented to find the type of failure (pullout or tensile rupture) for each crossed layer, that is, for each layer intersected by the potential failure surface. All possible combinations of failure are considered for the set of crossed layers (total of $2^{n_{crossed}}$) and for each combination (some of the crossed layers assumed to fail in tensile rupture and the rest in pullout) the required reinforcement strength $K_t/\gamma H$ is calculated with Eq. 3.22. Then, the initial assumption of failure for each layer is checked following the steps shown in Figure 3.5 and by comparing the pullout force (T_p) and the reinforcement strength (T) in each layer:

$$\frac{T_{p(i)}}{\gamma H^2} = 2\frac{L_{e(i)}}{H}\frac{z*_{(i)}}{H} f_b \tan\phi\,(1 - r_u) \tag{3.25}$$

$$\frac{T_{(i)}}{\gamma H^2} = \frac{K_t}{N\gamma H} \tag{3.26}$$

If for a given potential failure surface no possible combination with at least one layer failing in tension is feasible a final verification is carried out, corresponding to Mode 5 in Figure 3.5. In this verification, it is checked if the pullout of all of the crossed layers, together with the contributions of soil cohesion and of the facing would be sufficient to guarantee stability to the system. In this case, Eq. 3.22 would reduce to the following expression, from which the minimum length of reinforcement required to guarantee stability can be calculated:

$$2f_b \tan\phi\,(1-r_u)\,(C_1 L/H - C_2) \geq \left(\frac{r_0}{H}\right)^2 (f_1 - f_2 - f_3 - f_4 + f_5 + f_6 + r_u f_w) + \\ - \left(\frac{r_0}{H}\right)\left(\frac{c}{\gamma H}\right)(g_s) - \frac{P_f}{\gamma H^2} f_7 \tag{3.27}$$

If the predefined length used is smaller than the minimum required, the given length is too short for the case evaluated. Note that Mode 5 does not result in any required reinforcement strength $K_t/\gamma H$ since no layer fails in tensile rupture to contribute to internal energy dissipation (Eq. 3.27). However, it allows checking if the predefined length L/H is sufficient to guarantee stability for any potential failure surface.

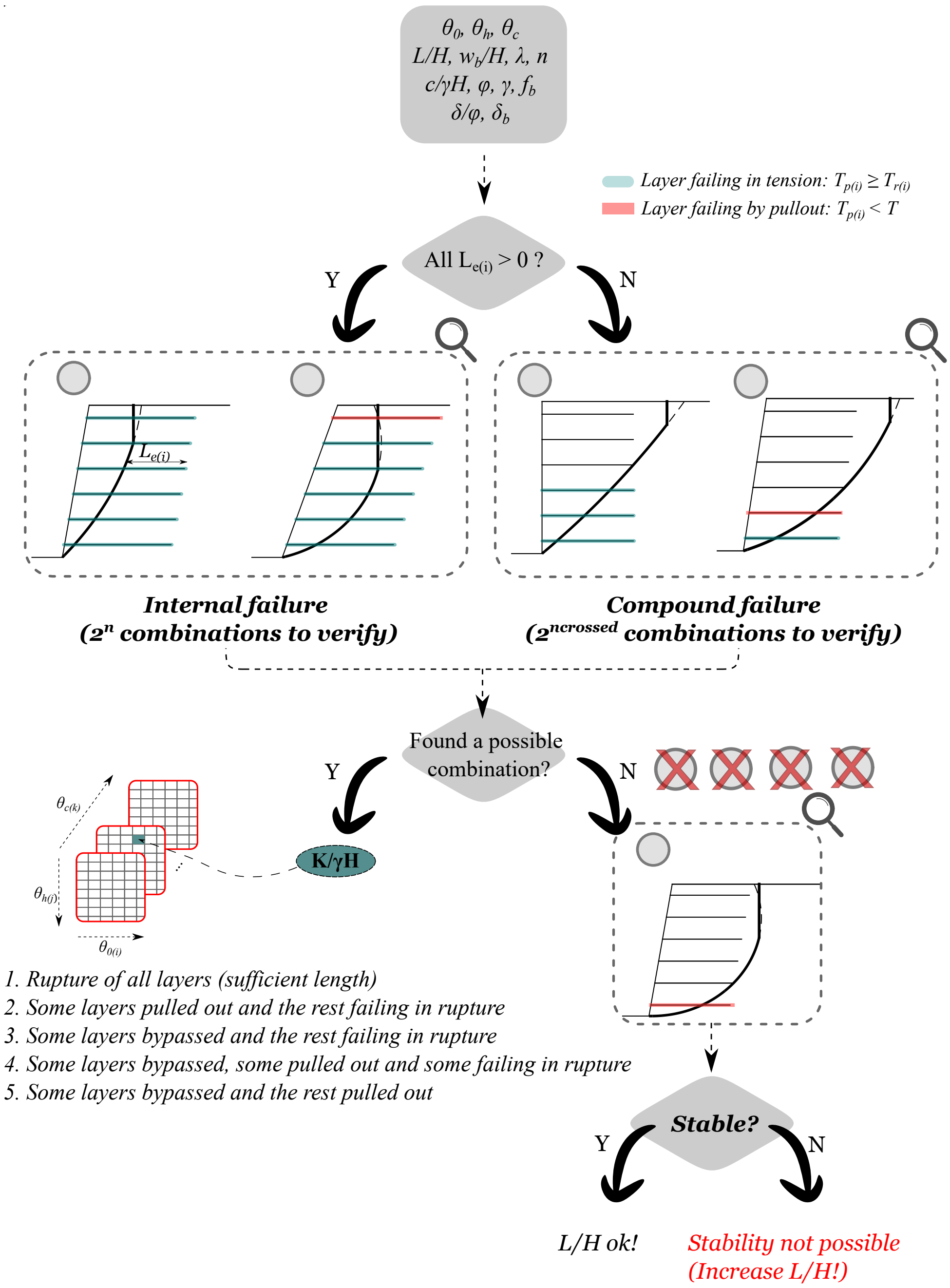

Figure 3.5: Failure modes considered

3.3.4 Failure mechanisms emerging at the wall facing

Note that due to tension cracks, potential failure mechanisms passing above the toe are no longer self-similar (UTILI, 2013) and therefore could in principle be critical. For this reason, Abd and Utili (2017) considered mechanisms daylighting above the toe for reinforced slopes in cohesive soils. In all the cases analysed the critical failure mechanism turned out to be the one passing at the toe. Here, the physics of the problem is different because of the stabilizing reaction force provided by the wall facing entering into the energy balance equation. The stability for mechanisms passing above the wall toe in this case will be a function of the presence of tension cracks, the interface friction between the facing blocks and the weight of the column of stacked blocks above the considered block-block interface intersected by the failure mechanism.

The values for inter-block friction may vary significantly since there is a range of block types commercially available (solid, with cores, with shear keys, etc., see Berg, Christopher, and Samtani (2009a) for examples) with different connection systems (HOLTZ; LEE, 2002a). BSI (2019) gives, for guidance, a minimum value of 0.4 for the coefficient of static friction at solid concrete-concrete interfaces, which is around 22°. Values in the range of 30° to 40° have been previously used in analytical and numerical analysis of reinforced soil walls (LESHCHINSKY; LESHCHINSKY; LESHCHINSKY, 2017; WU; PAYEUR, 2015). Hatami and Bathurst (2005) determined a value as large as 57° in laboratory shear tests for solid masonry concrete blocks with shear keys. Bathurst, Althoff, and Linnenbaum (2008) provide a set of results for interface shear behaviour of typical modular block units with varied interface shear transfer mechanisms and vertical loading arrangements. They found values ranging from 25° to 35° at 2% of block displacement and from around 30° to 40° in peak shear.

In cases where the geosynthetic connection to the wall face is achieved by friction (reinforcement placed between blocks), the reinforcement could also influence the block-block interface properties (LESHCHINSKY; LING; HANKS, 1995). Therefore, design values should be obtained from laboratory test results for the specific combination of facing blocks and geosynthetics to be used, for which standard methods can be found in ASTM D6916-18 (2018) and ASTM D6638-18 (2018).

In this thesis failure mechanisms emerging above the wall toe were considered for both UD and LID reinforcement distributions by discretising the wall facing for each block-block interface and calculating the minimum amount of required reinforcement associated to each mechanism. The equations are provided in Appendix C. Only reinforcement layers located above the failure mechanism exit point at the wall face were considered in the calculations (N' in Eq. C.4 of Appendix C).

For the results presented in Section 5 the number of blocks was assumed as twice the number of reinforcement layers, $N_b = 12$, with a block unit weight of 21.8 kN/m^3 and a block-block interface friction angle, δ_{bb}, of 38°. The critical failure mechanism remained passing through the wall toe for all the cases considered with $L/H = 0.7$ and $w_b/H > 0.05$, even with the presence of tension cracks, low soil friction angle and cohesion ($\phi = 15°$ and $c/\gamma H = 0.05$), thin block facing width ($w_b/H = 0.05$), vertical facing batter ($\beta = 90°$) and LID reinforcement distribution. An investigation of the effect of reducing the value of δ_{bb} was then performed and it was verified that instability in the region of the top blocks (above the top reinforcement) would only occur in the case of LID distribution for block-block friction angles below 17°, therefore it can be concluded the mechanism is not critical.

A case where mechanisms daylighting is critical was for UD reinforcement distribution, very thin block width ($w_b/H < 0.05$) and low soil friction angle and cohesion. In this case, the critical failure mechanism tends to daylight at the interface between the first and second wall blocks, from the wall toe, resulting in an increase in the needed reinforcement or Mode 5 type of failure (Figure 3.5). This is indicated in the results presented in Figure 4.5 of the next section. Increasing reinforcement density (here we used $N = 6$) would prevent this type of failure.

Note that the local stability of modular block facing walls should also be checked for connection failure, shear failure and crest toppling (NCMA, 2010). This last case refers to the local overturning failure of the top blocks in the unreinforced section of the structure, being particularly relevant for reinforcements distributed linearly along the wall height, in which reinforcement vertical spacings in the upper region of the wall are larger. The local facing stability checks are out of the scope of the paper.

4 Analytical Solution Results for the Design of Reinforced Cohesive Soil Walls

4.1 Method verification

Few studies have evaluated the influence of facing on the design of reinforced soil walls (ISMEIK; GULER, 1998; BAKER; KLEIN, 2004; LESHCHINSKY; ZHU; MEEHAN, 2010; XIE; LESHCHINSKY; YANG, 2016) and, to the best of our knowledge, none has considered the case of cohesive frictional backfills. Therefore, to validate the methodology developed herein (presented in Section 2.4) it was considered the example presented by Leshchinsky, Zhu, and Meehan (2010) for the case of cohesionless soils. The authors used a limit equilibrium approach assuming a log-spiral failure mechanism, accounting for the sliding resistance of the facing (toe resistance). The toe resistance was represented by the horizontal force acting at the wall toe (R_h in Figure 3.4), considered as an external force. The facing element was treated as part of the system (internal force) and thus no consideration of the location of the resultant lateral forces acting at the wall was required. Sufficient reinforcement length was considered so that all layers would fail in tensile rupture.

Leshchinsky, Zhu, and Meehan (2010) provided stability charts for prescribed values of R_h/nT that should be used in a trial-and-error process to obtain the required reinforcement strength. Therefore, the facing width is implicitly considered. To obtain comparable results, Eq. 3.17 should be re-written as a function of R_h/nT. The force sustained by the wall, P_f, can be represented as a function of the required reinforcement strength ($K_t/\gamma H$):

$$P_f = \frac{R_h}{\cos\delta_h} = \frac{\psi\left(\frac{K_t}{\gamma H}\right)\gamma H^2}{\cos\delta_h} \tag{4.1}$$

where $\psi = R_h/(nT)$.

Substitution of Eq. 4.1 into Eq. 3.17 gives:

$$\frac{K_t}{\gamma H} = \left[\frac{(f_1 - f_2 - f_3 - f_4 + f_5 + f_6 + r_u f_w)}{\left(\frac{H}{r_0}\right)(g_r)} - \left(\frac{c}{\gamma H}\right)\left(\frac{g_s}{g_r}\right)\right] \times \frac{1}{\left[1 + \left(\frac{H}{r_0}\right)\cdot\frac{\psi}{\cos\delta_h}\cdot\frac{f_7}{(g_r)}\right]} \tag{4.2}$$

The objective function in Eq. 4.2 considers a sufficient length for the reinforcement so

This chapter has been published in Géotechnique (see Franco, Utili, and Silva (2023)) all layers fail in tensile rupture. This expression was used to obtain $K_t/\gamma H$ for given values of ψ. Results obtained for $\phi = 30°$ are plotted in Figure 4.1 together with the results of Leshchinsky, Zhu, and Meehan (2010), for comparison. Curves for both UD and LID distributions are shown and, for consistency, the required reinforcement is represented as $2K_t/\gamma H$ in our calculation. The location of the force acting at the wall was assumed to be at one-third of the wall height ($D = H/3$). The chart in Figure 4.1 should be used iteratively, by first assuming a ψ value, then reading off the correspondent $K_t/\gamma H$ from the chart and finally verifying ψ by calculation of R_h:

$$R_h = R_v \tan \delta_{base} \tag{4.3}$$

where R_v is the normal force acting at the base of the facing (Figure 3.4).

Good agreement with the results of Leshchinsky, Zhu, and Meehan (2010) can be observed, with maximum differences not larger than 13% for UD distribution. In general, the minimum required reinforcement calculated with the extended formulation presented herein was slightly larger than the values reported by Leshchinsky, Zhu, and Meehan (2010), and therefore the difference is on the safe side. Nonetheless, smaller values were obtained for LID distribution and a vertical wall ($\beta = 90°$), since in Leshchinsky, Zhu, and Meehan (2010) UD and LID distributions gave the same results for$R_h/nT > 0$ and $\beta = 90°$.

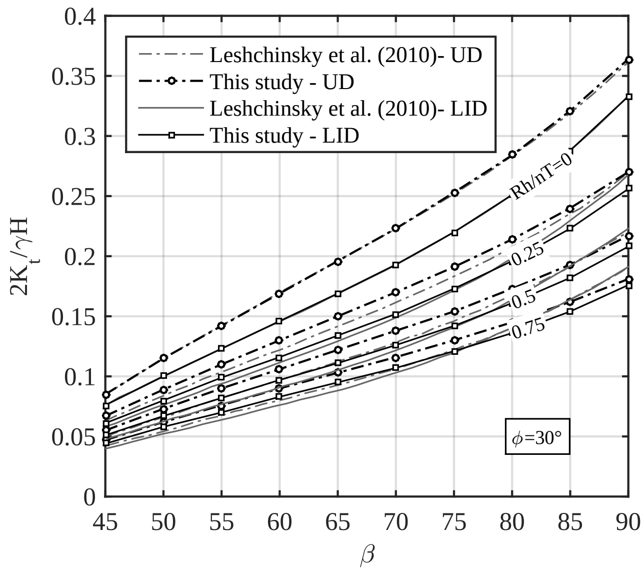

Figure 4.1: Comparison of required tensile strength in this study and in Leshchinsky, Zhu, and Meehan (2010) ($\phi = 30°$, $D = H/3$, modified force direction). $R_h$is the horizontal force at the wall toe as indicated in Figure 3.4.

4.2 Design charts

The formulation introduced here allows accounting for the influence of pore water pressure through the pore pressure coefficient r_u (BISHOP; MORGENSTERN, 1960), however for sake of simplicity the results presented here are for the case of drained soil ($r_u = 0$). The drainage system in reinforced soil walls with cohesive-frictional soils is particularly important since these materials present medium to low permeability that can cause the build-up of pore water pressure. Indeed, Koerner and Koerner (2018) have shown that faulty drainage in cohesive soils was a major cause of the wall failures investigated in their study. These arguments underline the critical importance of designing a suitable drainage system to keep the pore pressure within the prescribed values. Recommendations on drainage systems can be found in Koerner (2005) and Koerner and Koerner (2011), and in design guidelines such as in Berg, Christopher, and Samtani (2009a), NCMA (2010) and BSI (2010).

All the Matlab source codes developed are provided in Appendix D.

A parametric analysis was conducted to investigate the effect of the following parameters:

- normalized cohesion, $c/\gamma H$: 0.05 and 0.1;
- soil friction angle, ϕ: from 15° to 35°;
- facing batter, β: 70°, 80° and 90°;
- block width (toe to heel), w_b/H: 0, 0.05, 0.1, 0.15 and 0.25;
- location of the reaction force acting at the wall, D: $H/2$, $H/3$ and $H/4$;
- facing-backfill interface friction angle, δ/ϕ: 0, 1/3 and 2/3;
- facing-foundation interface friction angle, δ_b/ϕ: 0, 1/3 and 2/3;
- reinforcement length, L/H: 0.6, 0.7 and sufficiently long.

We selected the values for L/H based on recommendations of design standards for the minimum reinforcement length from Berg, Christopher, and Samtani (2009a), NCMA (2010), BSI (2010) and AASHTO (2017). It is common practice to adopt a minimum reinforcement length for reinforced soil structures around 70 percent of the structure's height. Design standards such as AASHTO, FHWA and BSI recommends $L \geq 0.7H$ with a minimum absolute length not less than 2.5 m for AASHTO (2017) and FHWA (ELIAS; CHRISTOPHER, 2001) and 3 m for BSI (2010). A minimum value of $0.6H$, not less than 1.2 m, is recommended by the private sector standard NCMA (2010) and by BSI for walls subjected to low thrust (but still with an absolute length not less than 3m).

The soil and facing block unit weights were set to 20 kN/m^3 and 21.8 kN/m^3, respectively. The number of layers $N = 6$, the bond coefficient between the soil and reinforcement $f_b = 0.5$, and the block-block interface friction $\delta_{bb} = 38°$ were kept the same in all analyses.

The results presented here are for the modified direction of the force acting at the wall, representative of a wall composed of stacked block units (Figure 3.4b). Charts for the conventional direction can be easily produced using $\delta_h = \delta + \beta - \pi/2$ in Eq. 3.16 and the substitution of f_7 related to the conventional direction given in Appendix B in the objective function to be optimized (Eq. 3.17, when a sufficient reinforcement length is assumed, or in Eq. 3.22, when a fixed length is given). In all analyses, for the calculation of the frictional capacity at the wall toe, both the wall weight and the vertical component of the interface friction between the reinforced soil and the wall facing were considered (Eq. 3.12).

For cohesive-frictional soils, we verified that Mode 1 (rupture of all layers) and Mode 4 (some layers bypassed, some pulled out and the rest failing in rupture) in Figure 3.5 were the more common modes of failure for the reinforcement lengths assumed ($L/H = 0.6$ and $L/H = 0.7$). Mode 3 (some layers bypassed and the rest failing in rupture) was not the critical mode of failure in any of the analyses with UD distribution carried out with $L/H = 0.7$. For $L/H = 0.6$ it was the critical mode in a few situations, mostly for large w_b/H and low ϕ. For LID distribution Mode 3 was critical for cases with $L/H = 0.7$ only with the lowest friction angle investigated ($\phi = 15°$), whereas for $L/H = 0.6$ more cases were detected.

Mode 5 (insufficient length) was critical and mostly not satisfied for the shorter length of $L/H = 0.6$ with UD distribution, and only for the lowest friction angle evaluated $\phi = 15°$ and $c/\gamma H = 0.05$, which means that the given length was too short and stability was not possible. Fewer cases were found not stable for LID distribution, restricted to $c/\gamma H = 0.05$, $\phi = 15°$, $L/H = 0.6$, $\beta = 70°$ and $w_b/H \leq 0.1$, as shown in Figure 4.2. In this case the failure surface crosses only the first reinforcement layer, closer to the wall toe.

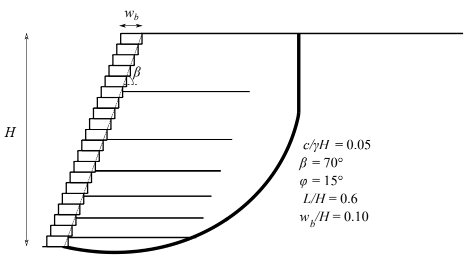

Figure 4.2: Case of unstable reinforced soil structure: predefined reinforcement length too short ($D = H/3$, modified force direction, LID distribution).

Michalowski (1997) found that for the case of non-cohesive reinforced soil slopes with significant pore water pressure the critical failure surface had the centre of rotation below the wall crest ($\theta_0 < 0$) and at some instances below the top reinforcement layer. When that is the case, the reinforcement layers above the failure surface centre of rotation ($\sin\theta_0 + z_i/r_0 < 0$) are subjected to compression and are likely to kink or buckle. Therefore, no energy is dissipated in those layers and the expression in Eq. 2.7 is reduced to the following expression, obtained by integration of the increment of the dissipation rate between 0 and θ_h:

$$\dot{D}_{r(B-D)} = \frac{1}{2} K_t \dot{\theta} r_0^2 \left\{ \exp\left[2\tan\phi\left(\theta_h - \theta_0\right)\right] \sin^2\theta_h \right\} \tag{4.4}$$

In this study, we found that compression of the top layers occurs in some particular cases and mostly for UD distribution. Figure 4.3 shows, for three wall facing batters and UD distribution, the required reinforcement strength obtained for the prescribed reinforcement lengths of $0.6H$ and $0.7H$. A set of curves calculated through Eq. 3.17 is also presented, in which case the length is assumed long enough so that all layers fail in tensile rupture. The blue 'x' markers on the charts indicate the points beyond which Mode 5 in Figure 3.5 becomes critical, indicating the need to increase the prescribed reinforcement length.

The curves in Figure 4.3 tend to converge as the soil angle of shearing resistance ϕ and the normalized cohesion $c/\gamma H$ increase. This means that for these cases and the given reinforcement length the analyses considering the possibility of combined failure leads to the same required reinforcement as the analyses that account only for the tensile rupture of all layers, approach adopted by Michalowski (1997).

By decreasing ϕ the curves begin to increasingly diverge, to such a point that the required reinforcement can be more than twice the value obtained for a sufficiently long reinforcement (Figure 4.4). This difference is more prominent for lower normalized cohesion (see curves for $c/\gamma H = 0.05$). The final choice then should consider the relative impact on the structure's cost of increasing the reinforcement length versus the reinforcement strength. Note that a longer reinforcement requires a larger volume of backfill, which will also have an impact on the structure's final cost. Similar results for LID distribution can be found in Appendix E, for which the required reinforcement is always less than the values obtained for UD distribution, as to be expected (ABD; UTILI, 2017; MICHALOWSKI, 1997).

The presence of tension cracks is more detrimental to stability especially for lower soil friction angles, larger cohesion and facing batter, as can be seen from the comparison of Figure 4.3a with Figure 4.3b and Figure 4.3c with Figure 4.3d, for a sufficiently long reinforcement. Adopting a predefined reinforcement length of $0.6H$ and $0.7H$, the influence of cracks becomes less pronounced (especially for $c/\gamma H = 0.05$).

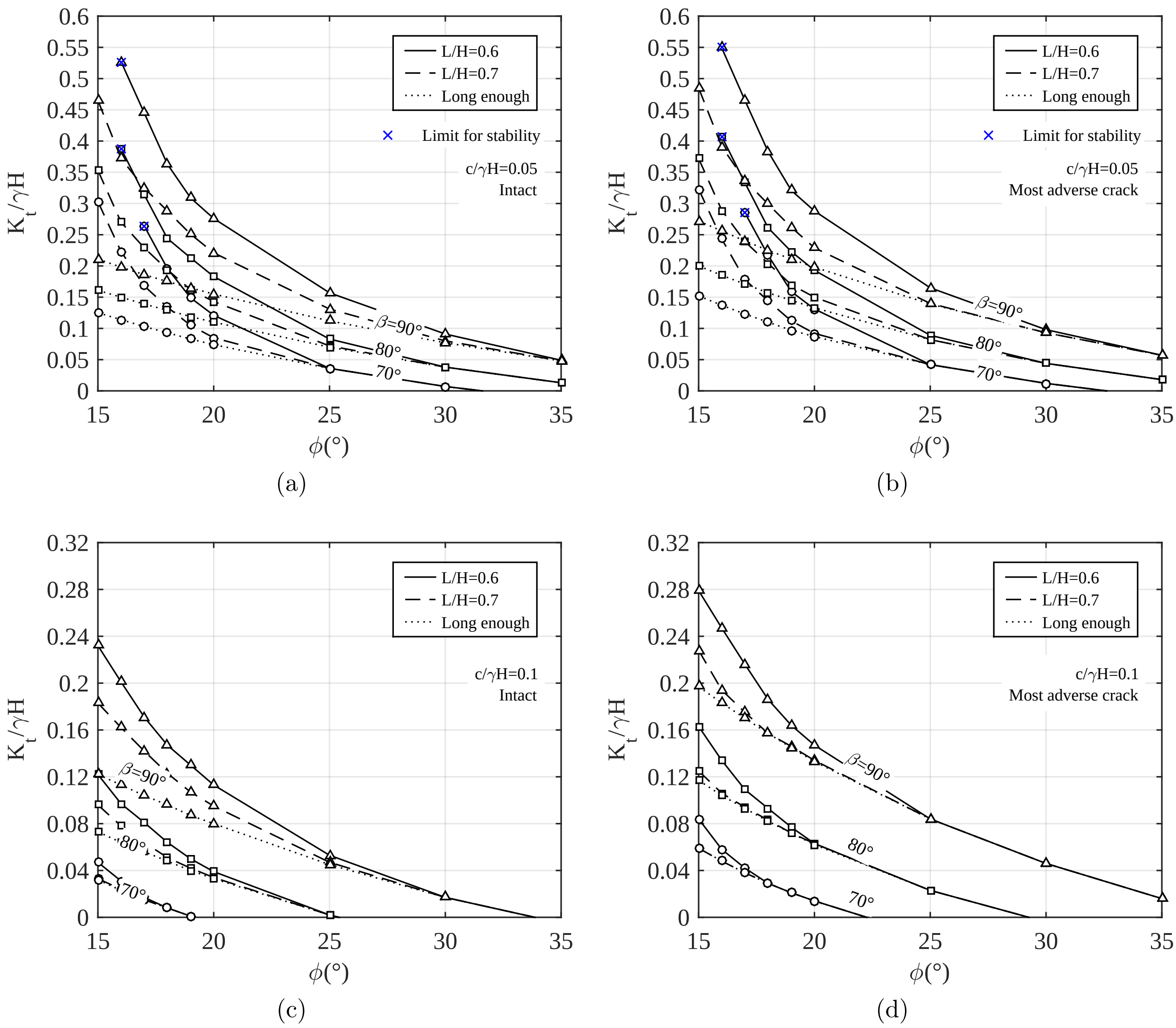

Figure 4.3: Required reinforcement versus wall facing batter β for different L/H (sufficient length for rupture of all layers, $0.6H$ and $0.7H$) ($w_b/H = 0.1$,$\delta = 2/3\phi$, $\delta_{base} = 15°$, $\delta_{bb} = 38°$, $D = H/3$, modified force direction, UD reinforcement distribution). (a) & (c) are for a reinforced soil wall in intact soil and in the presence of tension cracks for $c/\gamma H = 0.05$, respectively; while (b) & (d) are for $c/\gamma H = 0.1$. The most adverse crack to stability is considered. The blue 'x' markers indicate the limit for stability, beyond which the prescribed reinforcement length is not sufficient to provide stability.

Since $0.7H$ is a common reinforcement length used in design, the next charts to be presented were produced with this predefined value. Note however that for other lengths the required reinforcement strength will change, with the possibility to increase for smaller lengths and to decrease for longer reinforcements, as can be seen in Figure 4.4 for a vertical wall. For the next results, when not stated otherwise, normalized block width w_b/H was set as 0.1, the facing-reinforced fill interface friction δ as $2/3\phi$, the facing-foundation interface friction δ_{base} as 15°, and the location of the force acting at the wall at 1/3 of the wall height ($D = H/3$).

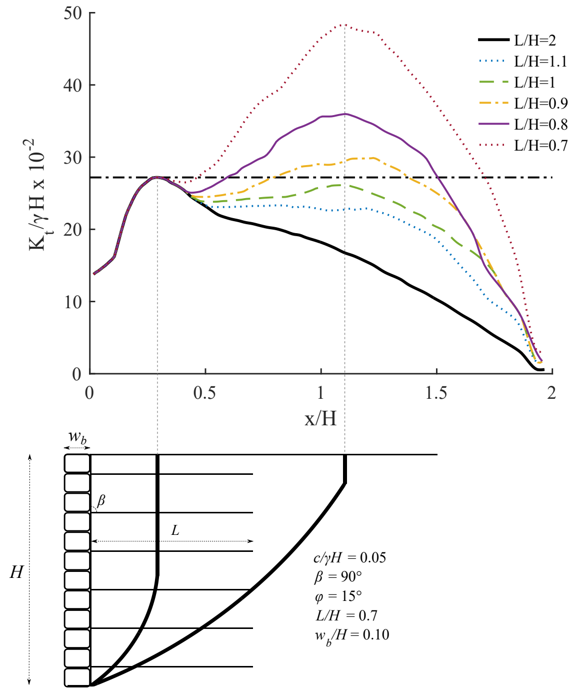

Figure 4.4: Comparison of required reinforcement strength for different values of L/H for a reinforced soil wall in the presence of tension cracks. The most adverse crack to stability is considered. ($\beta = 90°$, $w_b/H = 0.1$, $\delta = 2/3\phi$, $\delta_{base} = 15°$, $\delta_{bb} = 38°$, $D = H/3$, $c/\gamma H = 0.05$, $\phi = 15°$, modified force direction, UD reinforcement distribution).

The best lower bounds to the required reinforcement strength ($K_t/\gamma H$) for $L/H = 0.7$ were obtained by the maximization of the function in Eq. 3.21 and are shown in Figure 4.5 versus the normalized facing block width w_b/H. Commercial block units for reinforced soil walls are available in a range of dimensions that depend on the country. According to Berg, Christopher, and Samtani (2009a) the nominal front to back width for dry-stacked block facing typically ranges from 20 to 60 cm in the United States. In practice, this gives maximum values of w_b/H around 0.1. Indeed, typical normalized block widths from 0.03 to 0.1 have been reported in the literature for retaining wall applications (BATHURST et al., 1993; FISHMAN; DESAI; SOGGE, 1993; FARRAG; ABU-FARSAKH; MORVANT, 2004; RICCIO; EHRLICH; DIAS, 2014; ALLEN; BATHURST, 2014a,b; SALEM; HAMMAD; AMER, 2018). Therefore, values of w_b/H up to 0.1 in the charts in Figure 4.5 are considered to be representative of practical field values. Nevertheless, results for w_b/H up to 0.25 are here presented in order to evaluate the effect of a very thick facing, with the wall tending towards a gravitational structure.

From Figure 4.5 it can be observed that the facing element may provide a relevant contribution to wall stability, reducing the minimum required reinforcement in considerable amounts for lower soil friction angles. With wall thickness increasing, the mobilization of reinforcement loads decreases, with a smaller proportion of the soil load transferred to the reinforcement. In fact a larger block width implies a larger facing weight and frictional resistance at the wall/block base, which makes the facing element carry more load. However, it is worth mentioning that the designer should be careful in accounting for this contribution because it can be difficult to guarantee that the toe resistance will be present throughout all the life span of the structure. As in the previous charts, the impact of tension cracks is more significant for the higher cohesion (Figure 4.5c-d).

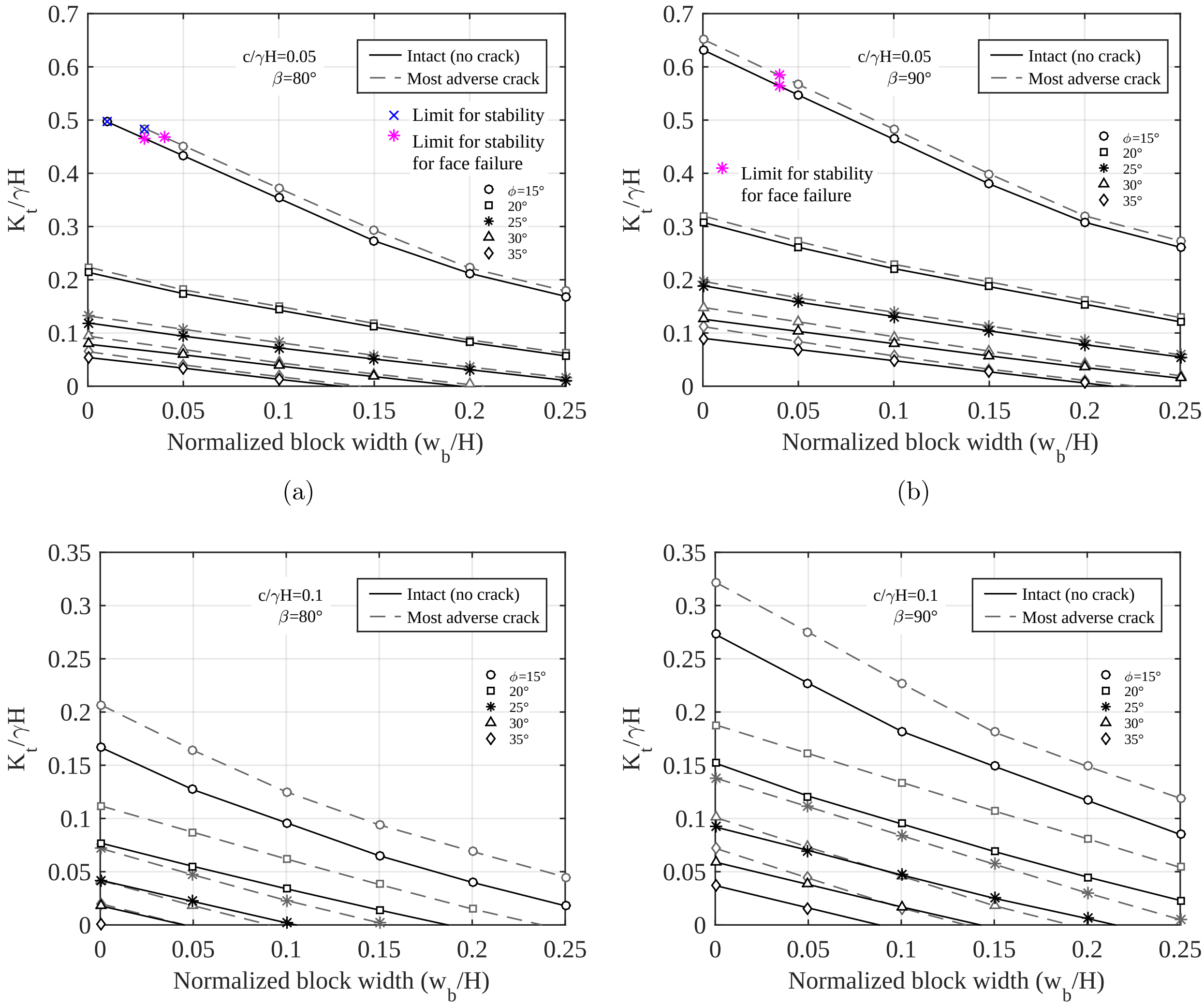

(a) (b)

(c) (d)

Figure 4.5: Required reinforcement versus w_b/H for a reinforced soil wall in intact soil and in the presence of tension cracks . The most adverse crack to stability is considered. (a) & (b) are for $c/\gamma H = 0.05$ and $\beta = 80°$ and $\beta = 90°$, respectively; while (c) & (d) are for $c/\gamma H = 0.1$ and $\beta = 80°$ and $\beta = 90°$, respectively. (δ =2/3ϕ, $\delta_{base} = 15°$, $\delta_{bb} = 38°$, $L/H = 0.7$, $D = H/3$, modified force direction, UD reinforcement distribution). The blue and pink 'x' markers indicate the limit for stability, for toe failure and failure surface emerging at the face, respectively, beyond which the prescribed reinforcement length is not sufficient to provide stability.

In Figure 4.6 the contribution of the horizontal toe resistance ($P_{f,h}$) relative to the soil horizontal thrust ($P_{f,h} + nT$) sustained by both the reinforcement and the facing element for $w_b/H = 0.1$ is illustrated. Results for UD (Fig 4.6a and Figure 4.6b) and LID

(Figure 4.6c and Figure 4.6d) reinforcement distributions are plotted, for $c/\gamma H = 0.05$ and $c/\gamma H = 0.1$. The facing lowest contributions, between 5% and 10% for UD distribution, and in the range of 10% and 20% for LID, are associated to the weaker soil ($\phi = 15°$ and $c/\gamma H = 0.05$), for which the load capacity of the wall is not sufficient to sustain the retained fill. In these cases, the stability is mostly relying on the reinforcement. By increasing the shear strength parameters of the soil (ϕ and $c/\gamma H$), the total thrust required to be sustained diminishes, and thus the load capacity of the facing becomes relatively more significant. For $\phi = 25°$ and $c/\gamma H = 0.05$, for example, the face carries around 20% of the load for a vertical wall and up to 50% for a wall batter of 70°. For a larger cohesion, $c/\gamma H = 0.1$, the relative contribution increases even further, with the influence of the wall batter and of the presence of cracks becoming more prominent: for vertical walls, the facing contribution situates around 25% - 43%, whereas for $\beta = 70°$ it reaches 100% regardless of reinforcement distribution or crack presence.

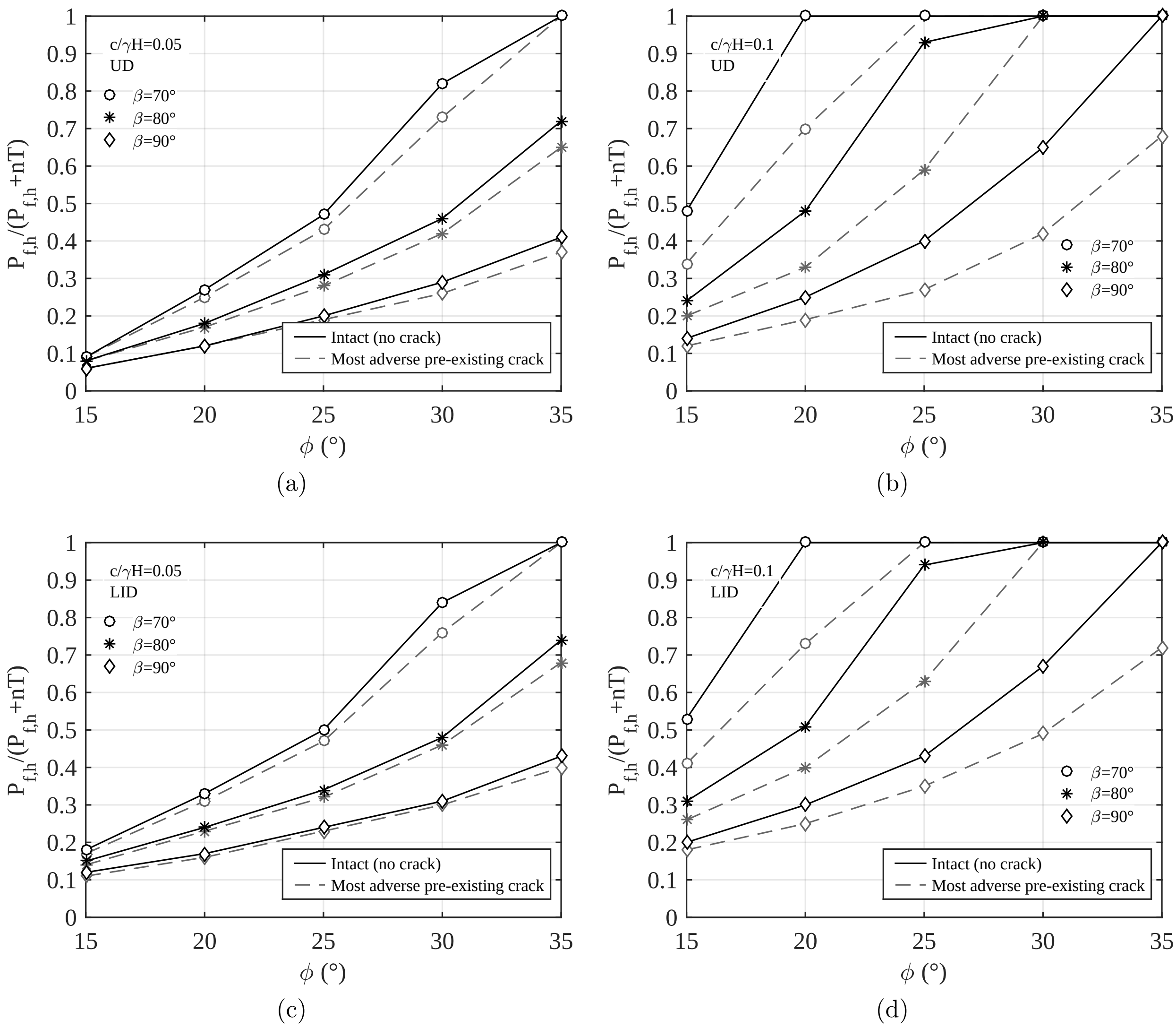

Figure 4.6: Relative horizontal toe resistance contribution $P_{f,h}/\left(P_{f,h}+nT\right)$ versus soil friction angle ϕ for a reinforced soil wall in intact soil (black lines) and in the presence of tension cracks (grey lines). The most adverse crack to stability is considered. ($\delta = 2/3\phi$, $\delta_{base} = 15°$, $\delta_{bb} = 38°$, $L/H = 0.7$, $D = H/3$, $w_b/H = 0.1$, modified force direction). $P_{f,h}$ is the horizontal component of P_f. (a) & (b) are for UD distribution, $c/\gamma H = 0.05$ and $c/\gamma H = 0.1$, respectively; while (c) & (d) are for LID distribution.

The effects of facing-backfill interface friction and foundation-block interface friction are investigated in Figure 4.7, with Figure 4.7a-b referring to $c/\gamma H = 0.05$ and Figure 4.7c-d to $c/\gamma H = 0.1$. The values were taken as 0, $1/3$ and $2/3$ and each combination of δ/ϕ and δ_b/ϕ is plotted in Figure 4.7. Two facing batters were considered: $\beta = 80°$ (Figure 4.7a-c) and $\beta = 90°$ (Figure 4.7b-d). For $c/\gamma H = 0.05$ the minimum required reinforcement, $K_t/\gamma H$, required in the presence of tension cracks ranges from 1 to 1.2 times the amount needed for intact soil, whereas for $c/\gamma H = 0.1$ it ranges from 1.2 to 3.2 times. Similar results were found for LID distribution and are shown in Appendix E (Figure D.3).

From Figure 4.7 it can be seen that the combined effect of facing-backfill interface friction and block-toe friction results in the most appreciable decrease in reinforcement loading. This stems from the vertical component of downdrag acting at the facing-backfill interface which results in an increased reaction/friction at the toe. For $\phi = 20°$, for example, going from $\delta/\phi = \delta_b/\phi = 2/3$ to $\delta/\phi = \delta_b/\phi = 0$ increases the amount of reinforcement required in 1.3 times for $c/\gamma H = 0.05$ and in 1.9 ($\beta = 80°$) and 1.5 times ($\beta = 90°$) for $c/\gamma H = 0.1$. By increasing the soil friction angle to $\phi = 30°$ the reduction in the required reinforcement is even more pronounced: for $c/\gamma H = 0.05$, by reducing δ/ϕ and δ_b/ϕ from $2/3$ to 0 the increase in the amount of reinforcement required is about 3.6 times for $\beta = 80°$ and about 2.1 times for $\beta = 90°$, while for $c/\gamma H = 0.1$ one goes from a situation where no reinforcement is needed to another where reinforcement is required.

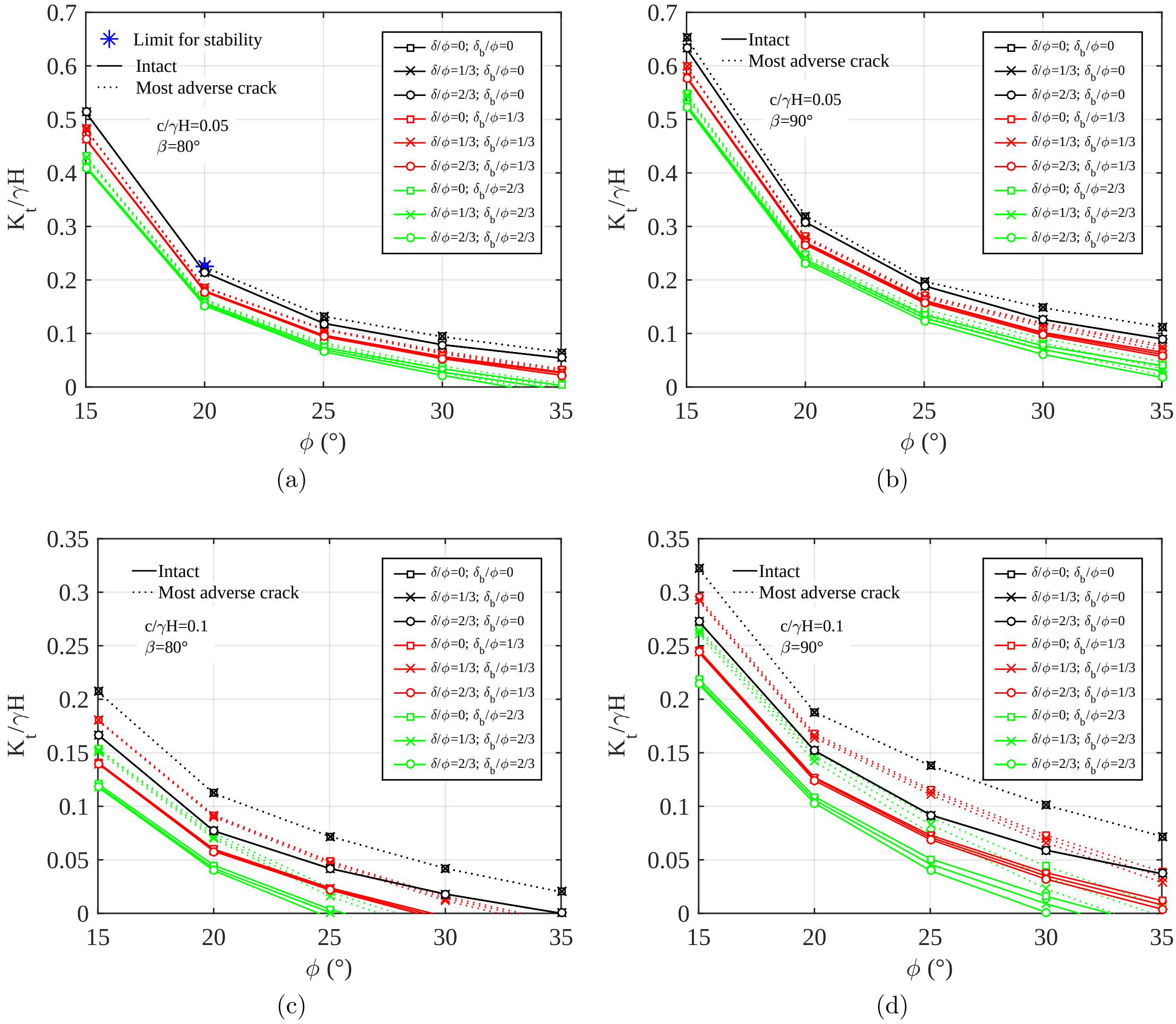

Figure 4.7: Effect of facing-backfill δ and foundation-block δ_{base} interface friction for a reinforced wall in intact soil (black lines) and in the presence of tension cracks (grey lines). The most adverse crack to stability is considered. ($L/H = 0.7$, $\delta_{bb} = 38°$, $w_b/H = 0.1$, $D = H/3$, modified force direction, UD reinforcement distribution). (a) & (b) are for $c/\gamma H = 0.05$, $\beta = 80°$ and $\beta = 90°$, respectively; while (c) & (d) are for $c/\gamma H = 0.1$. The blue 'x' markers indicate the limit for stability, beyond which the prescribed reinforcement length is not sufficient to provide stability.

For the previous analyses, we assumed the location of the force carried by the wall facing at one-third of the wall height ($D = H/3$). To investigate the sensitivity of the results on this assumption, other points of applications for the force were considered: at mid-height of the wall ($D = H/2$), at one-third of the wall height ($D = H/3$) and at a quarter of the wall height ($D = H/4$). Results for UD distribution are plotted in Figure 4.8 whilst the results for LID distribution are shown in Figure D.4 of Appendix E.

From Figure 4.8 emerges that the influence of the location, D, of the force stemming from the wall is significant only for large values of normalized cohesion ($c/\gamma H = 0.1$) and in the presence of tension cracks. For instance, for $\beta = 90°$, $c/\gamma H = 0.1$ and in the presence of tension cracks, for $\phi = 15°$ the facing carries around 12% of the load regardless of D, whereas for $\phi = 35°$ the facing contribution is around 70% for $D = H/4$ and $D = H/3$ and around 50% for $D = H/2$. Instead for $c/\gamma H = 0.05$ and in the presence of tension cracks D makes very little difference. The influence of D is less pronounced for LID distribution: for $\beta = 90°$, $c/\gamma H = 0.1$ and in the presence of tension cracks, around 17% of the load is carried by the facing when $\phi = 15°$, regardless of D, whereas the facing contribution for $\phi = 35°$ is around 70% for $D = H/4$ or $D = H/3$ and around 60% for $D = H/2$.

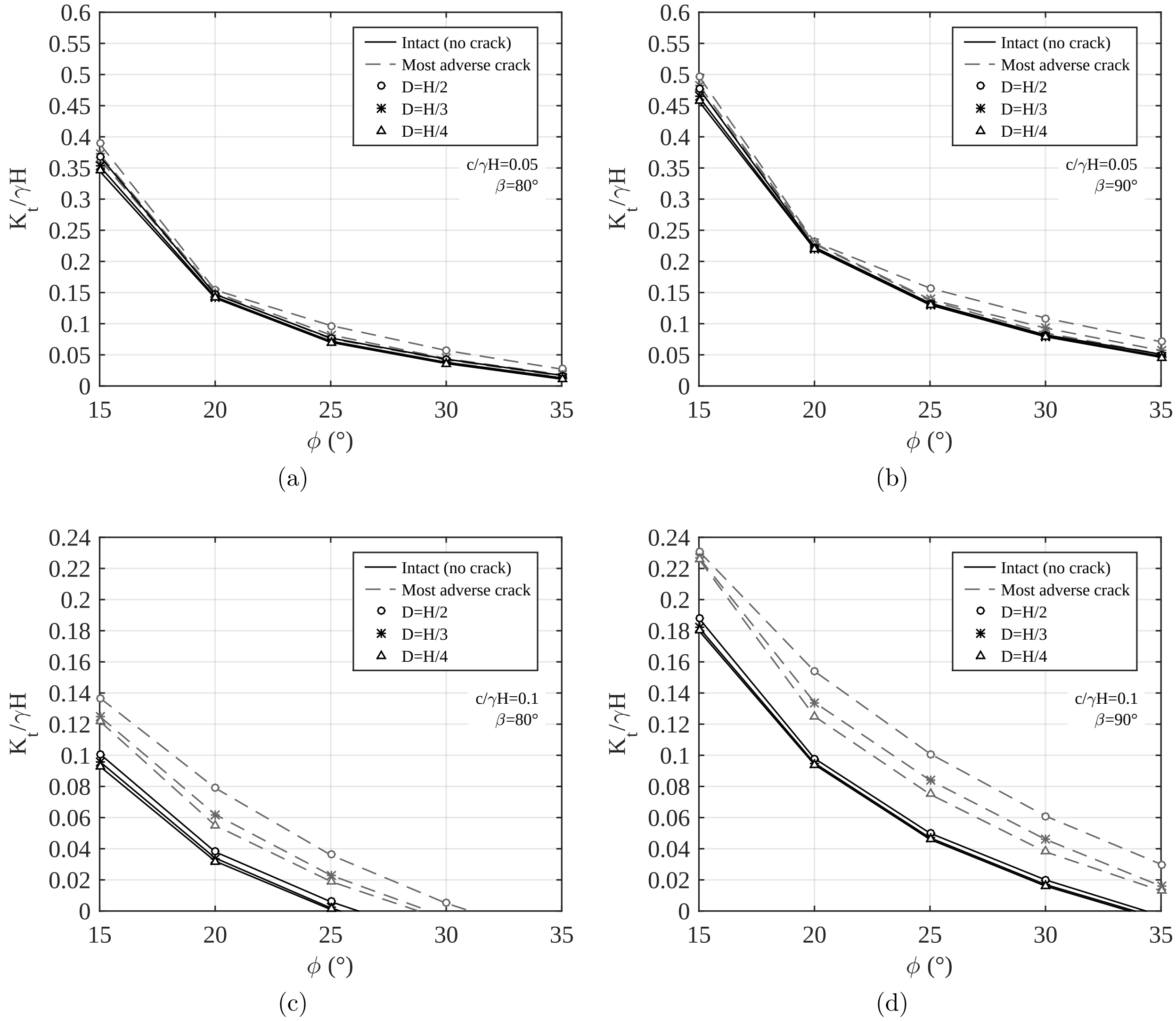

Figure 4.8: Effect of location of the reaction force acting at the facing (D) for a reinforced wall in intact soil (black lines) and in the presence of tension cracks (grey lines). The crack most adverse to stability is assumed. ($\phi = 20°$, $\delta = 2/3\phi$, $\delta_{base} = 15°$, $\delta_{bb} = 38°$, $L/H = 0.7$ and $w_b/H = 0.1$,modified force direction, UD reinforcement distribution). (a) & (b) are for $c/\gamma H = 0.05$, $\beta = 80°$ and $\beta = 90°$, respectively, while (c) & (d) are for $c/\gamma H = 0.1$, $\beta = 80°$ and $\beta = 90°$, respectively.

5 Experimental Program

5.1 Materials

5.1.1 General

The main materials used for the construction of the test wall in this research were:

1. Geosynthetic Reinforcement;

2. Backfill Soil;

3. Concrete Modular Block Facing Units.

The next sections describe in detail the characterization of each material.

5.1.2 Geosynthetic Reinforcement

The geosynthetic chosen as the reinforcement for the model wall in this study is a commercial polyester (PET) knitted geogrid, one of the weakest found in Brazilian market. The geogrid is called Fortrac 35T and was manufactured and made available by Huesker for this research. According to the supplier, this material shows high tenacity and low creep (strain-rate independent), being used primarily to soil reinforcement.

Table 5.1 summarises the geogrid geometric characteristics and its strength and deformability parameters, obtained from in-isolation wide-width tensile tests on specimens 200-mm wide (seven strands) and 300-mm long. The specimens were tested between roller clamps at a 10% strain/min rate at LabGsy Laboratory, in accordance with ASTM D6637-15 method of test (ASTM, 2015). The stress-strain response for the five samples tested is shown in Figure 5.1.

The reinforcement original aperture dimensions were 26 x 23 mm, measured in the laboratory. However, in an attempt to comply as much as possible with the scaling factors presented in Table 2.1 for the geosynthetic material, specially the ones concerning to the tensile strength-strain behaviour, it was used the technique adopted by Esfehani and Bathurst (2002) and Ezzein (2007) of cutting off two out of three longitudinal members of the material aiming to reduce its strength and stiffness. The end product was refereed as 'modified geogrid' (Figure 5.2) and its main parameters are presented in Table 5.2. It is worth noting that in this case there is not a perfect scaling-down for the geogrid material, since the requirements for frictional bond behaviour indicated by Viswanadham and König (2004), related to modelling rib cross-sectional area and opening sizes, are not achieved.

Direction	Parameter	Value (variation coefficient)
Longitudinal	Peak tensile strength, $T_{l,ult}$(kN/m)	26.8 (4.6%)
	Strain at peak, $\varepsilon_{l,peak}$(%)	8.4 (8.2%)
	Secant stiffness at 2% strain, $J_{l,2\%}$(kN/m)	360 (6.9%)
	Secant stiffness at 5% strain,$J_{l,5\%}$(kN/m)	308 (5%)
	Nominal longitudinal aperture, S_l(mm)	26
	Nominal longitudinal thickness,T_l(mm)	0.1
Transversal	Peak tensile strength,$T_{t,ult}$(kN/m)	18.9 (6.3%)
	Strain at peak,$\varepsilon_{t,peak}$(%)	9.0 (12.3%)
	Secant stiffness at 2% strain,$J_{t,2\%}$(kN/m)	270 (15.9 %)
	Secant stiffness at 5% strain,$J_{t,5\%}$(kN/m)	240 (9%)
	Nominal transversal aperture,S_t(mm)	23
	Nominal transversal thickness,T_t(mm)	0.05

Table 5.1: Geogrid Fortrac 35T original parameters (tested at 10% strain/min rate).

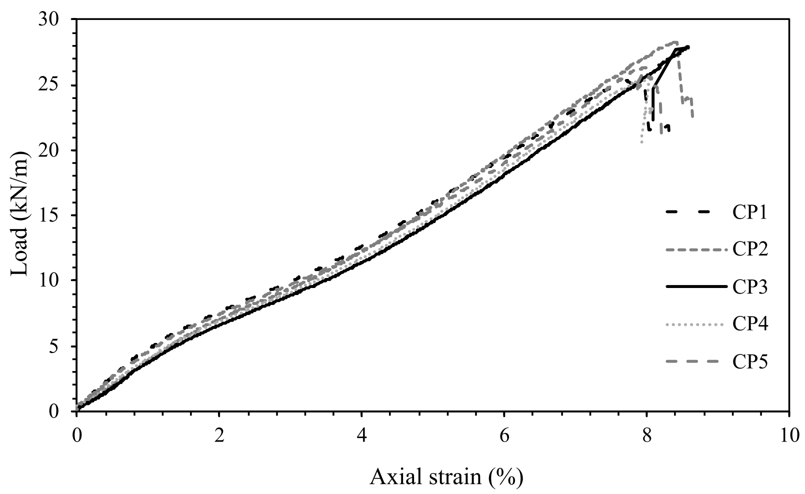

Figure 5.1: Load-strain curves from in-isolation wide-width strand tests at 10% strain per minute.

The 2%-strain tensile modulus of the model reinforcement (modified geogrid) was found to be 154.2 kN/m, which is equivalent to a stiffness of 2467.2 kN/m at prototype scale ($\lambda = 4$) from the scale factors shown in Table 2.1. The proper determination of reinforcement stiffness is of particular importance when converting reinforcement strain measurements to tensile load in physical modelling, supporting later numerical simulation calibration and parametric analysis (EZZEIN, 2007). All strains refereed to in this thesis are engineering strains.

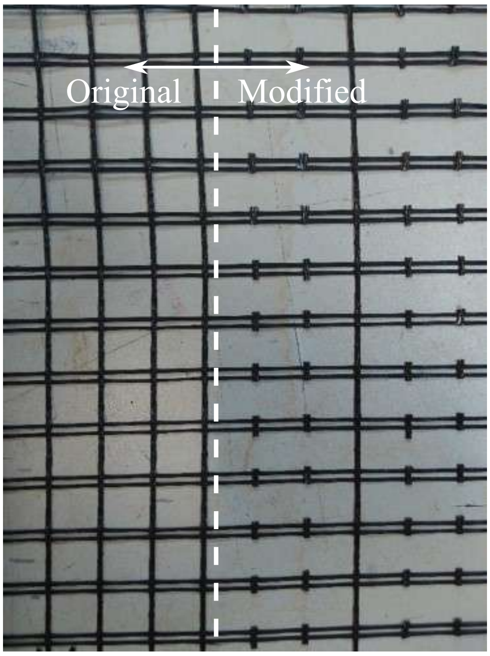

Figure 5.2: Geogrid Fortrac 35 T used in this research: at the left before trimming and at the right after trimming.

Parameter	Original geogrid	Modified geogrid
Aperture size (mm)	26x23	85x23
Peak tensile strength, $T_{l,ult}$(kN/m)	26.8	11.5
Secant stiffness at 2% strain,$J_{l,2\%}$(kN/m)	360	154.2
Secant stiffness at 5% strain,$J_{l,5\%}$(kN/m)	308	132

Table 5.2: Geogrid Fortrac 35T modified parameters for the longitudinal direction (used in the model walls).

5.1.3 Backfill Soil

The choice of the soil was based on the following considerations:

1. Past studies of soil/reinforcement interaction have focused mainly on coarse granular backfill materials, despite the common use of cohesive soils for reinforced soil structures construction in tropical regions such as Brazil;

2. The scaling law parameter for soil cohesion recommend by Iai (1989) and previously used in the studies of Esfehani and Bathurst (2002) sets a scale of $1/\lambda$ for soil cohesion, where λ is the prototype/model scale ratio. Therefore, is desirable that the fine-grained soil used for the model wall has a low cohesion so the correspondent soil cohesion for the prototype be compatible with common fine-grained soils used in field GRS-RW.

An extensive search on previous studies conducted in Brazil that employed cohesive soils from São Paulo state's countryside was carried on (CARMO, 1998; PATIAS, 2005; BENJAMIM, 2006; TAKEDA, 2006; PLÁCIDO, 2016; RINCÓN BARAJAS, 2016; KAKUDA, 2010; PORTELINHA, 2012). A total of 24 soils were first considered. Based on the above criteria and the distance from EESC/USP, the selected choices for preliminary testing were the soil from Campus II of USP at São Carlos-SP, Brazil, the same material used by Portelinha (2012), and the soil from highway Prof. Luis Augusto de Oliveira (SP 215), at km 170. This latter soil collection point was around 20 km ahead of the collection site of the soil used by Kakuda (2010).

The compaction curves for the candidate soils tested, obtained with Standard Proctor Tests (ASTM, 2012), are shown in Figure 5.3. At the same figure the curves for other soils from the area studied by previous authors are shown (CARMO, 1998; RINCÓN BARAJAS, 2016; KAKUDA, 2010). The maximum dry unit weights and optimum moisture contents obtained are shown in Table 5.3.

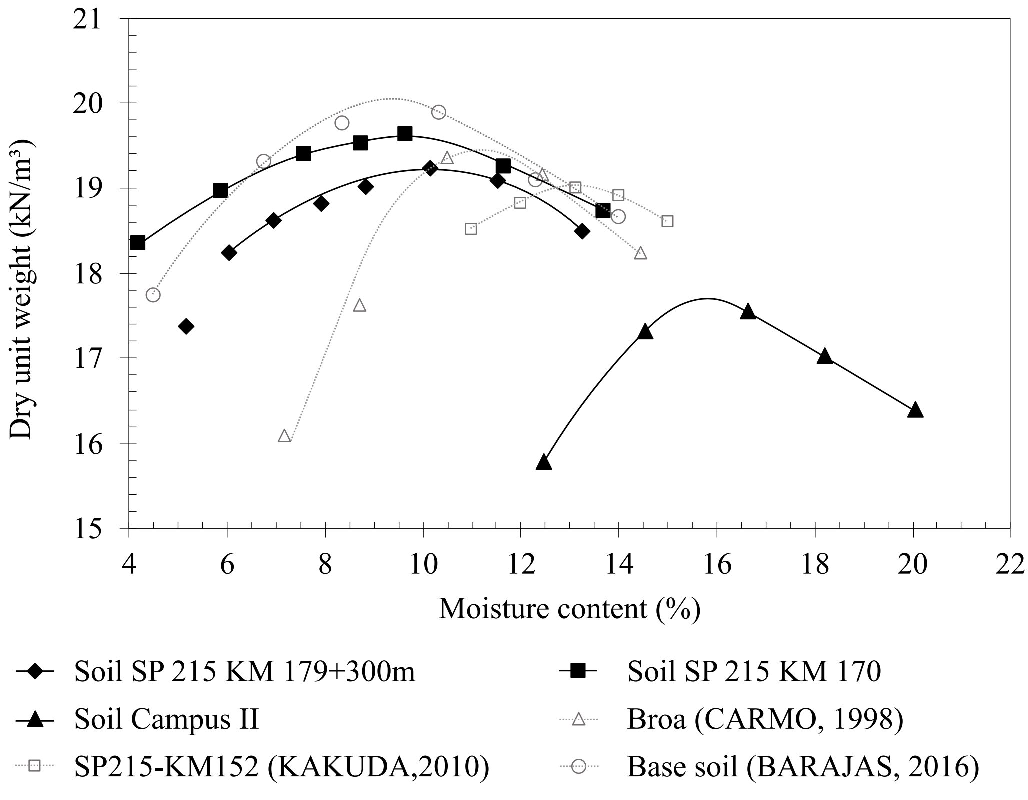

Figure 5.3: Compaction curves for the tested soils (SP 215 KM 170, and Campus II) and for other soils near São Carlos-SP, Brazil, used in previous researches.

Soil	$\gamma_{d,max}(kN/m^3)$	$w_{ot}(\%)$
SP 215 KM 170	19.6	9.38
Campus II	17.7	15.70

Table 5.3: Compaction test results for the soils evaluated (Standard Proctor Test)

The strength parameters were first investigated for Campus II soil, a material of interest specially due to its availability and proximity to the Geosynthetic Laboratory in

EESC/USP. Consolidated drained (CD) triaxial compression tests were performed on saturated soil specimens compacted at optimum water content and with compaction degree of 95%. Confining pressures ranging from 25kPa to 200 kPa were used. The samples were tested at EESC geotechnics laboratory.

The test specimens were prepared with a height of 110 mm and a diameter of 50 mm, resulting in a height/diameter ratio of 2.2, in the range of 2 to 2.5 recommended by ASTM-D7181 (ASTM, 2020). A displacement rate of 0.04 mm/min was used for the samples compacted with 95% degree of compaction. The saturation of each specimen was performed by increments of back pressure according to the procedures recommended by Head and Epps (2014) until the pore pressure parameter B reached a value equal or bigger than 0.95. From the test results, cohesion values for Campus II Soil situated around 29 kPa (Table 5.4). The stress x strain curves are shown in Figure 5.4.The cohesion value obtained was found to be higher than the desirable range needed to reflect a realistic cohesion intercept for the prototype wall. For this reason Campus II soil was considered not appropriate for the present study.

Soil SP 215 KM 170 was then further investigated by consolidated drained (CD) triaxial compression tests. These were carried out in a third partie laboratory, the Mauá Institute of Technology Laboratory, due to COVID restrictions on using EESC facilities. The tests were carried out in accordance with test method ASTM D7181 (ASTM, 2020), at 95% degree of compaction and at optimum moisture content, with specimens moulded in a cylindrical test apparatus 110 mm-long and 50 mm-diameter. Three tests were carried out, at confining stresses of 25 kPa, 50 kPa and 100 kPa and with the samples being sheared after complete saturation, at a shear displacement rate of 0.02 mm/min.

The load x strain curves obtained in the triaxial compression tests for soil SP 215 KM 170 are depicted in Figure 5.5, while the strength parameters obtained from linear regression of $s'xt'$ data are presented in Table 5.4 along with the results obtained for Campus II soil.

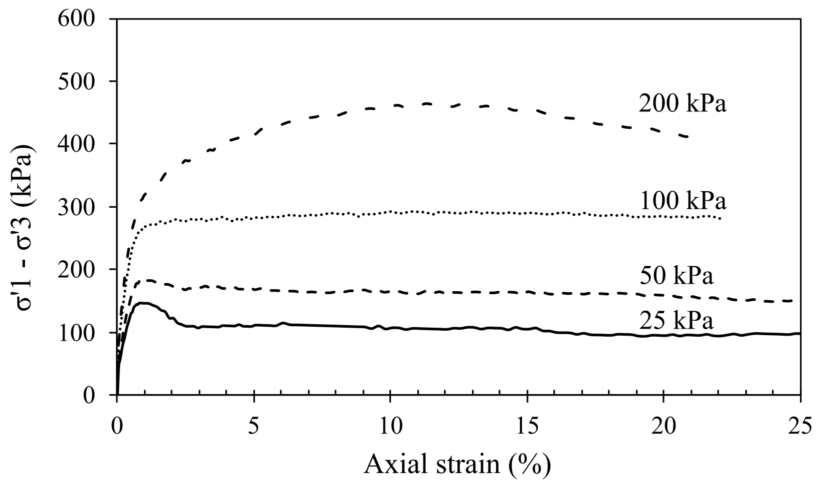

Figure 5.4: Triaxial compression test results for Campus II soil: 95% degree of compaction (EESC geotechnical laboratory).

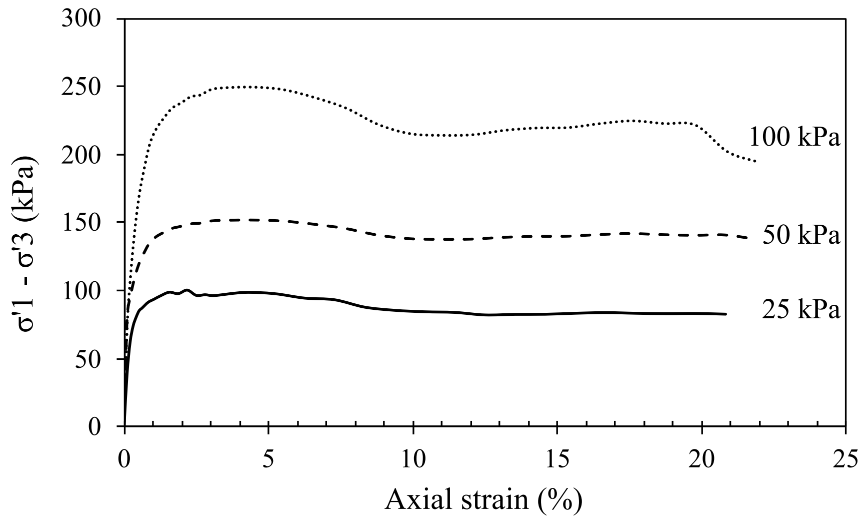

Figure 5.5: Triaxial compression test results for SP 215-KM170 soil, with 95% degree of compaction (Mauá Institute of Technology Laboratory Laboratory).

Soil	c(kPa)	$\varphi(°)$	R^2
SP 215 KM 170	14.8	29.9	1.000
Campus II	29.0	28.6	0.9997

Table 5.4: CD triaxial compression tests results: strength parameters for with 95% degree of compaction.

From Table 5.4 it can been seen that soil SP 215-KM170 presents the lowest cohesion intercept between the soil candidates tested. From the review of studies that used soils close to São Carlos city it was not found a better soil candidate to comply with the soil requirements summarized at the beginning of the present section. Therefore, soil SP 215-KM170 was chosen as the backfill soil for the model wall of the current study.

SP 215-KM170 soil is a frictional-cohesive material obtained from a road cut at highway Prof. Luis Augusto de Oliveira (SP 215), between the cities of São Carlos-SP and Ribeirão Bonito-SP, in Brazil (Figure 5.6). Prior to soil collection it was issued a permit from the Department of Highways of the State of São Paulo (DER-SP) for the removal of 10 m^3 of soil from the region specified (Figure 5.6). The material was stored at two soil bays at EESC's Geosynthetics Laboratory, close to the model wall test set-up room.

(a)

(b)

Figure 5.6: Soil collection point: (a) view of SP 215 at KM 170; (b) detail of area of soil collection in a cut in natural ground next to the highway.

The backfill soil particle size distribution is shown in Figure 5.7. The material is classified as a sandy clay (SC) according to the Unified Soil Classification System (USCS) with 14.6% fine content (i.e. passing sieve no. 200) . The soil SP 215-KM170 is classified as non-lateritic sand (NA) according to the MCT (Miniature, Compacted, Tropical) classification for fine-grained soils (NOGAMI; VILLIBOR, 1981). Note that, it was not possible to find a lateritic soil with low cohesion, as needed for this research, in a viable distance from LabGsy Laboratory. For this reason soil SP 215-KM170 was chosen even thought it is not lateritic.

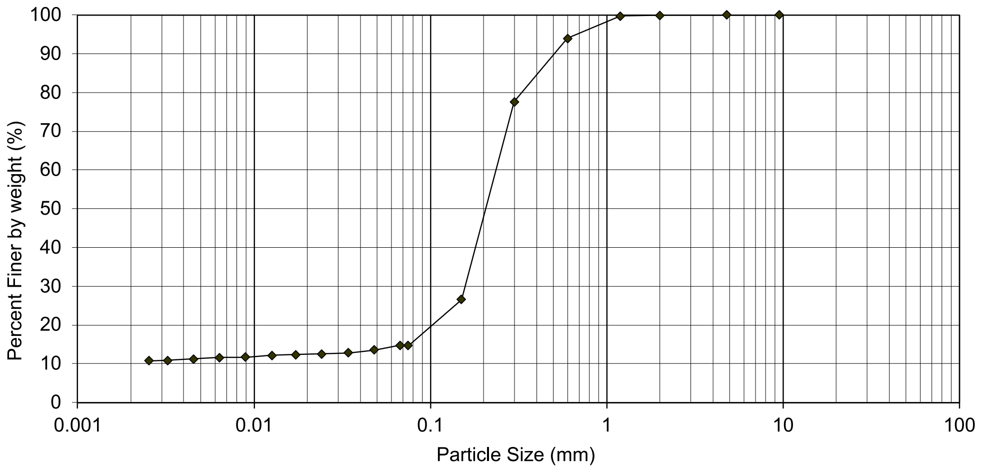

Figure 5.7: Particle size distribution for SP215-KM170 soil.

5.1.4 Concrete Modular Block Facing Units

For the model wall facing it was selected a modular block type to simulate a segmental retaining wall, similar to the one used by Burgess (1999) and Gregg (2008) in large-scale model walls tested in their studies. However, since there was not commercial blocks available with the dimensions needed for the model wall, the reduced-scale concrete units were specially manufactured for this research, with 140-mm in length, 150-mm in width (toe to heel) and 70-mm in height, and with a mass around 3.5 kg each. The blocks were design with a top shear key 10-mm high and 30-mm width and a corresponding slot at the bottom so when stacked, the model blocks would have an overall batter of 8 ° (Figure 5.8). These dimensions are representative of a prototype facing unit of 560 mm long x 600 mm wide x 280 mm high, that is slightly larger than the ones used in the construction of GRS walls in Brazil.

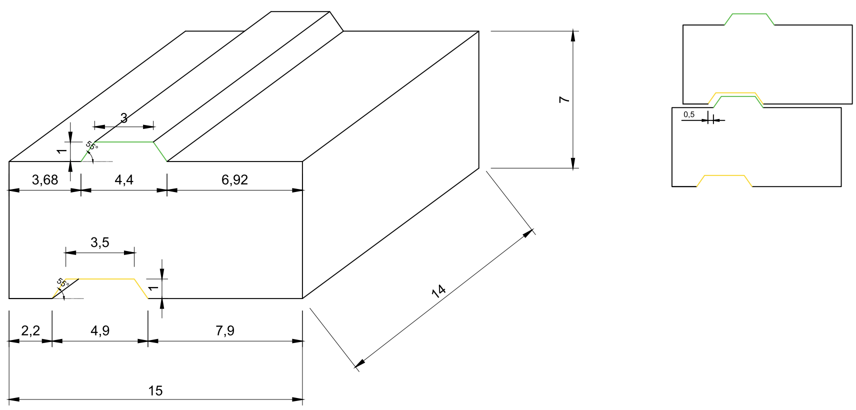

Figure 5.8: Facing block unit layout (dimensions in cm).

Note that in Brazil it is usually adopted hollow concrete units, rather than solid blocks as the ones applied in this research. The choice for a solid and simpler block aimed to simplify block placement during wall construction and to reduce block-block interaction complexness in order to facilitate interpretation of block-block interface parameters to use in future numeric simulation.

Corner blocks were fabricated with half of the length of the main block in order to allow a staggered (running joint) pattern for the wall facing. A total of 199 blocks of the main type and 22 corner block units were used for the construction of the model wall (Figure 5.9).

(a) (b)

Figure 5.9: Reduced-scale modular block facing units: a) manufacturing process; b) block cure; c) block storage at LabGsy laboratory.

The average unit weight of the fabricated concrete blocks was determined by weighting a sample block and determining its immersed volume by the hydrostatic balance method (Figure 5.10). First the block mass was taken and registered. Then the block was coated with a thin layer of paraffin wax in order to cover all of its pores and prevent water to penetrate into it. The coated block was mounted in a steel frame to allow connection to the hydrostatic balance set-up and the mass of the block + paraffin + steel frame set was taken. Finally, the coated block, connected to the hydrostatic balance set-up, was submerged in a bucket full of water to get its submerged mass. The unit weight of the block obtained was of 20.05 kN/m^3, close to the values for concrete blocks used in previous numerical studies (GULER; HAMDERI; DEMIRKAN, 2007; MIRMORADI; EHRLICH, 2017, 2018).

(a) (b) (c)

Figure 5.10: Determination of the unit weight of the modular block used in this research: (a) modular block coated with paraffin wax; (b) front view of the hydrostatic balance apparatus mounted, with the block submerged; (c) side view of the hydrostatic balance apparatus mounted.

5.1.5 Summary of prototype and reduced scale model parameters used

Table 5.5 summarizes the model parameters used in this research and its correspondent parameters for prototype scale, considering a scale factor (λ) of 4.

Parameter	Symbol	Scale factor (1g model)	Model	Prototype
Scale	λ	-	1/4	1
Wall height (m)	H	$1/\lambda$	1.47	5.88
Gravity	g	1	1g	1g
Soil unit weight, for a compaction degree of 95% (kN/m^3)	γ	1	21.7	21.7
Friction angle (deg)	φ	1	29.9	29.9
Cohesion (kPa)	c	$1/\lambda$	14.8	59.2
Normalized cohesion	$^{c}/_{\gamma H}$	1	0.46	0.46
Reinforcement peak tensile strength (kN/m)	T_{ult}	$1/\lambda^2$	11.5	184
Reinforcement stiffness at 2% strain (kN/m)	$J_{2\%}$	$1/\lambda^2$	154	2464
Reinforcement stiffness at 5% strain (kN/m)	$J_{5\%}$	$1/\lambda^2$	132	2112
Facing block width – toe to heel (cm)	w_b	$1/\lambda$	15	60
Normalized block width	$^{w_b}/_{H}$	1	0.1	0.1
Facing block height (cm)	h_b	$1/\lambda$	7	28
Facing block depth (cm)	d_b	$1/\lambda$	14	56

Table 5.5: Scalling parameters for the 1-g reduced scale model wall tested in the present study.

5.2 LabGsy Retaining Wall Test Facility

5.2.1 General

This chapter details the testing wall facility and instrumentation program used in this research, including the manufacturing of some of the instruments that were in-house made. A total of 75 automated sensors, 35 manual extensometers and 55 manual survey points were used to monitor the model wall during construction and surcharge. Detail of instrument construction, when applicable, calibration and placement are discussed, as well as a brief overview of the acquisition systems used.

5.2.2 Overview of the LabGsy Retaining Wall Test Facility

The LabGsy Retaining Wall Test Facility is a reduced-scale steel rigid box comprised of four walls and four pillars anchored at a concrete reaction floor, originally designed and built by Viana (2003) to support a maximum vertical stress of 200 kPa with minimal wall deflection. The multiple purpose test apparatus is 1.8-m long, 1.42-m wide and 1.8-m high (inner dimensions), with capacity to contain up to 5 m^3 of backfill material.

The testing box has been used in previous researches in LabGsy laboratory related to buried pipe behaviour (VIANA, 2003), geosynthetic reinforced pavement behaviour (CORREIA, 2014; PEDROSO, 2021) and geotextile wrapped facing retaining wall behaviour under moisture variation (PORTELINHA, 2012). For this last case and for the present research, in order to create space for the wall facing construction, one of the side walls of the test box was dismounted with the aid of a 2-ton capacity overhead crane (Figure 5.11).

Figure 5.11: Removal of the front wall of the test box.

5.2.3 Wall Test Facility Adjustments and Preliminary Tests

5.2.3.1 Front support beam

Due to the removal of the front box wall (Figure 5.11) a top reaction beam was needed to support the box lid and to promote force distribution towards the box's pillars. The beam was adapted from an existent one available at LabGsy laboratory that was probably the one used by Portelinha (2012). The beam ends were soldered in L-shaped steel brackets fixated to the box front pillars with steel screws (Figure 5.12).

Figure 5.12: Steel front support beam bolted to the front box pillars.

5.2.3.2 Box lid surcharge test

The box lid comprises of three separate pieces aiming to facilitate its handling (5.13a). However, two pieces of the box lid were somewhat warped, possibly due to excessive overload in previous uses. This was diminished by fixing tightly the lid screws with a pneumatic impact screwdriver, leaving a maximum final gap around 1.5 cm (Figure 5.13b). Even so, it was not possible to use fixation screws to connect the pieces of the top lid with each other, which could compromise forces distribution to the reaction floor and even the pressure distribution over the soil. It was considered to manufacture a new lid, however the costs involved could not be met at the time of the research.

To test for a possible non-uniformity in pressure distribution under the surcharge system it was conducted three preliminary surcharge tests, filling the test box with clean sand and placing five soil pressure cells on the top surface of the backfill sand, right under the surcharge system (Figure 5.14). It was used three 30-mm diameter diaphragm cell of the model KYOWA BE-2KC (CT-01, CT-02 and CT-03 in Figure 5.14a) and two 200-mm diameter confined fluid cells, specially manufactured for this research (SPC-01 and SPC-02 in Figure 5.14a). Surcharge steps of 50, 100 and 150 kPa were applied and maintained over a period of time to check readings stability. Four arrangements were tested: tests A and B were identical to check repeatability, with all the pressure cells buried under a thin layer of sand (∼20-cm thick); test C used the same layout as tests A and B but with the cells in direct contact with the surcharge airbag; test D was similar to test C, but with exchanging of cells SPC-01 and SPC-02 locations, since the front position is placed under a region of possible lower confinement due to the warped lid central piece.

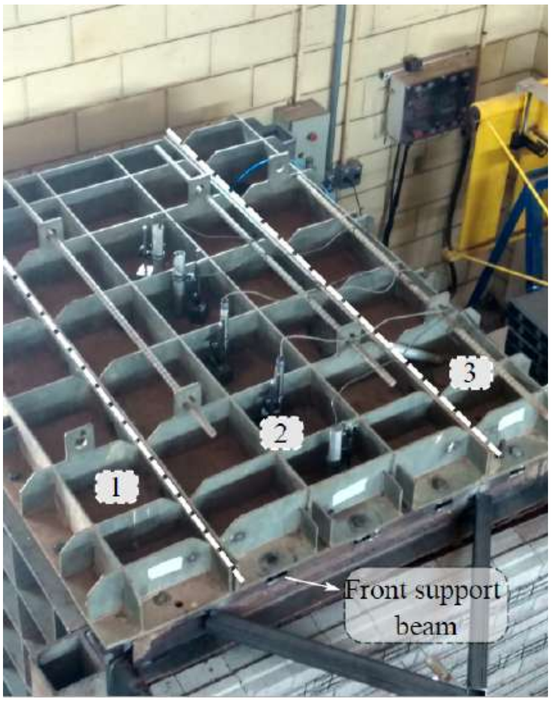

(a)

(b)

Figure 5.13: Detail of the test box three-piece reaction lid: (a) top view with the support beam; (b) front view before removal of the front wall, with detail of warped pieces (left and centre pieces).

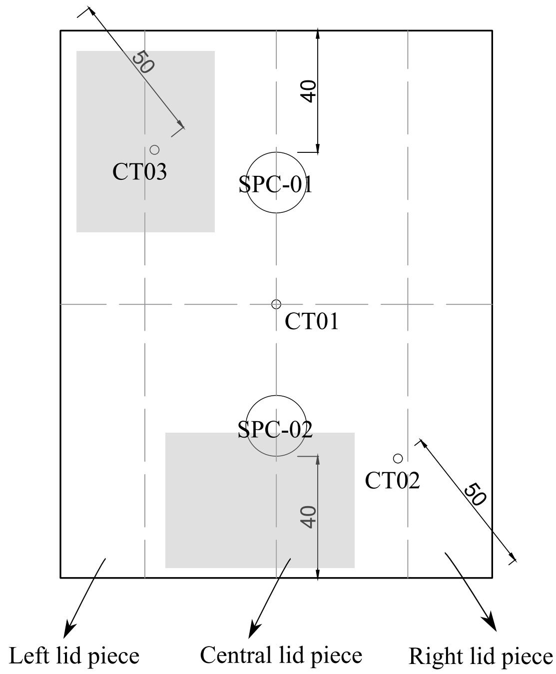

(a)

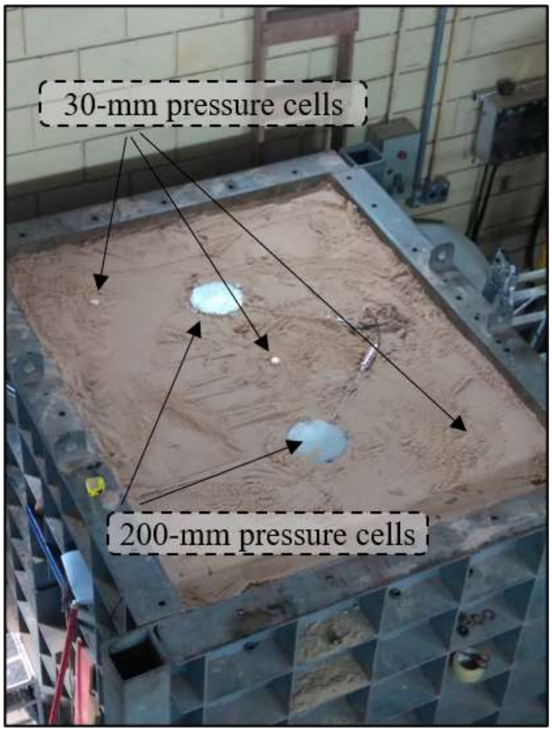

(b)

Figure 5.14: Detail of pressure cells layout for the surcharge test: (a) layout used for Test D; (b) top view of the pressure cells in-place. (grey areas indicates regions with possible lower confinement).

The plots in Figure 5.15 show the results obtained for each test, with cell readings in mV/V being converted to kPa by applying the calibration factor obtained within fluid and given by the manufacturer (800 kPa/mV/V for KYOWA cells and 0.04 kPa/mV for the larger cells). The results show a systematic underestimation of vertical stress for the larger cells, which puts in question the calibration factor given by the manufacturer. An adjusted factor of 0.067 kPa/mV, which accounts for a maximum output voltage of 3V instead of 5V, seems to be the correct one, as depicted by the plots in Figure 5.16, specially the ones correspondent to Test C and D, in which the pressure cells were in direct contact with the surcharge airbags.

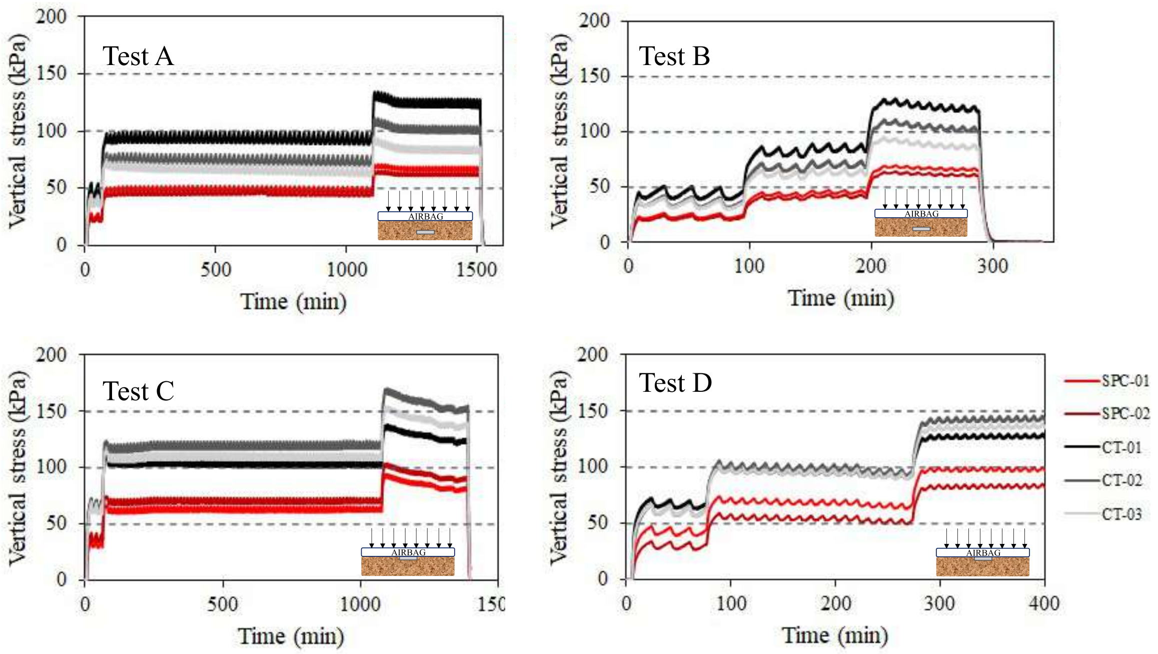

Figure 5.15: Results for the surcharge test conducted with backfill sand (cell calibration factors: 800 kPa/mV/V for CT-01, CT-02 and CT-03 and 0.04 kPa/mV for SPC-01 and SPC-02). Dashed horizontal lines represent the surcharge levels applied. (Test A and B are the same, with pressure cell buried in soil; Test C with cell in direct contact with airbag and SPC-01 at the front; Test D with cell in direct contact with airbag and SPC-02 at the front).

It is clear the effect of stress redistribution when the cells are buried in the backfill sand (Tests A and B), with the cells registering a lower pressure than the one applied in the system (Figure 5.15 and Figure 5.16). As expected, the cell located at the box central longitudinal axis at the front registered a slightly smaller pressure than the correspondent one located at the back (SPC-01 in Test C and SPC-02 in Test D) due to the warped lid piece. By taking the medium value of the measurements registered by the cells SPC-01 and SPC-02 at each surcharge step and comparing then it is possible to quantify the non-uniformity of vertical stresses, as shown in Table 5.6. The difference diminishes as increasing the surcharge applied, with the maximum difference observed in Test D for a

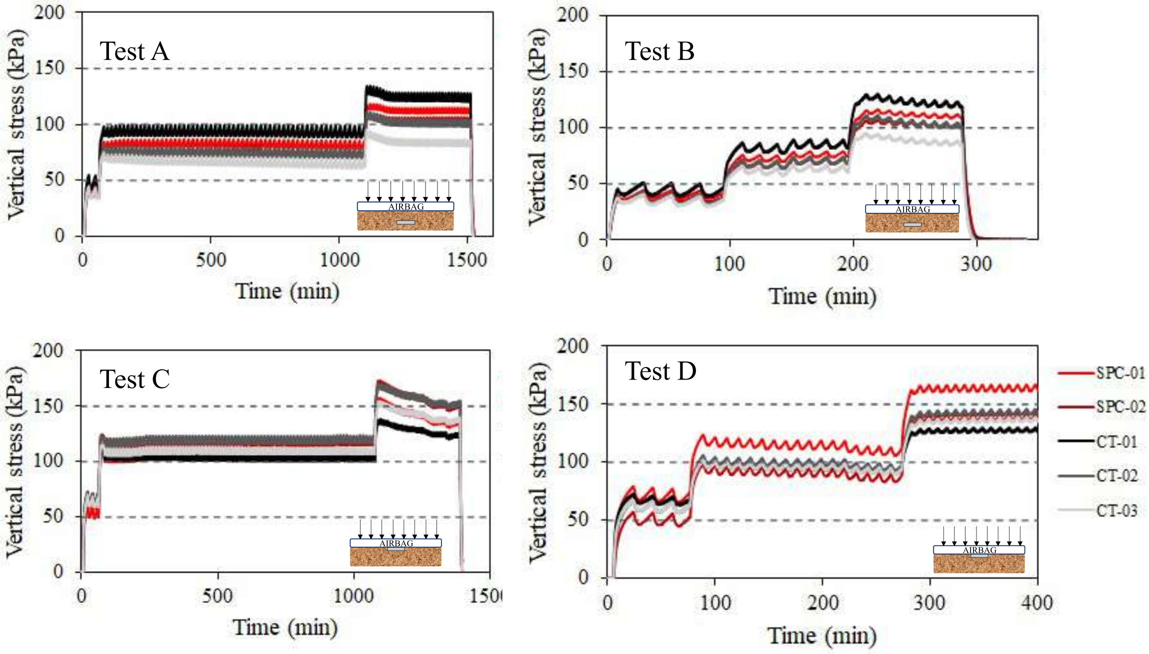

Figure 5.16: Results for the surcharge test conducted with backfill sand and adjusted calibration factor for SPC-01 and SPC-02 cells (cell calibration factors: 800 kPa/mV/V for CT-01, CT-02 and CT-03 and 0.067 kPa/mV for SPC-01 and SPC-02). Dashed horizontal lines represent the surcharge levels applied. (Test A and B are the same, with pressure cell buried in soil; Test C with cell in direct contact with airbag and SPC-01 at the front; Test D with cell in direct contact with airbag and SPC-02 at the front).

surcharge of 50 kPa, in which the front cell registered a pressure around 70% of the value registered by the back cell.

Surcharge (kPa)	Test C (SPC-01 in front)	Test D (SPC-02 in front)
50	85.9%	70.4%
100	89.2%	79.3%
150	90.3%	84.6%

Table 5.6: Pressure percentage of the front pressure cell measurement relative to the back cell, both positioned at the longitudinal central axis of the test box.

Regarding the smaller pressure cells, a smaller difference was noted with the minimum value around 90% of the maximum one (Table 5.7).

From the results obtained it was considered that conducting the physical test with the available box lid would be possible, keeping in mind that there would be some degree of non-uniformity in surcharge application to the model wall, specially for smaller stress levels.

Surcharge (kPa)	Test C	Test D
50	94.6%	91.0%
100	86.9%	96.6%
150	89.6%	90.0%

Table 5.7: Pressure percentage for the smaller pressure cells: minimum mean value relative to maximum mean value for each load step (cells positioned at the diagonal of the test box).

5.2.3.3 Facing blocks lateral support

In order to maintain the available box depth (180 cm) to be filled with the reinforced soil and keep the geogrid end distant from the box rear wall it was adapted two side 30-mm thick plywood boards to extend the lateral box walls. The two pieces were 163-cm high and 40-cm wide, with a lower indentation to fit into the pillar base. Each one was fixed to one of the front box pillars with three L-shaped angle brackets and hexagonal head screws along its length. To minimize outward deflection, wooden props were placed between the plywood sheet and the box pillar, as shown in Figure 5.17, while five 10-mm diameter tie-rods were transversely placed between the lateral plywood sheets and firmly tightened by means of nut adjustment (Figure 5.18). These rods also provided support for mounting the displacement transducers used to measure facing displacements during wall construction and functioned as a fixed reference for manual survey measurements. The same sidewall friction reducing membranes used for the box's walls was used to cover the lateral plywood sheets.

Additionally, a frontal plywood sheet was temporarily installed at the bottom of the test apparatus to provide lateral confinement for the compaction of the foundation soil. It was fixed to a steel plate anchored at the laboratory floor with three angle brackets (Figure 5.17).

Figure 5.17: Lateral plywood sheets installed to provide lateral support for the modular block facing and temporary frontal plywood sheet to provide confinement for the compaction of the foundation soil.

Figure 5.18: Transversal rods mounted between the lateral plywood sheets to provide block lateral restrain and support for the facing displacement transducers during wall construction.

5.2.4 Surcharge system

In the studies conducted at the Royal Military College (GREGG, 2008; BURGESS, 1999; REEVES, 2003; EZZEIN, 2007) it was used commercially available airbags employed for shipping containers. However, similar products were not found in Brazilian market with the dimensions needed for fitting in the test box. Therefore, the surcharging of the model wall was carried out by using two PVC inflatable airbags specially manufactured by the local company Formatto Coberturas Especiais for this research, aiming for a 200-kPa capacity. The airbags were 80-cm wide and 200-cm long, with two of its sides connected by spot-welding. They were designed with extra dimensions relative to the area of the box so it would be possible to fold the welded sides to prevent pressure concentration and a possible air leakage (Figure 5.19). It was kept a space between the two airbags to allow installation of the displacement transducers used to measure soil surface settlement during surcharging.

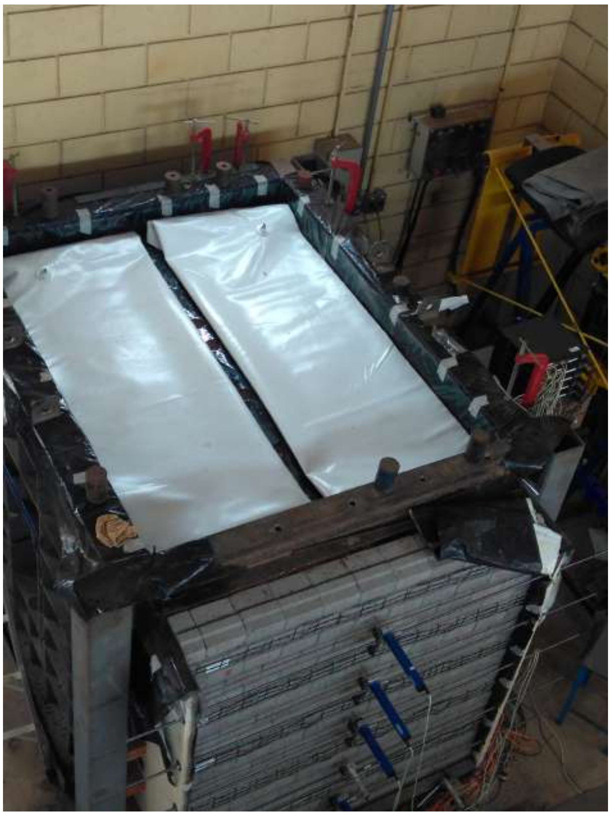

Figure 5.19: PVC airbags used to surcharge the model wall.

During the physical test the airbags were confined between the soil and a set-up comprised of three 25-mm thick plywood boards and two 18-mm thick MDF boards that reacted against the box lid fixated at the top of the test facility (Figure 5.32). The same friction reducing membranes used for the box's walls was used to cover the top soil surface (Figure 5.20), to reduce friction between the airbags and the soil. A non-woven geotextile was used to cover the airbags and minimize friction with the plywood board (Figure 5.20

to Figure 5.22).

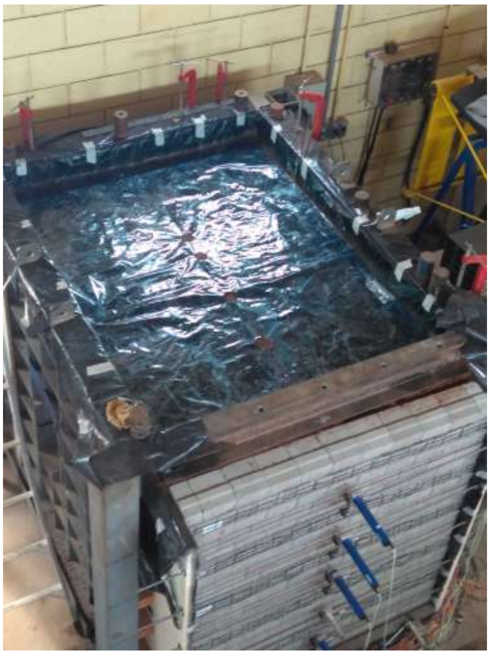

Figure 5.20: Soil top surface covered with friction reducing membranes.

Each airbag was manufactured with a water tank flange coupled with a 1/4 pneumatic push to quick connect fitting to connect to a 6-mm diameter air hose (Figure 5.23a) that conveyed the air pressure from a 100-L capacity air compressor with 140 PSI of capacity. The air hose passed through pre-drilled holes at the plywood and MDF boards placed over the airbags (Figure 5.23b).The lines for the two airbags were independently connected to a pressure panel with separated valves to allow isolation of each airbag in case of a leakage or rupture (Figure 5.24).

Figure 5.21: Non-woven geotextile sheets placed over airbags to minimize friction with plywood boards.

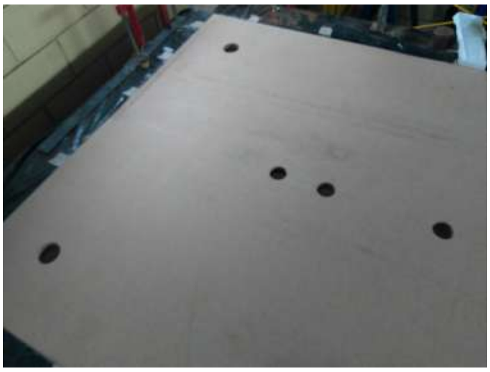

Figure 5.22: Plywood board placed over the airbag + geotextile set-up.

The pressure adjustment was achieved with an adjustable mechanical regulator connected to a brand new class A precision analogue pressure gauge with a scale range from 0 to 4 kgf/cm^2 (~392 kPa) and a resolution around 5 kPa mounted in a panel (Figure 5.24). It is worth noting that preliminary tests indicated that the pressure gauge already available at the LabGsy Laboratory was impaired, underegistering the applied pressures in over 80 kPa. This highlights the importance of testing all the equipments involved in the experimental program prior to conducting the actual experiment.

(a) (b)

Figure 5.23: Connection between the airbag and the air pressure hose: pneumatic push to quick connect fitting. (a) detail of connection; (b) detail of air pressure tube passing through pre-drilled holes at the plywood and MDF boards of the surcharging set-up.

Figure 5.24: Pressure panel used to control the air inflow and pressure to each airbag.

5.3 Instrumentation

5.3.1 General

Giving the data acquisition system and instrument limitations, the instrumentation scheme was designed to capture the data considered as the most relevant to understand wall behaviour, taking advantage of the instruments available at LabGsy Laboratory. Figure 5.25 shows an overall schematic of the instrumentation layout. A total of 75 automated sensors, 35 manual extensometers and 55 manual survey points were used to monitor the model wall during construction and surcharge, and detail description of each one is given in the following sections. A summary of the instruments used and the correspondent wall behaviour monitored is shown in Table 5.8. All instruments were powered by a 5 volt DC bridge excitation.

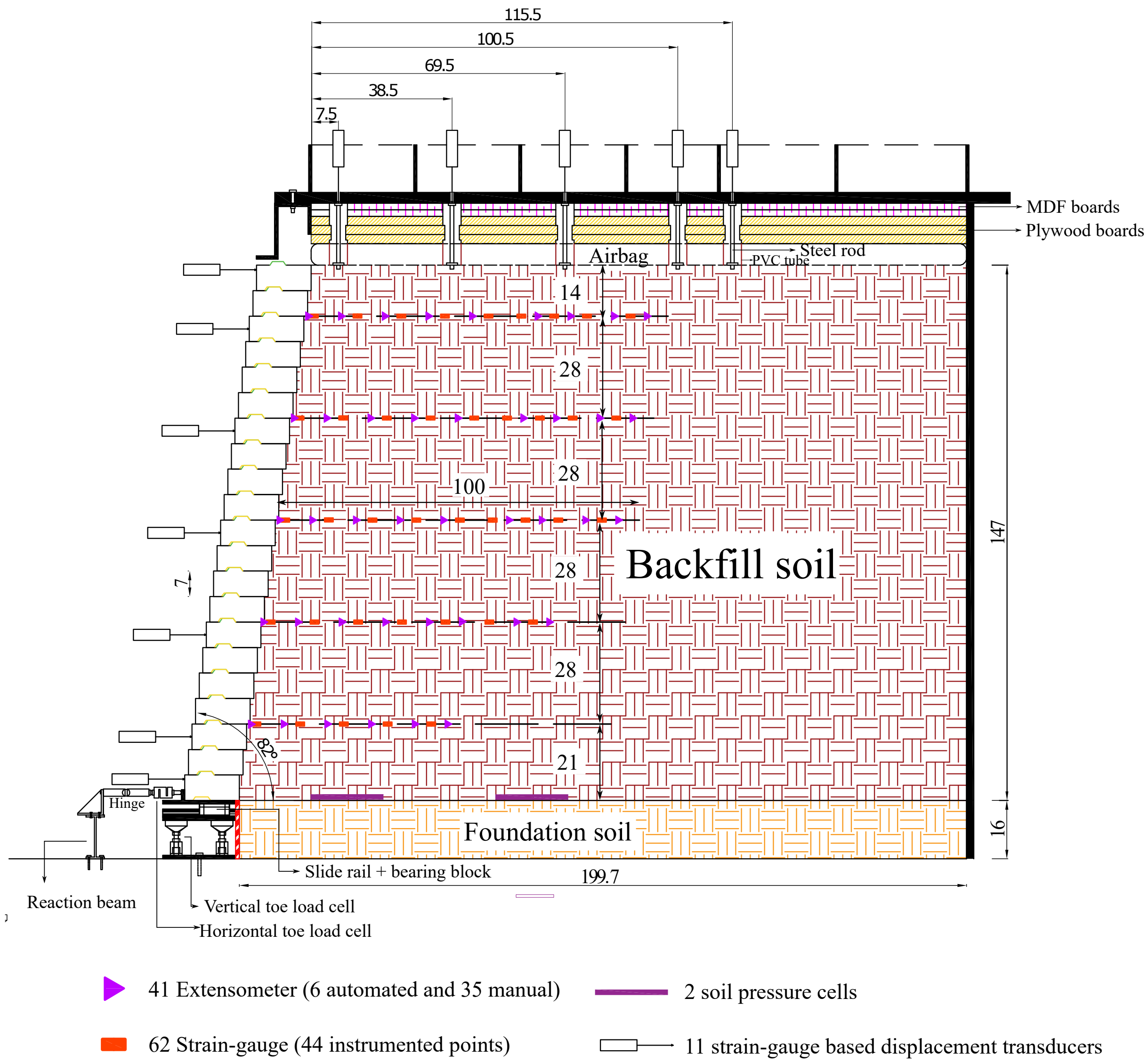

Figure 5.25: Cross-section view showing general schematic of the reduced scale reinforced soil model and instrumentation (dimensions in cm).

Behaviour	Measurement	Instrument Type	Quantity
Soil Movement	Facing deflections	Strain-gauge based displacement transducer	9
	Soil surface settlement	Strain-gauge based displacement transducer	5
Reinforcement	Horizontal movement	Draw wire potentiometer and manual extensometers	6 and 35, respectively
	Strain	High elongation strain gauges	44 instrumented points (62 strain-gauges)
Toe Forces	Horizontal forces	S-beam load cells	3
	Vertical forces	Single point load cells	6
Earth Pressures	Foundation stresses	Confined fluid earth pressure cells	2

Table 5.8: Summary of the instrumentation scheme used to monitor the model wall.

5.3.2 Data acquisition

During construction and surcharging the model wall was monitored and data registered with two types of data acquisition systems. LabGsy laboratory had available at the time of the experimental test two modules of System i5000 from Vishay Micro-Measurements, with 20 input channels each. From these, two sensor cards (10 channels) were for sensors with high-level voltage output while the rest was for strain-gage based transducers. One channel for strain-gage based transducers was impaired and could not be used. An additional module of System 8000 from Vishay Micro-Measurements, with 8 input channels was available at LabGsy laboratory. This system allows measurement of strain-gauges, strain-gauges based transducers, high-level voltage signal and thermocouples, without specific sensor cards.

The available number of input channels available at LabGsy laboratory (47 channels) was not sufficient to provide the desired instrumentation coverage to monitor the model wall behaviour. Therefore, additional 4 modules of System 8000 (32 additional channels) were lent by the Department of Structural Engineering of São Carlos School of Engineering. One channel, though, was impaired and could not be used. Therefore, the test ended up with 78 input channels available for wall monitoring (Figure 5.26). Clearly, the limitation of input channels available is a strong constraint on obtaining a comprehensive monitoring of physical model tests.

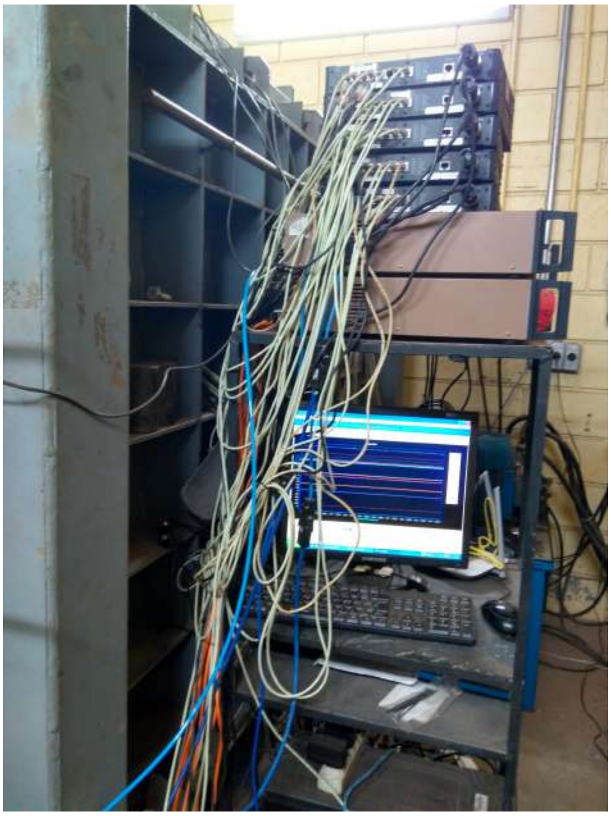

Figure 5.26: Data acquisition systems used for monitoring the physical test: 2 modules of system i5000 (below) and 5 modules of system 8000 (on top).

For both systems the same acquisition software was used, Strain Smart, although in different versions. The software allows real time and graphical visualization of the measurements taken. A personal computer (PC) was connected to the System 8000 modules while a desktop computer was used for System 5000 readings. The measurements were taken at a frequency of 1Hz and saved at regular periods of time (around 8h) to avoid data loss. During model wall construction instrumentation readings were taken before and after each soil lift placement, while during surcharging it was continuously registered, with interruptions only for saving the freshly recorded data. Real time monitoring of the surcharge phase was conducted in-place and remotely, by using the free software Any Desk, so any problem or inconsistency was readily detected and a course of action could be defined.

For the manual measurements (manual wire extensometers and facing survey) the data was taken before and after each construction layer (one block row) and before and after each surcharging increment.

5.3.3 Soil Movement

5.3.3.1 Horizontal Facing Displacements

Horizontal displacements of the wall facing were measured with automated strain-gauge displacement transducers and with manual facing survey. A central vertical line mounted with seven 100-mm stroke transducers was used, two already available at LabGsy Laboratory and manufactured by Vishay Micro-Measurements and the remaining in-house made. During wall construction the instruments were mounted at supports connected to the tie-rods used to restrain outward deflection of the lateral plywood sheets used to provide lateral constrain to the facing block (Figure 5.27).

The instruments were installed as the wall was constructed. During surcharging a stiffer structure was used, comprised of a square steel profile with its lower end bolted to the strong laboratory floor and its upper end fixated to the front beam installed to support the box lid. This was done by means of a truss arrangement composed of two square steel profiles welded to the beam (Figure 5.28). This set-up allowed a wider range of displacements to occur before needing to retrieve the transducers to avoid any damage due to excessive wall movement. The positions of the transducers were kept the same in both configurations, vertically spaced according to Figure5.25. The displacement transducers were positioned at middle height of the blocks immediately below the reinforcement layers, apart from the toe and the top displacement transducers, as shown in 5.25.

Figure 5.27: Displacement transducers support during wall construction: fixation on transversal tie rods.

Manual facing survey measurements were registered during surcharging at four vertical alignments at the face and at 5 measurement heights each, resulting in a total of 20 measurement points across the face of the test wall, as shown in the schematic in Figure 5.29. The readings were taken before and after each surcharge increment. The readings were taken with a 300-mm range digital paquimeter with 0.01-mm resolution and 0.04-mm

(a) (b)

Figure 5.28: Displacement transducers support during wall surcharging: (a) side view, with detail of the fixation to the front support beam (b) top view.

precision, using as reference the tie-rods used to restrain outward deflection of the lateral plywood boards as described in Section 5.2.3.3. Due to the inherent error associated with manual readings the measurements were registered with a resolution of 1 mm, aiming to reduce operator's influence on the measured data. The facing survey results were used as a redundancy to displacements measured by the displacement transducers, allowing a cross check between the different methods. Additionally, it allowed a wider coverage of the face and the detection of possible displacement non-uniformity across the wall facing.

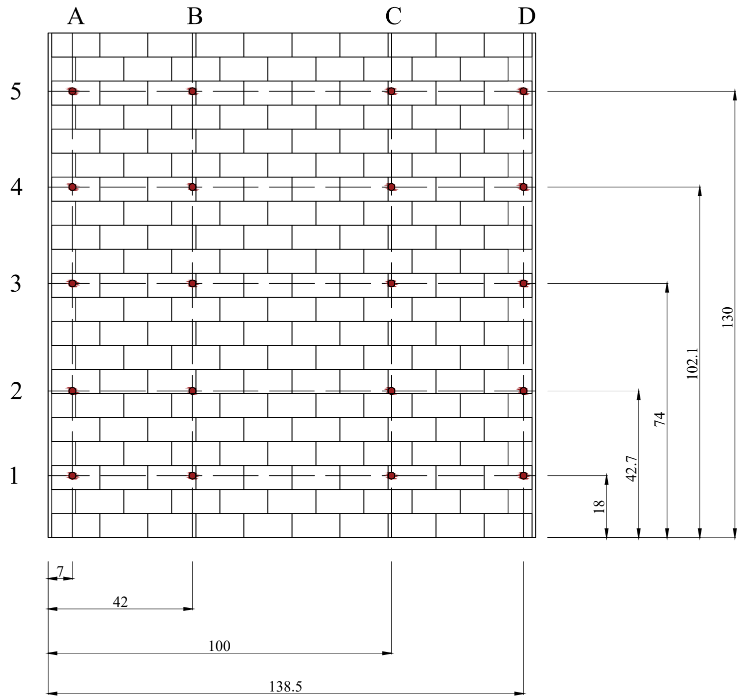

Figure 5.29: Facing survey measurement points (measurements in cm).

5.3.3.2 Horizontal Toe Displacements

To record toe displacements, three strain-gauge based displacement transducers were positioned along the first block row, at its middle height (Figure 5.30). The middle transducer was aligned with the other instruments used to measurement facing displacements so a displacement profile could be plotted.

Figure 5.30: Toe instrumentation: displacement transducers and load cells.

5.3.3.3 Soil Surface Vertical Displacements

During surcharging soil settlements at the top of the soil backfill were recorded with a row of five 100-mm stroke strain-gauge based displacement transducers manufactured by

Vishay Micro-Measurements and Kyowa. The sensors were positioned as shown in Figure 5.25, with the four instruments closest to the wall facing arranged along the reinforcement length projection and the fifth instrument, further from the face, positioned behind the reinforced zone projection. The measurements were taken at the centre line of the test box, between the two airbags.

As discussed in Section 5.2.4 the surcharging system comprised of two airbags placed directly on top of the soil backfill surface. To fill the gap between the airbags and the box lid a set of five boards (three 25-mm thick plywood boards and two 18-mm thick MDF boards) was placed above the airbags to provide reaction against the box lid. This arrangement put up a distance over 100 mm between the soil surface and the box lid, larger than the displacement transducer stroke, making impossible to place the sensor directly in contact with the top of the backfill soil. The solution was to adapt the measurement acquisition, using auxiliary 150-mm long steel rods with flat metal pieces at both of its ends which were positioned at pre-located holes at the plywood and MDF boards, as shown in 5.31.

Figure 5.31: Steel rod adapted to support the displacement transducers to measure soil surface settlement.

The rod tip in direct contact with the soil was buried into the soil to improve its anchorage, passing through 40-mm and 50-mm pre-made holes at the plywood and MDF boards of the surcharging system (Section 5.2.4).Nonetheless, a shortcoming of this set-up was that it could not be guaranteed rod proper alignment and position throughout surcharging, since soil movement could displace or rotate it. The tip of each displacement transducer passed through a hole made at the box lid and was positioned touching the correspondent top surface of the auxiliary rod, with a pre-given displacement to guarantee contact and sufficient available range of motion throughout the test.

To prevent contact between the airbags and the rods, that could potentially lead to rod displacement, PVC tubes with 50-mm length and 2-inch diameter were glued at fitting edges at the lower plywood board (Figure 5.32). In this way the rods were isolated from any contact with the airbags, being able to move freely with soil settlement.

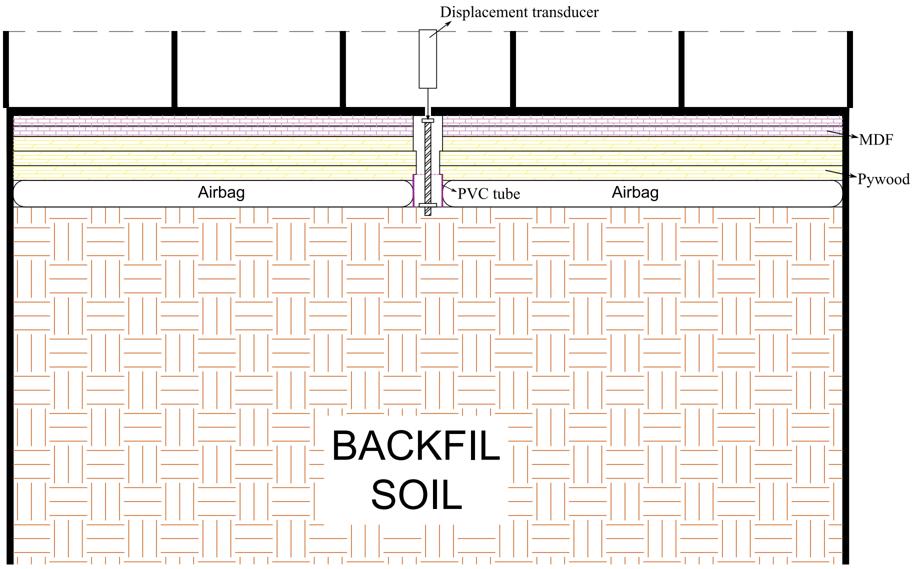

Figure 5.32: Arrangement to measure soil surface settlement: displacement transducer in direct contact with the rod adapter, anchored at the top surface of the backfill soil (cross section parallel to the wall facing).

5.3.3.4 Construction of the In-House Made Displacement Transducers

To complement the number of displacement transducers available in LabGsy Laboratory six new sensors were constructed in-house, with a stroke range of 100 mm. The design was similar to the one used in the commercially available sensors, comprised of a conical-shaped aluminium rod connected to the measurement arm mounted between two aluminium cantilever beams fixated in a base plate (Figure 5.33a). A set of 4 strain-gauges of model type PA-13-125BA-350-L with leadwires attached, manufactured by Excel Sensores, was bonded at the cantilever beams, close to the base plate, in a full-Wheatstone arrangement. The gauge-length was 3 mm and the gauge resistance was of 350 ohms, with a gauge factor of 2.06. The strain-gauges were self-compensated for temperature change for aluminium.

The strain-gauges were installed on both sides of the cantilever beam, at the reduced section (Figure 5.33a), near the fixed end, which is the region of greatest strain. During deflection of the beam, the external strain gages are subjected to compression while the internal ones are subjected to tension, so the strains in both sides are equal in modulus but have opposite signs.

When the instrument stroke is in motion, the conical-shaped rod slides between two low-friction rolling bearings located at the tip of the cantilever beams, thus deflecting them and causing a change in strain-gauge resistance. To reduce friction between the pieces during motion, the conical-shaped rod sides in contact with the bearings were well-polished.

Printed Circuit Board (PCB) plates were manufactured by Micropress Circuitos Impressos (São Paulo-SP, Brazil) and fixed at the base plate of the transducer core structure to facilitate wiring of the strain-gauges in the full-Wheatstone bridge arrangement. The PCB design is shown in Figure 5.33b. The bonding of the strain-gauges at the cantilever beams as well as the soldering and connection of the sensors were done in-house (5.34). The component pieces of the transducer structure was manufactured by SN Genera, in São Carlos-SP, Brazil.

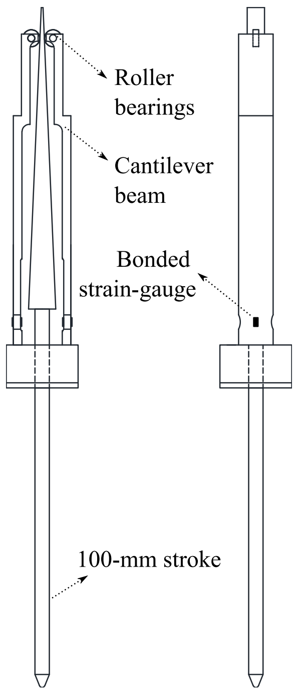

(a)

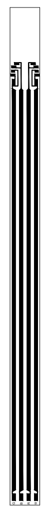

(b)

Figure 5.33: In-house made displacement transducer: (a) Inner design schematic (b) PCB board manufactured for strain-gauge wiring.

The materials used for strain-gauge bonding comprised of sandpaper #150 and #400, gauze, cotton swabs, isopropyl alcohol, conditioner (Excel Sensors), neutralizer (Excel Sensors), cyanoacrylate-based adhesive (instant adhesive type), silicone resin RK (Excel Sensors), tape, tweezers, adhesive tape, pencil, Teflon strip and glass plate. The materials for manipulating the strain-gauges, such as tweezers and glass plate, were duly cleaned with isopropyl alcohol before use to avoid contamination.

The procedures adopted for strain-gauge bonding are described as follows:

a) Surface preparation (Figure 5.34a-d): this step is important to ensure maximum adherence between the base surface and the strain-gauge, by means of the adhesive, guaranteeing a chemically clean area with adequate roughness. The base surface at the reduced section at both sides of the cantilever beam was sanded with random circular movements, first with sandpaper #150 (rough cleaning). After wiping out the residues, the surface was smoothly finished up with sandpaper #400 (fine cleaning) in order to leave it flat and uniform without bumps and indentations. The surface was then cleaned with gauze soaked in isopropyl alcohol (degreaser), always from the inside to the outside of the work area. Finally, with the help of cotton swabs, the final cleaning was done with conditioner and neutralizer solutions. Alignment marks (vertical and horizontal centrelines) were then drawn with a pencil around the target area to help with strain-gauge positioning.

b) Preparation and positioning of the strain-gauge (Figure 5.34e-f): after checking the strain-gauge resistance with the aid of a multimeter, the sensor element was removed from its packaging and placed on a clean glass plate with the aid of tweezers previously cleaned with isopropyl alcohol. A piece of transparent adhesive tape was then applied on top of the strain-gauge. Then, the tape/strain-gage assembly was carefully removed from the glass plate and positioned at the desired location on the surface of the freshly prepared beam surface, by matching the centre marks of the strain-gauge with the alignment marks previously drawn. With the correct positioning, the tape was carefully lifted by one of its ends until the strain-gauge bottom was exposed.

c) Strain-gage bonding: The adhesive was applied to the beam surface exposed and then the adhesive tape was lowered into the bonding position with the help of a gauze, in order to eliminate any excess of adhesive or air bubbles. Pressure was then applied with a metal clamp equipped with rubber pads for about 24 hours to ensure bonding (Figure 5.34g). Finally, the adhesive tape was removed by carefully pulling it by one of its end.

d) Waterproofing and protection: Soon after bonding, a thin layer of silicone resin was applied over the strain-gauge for its protection.

The connection of the strain-gauges in a full-Wheatstone bridge followed the bonding procedure, by soldering the end tip of the copper leadwires to the soldered terminals in the upper part of the PCB board fixed to the transducer inner structure, behind the cantilever beams (Figure 5.34i-k). A slack was maintained for all the leadwires to prevent tension. Leadwire end treatment consisted of cleaning the solders with a soldering cleaning solution. A 4x26 AWG cable was then connected to the soldered terminals located at the lower part of the PCB board, keeping it in a loop with a plastic hose clamp to avoid tension (Figure 5.34l). The other end was connected to a DB9 connector to allow connection to System i5000 data acquisition system.The connections were tested with a multimeter and finally the transducers were enclosed with an aluminium cylindrical case, with the AWG cable passing through a rubber lid (Figure 5.35)

Figure 5.35: Displacement transducer mounted.

5.3.3.5 Calibration of the Displacement Transducers

Both the commercial and the in-house made displacement transducers were calibrated before the test wall construction and surcharging. The majority of the commercial displacement transducers was calibrated by using a set of standard blocks with 20-mm high, for conference of the manufacturer calibration factor (Figure 5.36a). The in-house made transducers and two commercial transducers that needed repair were calibrated in an Instron Universal Testing Machine, in a displacement rate of 200 mm/min (Figure 5.36b). During calibration the sensors were connected to the same channels and excited using the same power supplies and connections used for the test wall monitoring. Data was recorded every 0.1 s.

The calibration factors, ratio between the displacement (δ) and sensor output signal (ΔV), and the respective R^2 values obtained are summarized in Table 5.9. The results indicate good similarity between the commercial and the in-house made transducers calibration factors, both showing good linearity in response (represented by R^2 values).

Additionally, cycles of displacements in the range of 0 - 70 mm were applied to test for output repeatability and hysteresis of the in-house made transducers. A total of 200 cycles were applied, with a displacement rate of 200 mm/min. The two repaired commercial transducers (DT01 and DT09) were also submitted to cyclic displacements in the Instron machine. A small linear hysteresis, not larger than 0.12 mm, was noted for the in-house made sensors (with exception for DT-HM06) and for the commercial sensor DT09 (50-mm stroke), as shown in Figure 5.37. The values obtained represent less than 0.12 % of the sensors full scale, which was considered negligible.

Figure 5.34: Displacement transducer construction: (a) surface sanding; (b) surface cleaning with isopropyl alcohol; (c) surface preparation: conditioner and neutralizer solution application; (d) drawing of alignment marks; (e) strain-gauge handling; (f) strain-gauge positioning at the cantilever beam with adhesive tape; (g) pressure application with metal clamp; (h) silicon resin protection; (i) PCB board fixing at the base of the transducer; (j) strain-gauges wiring in a full Wheatstone bridge; (k) detail of wiring; (l) connection of cabling at lower end of the PCB board.

(a)

(b)

Figure 5.36: Calibration of the strain-gauge displacement transducer: (a) Calibration with standard blocks; (b) Calibration in an Instron Universal Testing Machine.

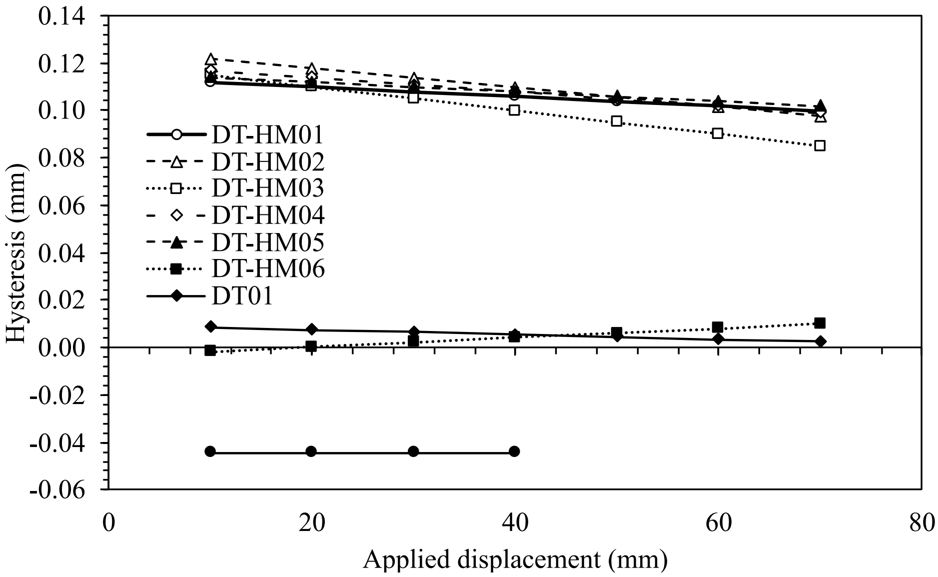

Figure 5.37: Hysteresis results from the cyclic tests performed with the displacement transducers (*HM refers to in-house made transducers).

Transducer ID*	Calibration method	Test wall location	Transducer stroke (mm)	Calibration factor ($\delta/\Delta V$)	R^2
DT01	Instron	Soil backfill top surface	100	20.01	1
DT02	Standard blocks	Soil backfill top surface	100	19.95	1
DT03	Standard blocks	Soil backfill top surface	100	18.83	1
DT04	Standard blocks	Test wall facing	50	10.11	0.9993
DT05	Standard blocks	Test wall facing	100	19.89	1
DT06	Standard blocks	Soil backfill top surface	100	19.05	1
DT07	Standard blocks	Soil backfill top surface	100	19.86	1
DT09	Instron	Toe displacement	50	10.02	0.9997
DT-HM01	Instron	Toe displacement	100	18.82	0.9999
DT-HM02	Instron	Toe displacement	100	18.03	0.9989
DT-HM03	Instron	Test wall facing	100	18.64	0.9985
DT-HM04	Instron	Test wall facing	100	17.99	0.9994
DT-HM05	Instron	Test wall facing	100	18.12	0.9996
DT-HM06	Instron	Test wall facing	100	18.20	0.9998

Table 5.9: Displacement transducer calibration factors (*HM refers to in-house made transducers)

5.3.4 Reinforcement Displacement and Strain

5.3.4.1 General

A total of 85 instrumented points were used to measure reinforcement horizontal displacement and reinforcement strain in the longitudinal direction, aiming to capture displacement and strain associated with outward movement of the facing. Draw wire potentiometers and manual wire extensometers were used to obtain the geogrid displacements, while the results from strain gages bonded to the geogrid (local strains) and the calculated strains from relative displacement between adjacent extensometers (global strains) were considered for reinforcement strain results. The location of each sensor is shown in Figure 5.38 to 5.40. Layer 1 is the first one from the bottom. Layers 4 and 5 were instrumented with the same layout as Layer 3 (Figure 5.40). Note that the location of the extensometers was purposely selected so between two adjacent extensometers a strain-gauge was placed, aiming for later comparison between global strains measured by the extensometers and local strains measured by strain-gauges.

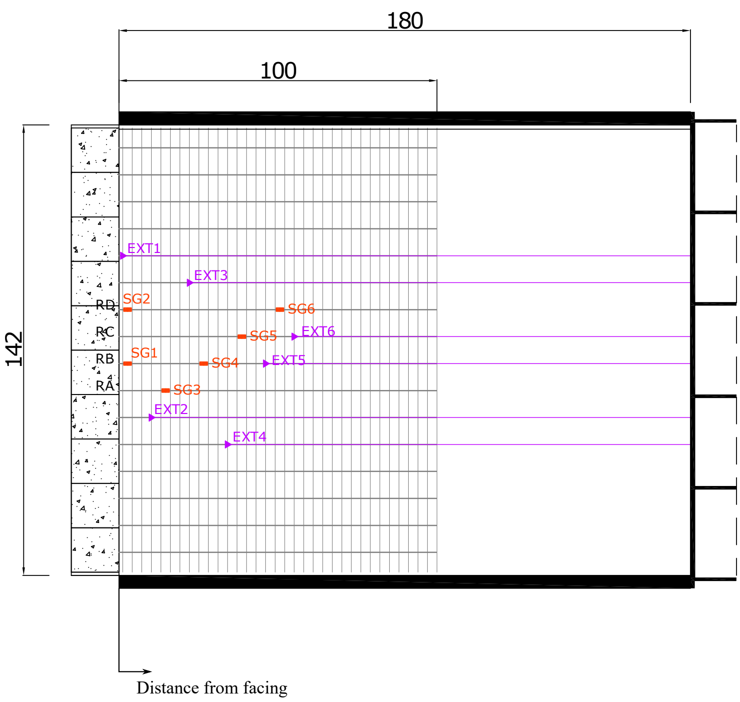

LAYER 1 - STRAIN-GAUGES				
SG	RIB	ID	Distance from facing	obs
1	B	LAYER 1_SG1_RIBB	2.71	*
2	D	LAYER 1_SG2_RIBD	2.71	*
3	A	LAYER 1_SG3_RIBA	14.71	*
4	B	LAYER 1_SG4_RIBB	26.71	
5	C	LAYER 1_SG5_RIBC	38.71	
6	D	LAYER 1_SG6_RIBD	50.71	

* *Problem during surcharging*

LAYER 1 - EXTENSOMETERS			
EXT	RIB	ID	Distance from face (cm)
1	D+2	LAYER 1_EXT1_RIBD+2	1.2
2	A-1	LAYER 1_EXT2_RIBA-1	10.2
3	D+1	LAYER 1_EXT3_RIBD+1	22.2
4	A-2	LAYER 1_EXT4_RIBA-2	34.2
5	B	LAYER 1_EXT5_RIBB	46.2
6	C	LAYER 1_EXT6_RIBC	58.2

Extensometer

Strain-gauge

All dimensions in cm

Figure 5.38: Extensometer and strain-gauge locations for layer 1, with distances of the measuring points from the facing summarized at the right tables (See Figure 5.25 for reinforcement layer elevations).

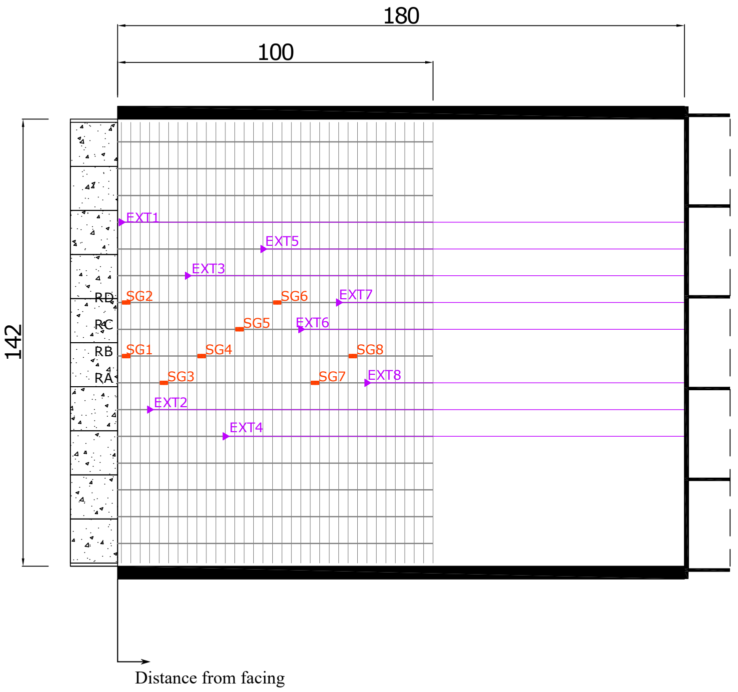

LAYER 2 - STRAIN-GAUGES				
SG	RIB	ID	Distance from facing	obs
1	B	LAYER 2_SG1_RIBB	2.71	
2	D	LAYER 2_SG2_RIBD	2.71	
3	A	LAYER 2_SG3_RIBA	14.71	
4	B	LAYER 2_SG4_RIBB	26.71	
5	C	LAYER 2_SG5_RIBC	38.71	
6	D	LAYER 2_SG6_RIBD	50.71	*
7	A	LAYER 2_SG7_RIBA	62.71	*
8	B	LAYER 2_SG8_RIBB	74.71	*

* Problem during surcharging

LAYER 2 - EXTENSOMETERS			
EXT	RIB	ID	Distance from face (cm)
1	D+3	LAYER2_EXT1_RIBD+3	1.2
2	A-1	LAYER2_EXT2_RIBA-1	10.2
3	D+1	LAYER2_EXT3_RIBD+1	22.2
4	A-2	LAYER2_EXT4_RIBA-2	34.2
5	D+2	LAYER2_EXT5_RIBD+2	46.2
6	C	LAYER2_EXT6_RIBC	58.2
7	D	LAYER2_EXT7_RIBD	70.2
8	A	LAYER2_EXT8_RIBA	79.2

Extensometer

Strain-gauge

All dimensions in cm

Figure 5.39: Extensometer and strain-gauge locations for layer 2, with distances of the measuring points from the facing summarized at the right tables (See Figure 5.25 for reinforcement layer elevations).

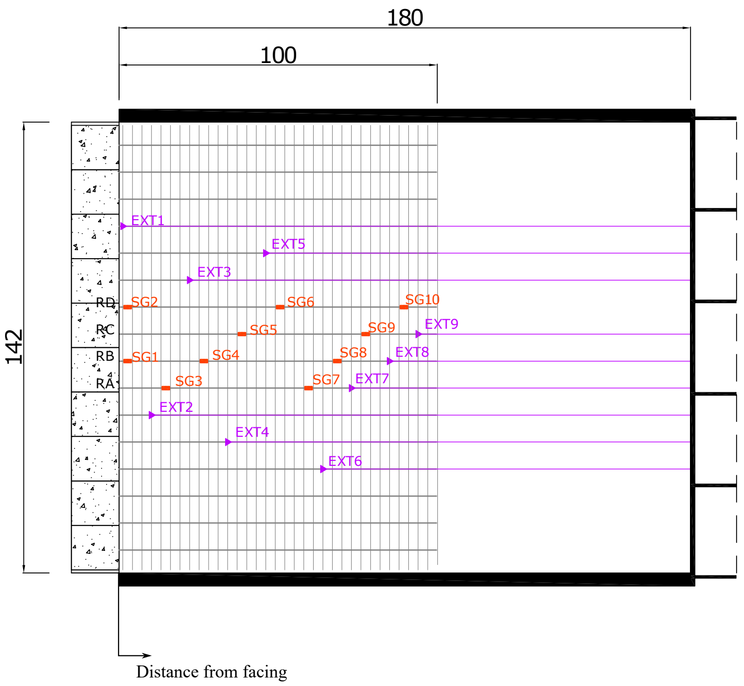

LAYER 3 - STRAIN-GAUGES				
SG	RIB	ID	Distance from facing	obs
1	B	LAYER 3_SG1_RIBB	2.71	
2	D	LAYER 3_SG2_RIBD	2.71	
3	A	LAYER 3_SG3_RIBA	14.71	*
4	B	LAYER 3_SG4_RIBB	26.71	
5	C	LAYER 3_SG5_RIBC	38.71	
6	D	LAYER 3_SG6_RIBD	50.71	
7	A	LAYER 3_SG7_RIBA	62.71	
8	B	LAYER 3_SG8_RIBB	74.71	
9	C	LAYER 3_SG9_RIBC	77.71	
10	D	LAYER 3_SG10_RIBD	89.71	*

* Problem during surcharging

LAYER 3 - EXTENSOMETERS			
EXT	RIB	ID	Distance from face
1	D+3	LAYER3_EXT1_RIBD+3	1.2
2	A-1	LAYER3_EXT2_RIBA-1	10.2
3	D+1	LAYER3_EXT3_RIBD+1	22.2
4	A-2	LAYER3_EXT4_RIBA-2	34.2
5	D+2	LAYER3_EXT5_RIBD+2	46.2
6	A-3	LAYER3_EXT6_RIBA-3	64.2
7	A	LAYER3_EXT7_RIBA	73.2
8	B	LAYER3_EXT8_RIBB	85.2
9	C	LAYER3_EXT9_RIBC	94.2

Extensometer

Strain-gauge

All dimensions in cm

Figure 5.40: Extensometer and strain-gauge locations for layer 3, with distances of the measuring points from the facing summarized at the right tables (See Figure 5.25 for reinforcement layer elevations). Same configuration for layers 4 and 5.

5.3.4.2 Reinforcement Horizontal Displacement

Horizontal displacement of selected nodes of the geogrid layers were measured using extensometers. For the first layer all of the 6 automated draw-wire potentiometers available at LabGsy were used while for the rest of the layers manual extensometers were employed, in an attempt to acquire a larger set of information on the reinforcement behaviour during the physical test. The location of each instrumented node is shown in Figure 5.38 to 5.40. The draw-wire potentiometers used were manufactured by UniMeasure (model type LX-PA 2.8), with a wire rope extension stroke of 29 mm.

The extensometers comprised of thin stainless steel cable (0.38-mm diameter) attached to the geogrid node by looping the wire through the geogrid fibres and enclosing it with a wire connector firmly tightened with pressure pliers (Figure 5.41). Finally the attachment point was stiffened using an epoxy adhesive, impregnating and surrounding the filaments of the reinforcement material around the wire. The remaining length of the wire inside the test box was protected with a small diameter plastic casing to enable free movement of the wire (Figure 5.42). The free end of the extensometer wires passed thorough pre-drilled holes at the rear wall of the test box.

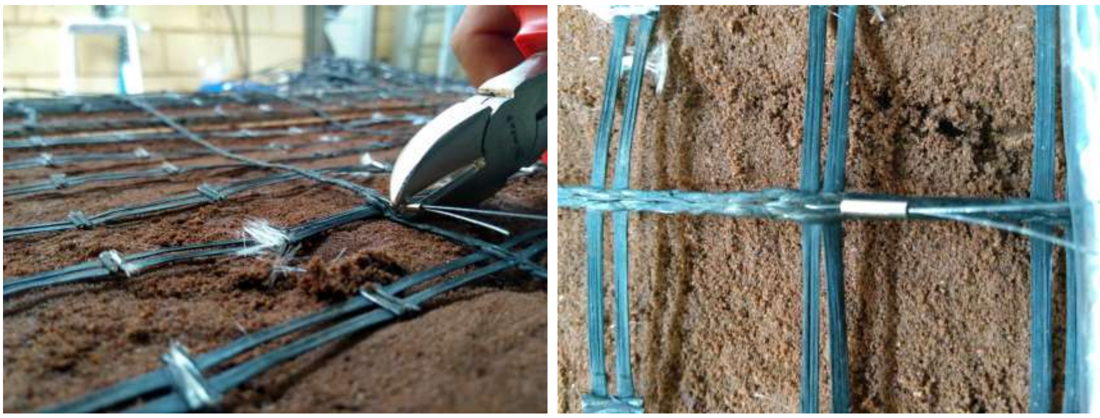

(a) (b)

Figure 5.41: Attachment of extensometer wire to geogrid node.

For the case of the first (lowest) geogrid layer the wire free ends were connected to the draw-wire potentiometers, mounted at a steel plate welded at outside of the rear wall. For the remaining reinforcement layers, the connection was done with a weight system, comprised of reference bars and cylindrical weights with a reference line (Figure 5.43). The weight system guaranteed that the wires remained stretched throughout the test and gave a reference for the displacement measurements, which was obtained with a paquimeter with 0.01- mm resolution and 0.04-mm precision.

Figure 5.42: Extensometer wiring enclosed by plastic tubes, extended up to the rear wall.

Figure 5.43: Weight system attached to extensometer wire end.

5.3.4.3 Calibration of the draw-wire potentiometers

The six draw-wire potentiometers were in-house calibrated by applying a know displacement and measuring the resultant output signal. Discrete displacements between

0 to 15 mm were imposed by moving the cursor of a Mitutoyo Digital Dial Indicator, that was attached to the eye fitting on the end of the wire rope (Figure 5.44). During calibration the sensors were connected to the same channels on the System i5000 acquisition system used during the physical test, and excited with the same power supply. The calibration factors obtained were compared to the calibration data given by the supplier, resulting in a maximum difference of 11.4 %, as shown in Table 5.10. Great linearity was obtained, with correlation factors (R^2) larger than 0.998. The calibration factors used to convert output signal to displacement during the physical test were the ones obtained from in-house calibration.

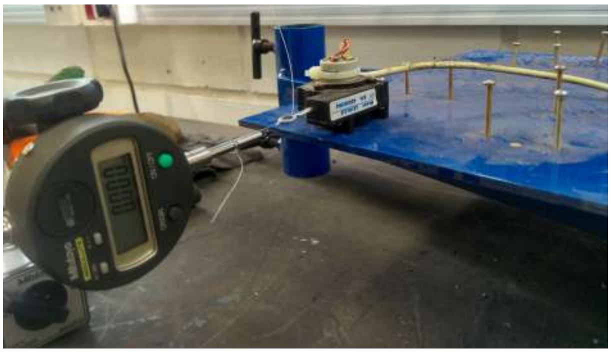

Figure 5.44: Calibration of the draw-wire potentiometers.

ID	Supplier(mV/mm)	In-house (mV/V)	Difference*
D1	321.69	327.90 (R^2 = 1.000)	1.89%
D2	322.16	293.00 (R^2 = 0.999)	-9.95%
D3	320.58	325.29 (R^2 = 1.000)	1.45%
D4	322.16	289.22 (R^2 = 0.999)	-11.39%
D5	320.04	296.95 (R^2 = 0.998)	-7.78%
D6	320.54	306.40 (R^2 = 1.000)	-4.62%

**(in-house - supplier)/supplier x 100*

Table 5.10: Draw-wire potentiometers calibration results.

5.3.4.4 Reinforcement Strains

Local strains in the longitudinal axis and at selected locations of the geogrid layers were measured directly by using high-elogation strain-gauges (model type KFEL-5-120-C1) manufactured by Kyowa Electronic Instruments Company of Japan. This model was chosen for its successful use in previous researches (EZZEIN, 2007; SANTOS, 2011; BURGESS, 1999; GREGG, 2008). According to the manufacturer the gauges are capable of measuring strains up to 15%, although the aforementioned studies indicated possible readings up to 5-10% when attached to geosynthetic material. The gauge-length was 5 mm and the gauge resistance was of 120 ohms, with a gauge factor of 2.11.

The method used for bonding the strain-gauges to the PET geogrid was adapted from the recommendations and description presented in previous studies, such as in Ezzein (2007), Santos (2011), Burgess (1999) and Gregg (2008).The CC-36 adhesive, manufactured by Kyowa, was used. The procedures adopted for strain-gauges bonding can be summarized as follows:

a) Surface preparation (Figure 5.46a-e): the PVC coating at the selected locations (Figure 5.45) of the geogrid longitudinal ribs was first carefully removed on both sides of the rib by using a soft brush, a cotton-tipped applicator and acetone. Next, the exposed fibres were cleaned with isopropyl alcohol and finally were impregnated with a small amount of CC-36 adhesive to create a flat surface for gauge bonding.

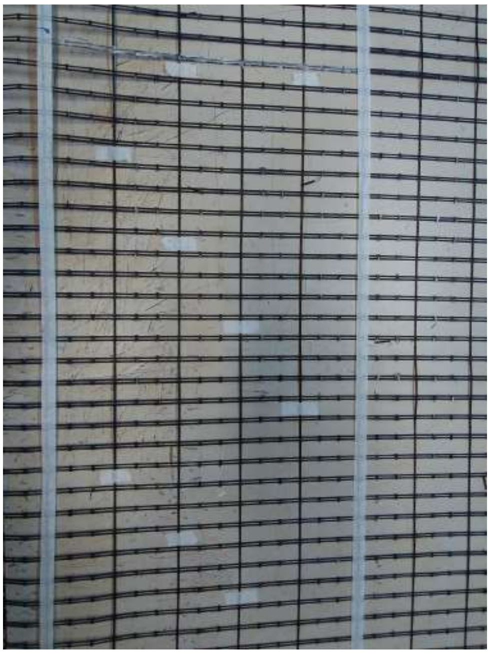

Figure 5.45: Modified geogrid marked for strain-gauge installation.

b) Strain-gage bonding (Figure 5.46a-c): the lower part of a metal clamp (manufactured for the present study) was positioned below the cleaned geogrid rib, with a piece of Teflon film between then, to prevent bondage between the geosynthetic and the clamp from adhesive excess. After checking the strain-gauge resistance with a multimeter, the sensor element was removed from its packaging with sterile tweezers and a small amount of CC-36 adhesive was placed at the back of the gauge, which was then positioned at the intended location at the cleaned rib. Immediately after, a piece of Teflon film was placed on top of the gauge and the top part of the metal clamp carefully connected to the lower one, avoiding to displace the gauge. The clamp was then tightened and kept during one day to provide pressure for adhesive curing.

d) Waterproofing and protection (Figure 5.46j): Soon after bonding, a thin layer of silicone resin was applied over the strain-gauge for its protection before wiring it.

Strain-gauge wiring followed the bonding procedure. At each reinforcement layer, the two instrumented locations closest to the wall facing (where is expected larger bending due to outward facing displacement and soil settlement) were connected in a half Wheatstone bridge to eliminate bending effects, by connecting two strain-gauges at the same rib but at opposite sides. For the remaining locations a quarter bridge arrangement was used, with gauges bonded to only the top side of the rib.

The leadwires from the strain-gauges were connected by twisting and soldering it with exposed tips of the terminal wires of a 4x26 AWG cable (Figure 5.46k), with a pre-solder in place. Strain relief of the leadwires was accomplished by inducing small bends in the wire prior to the connection with the AWG terminal wires. Leadwire end treatment consisted of cleaning the solders with a soldering cleaning solution.

Final waterproof and mechanical protection of the gauge and the wiring was done by encapsulating the area with a small-diameter flexible tube, cut lengthwise, filled with silicone (Figure 5.46l), as recommended by Warren, Christopher, and Howard (2010). The other end of the AWG cable was connected to a RJ45 connector to allow connection to System 8000 data acquisition system.

An attempt to measure global strains, which are measured over a larger length of the reinforcement, was done via extensometers. As used in previous studies (SANTOS, 2011; BURGESS, 1999; GREGG, 2008; WARREN; CHRISTOPHER; HOWARD, 2010; EZZEIN, 2007) global strains can be calculated by dividing the relative displacement between two adjacent extensometers by the original distance between then. This method enables the registration of larger strains, beyond the limit at which occurs strain-gauge rupture or debonding. However, as it will be seen in Section 6.2.6, the method used herein to measure the displacements with the manual wire extensometers was not reliable, giving scattered results that, unfortunately could not be used to calculate global strains.

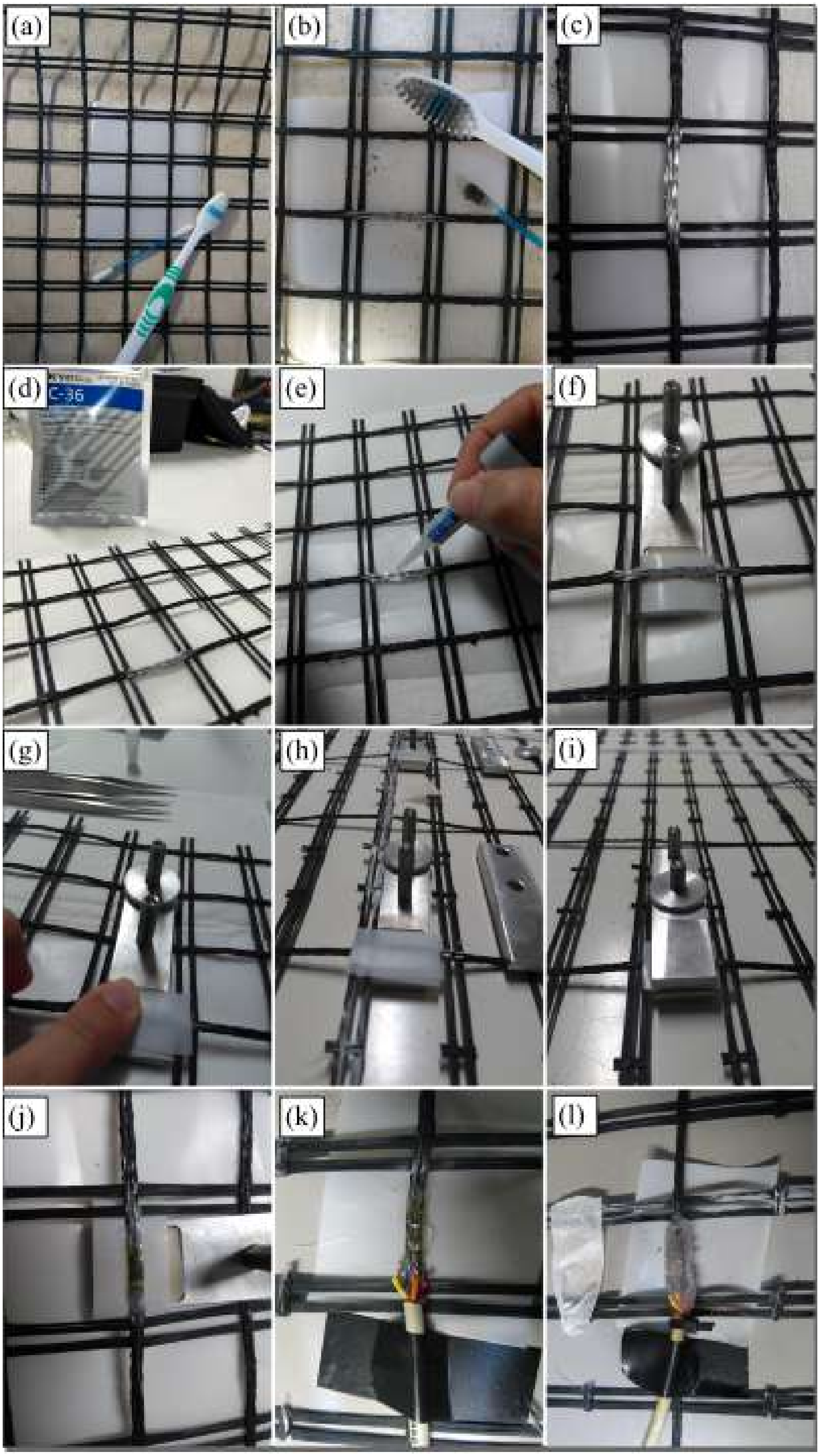

Figure 5.46: Strain-gauge installation at geogrid rib: (a) before rib PVC coating removal; (b) removal of rib PVC coating with acetone; (c) rib condition after PVC coating removal; (d) CC-36 adhesive; (e) CC-36 adhesive application on geogrid cleaned rib ; (f) rib impregnated with adhesive supported by clamp; (g) strain-gauge placement over adhesive on rib; (h) strain-gauge short after placement; (i) pressure sustained on recently bonded strain-gauge with a metal clamp; (j)strain-gauge bonded after 24-h curing, protected with a thin layer of silicone; (k) detail of wiring; (l) detail of strain-gauge protection with flexible tube filled with silicone.

5.3.4.5 Calibration of Strain-Gauges

The measurements registered by the strain-gauges bonded directly at the geogrid rib refers to local strains, that is, limited to the small area where the strain-gauge is placed. According to Bathurst, Allen, and Walters (2002) the local strain tends to be lower than the so-called global strain, measured over several geogrid apertures, since the bonding process usually generates a 'hard spot'. To convert local to global strain, which is required to reinforcement load estimation, a calibration factor (CF) that accounts for gauge type, bonding technique, reinforcement material and location of the gauge can be determined via constant-rate-of-strain, in-isolation wide-width tensile tests (ASTM, 2015), as done in the present study and described below.

Note that the loading conditions from constant-rate-of-strain, in-isolation wide-width tensile tests are not the same as the ones of the physical tests, in which the geogrid layers are loaded in a much slower rate during wall construction and in a step-load mode during surcharging, besides being in a confined state from soil burial. However, since PET geogrids tend to have much less time-dependent behaviour than polyolefin materials (BATHURST; NAFTCHALI, 2021) it was assumed that the calibration factor obtained via in-isolation wide-width tensile tests at 2% /min strain rate would be representative of the response in the physical test. As comparison, load-strain curves obtained from the calibration tests (strain rate of 2%/min) were plotted against the results from the tensile tests conducted to characterize the geogrid material presented in Section 5.1.2 (strain rate of 10%/min). The results are shown in Figure 5.47. Note that the curves are similar with no relevant difference in material behaviour due to change in the test strain rate.

In the present research a total of 5 in-isolation wide-width tensile tests were performed, at a constant strain rate of 2%/min. At each test, one strain-gauge was bonded to the geogrid central longitudinal rib at its middle section. The method for strain-gauge bonding at the geogrid rib and wiring was the same as described in Section 5.3.4.4, although for the calibration tests the set of protection casing + silicone was not used to allow better view of the gauge behaviour during geogrid elongation and of a potential gauge detachment.

Ideally, a modified geogrid sample (with two out of three longitudinal members cut out, giving a aperture transverse wide of 85 mm and $T_{ult} = 11.5$ kN/m) should be used for the calibration tests, in order to capture potential geogrid aperture size, strength and stiffness influence on the local to global strain response and to reflect as close as possible the physical test condition. However, due to size constrains of the roller clamps available at LabGsy Laboratory (maximum wide of 200 mm) it could not be possible to use a modified geogrid sample, since it would imply using less than five ribs in the cross-test direction wide as prescribed by ASTM (2015). For this reason a sample of the original product was used (aperture transverse wide of 26 mm and $T_{ult} = 26.8$ kN/m), with a specimen wide of 200 mm (7 ribs).

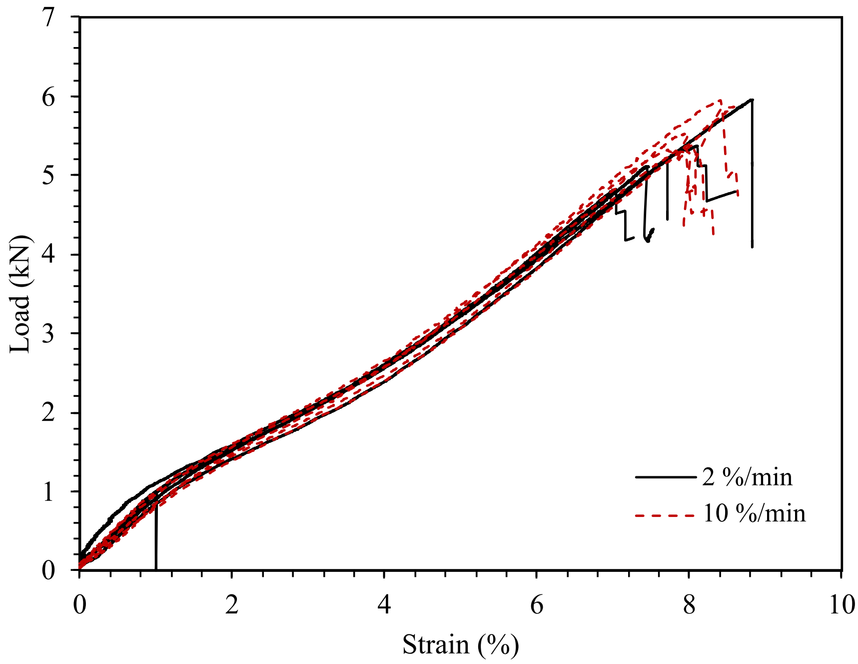

Figure 5.47: Strain-gauge calibration tests: load-strain curves from in-isolation wide-width strand tests at 2% and at 10% strain per minute (for the 2%/min tests one strain-gauge was bonded to the central geogrid rib).

The geogrid sample ends were wrapped around the testing machine roller clamps and fastened, adjusting it to maintain the instrumented rib approximately centred. Local strains were recorded by connecting the strain-gauge to a System 8000 acquisition module connected to a personal computer (Figure 5.48). During the tensile test global strains were simultaneously measured by using a video-extensometer device connected to the test machine software that tracks the relative displacement between two markers positioned along two geogrid apertures (Figure 5.49a). Measurements were taken at a frequency of 10 Hz and at a temperature controlled environment ($\sim$20°). The tests were carried on up to geogrid rupture by tensile stresses, which occurred after strain-gauge debonding (Figure 5.49b). Test results from strain-gauge readings are shown in Figure 5.50, in which strain-gauge debonding is clearly indicated by the lack of strain increase after a test time around 400 min.

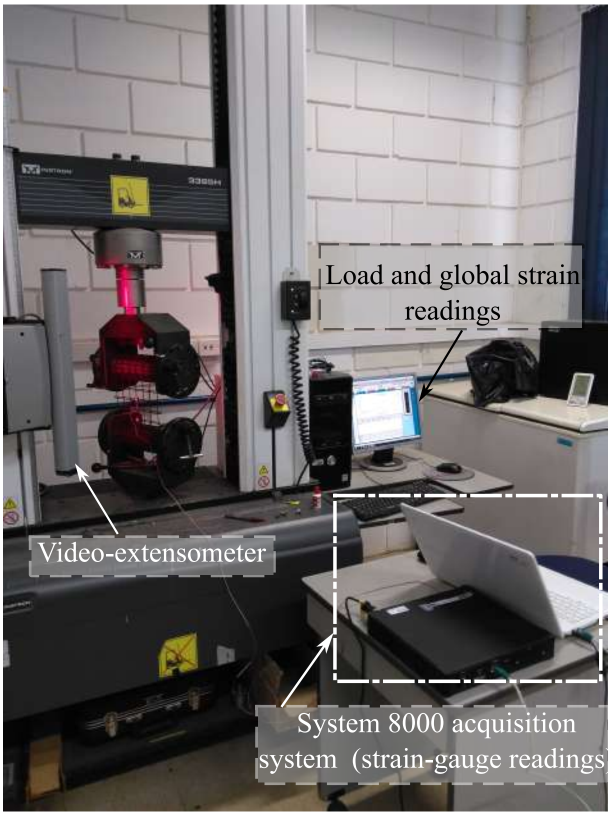

Figure 5.48: Strain-gauge calibration test set-up.

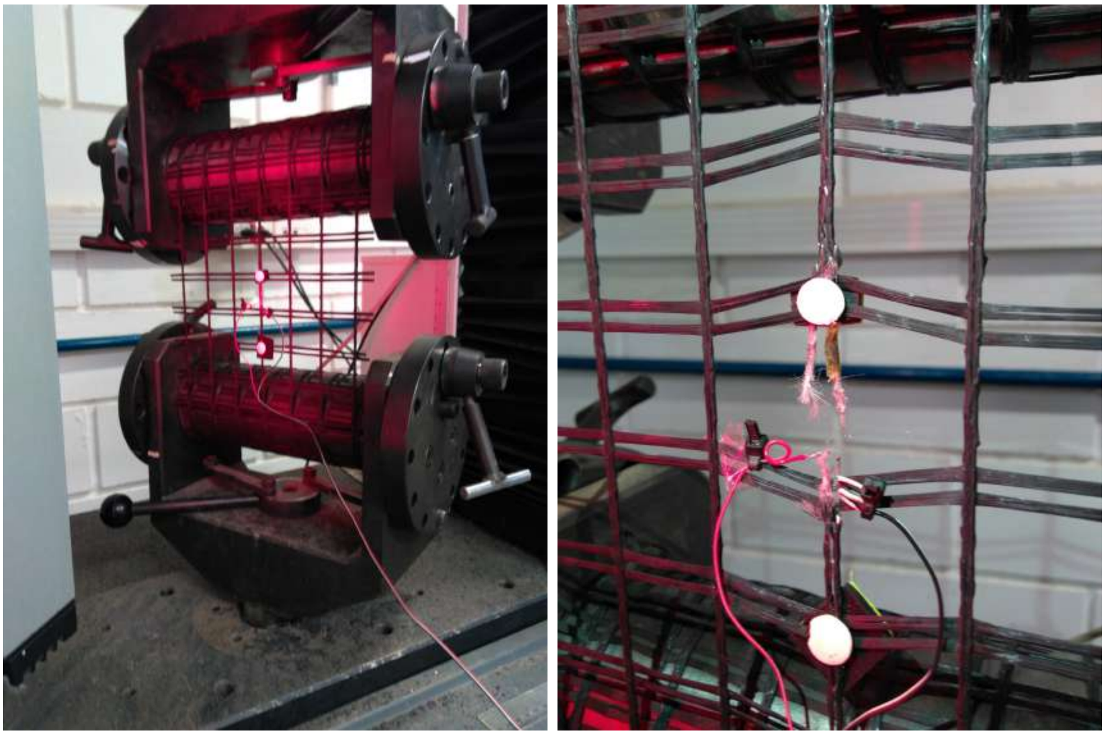

(a)

(b)

Figure 5.49: Strain-gauge calibration test: (a) geogrid mounted at the test machine (start of test); (b) geogrid after tensile failure (end of test).

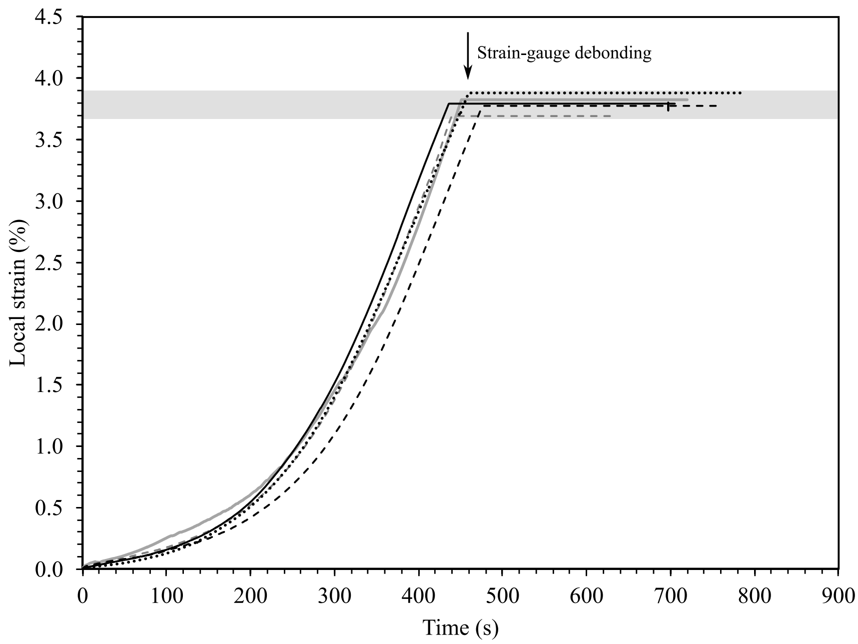

Figure 5.50: Strain-gauge calibration tests: time versus local strains with indication of strain-gauge debonding.

Figure 5.51 shows the calibration curve obtained from the tests (linear adjustment to test data), by plotting the results from strain-gage readings (local strains) against the video-extensometer measurements (global strains). Figure 5.51a refers to the measurements taken up to strain-gauge debonding, which occurred at strains around 3.5% (earlier than geogrid rupture) for all the test specimens, as shown in Figure 5.50. A calibration factor of 1.21 was obtained using a linear adjustment to the measured data. A slightly higher value ($CF = 1.37$) was obtained when considering only the strains up to 1.5% (Figure 5.51b), which represents the strain range experienced by the reinforcement at the physical test in the present research. For this reason, a $CF = 1.37$ was used to convert strain-gauge readings measured at the model wall to global strains. The evolution of the calibration factor as a function of local strain measured by the strain-gauge is shown in Figure 5.52, which shows a reducing trend of the value of CF as the local strain in the geogrid rib progress.

The values obtained in the present study are compatible with the ones found for similar materials in previous researches. Bathurst, Allen, and Walters (2002) presented results for in-isolation strain-gauge response versus global strain for a woven PET geogrid, with an index strength $T_{ult} = 16$ kN/m. The results from tests with varied strain rates (0.1 %/min, 1%/min and 2.5%/min) and tests with a constant load showed a relatively narrow band response, with a $CF = 2.2$ from the constant load test as a lower bound of the constant-rate-of-strain tests. For another woven PET geogrid ($T_{ult} = 39$ kN/m) a $CF = 1.4$ was found from the constant-rate-of-strain calibration curves, with differences being attributed to variation in product manufacture, strength, strain-gauge type and gauge adhesive. Thus the importance to obtain case-specific calibration factors.

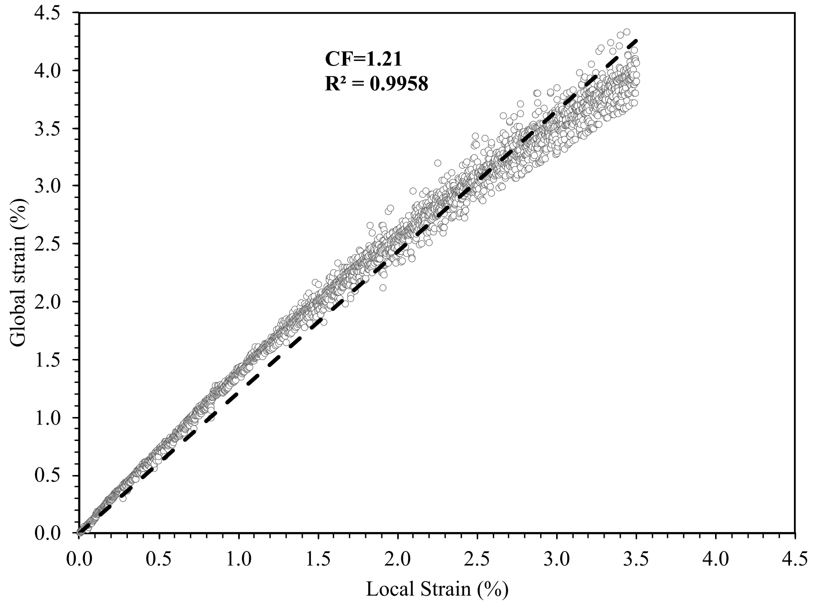

(a)

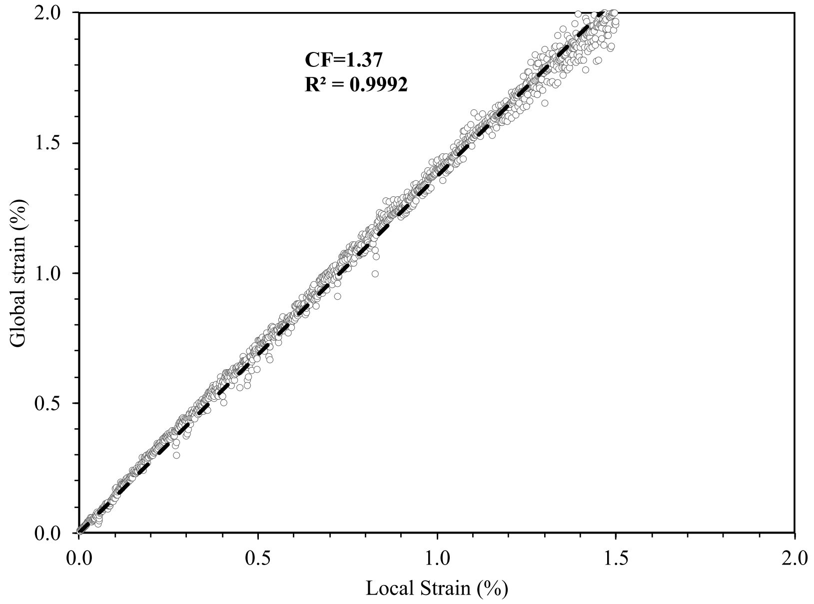

(b)

Figure 5.51: Local versus global strains test results: (a) calibration curve up to 4% local strain; (b) calibration curve up to 1.5% strain.

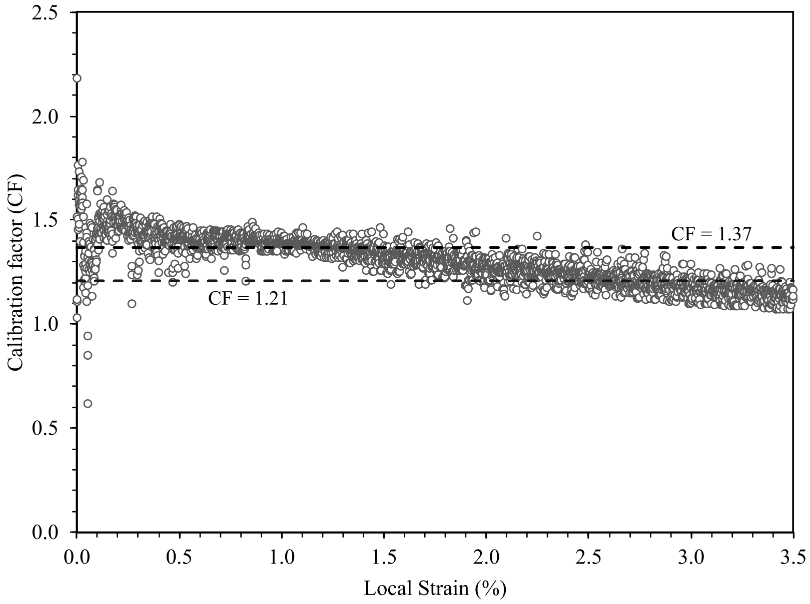

Figure 5.52: Strain-gauge calibration tests: local strain (strain-gauge reading) versus calibration factor.

5.3.5 Toe Forces

5.3.5.1 General

Horizontal and vertical forces exerted by the model wall system on the wall toe were independently measured by load cells. The vertical and horizontal toe loads were decoupled by using a set-up with three linear bearings at the base of the facing wall block, separating vertical and horizontal components of the toe force by preventing horizontal force transference to the vertical toe load cells. Further details of the toe set-up and the instrumentation are described below.

5.3.5.2 Toe set-up and instrumentation

The model wall toe set-up was designed to be as close as possible a fully restrained boundary condition and to allow independent measurements of horizontal and vertical toe forces (scheme is indicated in Figure 5.53). The base plate is a 3/8-inch steel plate (1420 mm long by 200 mm wide) fixated to the strong laboratory floor by using two parabolt anchors. Over the base plate shear-beam-type load cells (vertical toe load cells) were fixated, forming three rows with two load cells each perpendicular to the facing column (Figure 5.54). This arrangement aimed to capture possible wall facing rotation, by separately measuring vertical toe loads at the toe (front) and at the heel (back) of the footing. These load cells are commercially available (AEPH do Brasil) with a capacity of 30 kN each. The cells were connected to adjustable in height stainless steel articulated supports (30-kN capacity) to allow perfect decoupling of lateral forces during the vertical toe load measurement.

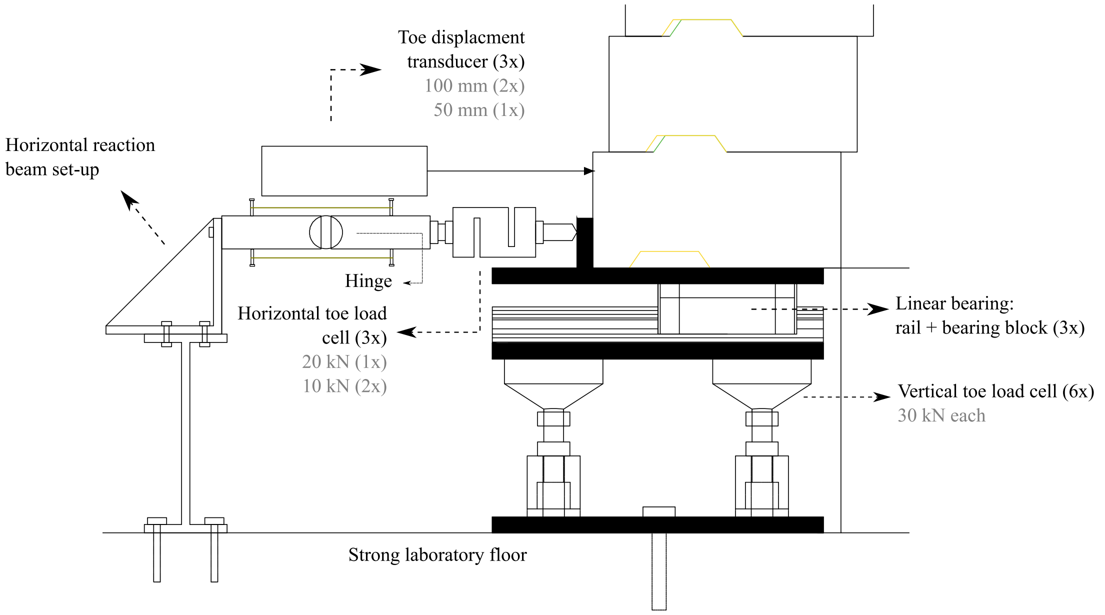

Figure 5.53: Wall toe set-up scheme.

Figure 5.54: Vertical load cells screw-mounted on the base plate of the toe set-up.

Over the six articulated supports, a second 3/8-inch steel plate was mounted (middle plate), levelled by adjusting the heights of the articulated supports. Over the middle plate, three 200-mm long linear bearings manufactured by G-motion were screw-mounted, aligned with the three vertical toe load cell rows below. Each linear bearing is comprised of one linear guide rail and a bearing block (model type HCH25), with 52-kN capacity, that allows for free movement of the facing block in the horizontal direction with minimal friction, thus providing full decoupling of horizontal and vertical toe loads.

The facing block base plate (a 3/8-inch steel plate) was screw-mounted over the bearing blocks, so it could move freely in the horizontal direction if no constraint was imposed. A steel flap (40-mm high and 1420-mm long) was welded to the facing block base plate, to provide alignment for the the first row of blocks during construction, to prevent movement between the facing block and the plate and to allow measurement of horizontal toe loads. (Figure 5.55).

Figure 5.55: Toe set-up: base plate with vertical toe load cells (bottom), middle plate with linear bearings and facing block base plate (top).

Three commercially available S-type beam load cells were used to measure horizontal toe loads developed during wall construction and surcharging. Due to LabGsy instrumentation availability, cells with two capacities were used: two cells were 10kN-capacity and one cell was 20-kN capacity. The cells were mounted on a stiff reaction beam bolted to the laboratory floor in front of the toe set-up at a sufficient distance to accommodate the load cells and the auxiliary pieces connected to the cells to guarantee force transfer without bending moments (minimize any load eccentricity in the load cell), by means of a hinge arrangement.

To ensure pre-loading of each load cell, each arrangement was placed tightly between the reaction beam and the flap at the facing block base plate, by adjusting the thread of the screw at the tip of the arrangement and in contact with the flap (Figure 5.56).

The toe arrangement was design to simulate an idealized rigid horizontal toe condition. Minimal displacement is expected though, due to cell arrangement compliance. Three strain-gauge based displacement transducers were used to measure these displacements and to allow later calculation of toe horizontal stiffness, by correlating the displacements with measured horizontal toe loads. Two of the transducers were in-house made with 100-mm stroke and the third one was a 50-mm stroke commercially available transducer, manufactured by Kyowa. The transducers were positioned around mid-height of the first block row, close to the horizontal load cells (Figure 5.57).

The vertical toe load cells were connected to System i5000 acquisition system while the horizontal toe load cells to System 8000.

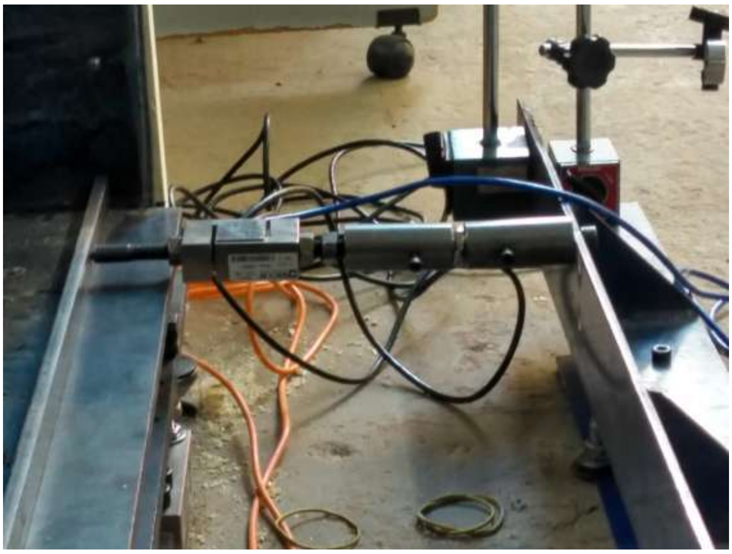

Figure 5.56: Horizontal toe load cell mounted between the stiff reaction beam and the flap at the facing block base plate.

(a) (b)

Figure 5.57: Instrumentation used to measure horizontal toe loads and horizontal toe displacements, with S-shaped load cells and strain-gauge based displacement transducers: (a) front view; (b) detail, showing displacement transducer and horizontal load cell arrangement.

5.3.6 Vertical Earth Pressures at Base of Test Facility

Pressure at the wall foundation was measured at two locations at the base of the test facility. The first cell, designated as SPC-01 was placed closer to the face (centre at 300 mm from the wall facing) while the second cell, SPC-02 was placed at the end of the reinforced zone, with its centre distant 800 mm from the wall facing.

Two confined fluid type soil pressure cells were manufactured specially for this research test program. They were designed with a diameter of 200 mm and a thickness of 7 mm, to maintain an aspect ratio (diameter/height) above 20.

Each cell was manufactured from two 304 stainless steel plates welded together around its periphery. The narrow gap between them was filled with silicon, which also filled a narrow tube connected to a piezorestitive pressure transducer responsible to convert the fluid pressure into an electrical signal, transmitted to the acquisition system via a signal cable. The cells were designed for an input voltage of 10Vcc, an output voltage of 0 to 5Vcc, with a pressure capacity of 200 kPa.

The earth pressure cells were embedded at the foundation compacted soil and placed in the horizontal position to measure vertical stresses at the foundation soil (Figure 5.58a). The installation process was carefully conducted aiming to maintain intimate contact between soil and cell throughout all its surface. First a circular hole was excavated in the foundation soil with a slightly larger diameter than the cell itself and with a depth similar to the cell's height. Second, it was excavated the region to fit the cell exit tube and transducer housing. Then the excavated hole bottom soil surface was carefully levelled and the cell put in place. To aid cell fixation, 4 screws were placed in the 4 mounting lugs around the cell's perimeter and fixated into the foundation soil (Figure 5.58b). The remaining lateral gap between the cell and the soil and between the transducer housing and the soil was filled with manually compacted soil. The transducer housing was protected with a layer of sand placed above it so the compaction of the above soil layers would not damage it (Figure 5.58c).

As recommended by Burgess (1999), based on the experience of RMC Geotechnical Group, the cells were calibrated *in-situ* by taking readings while each 70 mm lift of soil was placed and compacted (one block height). According to Ezzein (2007), the disadvantage of this method is the possible influence of boundary effects on instrument readings (specially for the cell closest to the wall facing) and the limitation of the calibration range to a maximum measured pressured of about 20 kPa as concluded by Nelson (2005) *apud* Gregg (2008), much smaller than the maximum surcharge pressure of about 150 kPa applied to the model.

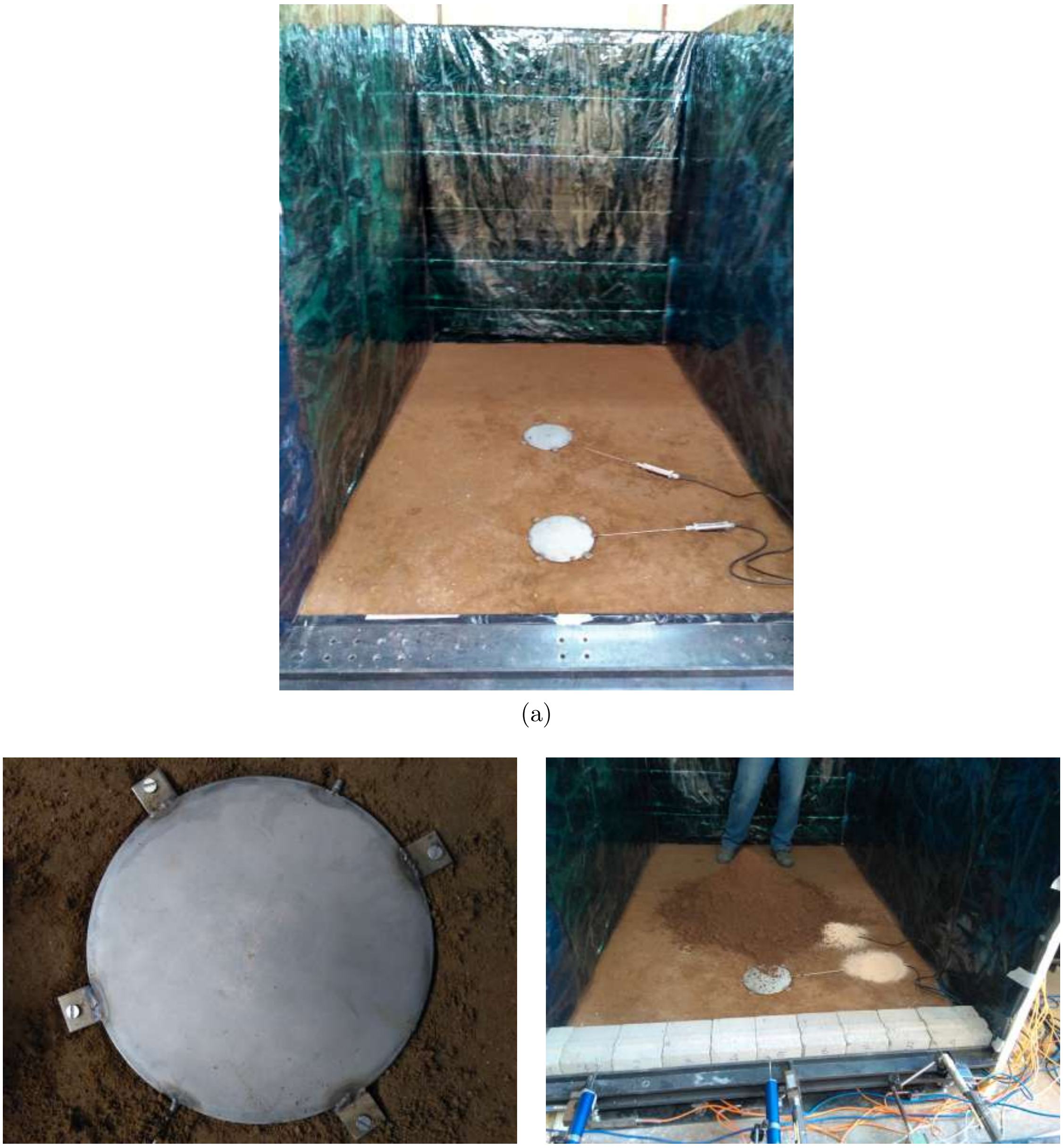

(a)

(b) (c)

Figure 5.58: Soil pressure cells installed at the foundation soil of the test wall model: (a) detail of cell arrangement; (b) detail of installed cell; (c) transducer housing protection with sand.

5.4 Testing Program and Procedure

5.4.1 General

The main goal of the Testing Program of this research was to construct, test and measure key aspects of behaviour of a Reduced Scale Geosynthetic Reinforced Soil Retaining Walls with a Frictional-Cohesive Backfill. A secondary objective was to test the model wall up to failure and compare the ultimate test surcharge to the one predicted by the design method proposed in Chapter 3 (after incorporating surcharging to the formulation), in an attempt to experimentally validate the design method. This chapter describes the construction and surcharging details of the physical test.

5.4.2 Model Wall Construction

5.4.2.1 General

The model wall was 1.47 m high and 1.42 m wide. The frictional-cohesive backfill soil was placed and compacted in 21 layers of 70 mm each (one block row) aiming for a degree of compaction larger than 95%. Five layers of the modified polyester geogrid, 1.42 m wide and 1.00 m long (behind the wall facing) were placed at pre-selected elevations in the model wall (Figure 5.25). Room temperature could not be controlled, varying in the range of 20° to 29°C during wall construction.

The construction of the model wall began on September, 9th, 2021 and took a total of 12 consecutive days for completion, with daily work shifts of approximately 8 hours. The construction history is depicted in Figure 5.59. Since this was the first model wall of this type constructed in LabGsy laboratory, it is notable the learning curve experienced during construction, with a lower rate of construction at the beginning and a speed-up from around mid-height of the wall towards the end.

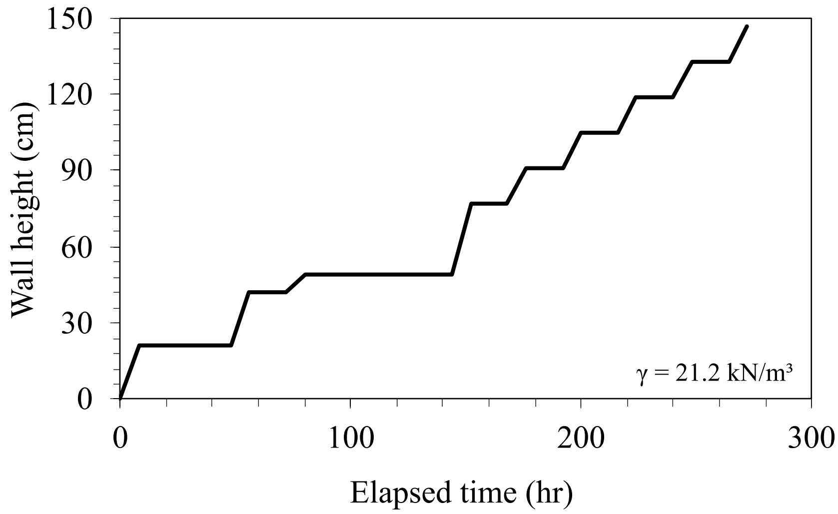

Figure 5.59: Construction history for the model wall.

Follow a brief description of the construction steps:

<u>Preparation:</u>

1. Installation of the facing blocks lateral support (plywood sheets);
2. Installation of side wall friction-reducing membranes (liners);

3. Construction of foundation base (compacted soil) and installation of foundation earth pressure cells;
4. Installation of toe set-up, with toe load cells and displacement transducers at the toe;
5. Paint markings on the rear wall to help to delimiter the elevations for reinforcement placement;
6. Zeroing of the instruments installed (toe load cells and foundation earth pressure cells).

Model construction:

1. Weighting and placement of block facing units in sequence with soil layers;
2. Mounting of the facing displacement transducer, if applicable, and setting it to zero;
3. Soil moisture adjustment and weighting;
4. Placement and compaction of soil layer (70 mm);
5. Instrumentation data register before and after each layer placement;
6. Record soil density and moisture contents between reinforcement layers (generally each 4 soil lifts), at 3 locations.
7. Placement of geogrid reinforcement layer and attachment to facing (wrapping around the above row block);
8. Connection of geogrid strain gauges to the data acquisition unit and setting them to zero;
9. Connection of extensometers to each reinforcement layer and to the acquisition unit (setting them to zero) or dead weights at the rear end of the the test box;
10. Placement of lubricated polyethylene sheet as friction-reducing liner at top of the soil backfill;
11. Installation of airbags over the top of the soil backfill;
12. Placement of non-woven geotextile as friction- reducing liner at top of the airbags;
13. Installation of plywood and MDF boards over the airbags;
14. Installation of auxiliary vertical rods to support the displacement transducers to measure soil backfill settlement;

15. Installation of test box lid;

16. Installation, over the text box lid, of the displacement transducers to measure soil backfill settlement.

Testing:

1. Initialization of all instrument readings;

2. Manual survey of wall facing and manual readings of the manual extensometers (reference);

3. Application of staged uniform surcharge by increasing pressure increments and holding each load step typically for 24h;

4. Before and after each load increment manual surveys of wall facing and manual readings of the manual extensometers;

5. Model unloading.

5.4.2.2 Preliminar Stability Analysis

To give an ideia of the stability condition of the model wall before surcharging it was conducted a preliminar slope stability analysis disconsidering the presence of the reinforcement. It was assumed a simplified planar failure surface emerging at the wall toe and it was used the Culmann's method, which expressions for the driving stress (τ_d) and for the resisnting stress (τ_r) are given in Das (2007) and are reproduced below:

$$\tau_d = \frac{1}{2}\gamma H \left[\frac{sin\,(\beta - \theta)}{sin\beta sin\theta}\right] sin^2\theta \tag{5.1}$$

$$\tau_r = c' + \frac{1}{2}\gamma H \left[\frac{sin\,(\beta - \theta)}{sin\beta sin\theta}\right] cos\theta sin\theta tan\phi' \tag{5.2}$$

where c' is the soil cohesion, γ is the soil unit weight, ϕ' is the soil effection friction angle, β is the slope angles (90° for the model wall) and θ is the angle of the planar failure surface with the horizontal.

The critical failure surface (θ_{cr}) is given by:

$$\theta_{cr} = \frac{\beta + \phi'}{2} \tag{5.3}$$

The safety factor can the be calculated by inserting the value obtained in Eq. 5.3 in Eq. 5.1and Eq. 5.2:

$$FS = \frac{\tau_r}{\tau_d} \tag{5.4}$$

Considering the soil parameters given in Section 5.1.3 and considering the model wall with a height of 1.47 m a factor of safety of 2.5 is obtained for the unreinforced model wall. Therefore, the reinforcement is expected to be mobilized only during surcharging.

5.4.2.3 Sidewall Friction Reducing Membranes

The inner walls of the test facility were treated to minimize soil/wall friction and maintain, as much as possible, plane strain condition throughout the test. First a 0.2-mm thick polyethylene (PE) sheet was fixated at the rigid walls and wiped clean with a solvent and allowed to dry (Figure 5.60a). Paint markings were drawn on the rear wall, over the PE sheet, to help delimiter the elevations for reinforcement placement (Figure 5.60c). Then a thin layer of lithium based grease was applied over the PE sheet (Figure 5.60b). A final 0.3-mm thick transparent polyvinyl chloride (PVC) sheet was placed unrestrained over the lubricated PE sheet (Figure 5.60c).

(a) (b) (c)

Figure 5.60: Sidewall Friction Reducing System: (a) fixed PE sheet; (b) placement of grease over the PE sheet; (c) placement of a PVC sheet over the lubricated PE sheet.

5.4.2.4 Compaction of Foundation Soil

Due to the toe set-up design the wall toe is positioned 160 mm above the test box floor. For this reason, it was necessary to create a 160-mm thick foundation layer over the test box concrete floor in order to level it with the facing block base plate of the toe set-up. The choice was for a compacted soil layer with minimum degree of compaction of 98% to provide a stiff foundation for the model wall. The soil used at the foundation was a clayey sand available at LabGsy laboratory and used in the research of Rincón Barajas (2016), who determined the compaction parameters by the Standard Proctor Test, obtaining $\gamma_{d,max} = 19.83$ kN/m^3 e $w_{ot} = 9.24\%$.

The soil was first sieved in a #4 automated sieve (4.5 mm) before compaction. Soil moisture adjustment was carried on before soil placement by using a concrete mixer with expedite moisture measurements via the frying pan method (D2216-19 ASTM, 2019a), which was later confirmed by the oven drying method (D4959-16 ASTM, 2016b). The soil were then placed at bags and weighted to adjust for the target layer weight (almost 1 ton). The soil bags were moved to the test box with a 2-ton capacity travelling crane.

To restrain soil lateral movement during compaction a 400-mm high temporary plywood board covered with a PE sheet was mounted at the front of the test box (Figure 5.61a). It was fixated to the toe set-up base plate with metal angle brackets and to the lateral plywood sheets (facing blocks lateral support) by screwing them together by using a wooden block. After soil compaction the temporary plywood board was removed and replaced by a 160-mm high one, to level with the wall toe (Figure 5.61b).

(a) (b)

Figure 5.61: Test box front foundation support (a) temporary support for soil foundation compaction (400 mm high); (b) permanent support (160 mm high).

The degree of compaction was achieved by using a hand-operated compactor, compacting the 160-mm layer in two lifts of 80 mm (Figure 5.62a). Final levelling of the soil foundation surface was done by manually compaction with a drop tamper (Figure 5.62b).

After foundation preparation, the toe set-up was assembled and the foundation earth pressure cells installed as described in Sections 5.3.5.2 and 5.3.6, respectively (Figure 5.58a).

(a) (b)

Figure 5.62: Foundation compaction: (a) hand operated compactor; (b) manual compactor for final adjustments.

5.4.2.5 Placement of Facing Blocks

Each facing block was individually numbered, weighed and recorded before placement in the facing wall. The blocks were assembled in a staggered (running joint) pattern, similar to the construction technique used in the field, with one layer placed before each soil lift. To guarantee fully engagement of the key connection from the start, each block was shifted forward during placement (Figure 5.63).

To prevent local overturning failure of the top blocks in the unreinforced section of the structure (above the last reinforcement) during surcharge loading the last three row of blocks was glued together with instant grout (Figure 5.64). Similar solution was used in the study of Guler and Enunlu (2009), who used ∅12mm re-bar between the modular blocks and concrete grout in the hollow space of the top blocks. Zheng and Fox (2016), when performing numerical investigation of geosynthetic-reinforced soil bridge abutments under static loading, assigned a larger tensile strength to concrete-concrete interfaces for the top three facing blocks to simulate the effect of block grouting.

Figure 5.63: Block placement at the wall facing.

Figure 5.64: Detail of instant grout used to glue together the top three rows of block.

5.4.2.6 Placement of the Backfill Soil

The soil backfill was placed in 70-mm lifts (one block row) aiming for a minimum of 95% degree of compaction.

The soil was first sieved in a #4 automated sieve (4.5 mm) close to the outdoor soil stockpile (Figure 5.65a), stored in big bags and moved to the indoor laboratory using a forklift truck. Soil moisture adjustment (Figure 5.65b and Figure 5.66) involved addition of water and was carried on before soil placement by using a concrete mixer with expedite moisture measurements via the frying pan method (D4959-16 ASTM, 2016b), which was later confirmed by the oven drying method.

(a) (b)

Figure 5.65: Soil preparation: (a) Soil sieving close to the outdoor soil stockpile; (b) Soil mixing and moisture adjustment.

Figure 5.66: Set-up for expedite determinations of soil moisture content: frying pan method.

The soil were then placed at bags and weighted to adjust for the target layer weight. The soil bags were moved to the test box with a 2-ton capacity travelling crane (Figure 5.67) and spread manually with shovels (Figure 5.68). Over 8 ton of wet soil was used to fill the test box and build the model wall (around 400 kg for each soil lift).

(a) (b)

Figure 5.67: Soil being placed at the test facility with a bag and a travelling crane.

Figure 5.68: Soil spreading before compaction.

The soil lift was manually compacted with a heavy drop hammer (15 kg), except for the region close to the wall facing (∼50-cm depth) that was compacted with a lighter drop hammer (hand-held steel plate tamper) to prevent facing displacement and uplifting of the block heel (Figure 5.69). In general, 3 passes of the hammer, with a falling height around 60 cm and with partially overlapping strokes were sufficient to achieve the target layer thickness. For the 3 upper layers of reinforcement, the lighter hammer was also used to compact a region of the first soil lift above the instrumented area of the reinforcement, since it was noticed strain-gage rupture and loss during compaction with the heavier hammer for the first two layers of geogrid.

Before placing the next soil lift the previous one was scarified to improve the contact between layers (Figure 5.70).

(a)

(b)

Figure 5.69: Soil lift manual compaction: (a) heavy drop hammer; (b) light drop rammer.

Nylon lines (mason's line) passing through stakes installed at the inner box corners were used to control the level of the soil lift. An aluminium flooring rule was used for final levelling of the soil surface.

Figure 5.70: Soil surface scarified between lifts.

At the end of each day of wall construction the top soil surface was protected with a PE sheet to reduce moisture loss until the next day of work (Figure 5.71).

Figure 5.71: Soil protection between days of work.

5.4.2.7 Installation of Geogrid Reinforcement

Each layer of geogrid reinforcement was instrumented with strain-gauges and supported by a geotextile sheet prior to installation. The geotextile sheet with the instrumented geogrid was moved into the test box and positioned behind the wall facing. Next, the geotextile sheet was slipped out from under the reinforcement and the geogrid was adjusted so 1-m long would be behind the facing and the remaining 50 cm of material would go over the row of blocks already in place (Figure 5.72).

The locking of the geogrid front end was provided by wrapping it around the immediately above row of blocks (Figure 5.73). In this way, the geosynthetic connection to the wall face is achieved by friction combined with the mechanical locking provided by the block shear key (reinforcement placed between blocks, common connection used at the field). However, with this set-up it was not possible to measure reinforcement connection loads at the wall facing.

Figure 5.72: Geogrid placement at the backfill soil by using an geotextile sheet.

(a) (b)

Figure 5.73: Geogrid connection to the wall facing: (a) before wrapping the reinforcement around the above row of blocks; (b) after wrapping it around.

After securing the connection to the wall facing, the steel wire for the extensometers (manual and automated) were attached to the geogrid as described in Section 5.3.4.2, protected with a small diameter plastic casing and connected to the draw-wire potentiometers (layer 1) or the dead weights (layers 2 to 5) placed outside the rear wall of the test box (Figure 5.74).

The draw-wire potentiometers were connected to the data acquisition system (System i5000) soon after installation. Strain-gauge cabling passed through pre-drilled holes (close to the reinforcement's elevations) at one side wall of the test box and were then connected to the data acquisition system (System 8000). The instruments were checked by applying a small manual tension on the instrumented rib to ensure a measurable response and zeroed before the next soil lift placement and compaction.

The instrumented geogrid edges were aligned with the test box and then lightly tensioned to prevent any warps or wrinkles in the material and ensure it was laid flat on the soil. To maintain the tension before the placement of the next soil lift, dead cylindrical weights were used to secure the rear end of the reinforcement in place and aligned (Figure 5.75).

The soil lift immediately above the geogrid layer was placed in sectors. First, an amount of material was placed and spread above the instrumented reinforcement. Then, the cylindrical weights that kept the geogrid in place and straight were removed and the remaining of the soil material was placed and spread. The compaction followed the procedures described in Section 5.4.2.6.

Figure 5.74: Manual extensometers connected to dead weights and draw-wire potentiometers (below) at the outside of the rear wall.

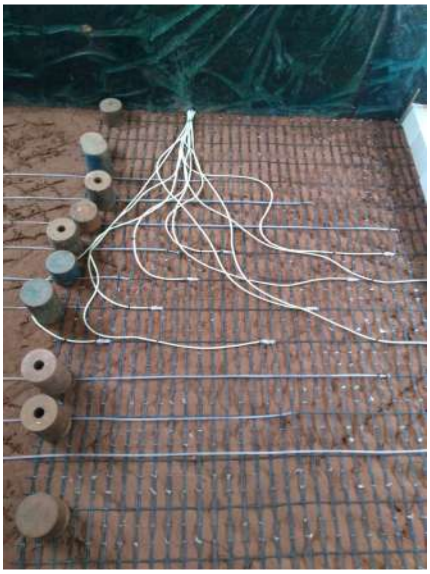

(a)

(b)

Figure 5.75: Instrumented geogrid in place before the next soil lift placement, with dead cylindrical weights securing its placement and straightness: (a) close view; (b) top view.

5.4.2.8 Compaction control

Density and moisture content were recorded with the sand-cone method (D1556 ASTM, 2016a) and the oven-dry method (D2216 ASTM, 2019b), respectively, over three locations along a diagonal. The average bulk unit weight of each layer used in the calculations is shown in Table 5.11, resulting in an overall average of 21.2 kN/m^3 with a coefficient of variation of 1.2%. Measurements were taken every four soil lifts (between reinforcement elevations), except for the first three measurements, taken after the first 3 soil lifts, as shown in Figure 5.76. Note that the last layer (layer 5) was below the target degree of compaction of 95%, however, all the remaining layers achieved high ° of compaction, above 98%. The maximum moisture deviation from optimum moisture content was -0.56%, deemed acceptable.

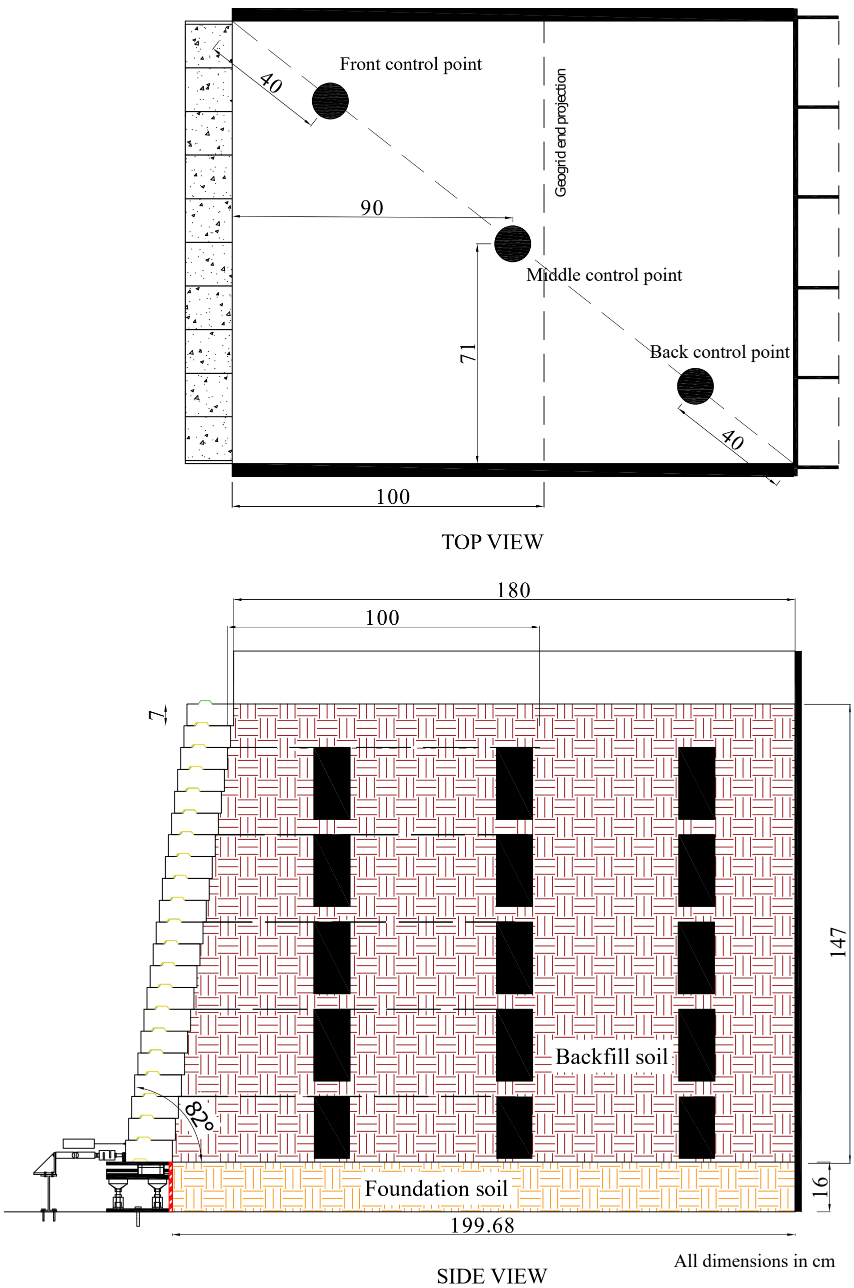

Figure 5.76: Location of density and moisture content measurements.

Layer	γ (kN/m^3)	w (%)	Δw (%)	GC (%)
1	22.33	8.82	-0.56	105.0
2	21.81	8.85	-0.53	102.5
3	21.47	9.12	-0.26	100.7
4	21.05	9.22	-0.16	98.6
5	19.48	8.82	-0.56	91.6

Table 5.11: Soil bulk unit weight and moisture content averages for each soil layer between reinforcement elevations.

5.4.2.9 Surcharging system construction

The airbag surcharging system was installed as outlined in Section 5.2.4, followed by the installation of the auxiliary rods to support the displacement transducers to measure soil top surface settlement as described in Section 5.3.3.3. Finally, each piece of the test box lid was carefully lifted with the overhead crane, positioned and aligned with the pre-drilled holes at the top surfaces of the test box side walls. After all pieces were proper aligned the screws were positioned and firmly tightened with a pneumatic impact screwdriver (total of 24 screws).

Finally, the displacement transducers used to measure soil surface settlement were installed (Figure 5.77). Its stroke tips passed through pre-drilled holes at the box lid and were positioned in direct contact with the upper flat metal piece of the auxiliary rods installed at the soil surface (Figure 5.78). A large displacement was applied at each transducer at the moment of installation to ensure that with soil settlement enough stroke range would be available to record the displacements. The instruments were then checked and zeroed. At this point, the model wall was considered to be at "end of construction" (EOC).

Prior to surcharging of the wall model the permanent support for the facing displacement transducers was installed as described in Section 5.3.3.1 and the instruments re-allocated. All instruments were re-zeroed at this point.

Figure 5.77: Displacement transducers installed at the model wall (passing through the box lid) to measure soil settlement.

Figure 5.78: Rod adapters installed inside the pre-drilled holes at the plywood and MDF boards of the surcharging set-up.

5.4.3 Surcharging

The initial surcharging of the model wall began on October, 10th, 2021. However, the model wall was unintentionally unloaded three times. The first two occasions the unloading occurred at a pressure of 75 kPa due to problems with the air compressor system and power loss in the laboratory. The third one occurred at a pressure of 90 kPa due to airbag leakage. It was then chosen to interrupt the surcharging and manufacture new airbags with stronger welds at a local company.

The re-loading of the model wall began on December, 13th, 2021 at 25 kPa. Load increments were applied in the consecutive days, reaching 150 kPa on December, 30th, 2021, when the airbag system reached its maximum capacity. A major air leakage made it impossible to proceed with wall loading to the target pressure of 200 kPa, resulting in rapid unloading of the model wall. The maximum surcharge pressured reached at the physical test was not great enough to achieve ultimate limit state for the model wall.

The entire surcharging history for the model wall is depicted in Figure 5.79, where day 0 corresponds to the first load increment applied (October, 10th, 2021). Figure 5.80 depicts the surcharging history after the installation of the new airbags, with the re-loading of the model wall (December, 13th, 2021).

The load increments were usually of 10 kPa, each one sustained for, at least, 24 hours. Only the first two increments were of 25 kPa, due to the pressure gauge resolution and precision at low pressures.

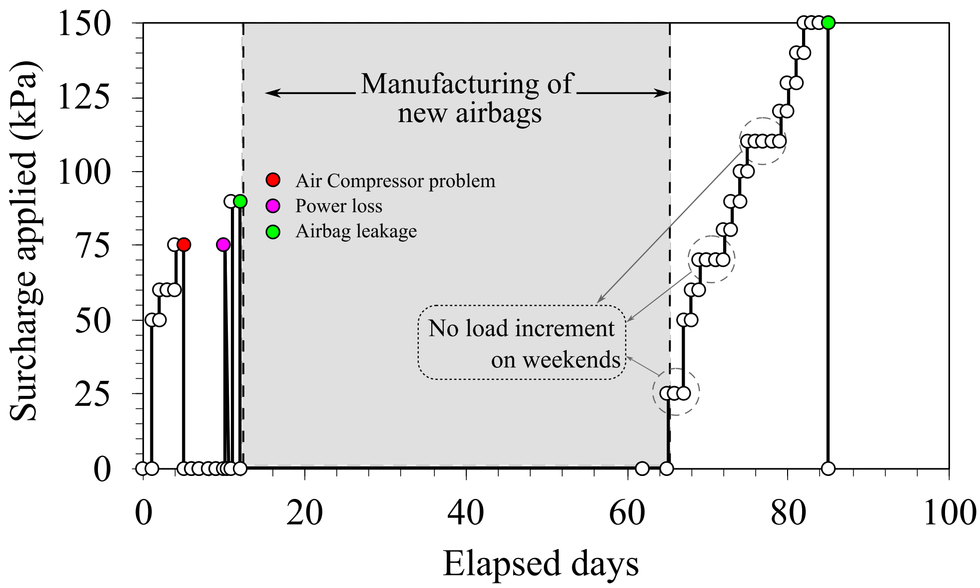

Figure 5.79: Surcharging (air pressure) history for the model wall (day 0 corresponds to the day of first loading of the wall model).

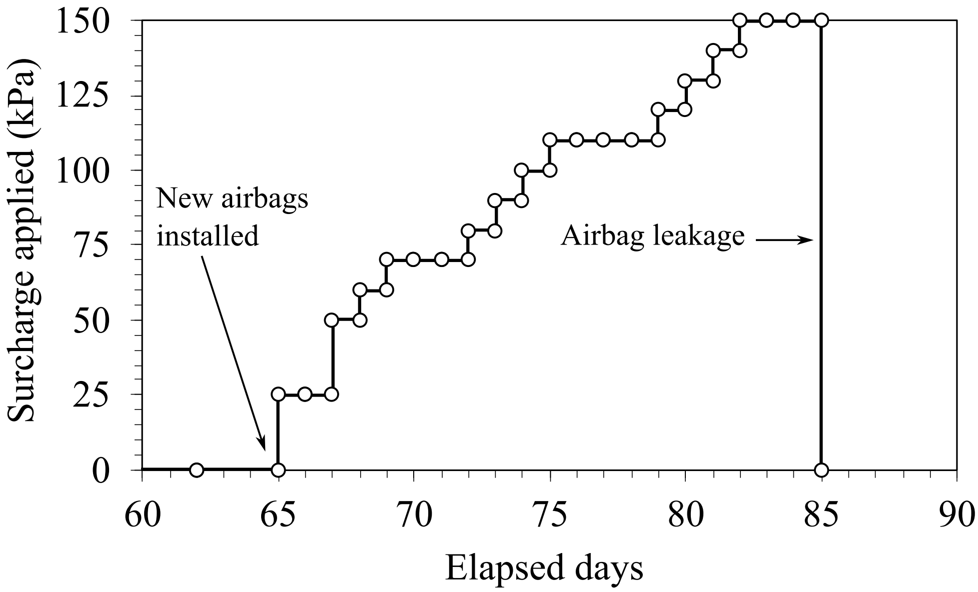

Figure 5.80: Detail of surcharging (air pressure) history after installation of new airbags.

6 Experimental Program Test Results and Discussion

6.1 General

This chapter presents the consolidated test results from monitoring model wall behaviour during construction and surcharging, along with the discussion of the data gathered. The results reported include:

1. Horizontal wall facing deflections;
2. Soil settlement at the surface of the backfill soil;
3. Reinforcement layer horizontal displacements and strain;
4. Horizontal and vertical toe loads;
5. Vertical earth pressures at the wall foundation.

During surcharging, measurements from the automated instruments were taken continuously during load application and recorded as an acquisition section called 'application'. Each load was sustained for at least 24h and the measured data in this period was recorded as an acquisition section called 'stabilization'.

In each of the following sections, if applicable, it is described the specific data filtering and treatment used to treat the measured data and exclude outliers or errors.

The time datum for the result plots was considered at the beginning of wall construction or at the end of construction (EOC), as indicated in the plots.

As outlined in Section 5.4.3 an initial surcharging attempt was made on October, 10th, 2021, that is, 22 days after the end of construction (EOC) of the model wall. However, the model wall was unintentionally unloaded three times and a considerable long period was needed to manufacture new airbags, with the surcharging re-starting only on December, 13th, 2021, 103 days after EOC. The results presented for the surcharge phase in the following sections are restricted to the measured data in this last load cycle, assuming that the previous attempts did not lead the model to experience plastic strains. Aiming to reduce the time gap between EOC and surcharging in the result plots and to facilitate the visualization, the results from surcharging were shifted back in time in the result plots.

6.2 Test Results

6.2.1 Initial Data Filtering

Readings from the automated instruments were registered every 0.1 s, periodically during construction and continuously during surcharging, which resulted in a large amount of data. Therefore, it was necessary to filter the measured data to capture relevant changes in the readings while allowing a wider spacing between measurements during periods of overall reading stabilization. A python script was written with this intention and is presented in Appendix F. The default step between readings to be recorded in the filtered data file was set to 500. The script runs through each raw data file and checks for variations between readings larger than a given tolerance to reduce the initial default step given. In this way the filtered data file captures reading variations during the physical test (smaller time intervals) while keeping a wider spacing between readings during periods of data stabilization, reducing significantly the file size and the amount of data to be handled for plotting the results.

A total of 210 raw data files was filtered, comprising measurements from 75 automated instruments during construction and surcharging and from acquisition systems System i5000 and System 8000.

6.2.2 Overall Model Wall Performance

The model wall was constructed in 12 consecutive days (8-hour work shifts) and surcharged over a period of 81 days. The long duration of surcharging was due to interruptions in load application due to problems with the air compression, airbag leakage and laboratory power loss.

The model wall was surcharged up to 150 kPa when airbag capacity was exceeded. Up to this point, post-construction (during surcharging) outward facing deflection was small, with maximum horizontal displacements around 2.6 mm (~0.2% of wall height) at the elevation 101.5 cm. The majority of the facing deflection took place during construction, with values up to 9.5 mm at wall mid-height. For this reason, facing batter at EOC deviated significantly from the designed batter of 8°.

At the end of surcharging (150 kPa) reinforcement strains up to 0.7% were recorded from strain-gauge readings while vertical and horizontal toe loads of 13.3 kN and 1.5 kN, respectively.

The maximum surcharge applied was not sufficient to reach ultimate limit state for the model wall, as intended. Although the box set up had a capacity for up 200 kPa of surcharge, the airbag capacity ended up to restrain the surcharge limit, with a major leakage after 150 kPa.

6.2.3 Soil Movement

6.2.3.1 Horizontal Toe Displacements

The toe displacement was measured over three locations along the wall toe, as described in Section 5.3.3.1. Figure 6.1 depicts the evolution of toe displacements during construction and surcharging at the left, centre and right locations of the toe monitored.

Despite being designed as a fully restrained toe, a small compliance at the toe set-up was verified, in the range of 0.4 mm to 1.0 mm. This is represented by the initial jump in toe displacements at the onset of wall construction on Figure 6.1. Similar observation was made by Ezzein (2007) when using horizontal load rings to simulate an idealized stiff toe condition, with a toe compliance of 1.3 mm. A slightly larger compliance was observed at the right and centre locations of the wall toe, indicating that the left horizontal toe load cell was better adjusted in a snug contact with the base plate flap than the other cells. Negligible incremental toe displacements occurred during construction and surcharging, indicating a stiff condition of the toe.

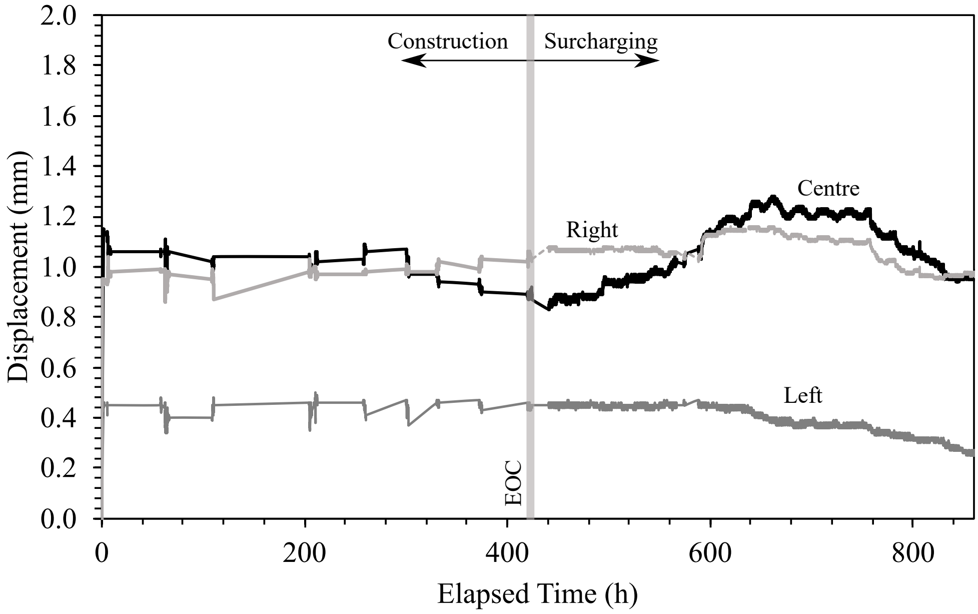

Figure 6.1: Toe displacement transducer measurements versus elapsed time (datum: start of construction).

The majority of the toe displacement and increment in horizontal toe load took place during construction, specially during placement and compaction of the first soil lifts, as shown in Figure 6.2. For the right and centre displacement transducers, it was observed a jump in displacement after compaction of the second and first soil lift, respectively. This was not verified for the left displacement transducer. Since the behaviour of the three displacement transducers were somewhat similar during wall construction, except for the initial soil lifts, there is a chance that during the process of placement and compaction of the first soil lifts the displacement transducers located at the centre and at the right of the wall facing toe were unintentionally touched and shifted from its original position.

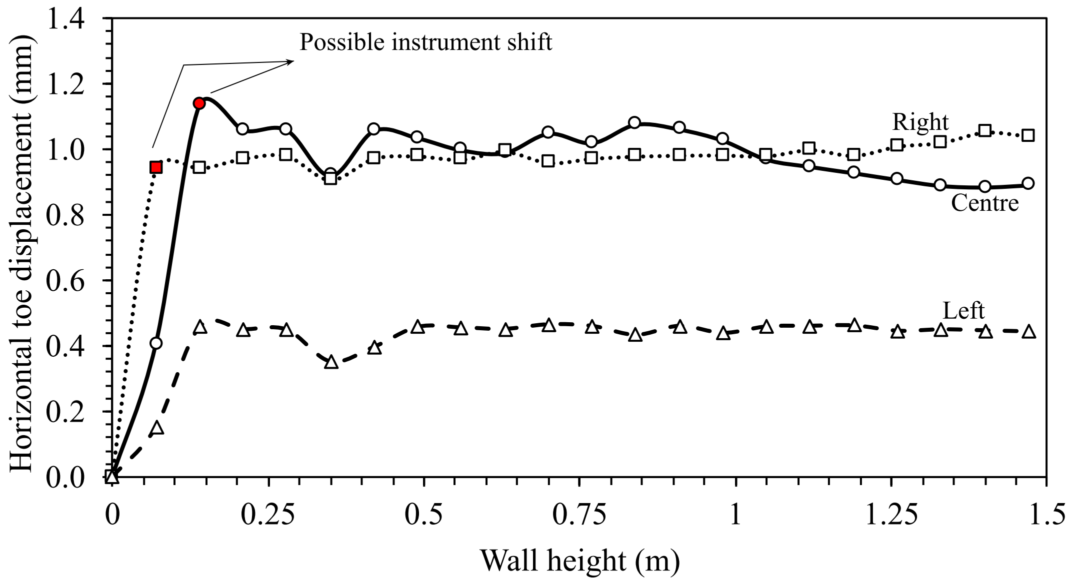

Figure 6.2: Horizontal toe behaviour as a function of wall height, during construction: horizontal toe displacements.

6.2.3.2 Horizontal Facing Displacements

As outlined in Section 5.3.3.1 outward displacement of the wall facing was monitored continuously by six displacement transducers positioned along the wall centreline and periodically by 20 points of manual survey at the facing, distributed over four vertical sections.

It was noticed frequent systematic error from the toe displacement transducers readings during wall construction, specially during the compaction of the soil lifts. Similar errors was detected for the facing displacement transducer positioned closer to the current soil lift compaction. This was attributed to possible unintended contact with the sensors or with the support transverse bars during soil compaction, shifting the transducer's zero reference. For future works it is then recommended to protect the displacement transducers at the facing, specially the toe ones. The recorded data showing systematic error was manually treated to shift the values to the original zero reference.

Figure 6.3 shows the measured relative facing displacements at different stages of wall construction and at the end of construction (EOC), while Figure 6.4 shows the evolution of the facing horizontal displacements at each measured elevation along wall construction. The representative values for each wall construction stage depicted in Figure 6.3 and in Figure 6.4 were taken as the mean value of the respective 'stabilization' acquisition section recorded after the correspondent soil lift compaction. The toe displacements depicted in these figures refers to the centre toe displacement transducer, which was aligned with the facing displacement transducers.

Since the wall facing moves during construction, the values plotted in Figure 6.3 refer to a moving datum, since they were taken at the time that the correspondent block row and soil lift were placed. Therefore the EOC curve is not representative of a wall profile at end of construction.

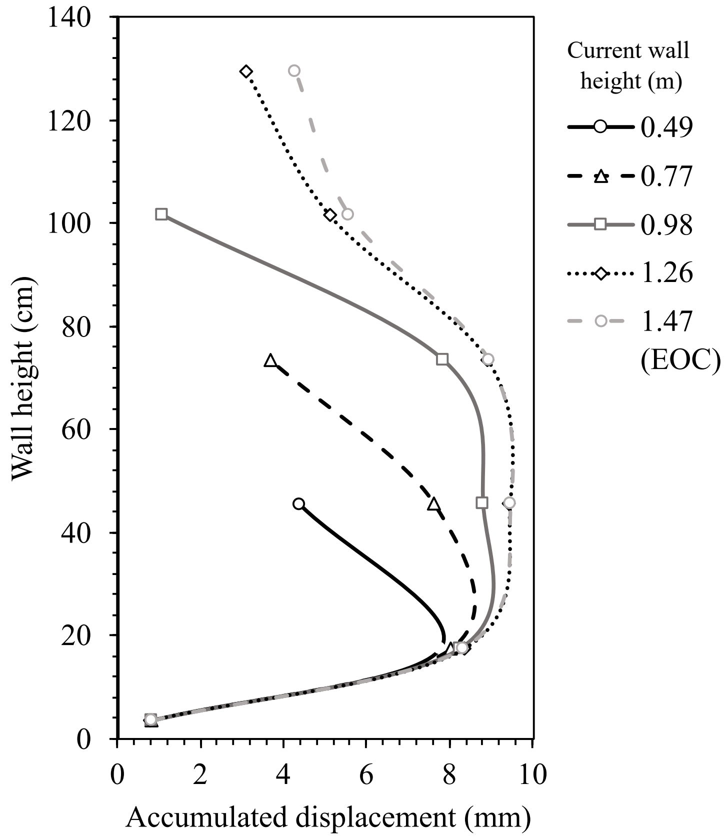

Figure 6.3: Facing displacements at different moments of wall construction (datum for each sensor refers to the placement of the respective block row at the wall facing).

From Figure 6.4 it can be seen that, during construction, the majority of the displacement at each monitored elevation occurred over the compaction process of the immediately above soil lifts, due to larger compaction-induced stresses at shallow depths. Larger displacements took place at the bottom one third of the wall height (close to reinforcement layers 1, 2 and 3), reaching almost 10 mm at the end of construction, which is equivalent to 0.7% of the wall height. Due to the nearly perfect restriction of the wall toe, the average toe displacement during wall construction presented small variation after the compaction of the first soil lifts, staying around 0.8 mm at EOC.

The displacement transducers measured only the displacements over the centreline of the wall facing, while the manual survey allowed to verify displacement non-uniformity over the facing, which is expected due to the type of facing (discrete modular construction).

Vertical and horizontal facing wall profiles at EOC are depicted in Figure 6.5 from the manual survey measurements at four vertical lines over the wall facing (A, B, C and D in Figure 5.29a), with the reference bars (Section 5.2.3.3) being mounted at a distance of 2.32 cm of the first block row face at its original position. The target facing batter

(8° in relation to the vertical) is also plotted in Figure 6.5a for comparison. From the manual survey results it is possible to verify that, as expected, displacements did not occur uniformly across the facing, especially for higher elevations, distant from the restricted wall toe. Slightly higher displacements took place at lines C and D (closer to the right side of the face), which is clearly illustrated at the horizontal facing wall profiles shown in Figure 6.5b. Note that a smaller distance to the reference bar, at a given elevation, means that the monitored point experienced a larger outward deflection.

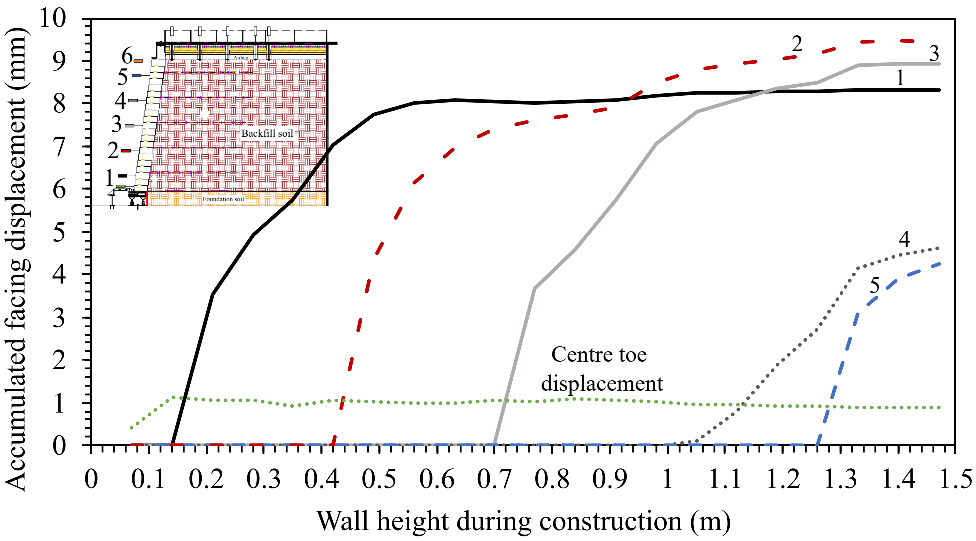

Figure 6.4: Facing displacement transducer measurements during wall construction (datum for each sensor refers to the placement of the respective block row at the wall facing).

Clearly, the displacements that took place during wall construction caused a significant deviation from the target batter (8° in relation to the vertical). Figure 6.6 illustrates this behaviour, showing maximum deviations in the range of 11.5 mm (line A) to 14.1 mm (line D) at the elevation of 130 mm (0.88H). The resultant facing batter at EOC was nearly vertical above the 7th block row (elevation 42.7 cm), specially at sections C and D located at the right side of the facing wall (indicated by the overlapped data points in 6.5b).

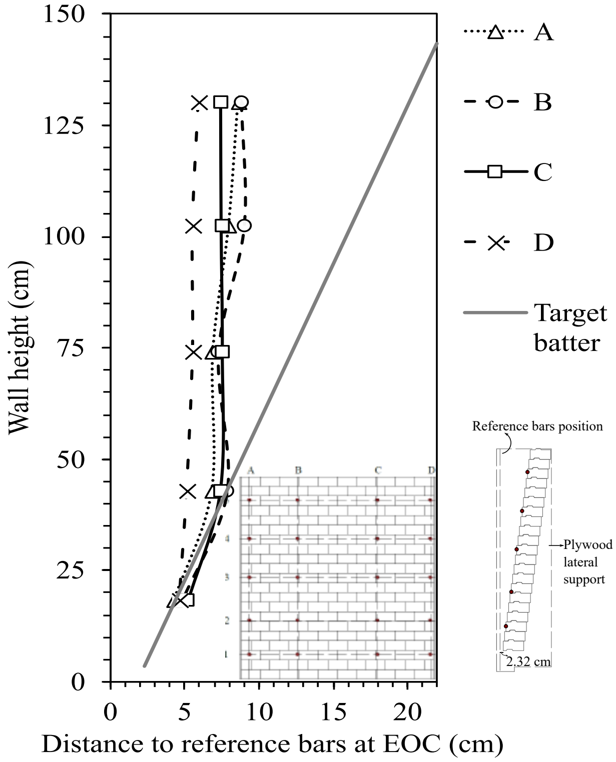

(a)

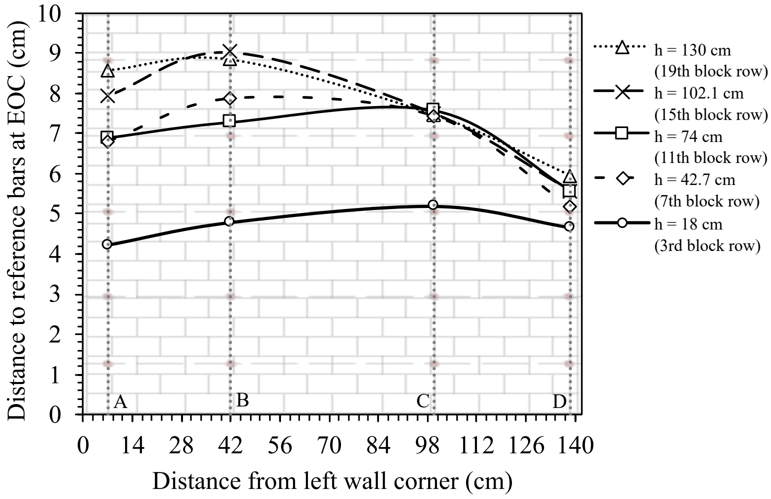

(b)

Figure 6.5: Manual survey results at EOC: (a) vertical facing profiles across the wall facing; (b) horizontal facing profiles across the wall facing.

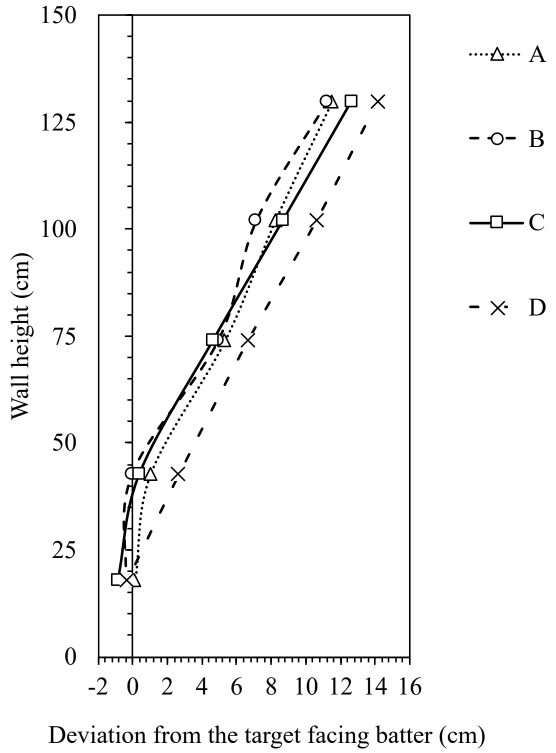

(a)

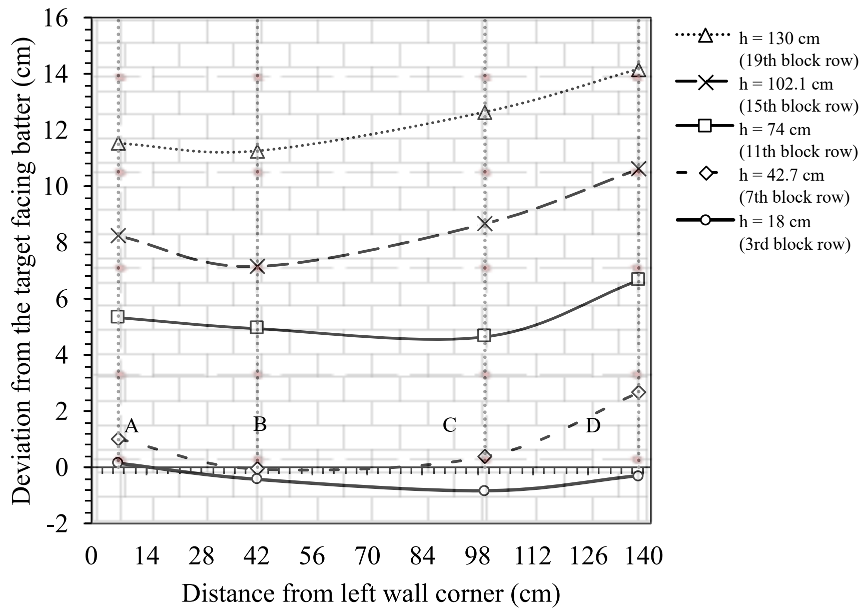

(b)

Figure 6.6: Deviation from target batter from manual survey results at EOC: (a) vertical deviation profiles across the wall facing; (b) horizontal deviation profiles across the wall facing.

The non-uniformity of the outward facing displacements can be viewed from the top view image of the wall model, shown in Figure 6.7.

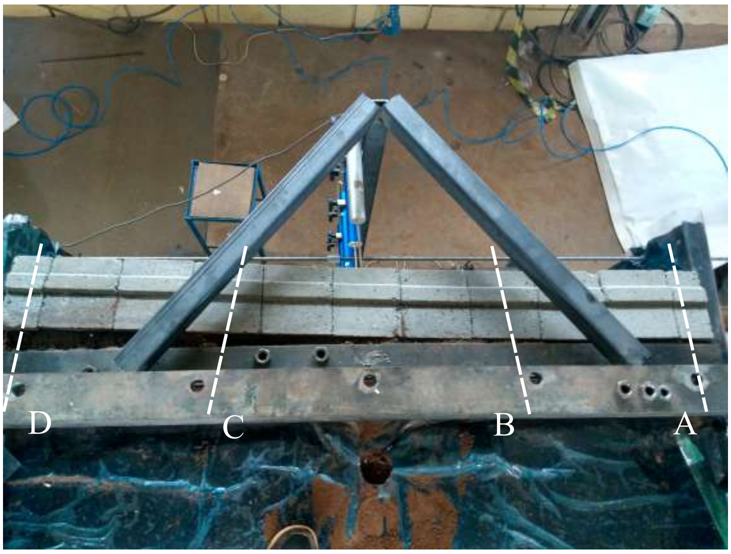

Figure 6.7: Top view of the wall facing showing the D section with larger outward deflection (left on the image).

Measurements continued to be recorded during the surcharging phase, with the displacement transducers being re-zeroed and repositioned at the fixed support as described in Section 5.3.3.1. However, during the application of the 110 kPa load increment, five displacement transducers showed anomalous behaviour, as if the wall was suddenly moving inwards (Figure 6.8a). This pattern was not validated by the manual survey results neither by the vertical toe load results and therefore it was considered as a systematic error possibly due to bumping into the transducer's support causing zero shifting. The anomalous data was treated to shift back the values to the original datum so the results could be used (Figure 6.8b). All the results presented in the following considers the corrected data.

In Figure 6.8 the representative values for each load increment were taken as the mean value of the respective 'stabilization' acquisition section record, in which the measurements after load application had already stabilized.

Figure 6.8 shows an increase in the outward wall deflection with increasing the surcharging increment, specially at layers 2 to 4 of the reinforcement, reaching maximum values around 2.6 mm. At the toe, the displacements were restricted by the restrained condition at this boundary. The displacements at the crest of the wall facing experienced an increase up to a surcharge of 110 kPa, after which it did not showed relevant incremental deflection. Similar behaviour was found by Burgess (1999).

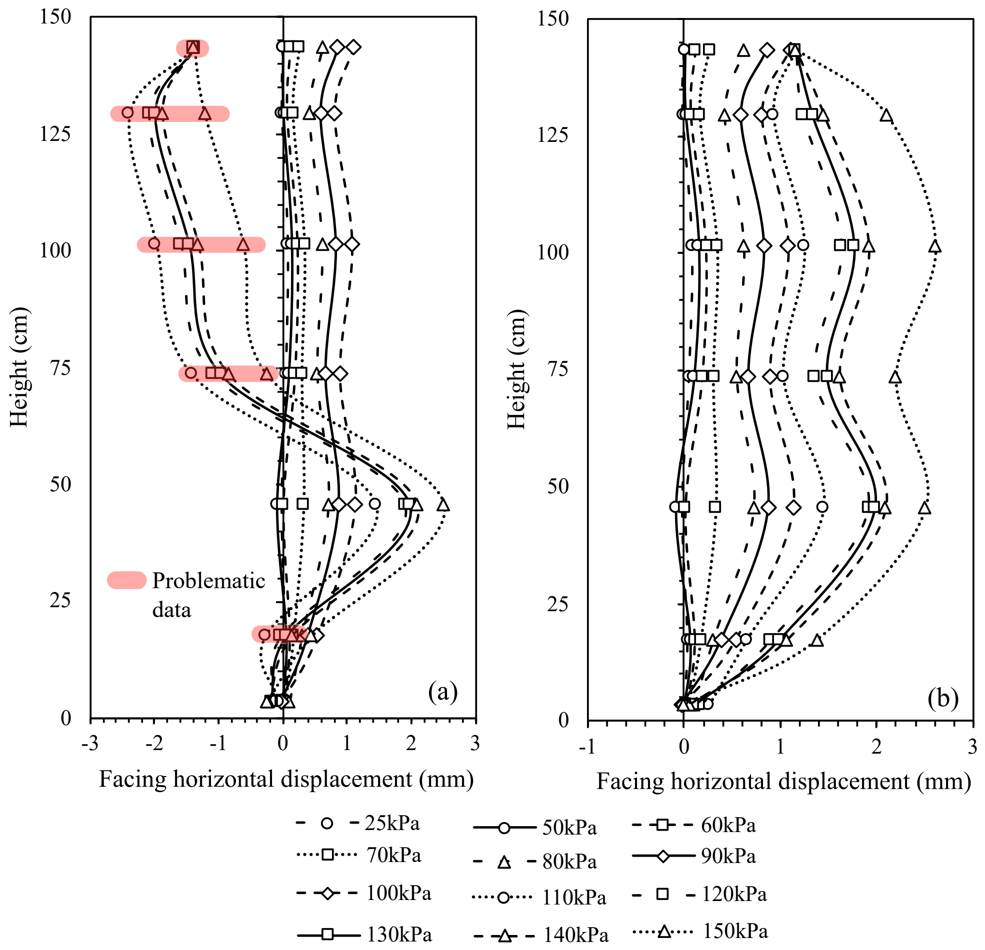

Figure 6.8: Facing displacement profiles during surcharging at wall mid-section: (a) measured data, without treatment; (b) treated data. (datum: EOC).

Figure 6.9 depicts the evolution of wall facing horizontal displacements during construction and surcharging. Clearly, the larger displacements took place during construction and compaction of the soil backfill, with the wall model being less sensitive to post-construction movements. According to Mirmoradi and Nascimento (2020) this effect can be attributed to a type of over-consolidation or pre-loading of the reinforced soil due to compaction effort. Indeed, the maximum post-construction displacements during surcharging reached a maximum of 2.61 mm at elevation 101.5 mm (reinforcement layer 4), about 70% of the wall height (0.7H). This displacement corresponds to only 0.18% of the wall height.

In Figure 6.10, registered data from manual survey during surcharging is plotted against the measurements from the displacement transducers positioned at wall mid-section for surcharging stages of 50 kPa, 100 kPa and 150 kPa. As well as in the construction phase, displacement non-uniformity across the wall facing took place during surcharging, represented by the different displacement profiles depicted in the plots for each surcharge level. Nonetheless, the displacement values at each elevation and surcharge

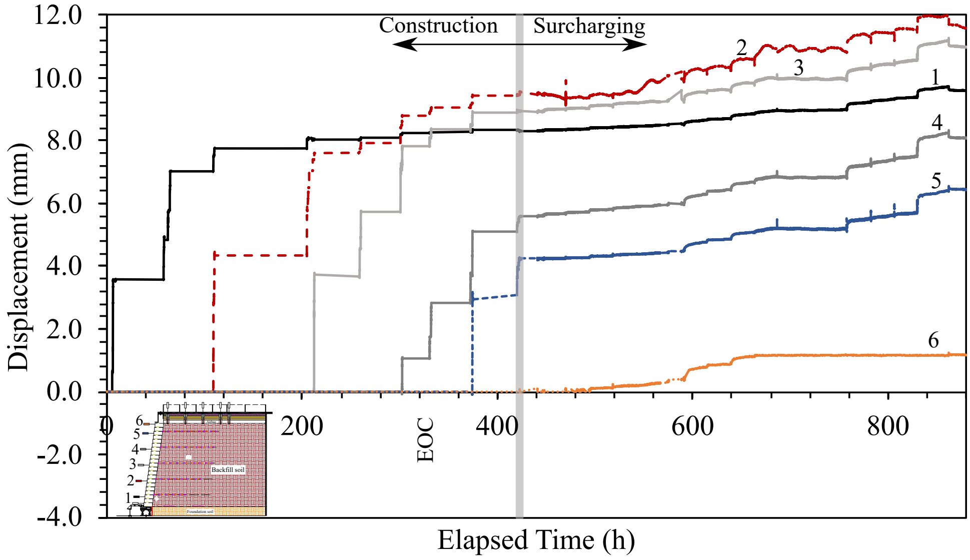

Figure 6.9: Facing displacement transducer measurements versus elapsed time (datum: start of construction).

level were of the same order of magnitude, with maximum differences around 2 mm. The largest outward deflections were registered at q = 150 kPa, at lines C and D (right side of the wall facing), locations that also presented larger displacements during construction. Overall, the displacements at wall mid-section, measured by the automated displacement transducers, have remained with intermediate values in relation to the displacement profiles measured by the manual survey. This validates the procedure described previously to correct the systematic error detected in the automated measurements during surcharging.

The small magnitude of wall facing deflections during construction and surcharging seems to indicate the the model wall was possibility under working stress conditions throughout the entire physical test, far from reaching failure. This can be attributed to the overconsolidated state of the backfill soil due to compaction effort, to the beneficial effect of cohesion on reinforced soil wall behaviour and to the influence of the restrained wall toe to carry part of the load.

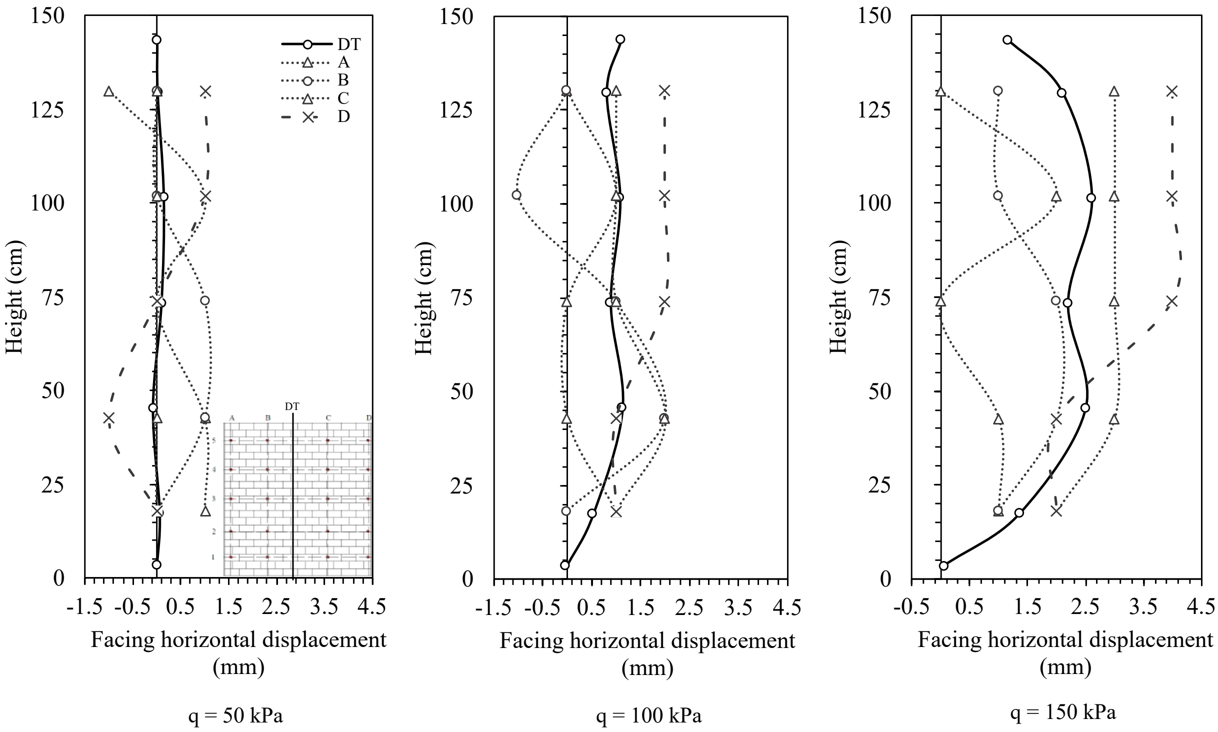

Figure 6.10: Facing displacement profiles at different stages of surcharging: comparison between manual face survey and displacement transducers (DT) measurements at wall mid-section (datum: EOC)

6.2.3.3 Soil Settlement

A set of five displacement transducers placed in contact with auxiliary rods anchored at the soil backfill (see Section 5.3.3.3 for details) were used to measure the vertical settlement of the backfill surface along a central section perpendicular to the wall facing, as shown in Figure 5.25. Figure 6.11 shows the settlement histories. The displacement transducer located at a distance of 69.5 cm from the wall facing did not registered any settlement, which was considered an error since this behaviour was not validated by the other sensors. Data from this sensor was therefore not included in the following plots.

Figure 6.12 depicts the displacement profiles at different surcharging steps while Figure 6.13 shows the evolution of soil surface settlement at each location monitored throughout surcharging. The representative values for each load increment were taken as the mean value of the respective 'stabilization' acquisition section record, in which the measurements after load application had already stabilized. Results for sensor 1, located closer to the wall facing at a distance of 7.5 cm, showed outliers throughout the test, but overall after a initial displacement around 12 mm at the beginning of surcharging the settlement remained somewhat constant. There is not an definitive pattern from the results plotted and no conclusive behaviour could be drawn from the data gathered.

There is a chance that the steel rods used to support the displacement transducer tips have rotated during surcharging, compromising the measurement of independent vertical movement of the soil surface.

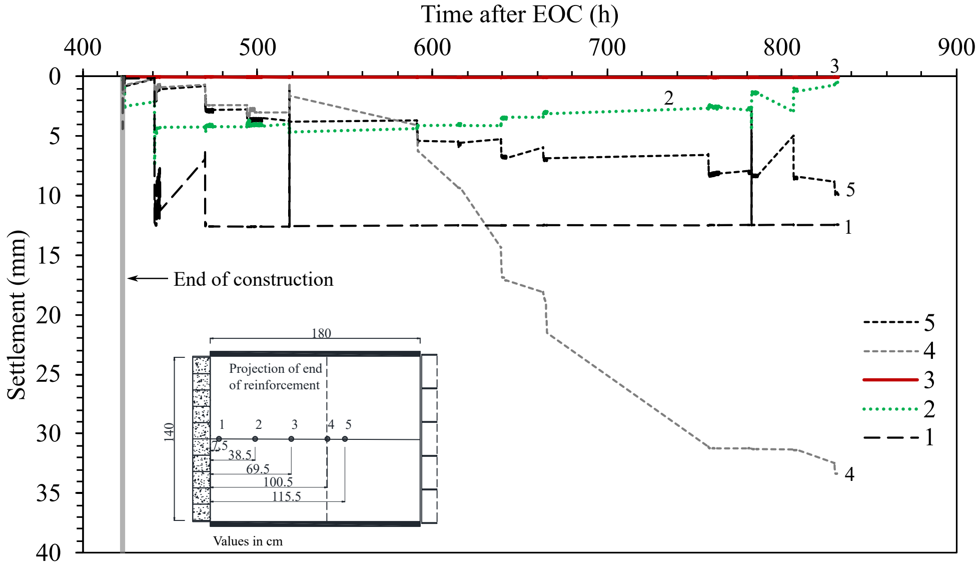

Figure 6.11: Soil surface vertical settlement versus elapsed time.

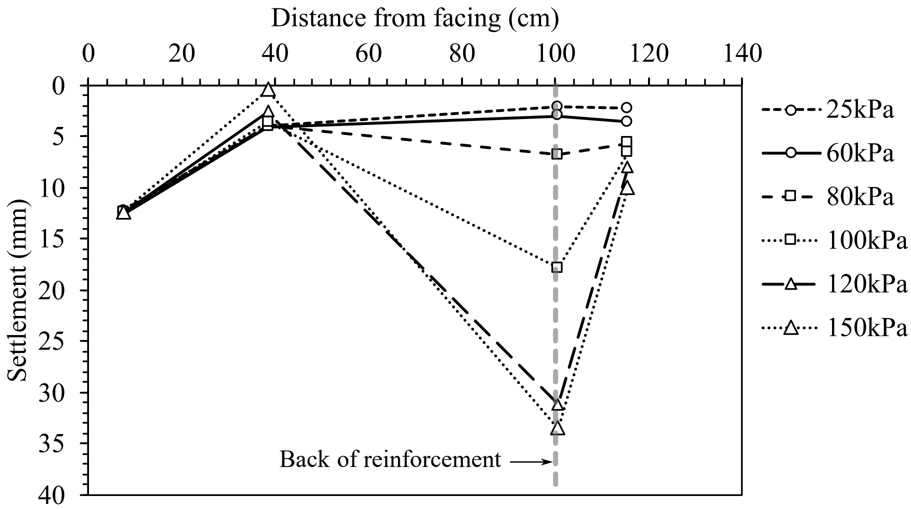

Figure 6.12: Soil surface settlement profiles at different surcharges.

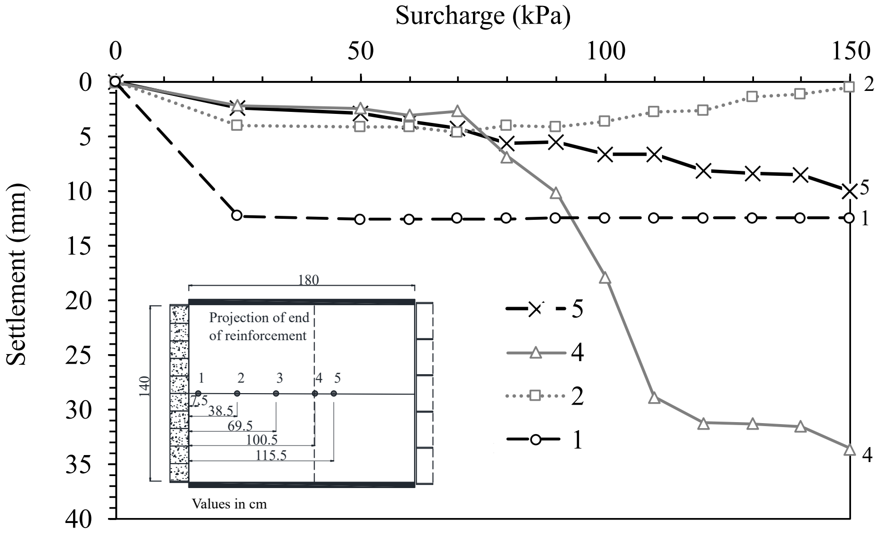

Figure 6.13: Evolution of soil surface settlement at different locations with surcharging.

6.2.4 Toe Forces

6.2.4.1 Vertical Toe Loads

Six load cells located under the wall facing were used to record decoupled vertical toe loads during wall construction and surcharging. Figure 6.14 depicts the time history of the total vertical toe load (sum of the six vertical load cells). Also shown in this figure is the sum of the three front load cells (toe), of the three back load cells (heel) and the facing self-weight (sum of all block measured weights across the full 1.42 m width of facing).

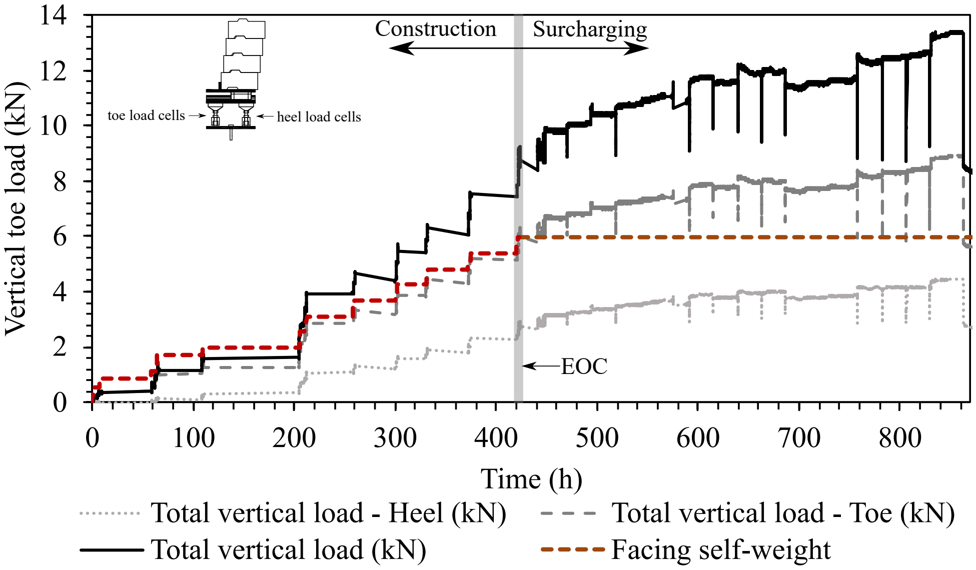

Figure 6.14: Total vertical footing loads versus time (EOC: End of Construction).

The vertical toe load increased with each soil lift during wall construction and with each new load increment during surcharging, remaining essentially constant during the stabilization periods (load sustained). The abrupt reading drops during surcharging occurred due to the problems with the airbags encountered during the test to sustain the surcharge pressure. At the end of construction (EOC), the total vertical toe load was approximately 8.3 kN while the full facing weight was around 5.96 kN, which is about 72% of the measured load. This is attributed to downdrag forces between the backfill soil and the back of the model blocks, which transfers vertical loads to the toe. The result of recorded vertical loads exceeding the facing self-weight has also been measured in previous experimental studies including large-scale field and laboratory tests (BATHURST, R.J.; WALTERS, D., et al., 2000; BATHURST, R.; WALTERS, et al., 2001; EZZEIN, 2007; GREGG, 2008; BURGESS, 1999; RICCIO; EHRLICH; DIAS, 2014), centrifuge tests (ZHANG; CHEN; YU, 2019) and numerical modelling studies (KARPURAPU; BATHURST, 1995; KERRY ROWE; SKINNER, 2001; HATAMI; BATHURST, 2005, 2006; MIRMORADI; EHRLICH, 2015b). However, it is worth noting that this behaviour was verified for walls with competent foundations. As indicated in the studies of Skinner and Rowe (2003), Ezzein (2007), Damians, Bathurst, Josa, and Lloret (2014) and Yoo and Song (2006) the foundation stiffness influences the amount of extra load carried by the toe, with a stiffer base yielding a higher force at the toe.

The majority of the vertical load was carried by the toe (front load cells) indicating wall rotation around the horizontally restrained toe of the wall. At EOC only 31% of the vertical load was carried by the wall heel, with a slightly increase at maximum surcharge, 33%. This indicates that wall rotation occurred mainly during wall construction.

At maximum surcharge (150 kPa) the total vertical toe load was approximately 13.3 kN, corresponding to 2.2 times the wall facing self-weight.

Figure 6.15 shows total vertical toe load results during construction while Figure 6.16 shows post-construction total vertical and horizontal toe load results versus surcharging pressure. The representative values for each load increment were taken as the mean values of the respective 'stabilization' acquisition sections record, in which the measurements after load application had already stabilized. Also shown in the figures is the facing self-weight, calculated by summing up the recorded weight of each block of the facing column at the respective wall height considered. As a general observation, it can be noted that the horizontal component of toe load reaction was less than the vertical component. Vertical toe load increased as the surcharge increased, achieving 160.7 % of post-construction load at 150 kPa of surcharge pressure.

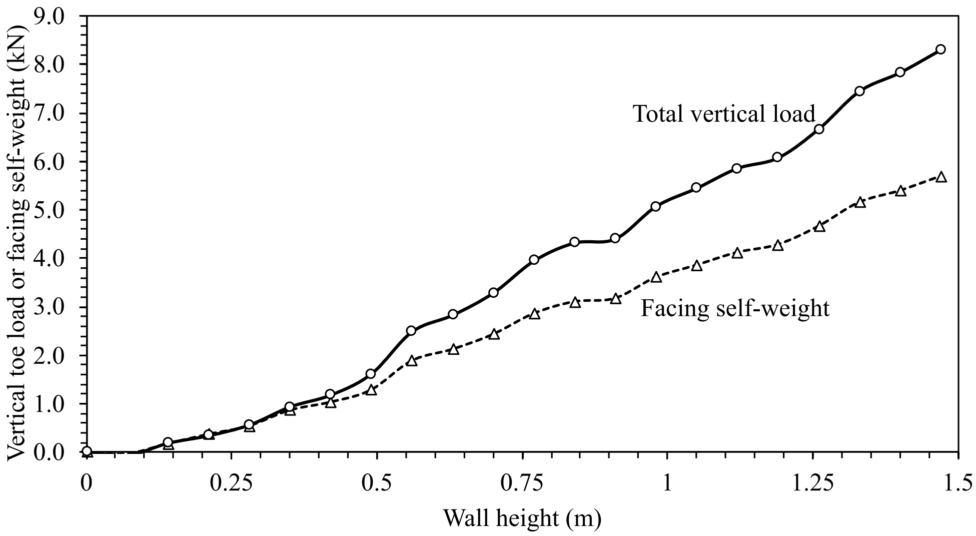

Figure 6.15: Toe vertical load as a function of wall height, during construction.

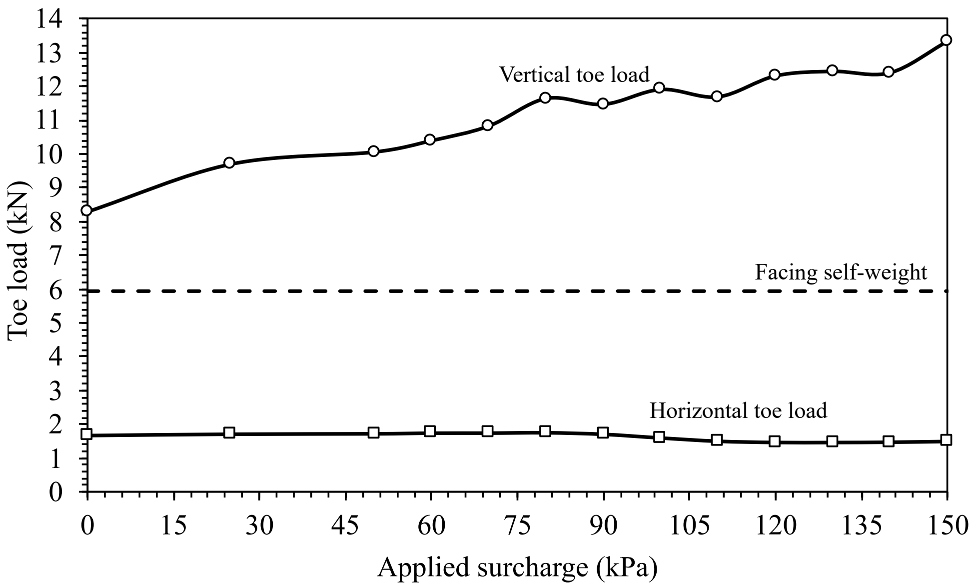

Figure 6.16: Total vertical and horizontal toe loads as a function of surcharge pressure.

6.2.4.2 Horizontal Toe Loads

Three load cells mounted horizontally against the toe were used to record decoupled horizontal toe loads during wall construction and surcharging (see details in Section 5.3.5.2). Figure 6.17 depicts the time history of the total horizontal toe load (sum of the three horizontal load cells). Individual readings of each cell are also depicted in this figure. Oddly, the load cell located at the right side of the wall facing recorded negligible readings compared with the other two cells, that measured similar forces during the test. This was not expected, since the toe displacement results showed in Figure 6.1 at Section 6.2.3.1 indicated outward displacement of the toe at the three monitored locations, which guarantees that the snug contact between the cell and the facing block was not lost. As discussed in Section 6.2.3.1 there is a chance that during the process of placement and compaction of the first soil lifts the displacement transducers located at the centre and at the right of the wall facing toe were unintentionally touched and shifted from its original position. The evolution of horizontal toe displacements and loads during construcion and surcharging is shown in Figure 6.18 and in Figure 6.19, respectively. Toe displacements and loads were much less sensitive to surcharge than to wall construction.

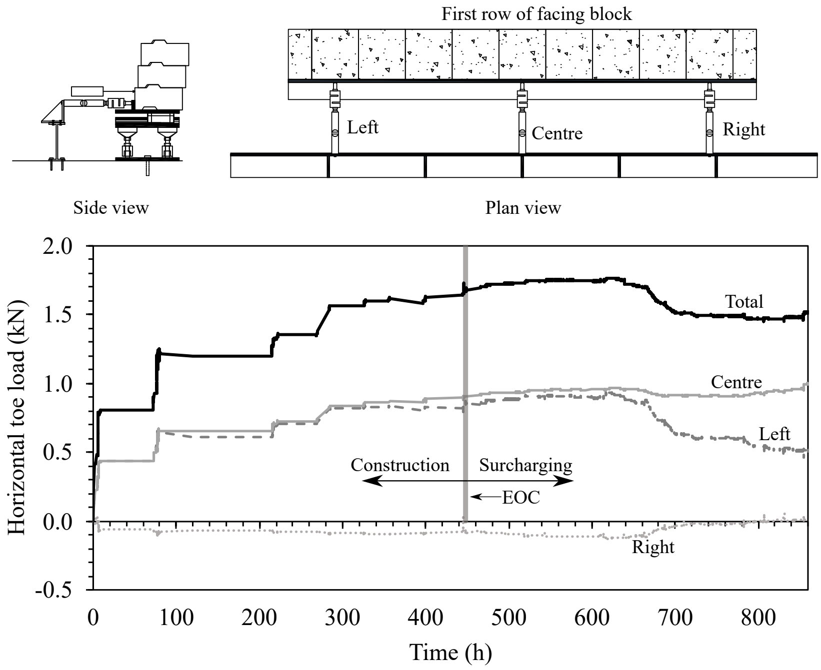

Figure 6.17: Total horizontal footing loads versus time (EOC: End of Construction).

Figure 6.20 shows the total horizontal toe load results during construction, which corresponds to the sum of the three load cells used to monitor horizontal toe loads. Horizontal toe load was practically constant during surcharging and similar to post-construction loads. A small decrease trend, however, was observed after the surcharge level of 80 kPa with a peaking up in load after the surcharge of 120 kPa, as detailed in 6.20b .

In previous studies that evaluated model wall behaviour under a condition of a fully restrained toe, horizontal toe load (EZZEIN, 2007) was more sensitive to surcharge pressure when compared with what was found in the present study. Gregg (2008) found that 35% of the peak horizontal toe load at 120 kPa of surcharge occurred during surcharging, with an increase at horizontal toe load immediately after applying each surcharge increment followed by a small increase with time. The author used a sand-silty soil with 60% of fines (passing sieve #200) with an average degree of compaction (measured) of 91,5%, based on measured bulk unit weight and soil moisture content during wall construction and the results from standard proctor tests. Ezzein (2007) found that 35.7% of the peak horizontal toe load at 41 kPa of surcharge occurred during surcharging for the model wall with the stiff toe (Wall 8). The difference in behaviour is possibly explained by the contribution of soil cohesion on resisting load, reducing the amount of load at the wall toe.

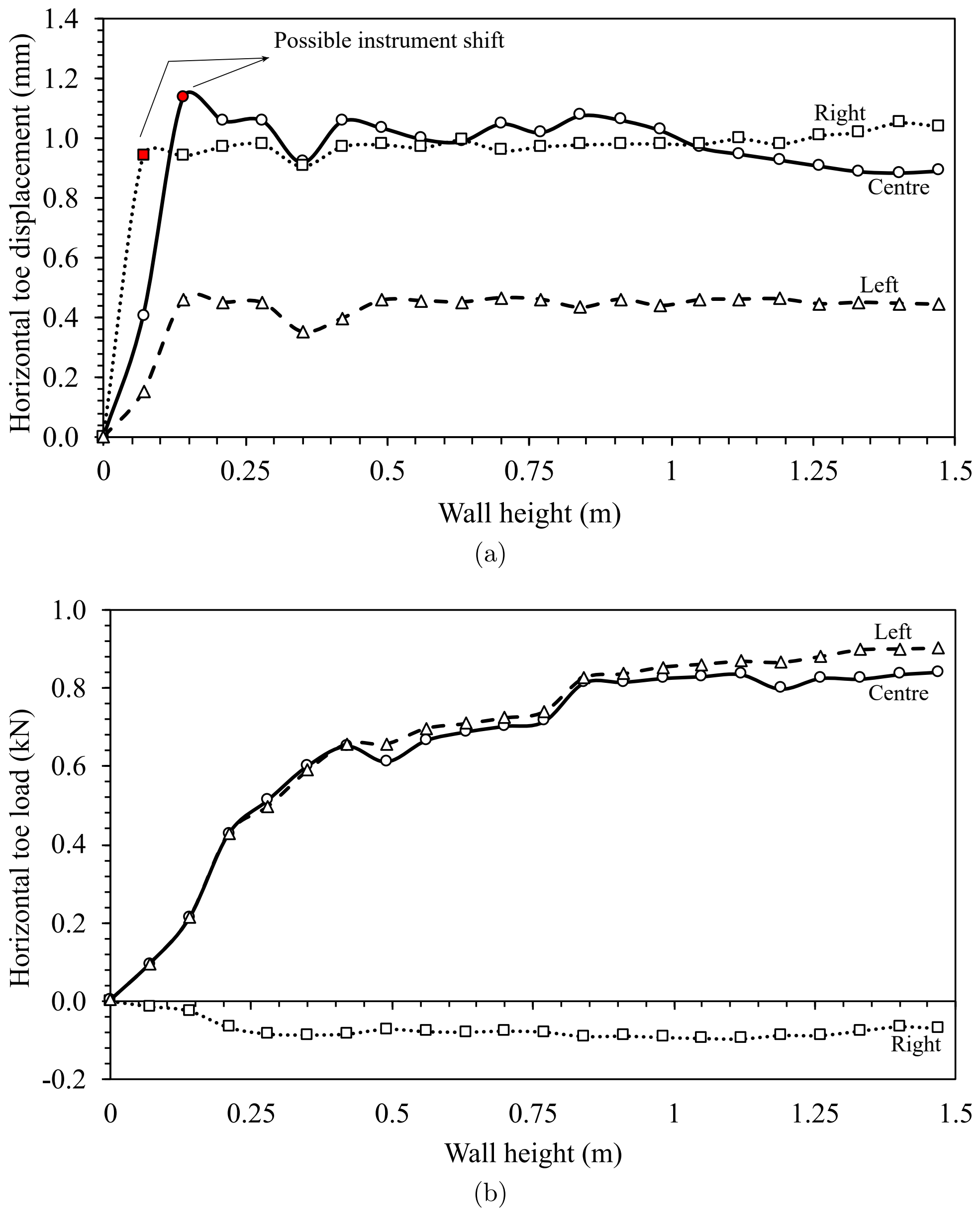

Figure 6.18: Horizontal toe behaviour as a function of wall height, during construction:. (a) horizontal toe displacements; (b) horizontal toe loads.

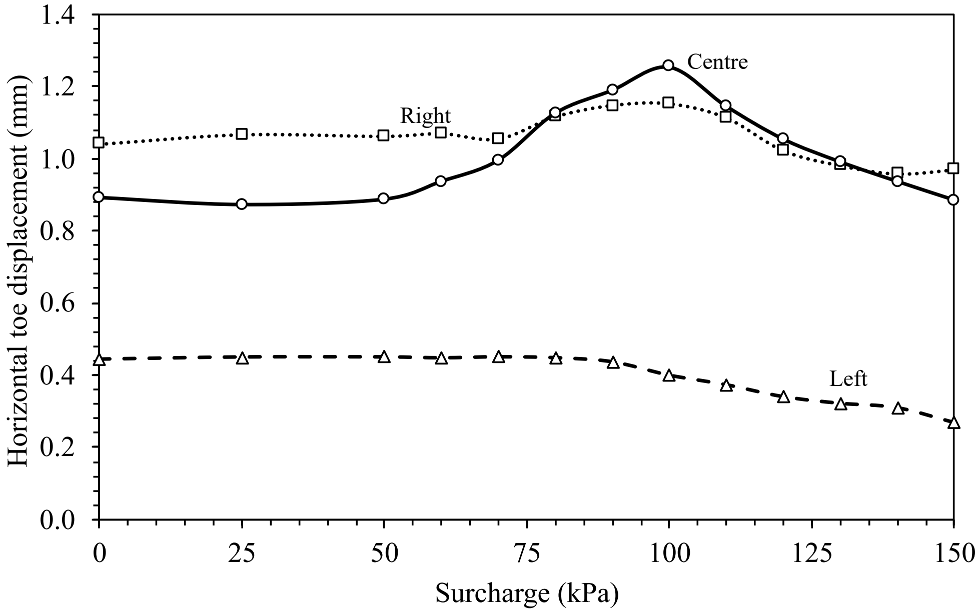

(a)

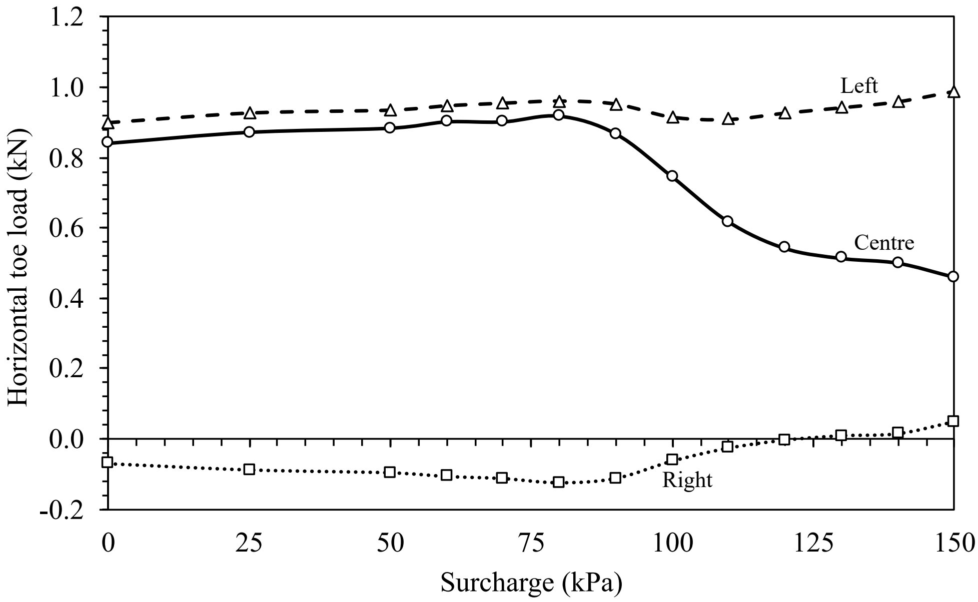

(b)

Figure 6.19: Horizontal toe behaviour as a function of wall height, during surcharging: (a) horizontal toe displacements; (b) horizontal toe loads.

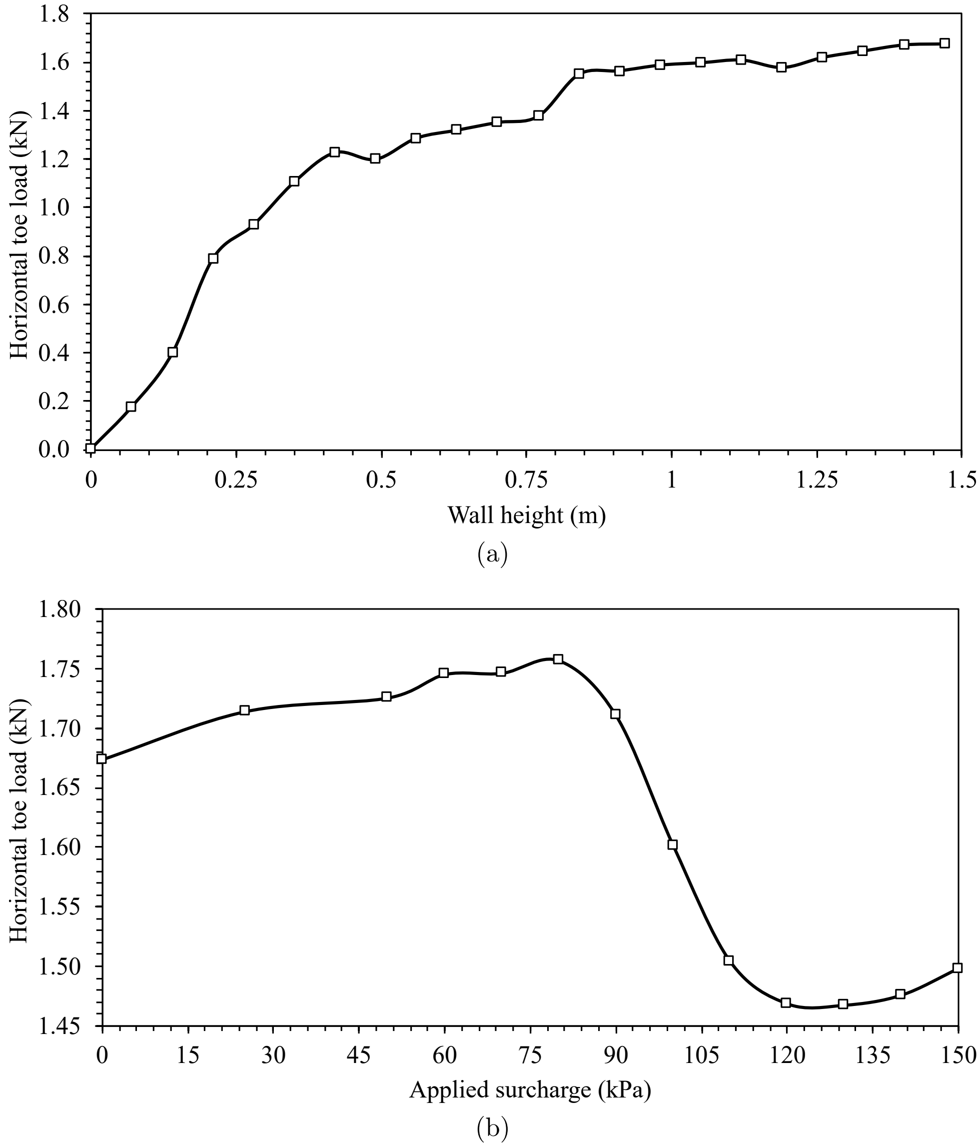

Figure 6.20: Total toe horizontal load (a) during construction; (b) during surcharging.

6.2.4.3 Horizontal toe stiffness

Considering the issues discussed related to the horizontal toe load measured at the right toe load cell and the possible shift in the right and centre displacement transducers, the horizontal toe stiffness (horizontal toe load / horizontal displacement), K_{toe}, was calculated considering only the coupled results of the toe load cell and the displacement transducer located at the left of the wall facing toe. Figure 6.21 shows the evolution of horizontal toe stiffness during construction and surcharging, with mean values of 1.59 MN/m and 2.46 MN/m, respectively. These are representative of a toe stiffness of 1.12 MN/m/m and 1.73 MN/m/m, considering the wall width of 1.42 m. These values are in the same order of magnitude as the value back-calculated by Ezzein (2007) for a model wall of similar dimensions: the author found a value of 0.96 MN/m for the 1.51-m high model wall that represented the stiffest toe condition (Wall 8) studied by him.

The knowledge of K_{toe} is of particular interest to conduct future numerical analysis of the model wall, since this is a boundary parameter that can help on model calibration.

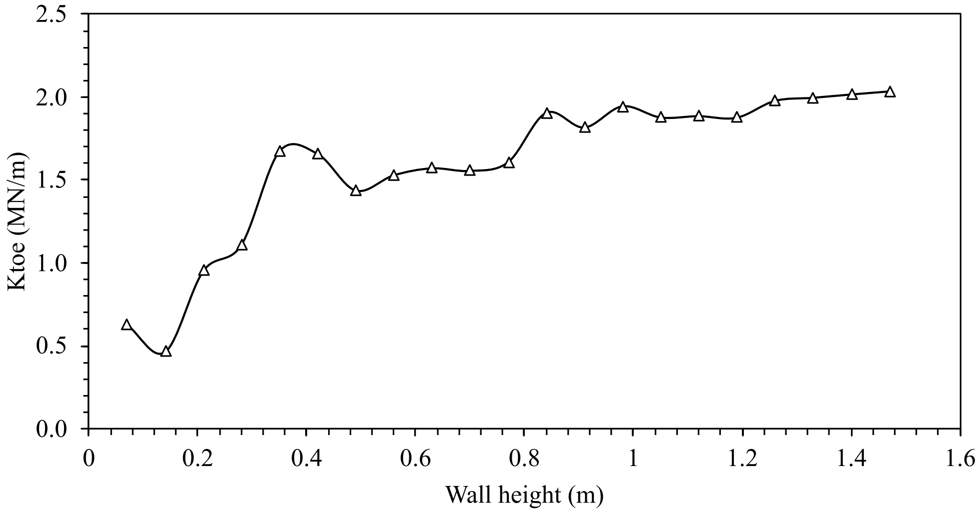

(a)

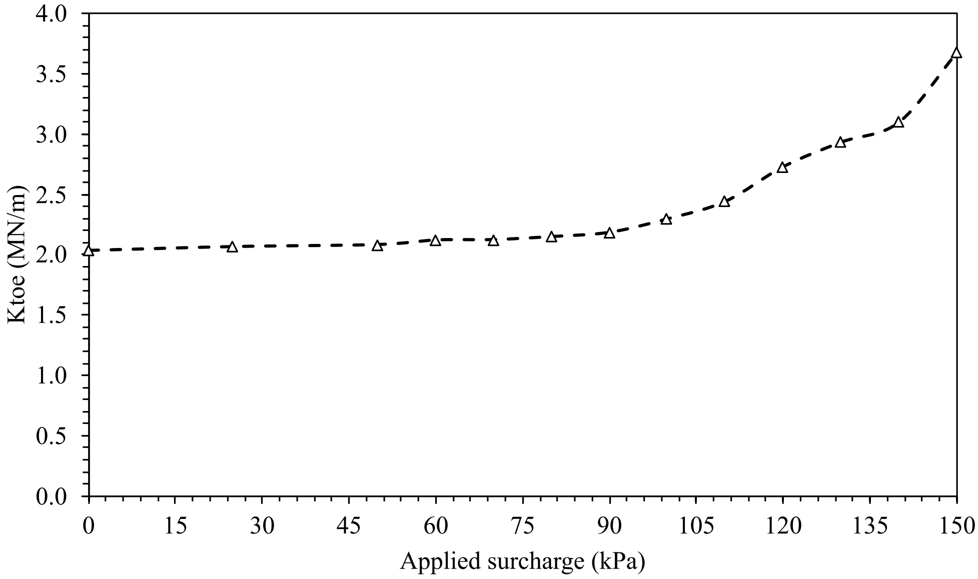

(b)

Figure 6.21: Toe horizontal stiffness. (a) during construction; (b) during surcharging.

6.2.5 Vertical Earth Pressures

An attempt to measure stresses at the foundation was made by using two pressure cells manufactured for the present research. One cell (SPC-01) was located 300 mm from the wall facing while the second cell (SPC-02) was located 800 mm behind the facing, close to the reinforcement free end (reinforcement length of 1000 mm behind the wall facing).

The method chosen to calibrate the pressure cells was the one used by Gregg (2008), who calibrated the sensors in situ by plotting equivalent vertical stresses (theoretical) calculated from the soil column above the sensors (soil unit weight versus soil column height) versus output signal from the cell, in volts, during wall construction. The soil unit weight for each soil lift was taken considering the results from the soil compaction control data summarized in Table 5.3 of Section 5.4.2.8.

Figure 6.22 depicts the calibration curves considering a maximum theoretical pressure around 20 kPa, as recommended by Ezzein (2007) and Burgess (1999). This corresponded to a wall height around 100 cm. Note that for SCP-02 it was obtained a poor correlation factor of 0.82, due to a change in readings trend around 12 kPa of theoretical pressure. For this reason, for SPC-02 the calibration factor was obtained by considering readings up to a theoretical pressure of 12 kPa, which is equivalent to a wall height of 56 cm (Figure 6.23). From the results presented, calibration factors of 6.52 kPa/mV and 5.03 kPa/mV were obtained for SPC-01 and SPC-02, respectively.

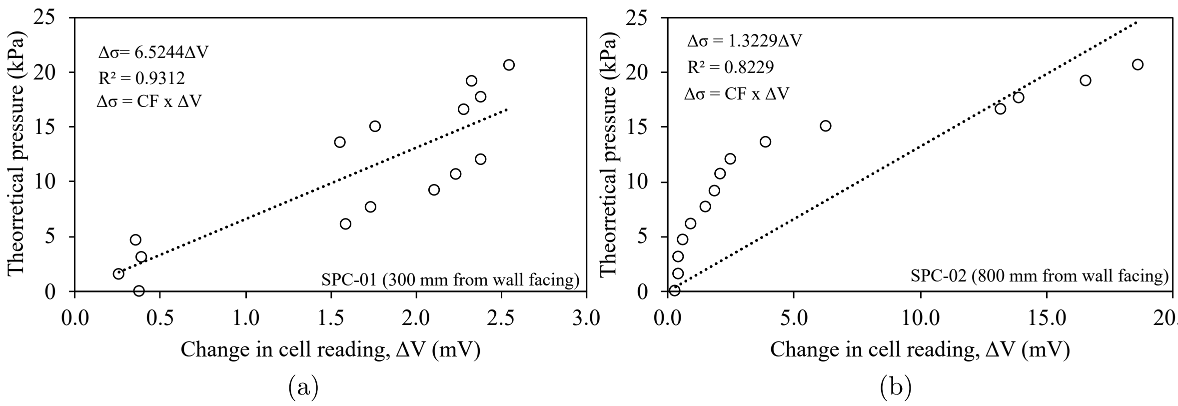

Figure 6.22: Soil pressure cells calibration curves obtained during wall construction up to a height of 98 cm (14 row blocks): (a) SPC-01 (b) SPC-02.

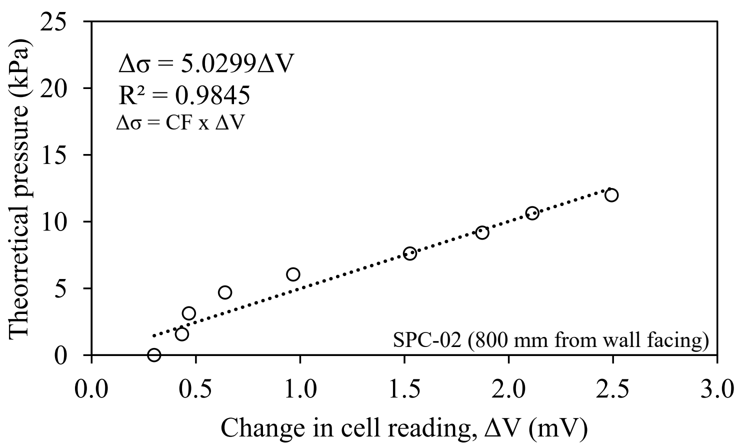

Figure 6.23: Soil pressure cell calibration curve for SPC-02 obtained during wall construction up to a height of 56 cm (9 row blocks).

Note that the in-situ calibration factors obtained during wall construction, with the pressure cells buried under the compacted backfill soil used, were significantly larger then the adjusted factor of 0.067 kPa/mV determined from the preliminary surcharging tests described in Section 5.2.3.2, in which the cells were either buried under a thin layer of sand or in direct contact with the surcharging airbags. During the surcharging tests, the change of output signal varied from around 500 mV up to 1000 mV, depending on test configuration, for a surcharge of 50 kPa. During the start of wall construction, up to the height considered for cell calibration, however, changes in cell readings were much lower: 2.32 mV for SPC-01 and 2.5 mV at 20 kPa and 12 kPa, respectively, of theoretical pressure. As comparison, changes in commercially available cell readings in previous researches (EZZEIN, 2007; GREGG, 2008), where a stiff toe was in place, varied in the range of 10 mV to 30 mV, at a theoretical pressure of 20 kPa. This rises some questions on the reliability of the readings of the cells used in this research under low stresses. It was also noted that under low stress levels, during load stabilization, cell readings were widely dispersed even under a constant vertical stress (soil weight), showing coefficients of variation generally higher than 10% and up to 135%, as shown in Table 6.1. On the other hand, under larger vertical stresses, during surcharging, the coefficients of variation during the stabilization load periods (constant load) were usually smaller than 5%.

Soil height (cm)	$\sigma_{v,\sigma_v,theoretical}$ (kPa)	Mean cell reading (mV)		Coefficent of variation of cell reading	
		SPC-01	SPC-02	SPC-01	SPC-02
0	0.0	0.4	0.3	58%	108%
7	1.6	0.3	0.4	135%	83%
14	3.1	0.4	0.5	90%	93%
21	4.7	0.4	0.6	125%	81%
28	6.1	1.6	1.0	29%	49%
35	7.6	1.7	1.5	35%	41%
42	9.2	2.1	1.9	20%	29%
49	10.7	2.2	2.1	21%	22%
56	12.0	2.4	2.5	24%	23%
63	13.5	1.6	3.9	34%	12%
70	15.1	1.8	6.3	29%	6%
77	16.6	2.3	13.2	32%	7%
84	17.7	2.4	13.9	21%	4%
91	19.2	2.3	16.6	23%	3%
98	20.6	2.5	18.6	20%	3%
105	22.1	20.6	19.0	3%	3%
112	21.8	20.8	13.0	3%	6%
119	23.2	58.0	8.3	1%	5%
126	24.6	73.3	12.0	1%	4%
133	25.9	129.1	14.4	0%	3%
140	27.3	135.5	11.9	0%	4%
147	28.7	154.3	13.1	0%	5%

Table 6.1: Mean cell reading at each stage of wall construction and respective coefficient of variation.

The low sensibility of the soil pressure cells used under low stress levels (during construction) is depicted in Figure 6.24a, in which the abrupt reading drops during surcharging indicates the problems encountered during the test to sustain the load over a long period of time. Figure 6.24b shows the results for cell readings considering only the stabilization load periods, that is, when the load increment was kept constant over a period of time. From the results presented in Figure 6.24 it can be seen that the cell closer to the wall facing (SCP-01) registered larger variations of output voltage with surcharging increment, indicating larger foundation pressures closer to the wall facing.

Some reasons could be raised in an attempt to explain the limitations on sensor measurement capacity under low levels of vertical stress. The first reason would be the inherent sensor range of application, with the pressure cell not being able to register low pressure levels. A second reason could be related to the relative stiffness between the pressure cell and the surrounding compacted soil, which could lead to stress redistribution around the sensor element that affected cell readings under low stress levels. Note that the surcharging tests described in Section 5.4.2.8 were conducted with dry sand as backfill material, while for the in-situ cell calibration a cohesive-friction material was used, compacted close to a degree of compaction of 98%. Finally, a third reason could be related to a poor cell anchorage at the soil foundation. Either way, for future research it is recommended to conduct calibration tests in a smaller box using the in-situ method and the thin sand layer calibration method used by Ezzein (2007) to evaluate the influence of different parameters in cell response.

For the reasons discussed herein it was not possible to conduct a reliable in-situ calibration of the soil pressure cells used and, as consequence, to estimate foundation pressures during model wall construction and surcharging.

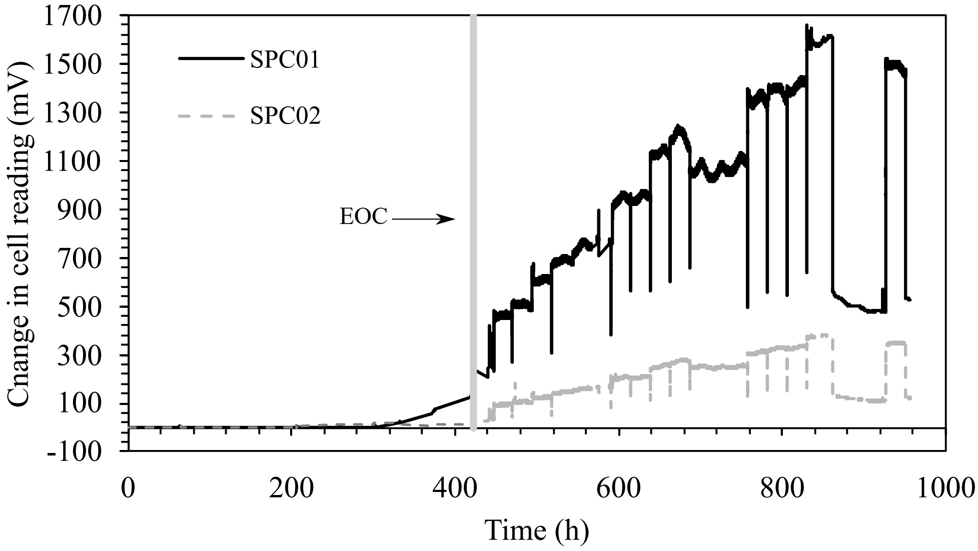

(a)

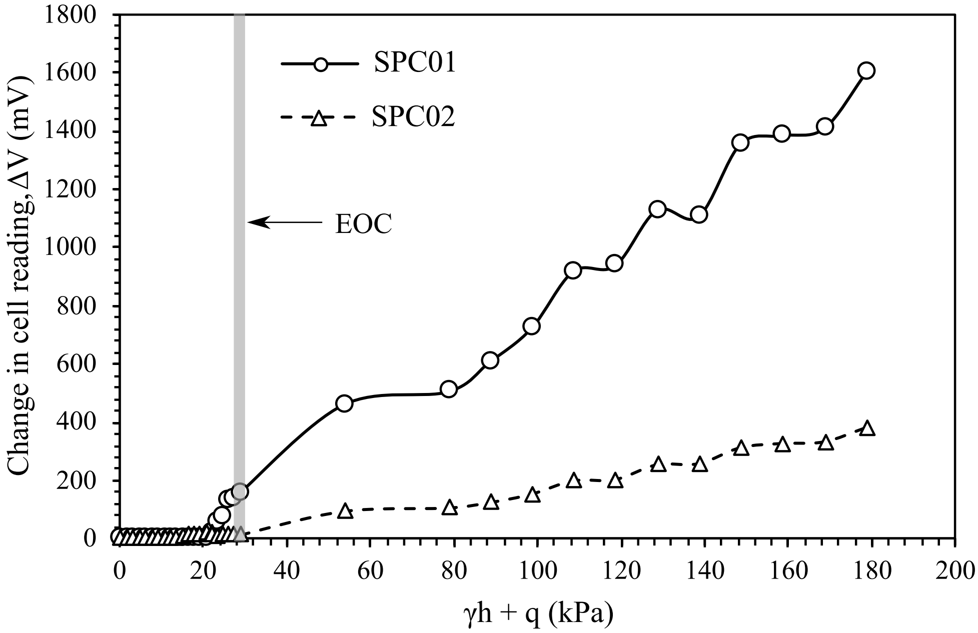

(b)

Figure 6.24: Soil pressure cells reading history during wall construction and surcharging: (a) cell reading vs time; (b) cell reading vs equivalent vertical stress (EOC: End of Construction).

6.2.6 Reinforcement Movement and Strain

Strain-gauges bonded directly to the geogrid longitudinal ribs and wire-line extensometers were used to obtain reinforcement strains throughout wall model construction and surcharging.

6.2.6.1 Extensometer displacement and strains

As indicated in previous studies (EZZEIN, 2007), extensometers readings are useful for deducing larger strains than the ones associated with strain gauge debonding. For this reason, the 5 geogrid layers were instrumented with a total of 41 extensometers: layer 1 with six automated draw-wire potentiometer, layer 2 with 8 manual extensometers and layers 3 to 5 with 9 manual extensometers each, as described in Section 5.3.4.2. However, the results for the manual readings were quite erratic, not showing any visible trend with surcharging increment. This was attributed to a possible systematic measurement error and/or displacements in the error range of the measurement method (readings conducted with a paquimeter). Therefore, since data reliability is questionable, the readings for the manual extensometers, installed at geogrid layers 2 to 5, will not be presented herein to illustrate model wall behaviour. In contrast, displacement results from the automated draw-wire potentiometers, installed at the lowest geogrid layer (layer 1), showed visible trends in displacement as will be detailed next.

Figure 6.25 shows the horizontal displacement history at 6 selected nodes of the lowest geogrid (layer 1, located at the height 0.21 m), measured by the draw-wire potentiometers, with the specific locations of each instrumented node illustrated in Figure 5.38.

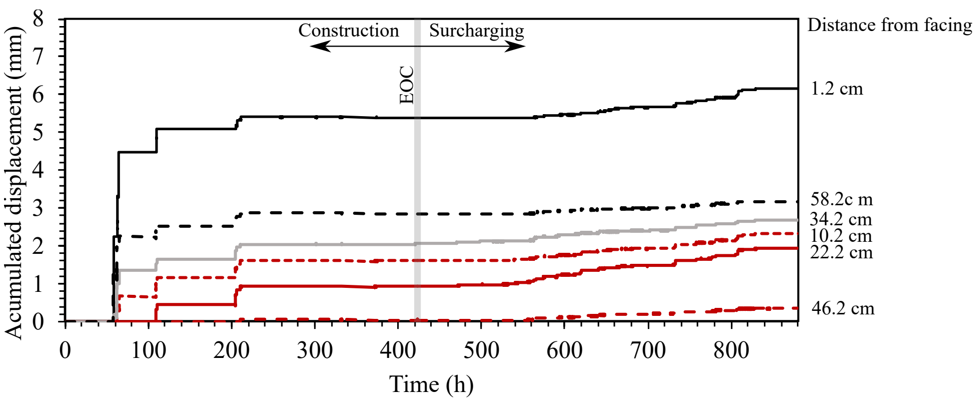

Figure 6.25: Horizontal displacement history of layer 1 (EOC: End of Construction). The position of each sensor is depicted in Figure 5.38.

Detailed result charts during wall construction and surcharging are shown in Figures 6.26 and 6.27, respectively. The largest displacements took place at the beginning of wall construction, with a trend to stabilize after the 10th soil lift placement and compaction, around 50% of the final wall height. This behaviour is probably associated with the restrained wall footing, which influences wall displacements at lower wall heights, in accordance with the behaviour of the facing displacements recorded at the lowest displacement transducer (DT-01) and shown in Figure 6.4. End of Construction displacement recorded by the closest extensometer to the wall facing (distant 1.2 cm) was around 5.4 mm, while facing displacement recorded by DT-01 (around the same level as geogrid layer 1 as depicted in Figure 5.25) was around 8.31 mm.

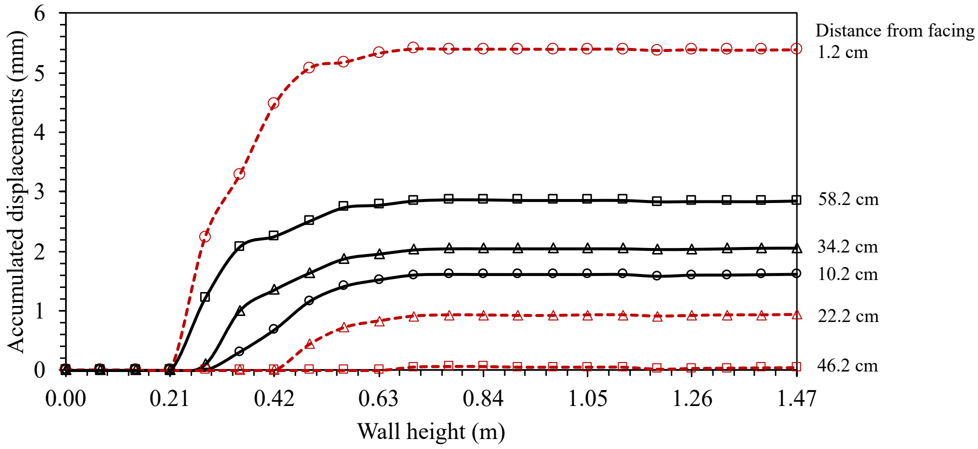

Figure 6.26: Accumulated displacements during wall construction at selected nodes of the lowest geogrid (layer 1, located at the height 0.21-m). The position of each measurement point is depicted in 5.38.

During the initial surcharging increments there was no observed deformation at layer 1 of reinforcement up to a surcharge of 50 kPa, as depicted in 6.27b. The increase in surcharging increment for values larger than 60 kPa caused a successive increase in deformation of Layer 1, specially for the geogrid node closer to the wall facing.

Figure 6.28 shows displacement profiles and strain profiles inferred from the wire-line potentiometers at end of construction and at different stages of surcharging. Clearly, the geogrid node located closer to the wall facing experienced the largest displacement, as expected. However, the expected pattern of reducing node displacement with the increasing of the distance to the wall facing, which would indicate geogrid tension, was not observed. Instead, negative inferred strains were detected at some locations, as shown in Figure 6.28b. These negative strains at the lowermost layer could be the result of foundation compressibility. No significant variation was observed in inferred strains at Layer 1 with increasing surcharge pressure. It is not clear why negative strains were obtained, however it is worth noting that the sensors were located at different geogrid ribs (see layout at Figure 5.38), and therefore the pattern detected could be related to strain non-uniformity throughout geogrid width, which would invalidate the assumption of strain uniformity that was considered to infer strains from extensometer measurements at different geogrid ribs. Ideally, it would be recommended in a future study to provide a larger set of automated extensometers at each geogrid layer to allow for redundancy and help to clarify odd behaviours.

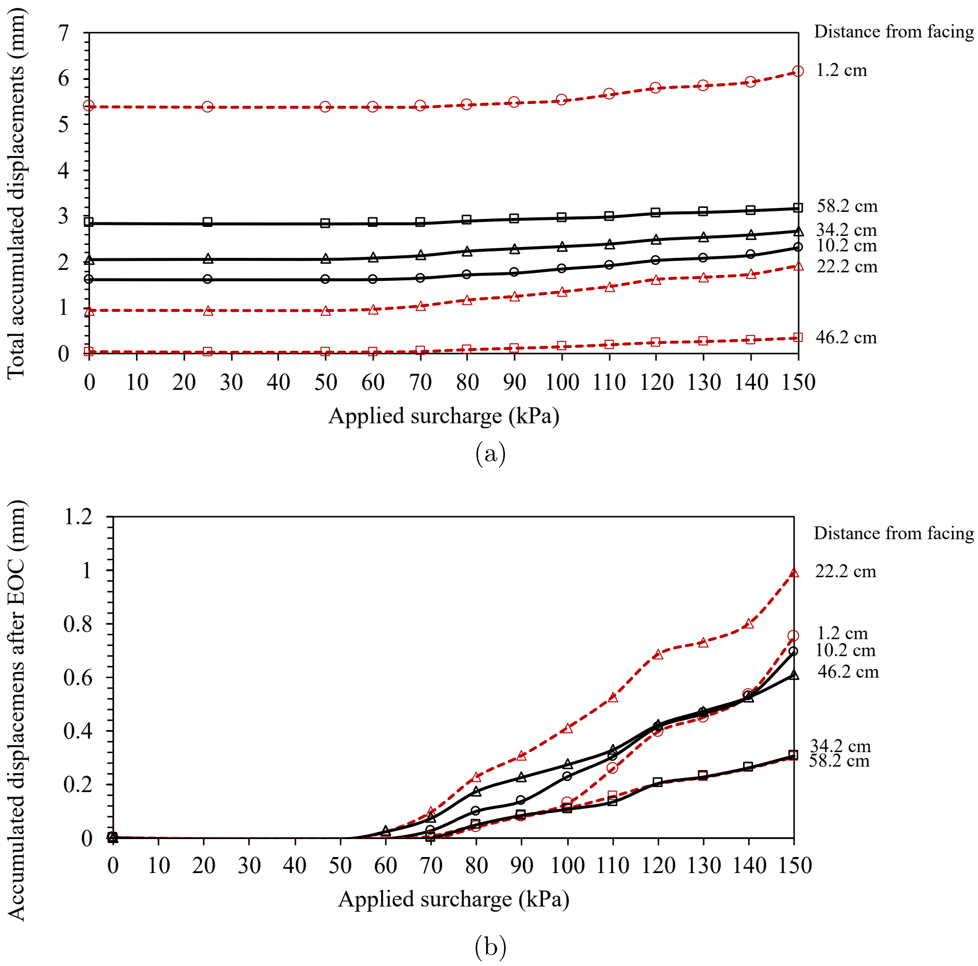

Figure 6.27: Accumulated displacements at selected geogrid nodes at layer 1 during surcharging, from draw-wire potentiometer readings: (a) reference at test start; (b) reference at End of Construction (EOC).

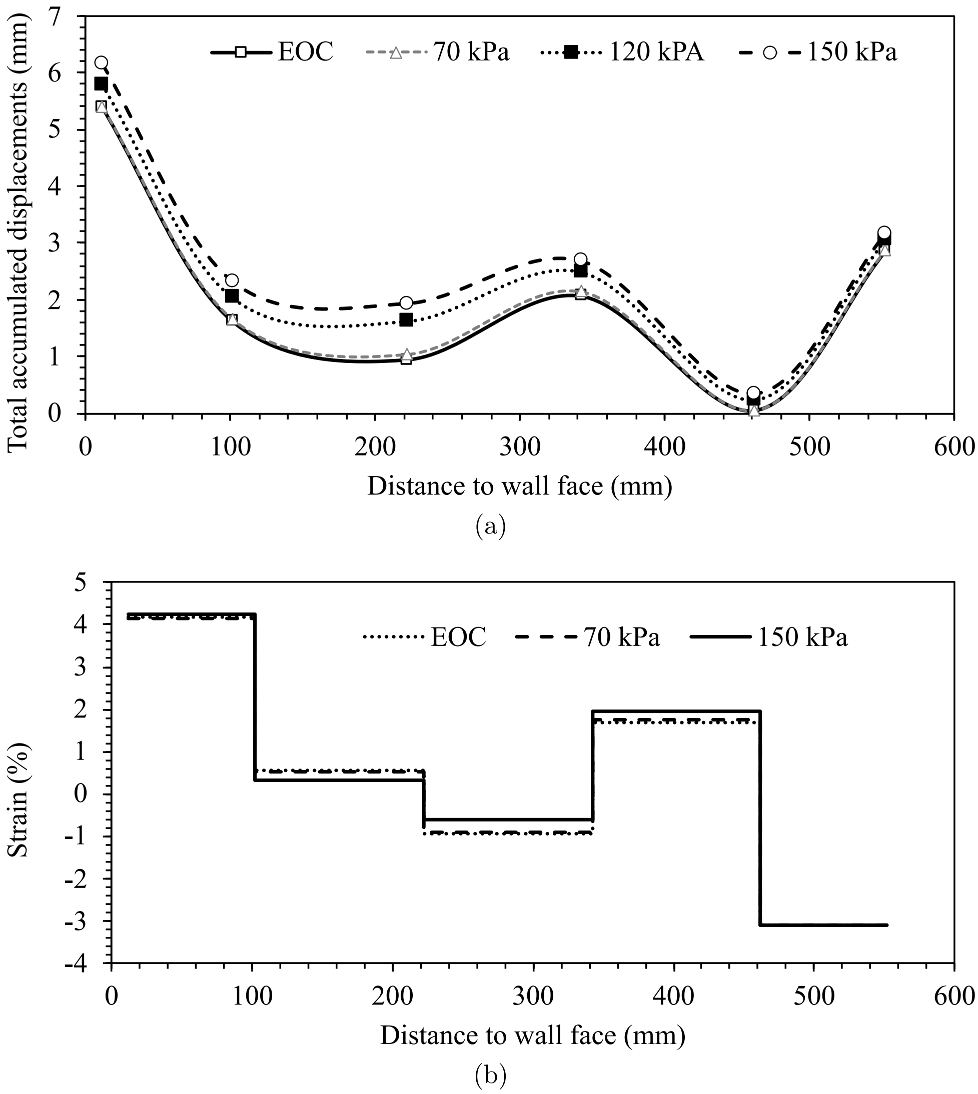

Figure 6.28: Results from the wire-line potentiometers at layer 1 and at End of Construction and different stages of surcharging: (a) displacement profiles; (b) inferred strain profiles.

6.2.6.2 Strains from strain-gauge readings

A total of 41 instrumented locations were monitored with strain-gauges bonded directly to the geogrid longitudinal rib. Layer 1 (the lowest) was monitored at 6 locations, layer 2 at 8 locations and layers 3 to 5 at 10 locations each, according to the layouts shown in Figures 5.38 to 5.40. However, some sensors were lost during soil compaction operations (L1-1B, L1-2D, L2-6D, L2-7A, L2-8B, L3-1B, L3-4B) or surcharging (L2-2D, L2-3A L2-4B, L2-5C, L3-3A, L3-10D, L5-9C). One strain-gauge (L1-3A) showed malfunction during signal testing, being discarded from the start of the test.

Global strains were calculated from local strains recorded from strain-gauge readings by applying the calibration factor adjusted for local strains up to 1.5% ($CF = 1.37$), as described in Section 5.3.4.5. Therefore, the results shown herein refers to converted global strains.

Figure 6.29 shows the strain profiles obtained at the end of construction and for different stages of surcharging for the five instrumented geogrid layers. In general, recorded strains were below 1%, with larger strains at layers 3 and 4. The breaks in strain profiles are indicative of sensor failure prior to the correspondent surcharge increment.

Overall the recorded strains by the strain-gauges at the end of surcharging were much lower than the ones measured in previous studies that used sand as backfill material (EZZEIN, 2007; BURGESS, 1999). However, the values found herein are in the same order of magnitude as the ones found by Gregg (2008) for the concrete modular block facing wall for strain-gauge measurements. Despite the differences in model wall geometry and materials (Gregg (2008) modelled a 3.6-m high wall) the aforementioned author used a sand-silty (non-select) soil backfill with 60% passing at sieve #200, soil friction angle of 40° and soil cohesion of 18 kPa. This is an indicative of the significant effect of soil cohesion on reducing reinforcement loads on reinforced soil walls. It is worth mention though that strain-gauge readings should not be taken as representative of maximum reinforcement strains, since it is usually more appropriate for small strains while a extensometer readings are more appropriate for larger strains. Unfortunately, manual extensometer measurements taken in this study were not reliable to allow an evaluation of maximum reinforcement strains at peak surcharge, as described in Section 6.2.6.1.

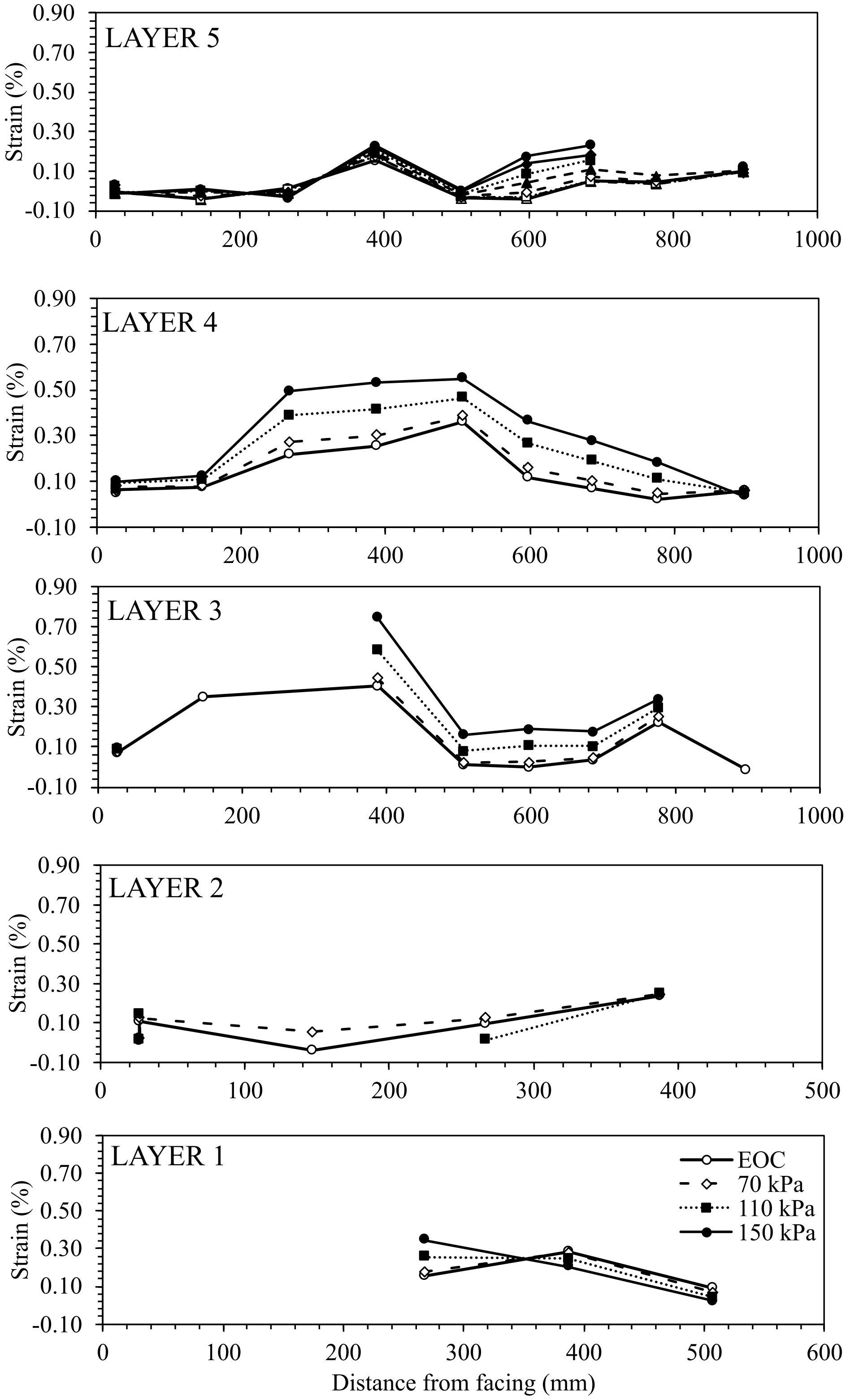

Figure 6.29: Geogrid layers strain profiles from strain-gauges. The position of each sensor is depicted in Figure 5.38.

6.2.6.3 Discussion on Reinforcement Movement and Strain

Since it was possible to infer geogrid strains from extensometer measurements only for Layer 1 (instrumented with automated draw-wire potentiometers) the comparison between strains obtained via extensometers and strain-gauges will be discussed solely for this reinforcement layer. Unfortunately, 50% of the strain-gauges bonded to layer 1 was discarded due to malfunction or failure during soil compaction, which left the reinforcement with only 3 working strain-gauges throughout surcharging, making it difficult to compare strain-gauge and extensometers results.

Figure 6.30 results from the overlapping of Figure 6.28b with Figure 6.29 for Layer 1. It is possible to note some discrepancy from a distance from the facing around 267 mm up to 500 mm, section in which it was possible to obtain measurements from strain-gauges throughout surcharging. However, due to strain-gauge failure during surcharging it is difficult to find the maximum strains from strain-gauge readings. Besides, strains obtained from extensometer readings showed less sensitiveness to surcharge increment than strain-gauge measurements. Despite the observed differences, it is worth noting that the sensors were located at different geogrid ribs (see layout at Figure 5.38), and therefore the differences detected could be related to strain non-uniformity throughout geogrid width and even to a possible effect of transverse member bending on geogrid behavior.

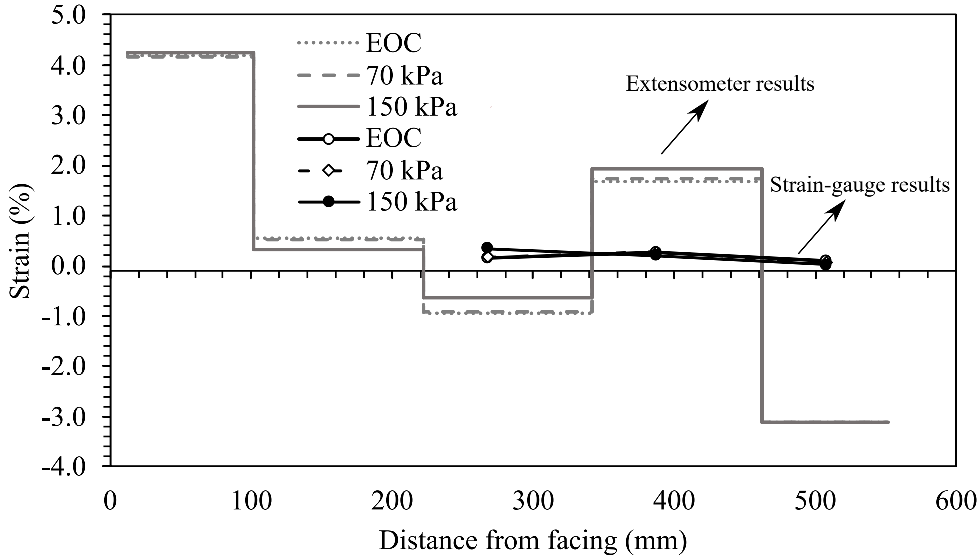

Figure 6.30: Overlapping of strain profiles from extensometers and strain-gauges for Layer 1 (EOC: End of Construction)

Figure 6.31 shows the strain history from the three working strain-gauges at Layer 1 of reinforcement during construction and surcharging. Also shown in this figure is the strain history calculated from extensometers that spanned the location of the correspondent strain-gauge. Note that for all cases the draw-wire potentiometers recorded a significant jump at the onset of the readings (during construction, after reinforcement layer 1 placement and with the above soil lift compaction). The readings from the displacement transducer located at the third block row (close to layer 1 height, at 0.21 m), to measure facing displacements, also showed larger displacements at the beginning, with a tendency to reach a plato around a height around of 0.6 m during wall construction (see Figure 6.4). However, this behaviour was not captured by the strain-gauges located further than 267 mm from the wall facing. Strain-gauges closer to the facing failed or presented signal problems before the onset of the readings.

Therefore, due to the small amount of available data it not possible to make a conclusion regarding reinforcement strain behaviour throughout the test. Nonetheless, it is worth noting that from the strenght parameters of the model soil the model wall would be stable without reinforcement at the initial stage (before surcharging), as shown in Section 5.4.2.2. As the cohesion (~15 kPa) of the soil in the model is large, the reinforcement layers played a minor role for the stability of the system.

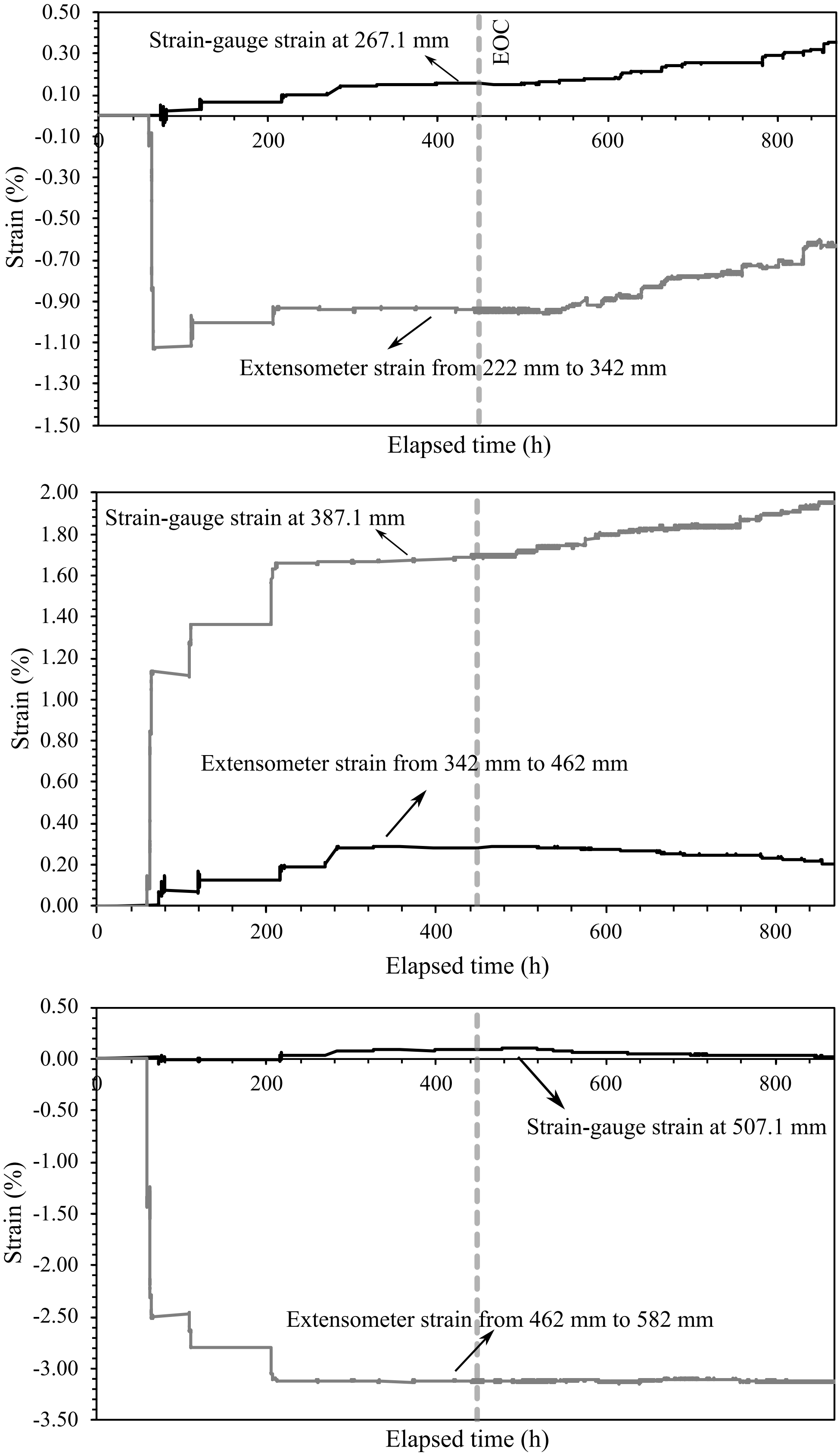

Figure 6.31: Strain history at different locations at Layer 1 from strain-gauge and extensometer results. The position of each sensor is depicted in Figure 5.38. (EOC: End of Construction)

7 PLAXIS Remote Scripting with Python

Recent versions of PLAXIS allow the user to design and run models using Python scripting, which is specially useful when a series of models of similar applications must be calculated, such as for parametric analyses. To this end, with the intention of laying the basis for a future numerical study involving automated parametric analysis of reinforced soil walls, it was used the remote scripting interface and its Python wrapper to define, run and save relevant results from reinforced soil wall models. In this way, all the steps in the analysis are automated. It was used Python 3.7.4, version compatible with PLAXIS 2D 2020, and the Pycharm editor (2020.2.3). The scripts were developed considering only the construction process of the reinforced soil wall, but a surcharging load can easily be implemented in the script to simulate the surcharging of the model.

To develop the code it was used the python syntax indicated in Plaxis Reference Manual (Bentley (2020)) and PLAXIS Command Reference manual which comes with the installation of the software. The first step when using remote scripting in PLAXIS is to configure the remote server in order to establish a secure connection between the server and the remote scripting interface. For automated analysis this can be done by using the following code:

```
from plxscripting.easy import *  # scripting library, *import all names that a module defines

inputport = 10000
outputport = 10001
plaxispw = r'1/WkZB%SCf2t^EN@'
plaxis_path = r'C:\Program Files\Bentley\Geotechnical\PLAXIS 2D CONNECT Edition V20'
plaxis_input = 'PLAXIS2DxInput.exe'

args = [os.path.join(plaxis_path, plaxis_input),
        "--AppServerPort={}".format(inputport),
        "--AppServerPassWord={}".format(plaxispw),
        "NO_CONTROLLERS"]
process_name="Plaxis2DXInput.exe"

if process_name not in (p.name() for p in psutil.process_iter()): # checks if Plaxis is already opened and with server running
        inputprocess = subprocess.Popen(args)

# # then initialize the new_server with additional waiting time due to startup of PLAXIS
s_i, g_i = new_server('localhost', inputport, password=plaxispw, timeout
```

```
    =10.0)
s_i.new()
```

Note that, in the code above, s_i is bound to an object representing the PLAXIS application (Plaxis server object) while g_i refers to a global object of the current PLAXIS section (allow the user to manipulate the current model).

A series of python scripts (provided in Appendix G) were written comprising of the following procedures, embedded in the main routine (Appendix G.2):

1. Retrieve model inputs from an input .txt file in a standard format (see Appendix H) to set model geometry (facing batter, block dimensions, wall height, number of reinforcement layers, reinforcement length, height of compaction lift, connector stiffness, etc), mesh settings (mesh factor), material properties (soil, reinforcement, block, soil/block interface, block/block interface, reinforcement/facing connector), surcharging values (to simulate compaction of soil layers during construction) and boundary conditions (toe restraint, represented by an anchor) by calling up the function set_wall_model, included in the script file_processing (Appendix G.1). The function set_wall_model calls up the function import_data_from_file, also included in the script file_processing.py.

2. Create a new project (s_i.new ()) and set model geometry and material properties in Plaxis from the input data retrieved: from the main script commands PLAXIS assigns the parameters and constitutive models for all the materials (soil, reinforcement, block, interfaces and toe anchor) as retrieved from the input data. Next, it draws the external geometry and the subregions needed to material attribution (soil layers, blocks, reinforcement lines, connectors and interfaces positions);

3. Set boundary conditions - prescribed displacements and groundwater flow;

4. Generate mesh (g_i.gotomesh()): PLAXIS defines the mesh according to a general coarseness factor defined by the user (retrieved from the input data) by using the command g_i.mesh (coarseness factor). The script imposes a refinement in local areas such as around the reinforcement layers, the connection between the reinforcement and the facing, interfaces and for the first wall block where the anchor that represents the toe restraint are connected, in order to obtain more representative values for toe reactions;

5. Add notable points for post-processing: upper left point of the wall, points at the centre of the block wall at the same elevation as the reinforcement, toe point. To this end, the code opens up the output module of Plaxis - s_o, g_o = new_server('localhost', outputport, password=plaxispw) in order to use select specific mesh points;

6. Phase Construction (g_i.gotostages()): part of the code in which the wall construction is simulated according to the number of soil layers given in the input data. Compaction effort is simulated by using a transient surcharging (applied only above or on both sides, with opposite signs, of the soil layer, as specified by the user with the parameter surcharge_type, given in the input data);

7. Calculate model (g_i.calculate());

8. Record results for End of Construction (g_o.getcurveresults ()): record in .txt files facing and toe displacements and toe reaction forces by calling up the functions record_facedisp, record_toe_facedisp, record_top_facedisp, record_toe_reactions included in the script Record_Results.py (Appendix G.4). After ending data extraction it is recommended to close the output project by using the command s_o.close().

Auxiliary scripts were written to conduct mesh convergence analysis (with reference to the displacement of left uppermost point in the model) and to plot the results and . These are presented in Appendix G.3 and Appendix G.5, respectively.

8 Final remarks

8.1 Conclusions

This thesis evaluated the influence of soil cohesion and a structural facing on the stability of reinforced soil walls by using two approaches: the first was a semi-analytical approach while the second one an experimental approach. In addition, with the intention of laying the basis for a future numerical study involving automated parametric analysis, a series of python scripts were developed during the present study to conduct automated numerical analysis in Plaxis 2D. These are presented in Appendix G.

In the first half of the present thesis it was presented a new semi-analytical method based on limit analysis to design the reinforcement strength required by geosynthetic reinforced walls in cohesive soils accounting for the contribution of cohesion and wall facing to wall stability and the onset of tension cracks.

A parametric analysis was performed producing several dimensionless design charts for both uniform and linearly increasing reinforcement distributions. The effect of soil cohesion, soil friction angle, facing batter, block width, location of the reaction force acting on the face, facing/backfill interface friction angle, facing/foundation interface friction angle, and reinforcement length was investigated. The results from the parametric analysis showed that:

1. Accounting for the presence of cohesion and the facing element can lead to significant savings in the overall level of reinforcement. For normalized cohesion values of $c/\gamma H = 0.05$ and 0.1 savings up to 57% and 82% of the amount of reinforcement, respectively, could be achieved;

2. The contribution of the facing to structure stability relies on the facing self-weight and the toe restraint condition. In this study, the toe restraint was considered through the interface friction between the base of the facing and the foundation soil. The magnitude of this interface friction angle exhibits a major influence on the load capacity of the facing element, being able to drastically reduce the requirement for reinforcement;

3. The presence of tension cracks has a detrimental effect on wall stability, especially for high values of cohesion. Neglecting the presence of cracks in the design may, therefore, severely underestimate the required reinforcement and possibly risk the safety of the structure;

4. Adopting common reinforcement lengths employed in the design of reinforced soil walls ($0.6H$ and $0.7H$), due to the recommendations of technical standards, resulted

mostly in two types of critical failure modes for the ones considered herein: internal failure with rupture of all layers of reinforcement and compound failure with the crossed layers failing in tensile rupture and pullout. Note that, in this work it was not considered the failure mechanism of direct sliding over one reinforcement layer;

It was shown the potential for substantial savings to be made on the amount of geo-reinforcement to be employed in reinforced walls by accounting for the contributions of facing and soil cohesion to stability. Nevertheless, these gains can be realized under the condition that a proper drainage system is in place for the cohesive backfill throughout the design lifetime of the wall and the amount of cohesion assumed in design is conservatively estimated accounting for its potential degradation over time.

The second part of the present thesis comprised the construction and testing of a 1.47 m high reinforced soil wall model, constructed with a frictional-cohesive soil and a modular block wall facing with a restrained toe. It was presented the materials, methods, instrumentation design and construction and test box adaptations needed to surcharging the wall model up to 150 kPa. From the test results the following general conclusions can be drawn:

1. Post-construction outward facing deflection was small, with maximum horizontal displacements around 2.6 mm ($\sim$0.2% of wall height) at the elevation 101.5 cm. The majority of the facing deflection took place during construction, with values up to 9.5 mm ($\sim$0.6% of wall height) at wall mid-height. For this reason, facing batter at EOC deviated significantly from the designed batter of 8°.

2. At the end of surcharging (150 kPa) reinforcement strains up to 0.7% were recorded from strain-gauge readings while vertical and horizontal toe loads of 13.3 kN and 1.5 kN, respectively;

3. The majority of the toe displacement and increment in horizontal toe load took place during construction, specially during placement and compaction of the first soil lifts;

4. Negligible incremental toe displacements occurred during construction and surcharging, indicating a stiff condition of the toe. The maximum to displacements were in the range of 0.4 mm to 1.0 mm;

5. Displacements showed non-uniformity over the facing, which is expected due to the type of facing (discrete modular construction);

6. the larger displacements took place during construction and compaction of the soil backfill, with the wall model being less sensitive to post-construction movements;

7. Under 150 kPa of surcharging (airbag capacity before major leakage) the model wall was probably under work stress conditions, being possibly far from failure from the small magnitude of displacements observed;

8. It was not possible to detected a definitive pattern from the results from the soil backfill surface settlement measurements and no conclusive behaviour could be drawn from the data gathered. It should be evaluated a better arrangement to conduct the measurements in a future study;

9. At the end of construction (EOC), the total vertical toe load was approximately 8.3 kN while the full facing weight was around 5.96 kN, which is about 72% of the measured load. At maximum surcharge (150 kPa) the total vertical toe load was approximately 13.3 kN, corresponding to 2.2 times the wall facing self-weight. This is attributed to downdrag forces between the backfill soil and the back of the model blocks, which transfers vertical loads to the wall toe;

10. It was observed wall rotation mainly during wall construction, with the front of the model wall toe carrying around 70% of the toe vertical load, when compared to the heel of the toe;

11. Overall the recorded strains by the strain-gauges at the end of surcharging were much lower than the ones measured in previous studies that used sand as backfill material. This could be an indicative of the significant effect of soil cohesion on reducing reinforcement loads on reinforced soil walls. However, due to the small amount of available reliable data it was not possible to make a conclusion regarding reinforcement strain behaviour throughout the test.

The small magnitude of wall facing deflections during construction and surcharging seems to indicate the the model wall was possibility under working stress conditions throughout the entire physical test, far from reaching failure. This can be attributed to the over-consolidated state of the backfill soil due to compaction effort, to the beneficial effect of cohesion on reinforced soil wall behaviour and to the influence of the restrained wall toe to carry part of the load.

8.2 Recommendations for future work

The recommendations based on the results and conclusions of this thesis are:

1. Conduct compression tests to determine stress-strain behaviour of the reduced-scale modular blocks used in this research to obtain parameters to use in numerical analysis;

2. Conduct block-block interface tests to determine interface parameters to use in numerical analysis;

3. Conduct direct shear tests on specimens of the backfill soil and the friction reducing system used in this research to evaluate the efficiency of the solution in reducing boundary effects;

4. Conduct calibration tests of the soil pressure cells (foundation cells) in a smaller box using the in-situ method and the thin sand layer calibration method used by Ezzein (2007) to evaluate the influence of different parameters in cell response;

5. Construct and test other model walls, changing key parameters to obtain a wider set of data on reinforced soil walls with cohesive soil. The instrumentation should be adapted and improved to cover a wider range of reliable test results (improvement is needed for the surface backfill settlement, reinforcement displacements and foundation pressure measurements);

6. Evaluate the influence of cutting geogrid ribs (change in geogrid geometry, stiffness and strength) on calibration factors (local versus global strains) for strain-gauges bonded to the geogrid;

7. Calibrate numerical codes for reinforced soil wall models with cohesive soil by comparing numerical results to the physical test results presented in this thesis.If using PLAXIS the scripts to conduct automated analysis can be found in Appendix G of this thesis. After the calibration of the numerical model a series of parametric analysis can be conducted to evaluate the influence of changing other parameters on wall performance (toe restrain, reinforcement stiffness and length, soil cohesion, wall height, block size, etc.);

8. Expand the semi-analytical method by including surcharging and use the calibrated numerical model to validate the semi-analytical method by comparing the peak surcharge that leads to wall failure;

9. Study better options of airbags that can sustain larger pressures before leakage, aiming to bring future model walls to be constructed in LabGsy laboratory to failure. The results of these test can than be used to validate the expanded semi-analytical method with surcharging, by comparing the value of surcharge that leads the model to failure with the value estimated by the semi-analytical calculations.

Bibliography

AASHTO. **Bridge Design Specifications 6th ed.** Washington D.C., 2012.

________. **LRFD Bridge Design Specifications 8th ed.** Washington D.C., 2017.

ABD, A.H. **Geosynthetic-Reinforced and Unreinforced Soil Slopes Subject to Cracks and Seismic Action : Stability Assessment and Engineered Slopes**. 2017. s. 214. PhD thesis – University of Warwick.

ABD, A.H.; UTILI, S. Design of geosynthetic-reinforced slopes in cohesive backfills. **Geotextiles and Geomembranes**, Elsevier Ltd, v. 45, n. 6, p. 627–641, 2017. ISSN 02661144. DOI: `10.1016/j.geotexmem.2017.08.004`.

ALLEN, T.M.; BATHURST, R.J. Comparison of working stress and limit equilibrium behavior of reinforced soil walls. English. **Geotechnical Special Publication**, Washington State Department of Transportation, State Materials Laboratory, Olympia, WA, 98504-7365, United States, n. 230, p. 500–514, 2013. ISSN 08950563 (ISSN).

________. Design and performance of 6.3-m-high, block-faced geogrid wall designed using k-stiffness method. **Journal of Geotechnical and Geoenvironmental Engineering**, v. 140, n. 2, p. 1–12, 2014. ISSN 10900241. DOI: `10.1061/(ASCE)GT.1943-5606.0001013`.

________. Improved Simplified Method for Prediction of Loads in Reinforced Soil Walls. English. **Journal of Geotechnical and Geoenvironmental Engineering**, American Society of Civil Engineers (ASCE), Washington State Dept. of Transportation Olympia, Washington, DC, United States, v. 141, n. 11, p. 04015049, Nov. 2015. ISSN 1090-0241. DOI: `10.1061/(ASCE)GT.1943-5606.0001355`.

________. Performance of an 11 m high block-faced geogrid wall designed using the K -stiffness method. English. **Canadian Geotechnical Journal**, Washington State Department of Transportation, State Materials Laboratory, Olympia, WA 98504-7365, United States, v. 51, n. 1, p. 16–29, Jan. 2014. ISSN 0008-3674. DOI: `10.1139/cgj-2013-0261`.

________. Soil reinforcement loads in geosynthetic walls at working stress conditions. English. **Geosynthetics International**, Washington State Dept. of Transp., Olympia, WA 98504-7365, United States, v. 9, n. 5-6, p. 525–566, 2002. ISSN 10726349 (ISSN). DOI: `10.1680/gein.9.0227`.

ALLEN, T.M.; BATHURST, R.J.; HOLTZ, R.D.; WALTERS, D.; LEE, W.F. A new working stress method for prediction of reinforcement loads in geosynthetic walls. English. **Canadian Geotechnical Journal**, State Materials Laboratory, Washington State Dept. Transp., Olympia, WA 98504-7365, United States, v. 40, n. 5, p. 976–994, 2003. ISSN 00083674 (ISSN). DOI: `10.1139/t03-051`.

ANDERSON, D.G.; MARTIN, G.R.; LAM, I.P.; WANG, J.N. **Seismic Analysis and Design of Retaining Walls, Slopes and Embankments, and Buried Structures, NCHRP Report 611**. Washington, DC,USA, 2008.

ASTM. **D1556/D1556M-15e1 - Standard Test Method for Density and Unit Weight of Soil in Place by Sand-Cone Method**. West Conshohocken, PA: ASTM INTERNATIONAL, 2016. p. 8. DOI: `10.1520/D1556_D1556M-15E01`.

_______. **D2216-19 - Standard Test Methods for Laboratory Determination of Water (Moisture) Content of Soil and Rock by Mass**. West Conshohocken, PA: ASTM International, 2019. p. 7.

_______._______. West Conshohocken, PA: ASTM INTERNATIONAL, 2019. p. 7.

_______. **D4959-16 - Standard Test Method for Determination of Water Content of Soil By Direct Heating**. West Conshohocken, PA: ASTM International, 2016. p. 6.

_______. **D6638-18 - Standard Test Method for Determining Connection Strength Between Geosynthetic Reinforcement and Segmental Concrete Units (Modular Concrete Blocks)**. West Conshohocken, PA, 2018. p. 1–9. DOI: `10.1520/D6638-18.Copyright`.

_______. **D698-12 - Standard Test Methods for Laboratory Compaction Characteristics of Soil Using Standard Effort (12 400 ft-lbf / ft 3 (600 kN-m / m 3))**. West Conshohocken, PA: ASTM INTERNATIONAL, 2012. p. 1–13. DOI: `10.1520/D0698-12E01.1`.

_______. **D7181 - Standard test method for consolidated drained triaxial compression test for soils**. West Conshohocken, PA: ASTM INTERNATIONAL, 2020. p. 11. DOI: `10.1520/D7181-11.Copyright`.

_______. **Standard Test Method for Determining Tensile Properties of Geogrids by the Single or Multi-Rib Tensile Method**. [S.l.], 2015. p. 1–6. DOI: `10.1520/D6637`.

BAKER, R. Tensile Strength, Tension Cracks, and Stability of Slopes. **Soils and Foundations**, v. 21, n. 2, p. 1–17, June 1981. ISSN 00380806.

BAKER, R.; KLEIN, Y. An integrated limiting equilibrium approach for design of reinforced soil retaining structures: Part I-formulation. **Geotextiles and Geomembranes**, v. 22, n. 3, p. 119–150, 2004. ISSN 02661144. DOI: `10.1016/j.geotexmem.2003.10.002`.

BATHURST, R.; WALTERS, D.; HATAMI, K.; ALLEN, T. Full-scale performance testing and numerical modelling of reinforced soil retaining walls(Invited Keynote paper). In: ________. January. **Landmarks in Earth Reinforcement**. Fukuoka, Japan: A. A. Balkema, 2001. v. 2, p. 777–799. ISBN 9026518641.

BATHURST, R.J. Investigation of Footing Restraint on Stability of Large-scale Reinforced Soil Wall Tests. In: 46'TH Canadian Geotechnical Conference. Saskatoon, Saskatchewan, Canada: [s.n.], 1993. p. 389–398.

BATHURST, R.J.; ALLEN, T.M.; HUANG, B.Q. Current issues for the internal stability design of geosynthetic reinforced soil. In: 9TH International Conference on Geosynthetics. [S.l.]: IGS - Brazil, 2010. p. 533–546.

BATHURST, R.J.; ALLEN, T.M.; WALTERS, D.L. Reinforcement loads in geosynthetic walls and the case for a new working stress design method. English. **Geotextiles and Geomembranes**, Department of Civil Engineering, GeoEngineering Centre at Queen's-RMC, Royal Military College of Canada, Kingston, Ont. K7K 7B4, Canada, v. 23, n. 4, p. 287–322, 2005. ISSN 02661144 (ISSN). DOI: `10.1016/j.geotexmem.2005.01.002`.

________. Short-Term Strain and Deformation Behavior of Geosynthetic Walls at Working Stress Conditions. **Geosynthetics International**, v. 9, n. 5-6, p. 451–482, Jan. 2002. ISSN 1072-6349. DOI: `10.1680/gein.9.0225`.

BATHURST, R.J.; ALTHOFF, S.; LINNENBAUM, P. Influence of test method on direct shear behavior of segmental retaining wall units. **Geotechnical Testing Journal**, v. 31, n. 2, p. 157–165, 2008. ISSN 01496115. DOI: `10.1520/gtj100911`.

BATHURST, R.J.; MIYATA, Y.; NERNHEIM, A.; ALLEN, A.M. Refinement of K-stiffness Method for geosynthetic-reinforced soil walls. English. **Geosynthetics International**, GeoEngineering Centre at Queen's-RMC, Department of Civil Engineering, Royal Military College of Canada, Kingston, ON K7K 7B4, Canada, v. 15, n. 4, p. 269–295, 2008. ISSN 10726349 (ISSN). DOI: `10.1680/gein.2008.15.4.269`.

BATHURST, R.J.; NAFTCHALI, F.M. Geosynthetic reinforcement stiffness for analytical and numerical modelling of reinforced soil structures. **Geotextiles and Geomembranes**, Elsevier Ltd, v. 49, n. 4, p. 921–940, Aug. 2021. ISSN 02661144. DOI: `10.1016/j.geotexmem.2021.01.003`.

BATHURST, R.J.; NERNHEIM, A.; WALTERS, D.L.; ALLEN, T.M.; BURGESS, P.; SAUNDERS, D.D. Influence of reinforcement stiffness and compaction on the performance of four geosynthetic-reinforced soil walls. **Geosynthetics International**, v. 16, n. 1, p. 43–59, Feb. 2009. ISSN 1072-6349. DOI: 10.1680/gein.2009.16.1.43.

BATHURST, R.J.; SIMAC, M.R. Review of Three Instrumented Geogrid Reinforced Soil Retaining Walls. In: 6TH Annual One Day Symposium. [S.l.: s.n.], 1991. p. 15–24.

BATHURST, R.J.; SIMAC, M.R.; BERG, R.R. Review of NCMA Segmental Retaining Wall Design Manual for Geosynthetic Reinforced Structures. **Transportation Research Record**, v. 1414, p. 16–25, 1993.

BATHURST, R.J.; SIMAC, M.R.; CHRISTOPHER, B.R.; BONCZKIEWICZ, C. A Database of Results from a Geosynthetic Reinforced Modular Block Soil Retaining Wall. In: PROCEEDINGS of Soil Reinforcement: Full Scale Experiments of the 80s, [s.l.: s.n.], 1993.

BATHURST, R.J.; VLACHOPOULOS, N.; WALTERS, D.L.; BURGESS, P.G.; ALLEN, T.M. The influence of facing stiffness on the performance of two geosynthetic reinforced soil retaining walls. **Canadian Geotechnical Journal**, v. 43, n. 12, p. 1225–1237, Dec. 2006. ISSN 0008-3674. DOI: 10.1139/t06-076.

BATHURST, R.J.; WALTERS, D.; VLACHOPOULOS, N.; BURGESS, P.; ALLEN, T.M. Full Scale Testing of Geosynthetic Reinforced Walls. Invited keynote paper. In: ________. **Advances in Transportation and Geoenvironmental Systems using Geosynthetics: Proceedings of Sessions of Geo-Denver**. Denver, Colorado: American Society of Civil Engineers (ASCE), 2000. p. 201–217. ISBN 9780784405154. DOI: 10.1061/40515(291)14.

BATHURST, R.J.; WALTERS, D.L. Lessons learned from full scale testing of geosynthetic reinforced soil retaining walls. In: GEOENG2000. Melbourne, Australia: [s.n.], 2000.

BATHURST, R.J.; WALTERS, D.L.; HATAMI, K.; SAUNDERS, D.D.; VLACHOPOULOS, N.; BURGESS, G.P.; ALLEN, T.M. Performance testing and numerical modelling of reinforced soil retaining walls. In: SEVENTH International Geosynthetics Conference. Nice, France: [s.n.], 2002. ISBN 9058095231.

BENJAMIM, C.V.S. **Avaliação experimental de protótipos de estruturas de contenção em solo reforçado com geotêxtil**. 2006. s. 294. PhD thesis – Escola de Engenharia de São Carlos.

BENJAMIM, C.V.S.; BUENO, B.S.; ZORNBERG, J.G. Field monitoring evaluation of geotextile-reinforced soil-retaining walls. **Geosynthetics International**, v. 14, n. 2, p. 100–118, Apr. 2007. ISSN 1072-6349. DOI: 10.1680/gein.2007.14.2.100.

BENTLEY. **PLAXIS 2D-Reference Manual**. Ed. by Bentley. 20.04. ed. [S.l.: s.n.], 2020. p. 1–570.

BERG, R.; CHRISTOPHER, B.; SAMTANI, N. **Design and construction of mechanically stabilized earth walls and reinforced soil slopes**. [S.l.]: Federal High Way Administration (FHWA), 2009. v. I. ISBN FHWA-NHI-10-024. DOI: FHWA-NHI-10-024&FHWA-NHI-10-025.

________. **Design and construction of mechanically stabilized earth walls and reinforced soil slopes–Volume II**. v. II. [S.l.], 2009. ISBN FHWA-NHI-10-024. DOI: FHWA-NHI-10-024&FHWA-NHI-10-025.

BISHOP, A.W.; MORGENSTERN, N. Stability coefficients for earth slopes. **Géotechnique**, v. 10, n. 4, p. 129–153, 1960. DOI: 10.1680/geot.1960.10.4.129.

BSI. **BS 5975:2019 - Code of practice for temporary works procedures and the permissible stress design of falsework**. [S.l.], 2019.

________. **BS 8006-1:2010+A1:2016 - Code of practice for strengthened / reinforced soils and other fills**. [S.l.: s.n.], 2010. ISBN 978-0-580-53842-1.

BUHAN, P. de; MANGIAVACCHI, R.; NOVA, R.; PELLEGRINI, G.; SALENÇON, J. Yield design of reinforced earth walls by a homogenization method. **Géotechnique**, v. 39, n. 2, p. 189–201, June 1989. ISSN 0016-8505. DOI: 10.1680/geot.1989.39.2.189.

BURGESS, G.P. **Performance of two full-scale model geosynthetic reinforced segmental retaining walls**. 1999. s. 227. PhD thesis – Royal Military College of Canada.

CARMO, C.A.T. do. **A avaliação do módulo de resiliência através de ensaios triaxiais dinâmicos de dois solos compactados e a sua estimativa a partir de ensaios rotineiros**. 1998. s. 131. PhD thesis – São Carlos School of Engineering - University of São Paulo. DOI: 10.11606/D.18.2018.tde-14032018-111408.

CHEHADE, H.A.; DIAS, D.; SADEK, M.; JENCK, O.; CHEHADE, F.H. Seismic analysis of geosynthetic-reinforced retaining wall in cohesive soils. **Geotextiles and Geomembranes**, Elsevier, v. 47, n. 3, p. 315–326, 2019. ISSN 0266-1144. DOI: 10.1016/j.geotexmem.2019.02.003.

________. Upper bound seismic limit analysis of geosynthetic-reinforced unsaturated soil walls. **Geotextiles and Geomembranes**, Elsevier, v. 48, n. 4, p. 419–430, Aug. 2020. ISSN 02661144. DOI: 10.1016/j.geotexmem.2020.02.001.

CHEN, W. **Limit analysis and soil plasticity**. [S.l.]: Elsevier, 1975. p. 638. ISBN 0444412492.

CHEN, Y.; GAO, Y.; YANG, S.; ZHANG, F. Required unfactored geosynthetic strength of three-dimensional reinforced soil structures comprised of cohesive backfills. **Geotextiles and Geomembranes**, Elsevier, v. 46, n. 6, p. 860–868, 2018. ISSN 02661144. DOI: `10.1016/j.geotexmem.2018.08.004`.

CLAYBOURN, A.F.; WU, J.T.H. Geosynthetic-reinforced soil wall design. **Geotextiles and Geomembranes**, v. 12, n. 8, p. 707–724, Jan. 1993. ISSN 02661144. DOI: `10.1016/0266-1144(93)90047-R`.

CORREIA, N.d.S. **Performance of flexible pavements enhanced using geogrid-reinforced asphalt overlays**. 2014. s. 205. PhD thesis.

DAMIANS, I.P.; BATHURST, R.J.; JOSA, A.; LLORET, A. Numerical study of the influence of foundation compressibility and reinforcement stiffness on the behavior of reinforced soil walls. English. **International Journal of Geotechnical Engineering**, Maney Publishing, Department of Geotechnical Engineering and Geo-Sciences (ETCG), School of Civil Engineering (ETSECCP), Universitat Politècnica de Catalunya - BarcelonaTech (UPC), Spain, v. 8, n. 3, p. 247–259, 2014. ISSN 19386362 (ISSN). DOI: `10.1179/1939787913Y.0000000039`.

DAMIANS, I.P.; BATHURST, R.J.; JOSA, A.; LLORET, A.; ALBUQUERQUE, P.J.R. Vertical-Facing Loads in Steel-Reinforced Soil Walls. **Journal of Geotechnical and Geoenvironmental Engineering**, v. 139, n. 9, p. 1419–1432, Sept. 2013. ISSN 1090-0241. DOI: `10.1061/(ASCE)GT.1943-5606.0000874`.

DAS, B.M. **Fundamentals of Geotechnical Engineering**. 3. ed. [S.l.]: CL-Engineering, 2007. p. 622. ISBN 0-495-29572-8.

DAVIS, E.H. Theories of plasticity and failure of soil masses. In: LEE, I. K. (Ed.). **Soil mechanics: selected topics**. New York, NY, USA: Elsevier, 1968. p. 341–354.

EHRLICH, M.; MIRMORADI, S.H. A simplified working stress design method for reinforced soil walls. **Géotechnique**, v. 66, n. 10, p. 854–863, Oct. 2016. ISSN 0016-8505. DOI: `10.1680/jgeot.16.P.010`.

________. Evaluation of the effects of facing stiffness and toe resistance on the behavior of GRS walls. **Geotextiles and Geomembranes**, Elsevier Ltd, v. 40, p. 28–36, 2013. ISSN 02661144. DOI: `10.1016/j.geotexmem.2013.07.012`.

EHRLICH, M.; MITCHELL, J.K. Working Stress Design Method for Reinforced Soil Walls. **Journal of Geotechnical Engineering**, v. 120, n. 4, p. 625–645, Apr. 1994. ISSN 0733-9410. DOI: `10.1061/(ASCE)0733-9410(1994)120:4(625)`.

ELIAS, V.E.; CHRISTOPHER, B.R. **Mechanically stabilized earth walls and reinforced soil slopes: design and construction guidelines**. [S.l.], 2001. p. 418.

EL-EMAM, M.M.; BATHURST, R.J. Facing contribution to seismic response of reduced-scale reinforced soil walls. English. **Geosynthetics International**, GeoEngineering Centre at Queen's-RMC, Queen's University, Kingston, Ont. K7L 3N6, Canada, v. 12, n. 5, p. 215–238, 2005. ISSN 10726349 (ISSN). DOI: 10.1680/gein.2005.12.5.215.

ESFEHANI, M.; BATHURST, R.J. Influence of Fines Content on Reinforced Soil Retaining Wall Behaviour. In: 55TH Canadian Geotechnical Conference. Niagara Falls, Ontario: Canadian Geotechnical Society, 2002. p. 8.

EZZEIN, F.M. **INFLUENCE OF FOUNDATION STIFFNESS ON REINFORCED SOIL WALL BEHAVIOUR**. 2007. PhD thesis – Queen's University.

FARRAG, K.; ABU-FARSAKH, M.; MORVANT, M. Stress and Strain Monitoring of Reinforced Soil Test Wall. **Transportation Research Record: Journal of the Transportation Research Board**, v. 1868, p. 89–99, Jan. 2004. ISSN 0361-1981. DOI: 10.3141/1868-10.

FISHMAN, K.L.; DESAI, C.S.; SOGGE, R.L. Field Behavior of Instrumented Geogrid Soil Reinforced Wall. **Journal of Geotechnical Engineering**, v. 119, n. 8, p. 1293–1307, Aug. 1993. ISSN 0733-9410. DOI: 10.1061/(ASCE)0733-9410(1993)119:8(1293).

FRANCO, Y.B.; UTILI, S.; SILVA, J.L. Design of reinforced cohesive soil walls accounting for wall facing contribution to stability. **Géotechnique**, v. 73, n. 8, p. 667–688, Aug. 2023. ISSN 0016-8505. DOI: 10.1680/jgeot.21.00119.

GONZÁLEZ-CASTEJÓN, J.; SMITH, C.C. Optimised design of soil reinforcement layout. **Géotechnique**, p. 1–10, 2021. ISSN 0016-8505. DOI: 10.1680/jgeot.19.p.326.

GREGG, R. **Performance of Two Full-Scale Model GeosyntheticReinforced Retaining Walls Constructed with a Sandy silt Backfill Soil**. 2008. s. 206. PhD thesis – Royal Military College of Canada. ISBN 9780494421352. DOI: 10.1016/b978-012397720-5.50034-7.

GULER, E.; ENUNLU, A.K. Investigation of dynamic behavior of geosynthetic reinforced soil retaining structures under earthquake loads. **Bulletin of Earthquake Engineering**, v. 7, n. 3, p. 737–777, 2009. ISSN 1570761X. DOI: 10.1007/s10518-009-9106-9.

GULER, E.; HAMDERI, M.; DEMIRKAN, M.M. Numerical analysis of reinforced soil-retaining wall structures with cohesive and granular backfills. **Geosynthetics International**, v. 14, n. 6, p. 330–345, 2007. ISSN 1072-6349. DOI: 10.1680/gein.2007.14.6.330.

HATAMI, K.; BATHURST, R.J. Development and verification of a numerical model for the analysis of geosynthethic-reinforced soil segmental walls under working stress conditions. English. **Canadian Geotechnical Journal**, GeoEngineering Centre at Queen's-RMC, Department of Civil Engineering, Royal Military College of Canada, Kingston, Ont. K7K 7B4, Canada, v. 42, n. 4, p. 1066–1085, 2005. ISSN 00083674 (ISSN). DOI: 10.1139/t05-040.

________. Numerical Model for Reinforced Soil Segmental Walls under Surcharge Loading. **Journal of Geotechnical and Geoenvironmental Engineering**, v. 132, n. 6, p. 673–684, June 2006. ISSN 1090-0241. DOI: 10.1061/(ASCE)1090-0241(2006)132:6(673).

HEAD, K.H.; EPPS, R.J. **Manual of Soil Laboratory Testing - Volume 3: Effective Stress Tests**. 3. ed. Scotland, UK: Whittles Publishing, 2014. v. 3, p. 414. ISBN 0471977950.

HO, S.K.; ROWE, R.Kerry. Effect of wall geometry on the behaviour of reinforced soil walls. **Geotextiles and Geomembranes**, v. 14, n. 10, p. 521–541, Oct. 1996. ISSN 02661144. DOI: 10.1016/S0266-1144(97)83183-4.

HOLTZ, R.D.; LEE, W.F. **Internal Stability Analyses of Geosynthetic Reinforced Retaining Walls. No. WA-RD 532.1.** Olympia, WA, USA, 2002.

________. WA-RD 532.1: Internal Stability Analyses of Geosynthetic Reinforced Retaining Walls. **Washington State Transportation Center (TRAC)**, January 2002, 2002.

HUANG, B.; BATHURST, R.J.; HATAMI, K.; ALLEN, T.M. Influence of toe restraint on reinforced soil segmental walls. **Canadian Geotechnical Journal**, v. 47, n. 8, p. 885–904, Aug. 2010. ISSN 0008-3674. DOI: 10.1139/T10-002.

IAI, S. Similitude for Shaking Table Tests on Soil-Structure-Fluid Model in 1g Gravitational Field. **Soils and Foundations**, v. 29, n. 1, p. 105–118, Mar. 1989. ISSN 00380806. DOI: 10.3208/sandf1972.29.105.

ISMEIK, M.; GULER, E. Effect of Wall Facing on the Seismic Stability of Geosynthetic-Reinforced Retaining Walls. **Geosynthetics International**, v. 5, n. 1-2, p. 41–53, Jan. 1998. ISSN 1072-6349. DOI: 10.1680/gein.5.0113.

JEWELL, R.A. Application of revised design charts for steep reinforced slopes. **Geotextiles and Geomembranes**, v. 10, n. 3, p. 203–233, 1991. ISSN 02661144. DOI: 10.1016/0266-1144(91)90056-3.

________. Revised design charts for steep reinforced slopes. In: REINFORCED embankments, theory and practice. London, England: Thomas Telford, 1990. p. 1–30. DOI: 10.1680/re.15456.0001.

________. **Soil reinforcement with geotextiles**. London, UK: CIRIA and Thomas Telford, 1996.

JEWELL, R.A.; PAINE, N.; WOODS, R.I. Design methods for steep reinforced embankments. In: POLYMER Grid Reinforcement in Civil Engineer. London: [s.n.], 1984. p. 70–81. ISBN 0727702424.

JONES, C.J.F.P. **Earth Reinforcement and Soil Structures**. 3. ed. [S.l.: s.n.], 1996. p. 379. ISBN 9780408035491.

KAKUDA, F.M. **Desenvolvimento e a utilização de um equipamento de grandes dimensões na análise do comportamento mecânico de uma seção de pavimento sob carregamento cíclico.** 2010. s. 290. PhD thesis – São Carlos School of Engineering.

KARPURAPU, R.; BATHURST, R.J. Behaviour of geosynthetic reinforced soil retaining walls using the finite element method. **Computers and Geotechnics**, v. 17, n. 3, p. 279–299, Jan. 1995. ISSN 0266352X. DOI: 10.1016/0266-352X(95)99214-C.

KERRY ROWE, R.; SKINNER, G.D. Numerical analysis of geosynthetic reinforced retaining wall constructed on a layered soil foundation. **Geotextiles and Geomembranes**, v. 19, n. 7, p. 387–412, Sept. 2001. ISSN 02661144. DOI: 10.1016/S0266-1144(01)00014-0.

KOERNER, R.M. **Designing with geosynthetics**. 5th. New Jersey: Pearson Prentice Hall, 2005. ISBN 0131454153.

KOERNER, R.M.; KOERNER, G.R. A data base, statistics and recommendations regarding 171 failed geosynthetic reinforced mechanically stabilized earth (MSE) walls. **Geotextiles and Geomembranes**, v. 40, p. 20–27, Oct. 2013. ISSN 02661144. DOI: 10.1016/j.geotexmem.2013.06.001.

________. An extended data base and recommendations regarding 320 failed geosynthetic reinforced mechanically stabilized earth (MSE) walls. **Geotextiles and Geomembranes**, Elsevier, v. 46, n. 6, p. 904–912, 2018. ISSN 02661144. DOI: 10.1016/j.geotexmem.2018.07.013.

________. The importance of drainage control for geosynthetic reinforced mechanically stabilized earth walls. English. **Journal of GeoEngineering**, Taiwan Geotechnical Society, Drexel University, Geosynthetic Institute, Folsom, PA, United States, v. 6, n. 1, p. 3–13, 2011. ISSN 19908326 (ISSN). DOI: 10.6310/jog.2011.6(1).1.

LEE, K.L.; ADAMS, B.D.; VAGNERON, J.J. Reinforced Earth Retaining Walls. **Journal of the Soil Mechanics and Foundations Division**, v. 99, n. 10, p. 745–764, 1973.

LESHCHINSKY, D. Design dilemma: Use peak or residual strength of soil. **Geotextiles and Geomembranes**, v. 19, n. 2, p. 111–125, 2001. ISSN 02661144. DOI: 10.1016/S0266-1144(00)00007-8.

________. Discussion on The influence of facing stiffness on the performance of two geosynthetic reinforced soil retaining walls. **Canadian Geotechnical Journal**, v. 44, n. 12, p. 1479–1482, Dec. 2007. ISSN 0008-3674. DOI: 10.1139/T07-102.

LESHCHINSKY, D.; BOEDEKER, R.H. Geosynthetic Reinforced Soil Structures. **Journal of Geotechnical Engineering**, v. 115, n. 10, p. 1459–1478, Oct. 1989. ISSN 0733-9410. DOI: 10.1061/(ASCE)0733-9410(1989)115:10(1459).

LESHCHINSKY, D.; EBRAHIMI, S.; VAHEDIFARD, F.; ZHU, F. Extension of Mononobe-Okabe approach to unstable slopes. **Soils and Foundations**, Elsevier, v. 52, n. 2, p. 239–256, 2012. ISSN 00380806. DOI: 10.1016/j.sandf.2012.02.004.

LESHCHINSKY, D.; LESHCHINSKY, B.; LESHCHINSKY, O. Limit state design framework for geosynthetic-reinforced soil structures. **Geotextiles and Geomembranes**, Elsevier Ltd, v. 45, n. 6, p. 642–652, 2017. ISSN 02661144. DOI: 10.1016/j.geotexmem.2017.08.005.

LESHCHINSKY, D.; LING, H.; HANKS, G. Unified Design Approach to Geosynthetic Reinforced Slopes and Segmental Walls. **Geosynthetics International**, v. 2, n. 5, p. 845–881, Jan. 1995. ISSN 1072-6349. DOI: 10.1680/gein.2.0039.

LESHCHINSKY, D.; PERRY, E.B. On the design of geosynthetic-reinforced walls. English. **Geotextiles and Geomembranes**, Department of Civil Engineering, University of Delaware, Newark, DE 19716, United States, v. 8, n. 4, p. 311–323, 1989. ISSN 02661144 (ISSN). DOI: 10.1016/0266-1144(89)90014-9.

LESHCHINSKY, D.; VULOVA, C. Numerical Investigation of the Effects of Geosynthetic Spacing on Failure Mechanisms in MSE Block Walls. **Geosynthetics International**, v. 8, n. 4, p. 343–365, Jan. 2001. ISSN 1072-6349. DOI: 10.1680/gein.8.0199.

LESHCHINSKY, D.; ZHU, F.; MEEHAN, C.L. Required unfactored strength of geosynthetic in reinforced earth structures. English. **Journal of Geotechnical and Geoenvironmental Engineering**, Dept. of Civil and Environmental Engineering, Univ. of Delaware, 301 DuPont Hall, Newark, DE 19716, United States, v. 136, n. 2, p. 281–289, 2010. ISSN 10900241 (ISSN). DOI: 10.1061/(ASCE)GT.1943-5606.0000209.

LI, Z.; YANG, X. Active earth pressure for soils with tension cracks under steady unsaturated flow conditions. **Canadian Geotechnical Journal**, v. 55, n. 12, p. 1850–1859, 2018. ISSN 0008-3674. DOI: 10.1139/cgj-2017-0713.

LI, Z.W.; YANG, X.L. Active earth pressure for retaining structures in cohesive backfills with tensile strength cut-off. **Computers and Geotechnics**, v. 110, August 2018, p. 242–250, June 2019. ISSN 0266352X. DOI: 10.1016/j.compgeo.2019.02.023.

LING, H.I.; LESHCHINSKY, D. Finite element parametric study of the behavior of segmental block reinforced-soil retaining walls. **Geosynthetics International**, v. 10, n. 3, p. 77–94, June 2003. ISSN 1072-6349. DOI: 10.1680/gein.2003.10.3.77.

LING, H.I.; LESHCHINSKY, D.; CHOU, N.N.S. Post-earthquake investigation on several geosynthetic-reinforced soil retaining walls and slopes during the ji-ji earthquake of Taiwan. English. **Soil Dynamics and Earthquake Engineering**, Dept. Civ. Eng. and Eng. Mechanics, Columbia Univ., 500 W. 120th Street, New York, NY 10027, United States, v. 21, n. 4, p. 297–313, 2001. ISSN 02677261 (ISSN). DOI: 10.1016/S0267-7261(01)00011-2.

MICHALOWSKI, R.L. Limit analysis in stability calculations of reinforced soil structures. **Geotextiles and Geomembranes**, v. 16, n. 6, p. 311–331, 1998. ISSN 02661144. DOI: 10.1016/S0266-1144(98)00015-6.

________. Stability assessment of slopes with cracks using limit analysis. **Canadian Geotechnical Journal**, v. 50, n. 10, p. 1011–1021, 2013. ISSN 00083674. DOI: 10.1139/cgj-2012-0448.

________. Stability of Uniformly Reinforced Slopes. **Journal of Geotechnical and Geoenvironmental Engineering**, v. 123, n. 6, p. 546–556, June 1997. ISSN 1090-0241. DOI: 10.1061/(ASCE)1090-0241(1997)123:6(546).

MICHALOWSKI, R.L.; ZHAO, A. Continuum versus Structural Approach to Stability of Reinforced Soil. **Journal of Geotechnical Engineering**, v. 121, n. 2, p. 152–162, Feb. 1995. ISSN 0733-9410. DOI: 10.1061/(ASCE)0733-9410(1995)121:2(152).

MIRMORADI, S.H.; EHRLICH, M. Effects of facing, reinforcement stiffness, toe resistance, and height on reinforced walls. **Geotextiles and Geomembranes**, Elsevier Ltd, v. 45, n. 1, p. 67–76, 2017. ISSN 02661144. DOI: 10.1016/j.geotexmem.2016.07.006.

________. Modeling of the compaction-induced stress on reinforced soil walls. **Geotextiles and Geomembranes**, v. 43, p. 82–88, Feb. 2015. ISSN 02661144. DOI: 10.1016/j.geotexmem.2014.11.001.

________. Numerical Evaluation of the Behavior of GRS Walls with Segmental Block Facing under Working Stress Conditions. **Journal of Geotechnical and Geoenvironmental Engineering**, v. 141, n. 3, p. 04014109, Mar. 2015. ISSN 1090-0241. DOI: 10.1061/(ASCE)GT.1943-5606.0001235.

MIRMORADI, S.H.; EHRLICH, M. Numerical simulation of compaction-induced stress for the analysis of RS walls under working conditions. **Geotextiles and Geomembranes**, Elsevier, v. 46, n. 3, p. 354–365, 2018. ISSN 02661144. DOI: `10.1016/j.geotexmem.2018.01.006`.

MIRMORADI, S.H.; NASCIMENTO, G. Investigation of the Effect of Compaction-Induced Stress on the Behavior of Reinforced Soil Walls. v. 43, n. 3, p. 419–439, 2020.

MITCHELL, J.K.; VILLET, W.C.B.; BOARD, N.R.C.U.S..T.R. **Reinforcement of earth slopes and embankments**. Washington, 1987. p. 323. ISBN 0309040248.

MIYATA, Y.; BATHURST, R.J. Development of the K-stiffness method for geosynthetic reinforced soil walls constructed with c-π soils. English. **Canadian Geotechnical Journal**, v. 44, n. 12, p. 1391–1416, 2007. ISSN 00083674 (ISSN). DOI: `10.1139/T07-058`.

MIYATA, Y.; BATHURST, R.J.; MIYATAKE, H. Performance of three geogrid-reinforced soil walls before and after foundation failure. **Geosynthetics International**, v. 22, n. 4, p. 311–326, Aug. 2015. ISSN 1072-6349. DOI: `10.1680/gein.15.00014`.

MURARO, S.; MADASCHI, A.; GAJO, A. Passive soil pressure on sloping ground and design of retaining structures for slope stabilisation. **Géotechnique**, v. 65, n. 6, p. 507–516, June 2015. ISSN 0016-8505.

NCMA. **Design Manual for Segmental Retaining Walls**. Ed. by M. Bernardi. 3. ed. Herndon, VA: [s.n.], 2010.

NELSON, R. **Perfomance of two full-scale reinforced retaining walls - modular block and incremental panel**. 2005. s. 254. Master of Engineering – Royal Military College, Kingston, Ontario, Canada.

NOGAMI, J.S.; VILLIBOR, D.F. A new geotechnical classification for tropical soils. In: BRAZILIAN Symposium of Tropical Soil in Engineering. Rio de Janeiro, Brazil: [s.n.], 1981. p. 30–41.

PATIAS, J. **Avaliação do uso de solos não convencionais em estruturas de solo reforçado**. 2005. PhD thesis – São Carlos School of Engineering.

PEDROSO, G.O.M. **Performance of geosynthetic base stabilization under cyclic moving wheel loads by laboratory and numerical evaluation**. 2021. PhD thesis – São Carlos School of Engineering - University of São Paulo.

PERRY, J. A technique for defining non-linear shear strength envelopes, and their incorporation in a slope stability method of analysis. **Quarterly Journal of Engineering Geology**, v. 27, n. 3, p. 231–241, 1994. ISSN 04812085. DOI: 10.1144/gsl.qjegh.1994.027.p3.04.

PLÁCIDO, R.R. **Análises de campo e laboratório do comportamento ao longo do tempo de muros de solos tropicais finos reforçados com geossintéticos**. 2016. PhD thesis – Escola Politécnica da Universidade de São Paulo.

PORBAHA, A.; GOODINGS, D.J. Laboratory Investigation of Nonuniformly Reinforced Soil-Retaining Structures. **Geotechnical Testing Journal**, v. 20, n. 3, p. 289–295, 1997. ISSN 01496115. DOI: 10.1520/gtj19970004.

PORBAHA, A.; ZHAO, A.; KOBAYASHI, M.; KISHIDA, T. Upper bound estimate of scaled reinforced soil retaining walls. **Geotextiles and Geomembranes**, v. 18, n. 6, p. 403–413, 2000. ISSN 02661144. DOI: 10.1016/S0266-1144(99)00036-9.

PORTELINHA, F.H.M. **Avaliação experimental da influência do avanço do umedecimento no comportamento de muros de solos finos reforçados com geotêxteis não tecidos**. 2012. PhD thesis – São Carlos School of Engineering - University of São Paulo.

POTTS, D.M.; FOURIE, A.B. A numerical study of the effects of wall deformation on earth pressures. **International Journal for Numerical and Analytical Methods in Geomechanics**, v. 10, n. 4, p. 383–405, July 1986. ISSN 0363-9061. DOI: 10.1002/nag.1610100404.

POTTS, D.M.; KOVACEVIC, N.; VAUGHAN, P.R. Delayed collapse of cut slopes in stiff clay. **Géotechnique**, v. 47, n. 5, p. 953–982, Oct. 1997. ISSN 0016-8505. DOI: 10.1680/geot.1997.47.5.953.

REEVES, J.W. **Performance of a full-scale wrapped face welded wire mesh reinforced retaining wall.PDF**. 2003. PhD thesis.

RESL, S. Soil-reinforced mechanisms of nonwoven geotextiles. In: GEOTEXTILES, geomembranes and related products. Rotterdam: Balkema, 1990. p. 93–96.

RICCIO, M.; EHRLICH, M.; DIAS, D. Field monitoring and analyses of the response of a block-faced geogrid wall using fine-grained tropical soils. **Geotextiles and Geomembranes**, v. 42, n. 2, p. 127–138, Apr. 2014. ISSN 02661144. DOI: 10.1016/j.geotexmem.2014.01.006.

RINCÓN BARAJAS, S.A. **Estudo comparativo da interação solo-geogrelha por meio de ensaios de arrancamento monotônico e cíclico utilizando equipamentos de pequenas e grandes dimensões**. 2016. s. 191. PhD thesis – São Carlos School of Engineering - University of São Paulo.

ROWE, R.K.; HO, S.K. A review of the behaviour of reinforced soil walls. In: OCHIAI, Hidetoshi; HAYASHIC, Shigenori; ORANI, J.ORANI (Eds.). **International symposium on earth reinforcement**. Rotterdam: A. A. Balkema, 1992. p. 801–830.

SALEM, M.A.; HAMMAD, M.A.; AMER, M.I. Field monitoring and numerical modeling of 4.4 m-high mechanically stabilized earth wall. **Geosynthetics International**, n. 5, p. 1–45, 2018. ISSN 1072-6349. DOI: `10.1680/jgein.18.00027`.

SANTOS, E.C.G.D. **Avaliação experimental de muros reforçados executados com resíduos de construção e demolição reciclados (RCD-R) e solo fino**. 2011. s. 248. PhD thesis – UNB.

SAWICKI, A. Plastic Limit Behavior of Reinforced Earth. **Journal of Geotechnical Engineering**, ASCE McGraw Hill ©ASCE, v. 109, n. 7, p. 1000–1005, July 1983. ISSN 0733-9410. DOI: `10.1061/(ASCE)0733-9410(1983)109:7(1000)`.

SCHLOSSER, F.; DELAGE, P. Reinforced soil retaining structures and polymeric materials. In: ________. **NATO ADVANCED RESEARCH WORKSHOP ON APPLICATION OF POLYMERIC REINFORCEMENT IN SOIL RETAINING STRUCTURES**. Kingston, Ontario: Kluwer Academic Publishers, 1987. p. 71–125.

SKINNER, G.D.; ROWE, R.K. Design and behaviour of geosynthetic-reinforced soil walls constructed on yielding foundations. **Geosynthetics International**, v. 10, n. 6, p. 200–214, Dec. 2003. ISSN 1072-6349. DOI: `10.1680/gein.2003.10.6.200`.

SLOAN, S.W. Geotechnical stability analysis. **Géotechnique**, v. 63, n. 7, p. 531–572, 2013. DOI: `10.1680/geot.12.RL.001`.

SUAH, P.G.; GOODINGS, D.J. Failure of Geotextile-Reinforced Vertical Soil Walls with Marginal Backfill. **Transportation Research Record: Journal of the Transportation Research Board**, v. 1772, n. 1, p. 183–189, Jan. 2001. ISSN 0361-1981. DOI: `10.3141/1772-22`.

TAKE, W.A.; BOLTON, M.D. Seasonal ratcheting and softening in clay slopes, leading to first-time failure. **Géotechnique**, v. 61, n. 9, p. 757–769, Sept. 2011. ISSN 0016-8505. DOI: `10.1680/geot.9.P.125`.

TAKEDA, M.C. **A Influência da variação da umidade pós-compactação no comportamento mecânico de solos de rodovias do interior paulista**. 2006. s. 255. PhD thesis.

TATSUOKA, F.; TATEYAMA, M.; UCHIMURA, T.; KOSEKI, J. Geosynthetic-reinforced soil retaining walls as important permanent structures. **Geosynthetics International**, v. 4, n. 2, p. 81–136, 1998. ISSN 10726349. DOI: `10.1680/gein.4.0090`.

TESTING, American Society for; MATERIALS. **D6916-18 - Determining the Shear Strength Between Segmental Concrete Units (Modular Concrete Blocks)**. West Conshohocken, PA, 2018. p. 1–7. DOI: 10.1520/D6916-18.2.

THUSYANTHAN, N.I.; TAKE, W.A.; MADABHUSHI, S.P.G.; BOLTON, M.D. Crack initiation in clay observed in beam bending. **Géotechnique**, v. 57, n. 7, p. 581–594, Sept. 2007. ISSN 0016-8505. DOI: 10.1680/geot.2007.57.7.581.

UTILI, S. Investigation by limit analysis on the stability of slopes with cracks. **Géotechnique**, v. 63, n. 2, p. 140–154, Feb. 2013. ISSN 0016-8505. DOI: 10.1680/geot.11.P.068.

UTILI, S.; ABD, A.H. On the stability of fissured slopes subject to seismic action. **International Journal for Numerical and Analytical Methods in Geomechanics**, v. 40, n. 5, p. 785–806, Apr. 2016. ISSN 0363-9061. DOI: 10.1002/nag.2498.

UTILI, S.; NOVA, R. On the optimal profile of a slope. **Soils and Foundations**, v. 47, n. 4, p. 717–729, 2007. ISSN 00380806. DOI: 10.3208/sandf.47.717.

VAHEDIFARD, F.; LESHCHINSKY, B.A.; MORTEZAEI, K.; LU, N. Active Earth Pressures for Unsaturated Retaining Structures. **Journal of Geotechnical and Geoenvironmental Engineering**, v. 141, n. 11, p. 04015048, Nov. 2015. ISSN 1090-0241. DOI: 10.1061/(ASCE)GT.1943-5606.0001356. arXiv: 1612.06814.

VAHEDIFARD, F.; LESHCHINSKY, B.A.; SEHAT, S.; LESHCHINSKY, D. Impact of cohesion on seismic design of geosynthetic-reinforced earth structures. English. **Journal of Geotechnical and Geoenvironmental Engineering**, American Society of Civil Engineers (ASCE), Dept. of Civil and Environmental Engineering, Mississippi State Univ, Mississippi State, MS, United States, v. 140, n. 6, 2014. ISSN 10900241 (ISSN). DOI: 10.1061/(ASCE)GT.1943-5606.0001099.

VIANA, P.M.F. **Geovala : Um Novo Processo Construtivo**. 2003. s. 265. PhD thesis – São Carlos School of Engineering - University of São Paulo.

VIDAL, H. La Terre Armée. In: ANNALES de l'institut technique du batiment et des travaux publics. [S.l.: s.n.], 1966.

VISWANADHAM, B.V.S.; KÖNIG, D. Studies on scaling and instrumentation of a geogrid. **Geotextiles and Geomembranes**, v. 22, n. 5, p. 307–328, 2004. ISSN 02661144. DOI: 10.1016/S0266-1144(03)00045-1.

WARREN, K.A.; CHRISTOPHER, B.; HOWARD, I.L. Geosynthetic strain gage installation procedures and alternative strain measurement methods for roadway applications. **GEOSYNTHETICS INTERNATIONAL**, ICE PUBL, 40 MARSH WALL, 2 FL, LONDON E14 9TP, ENGLAND, v. 17, n. 6, p. 403–430, 2010. ISSN 1072-6349. DOI: 10.1680/gein.2010.17.6.403.

WOOD, D.M. **Geotechnical modelling**. [S.l.: s.n.], 2004. p. 1–488. ISBN 9781482288315. DOI: 10.1201/9781315273556.

WU, J.T.H.; PAYEUR, J.B. Connection Stability Analysis of Segmental Geosynthetic Reinforced Soil (GRS) Walls. **Transportation Infrastructure Geotechnology**, v. 2, n. 1, p. 1–17, 2015. ISSN 21967210. DOI: 10.1007/s40515-014-0013-4.

XIE, Y.; LESHCHINSKY, B.; YANG, S. Evaluating reinforcement loading within surcharged segmental block reinforced soil walls using a limit state framework. English. **Geotextiles and Geomembranes**, Elsevier Ltd, Dept. of Civil and Construction Engineering, Oregon State University, 101 Kearney Hall, Corvallis, OR, United States, v. 44, n. 6, p. 832–844, 2016. ISSN 02661144 (ISSN). DOI: 10.1016/j.geotexmem.2016.06.010.

YOO, C.S.; SONG, A.R. Effect of foundation yielding on performance of two-tier geosynthetic-reinforced segmental retaining walls: A numerical investigation. English. **Geosynthetics International**, Department of Civil and Environmental Engineering, Sungkyunkwan University, 300 Chun-Chun Dong, Jan-An Gu, Suwon, Kyong-Gi Do 440-746, South Korea, v. 13, n. 5, p. 181–194, 2006. ISSN 10726349 (ISSN). DOI: 10.1680/gein.2006.13.5.181.

ZHANG, W.; CHEN, J.; YU, Y. Influence of toe restraint conditions on performance of geosynthetic-reinforced soil retaining walls using centrifuge model tests. **Geotextiles and Geomembranes**, Elsevier, v. 47, n. 5, p. 653–661, Oct. 2019. ISSN 02661144. DOI: 10.1016/j.geotexmem.2019.103469.

ZHAO, A. Limit Analysis of Geosynthetic-Reinforced Soil Slopes. **Geosynthetics International**, v. 3, n. 6, p. 721–740, Jan. 1996. ISSN 1072-6349. DOI: 10.1680/gein.3.0082.

ZHENG, Y.; FOX, P.J. Numerical Investigation of Geosynthetic-Reinforced Soil Bridge Abutments under Static Loading. **Journal of Geotechnical and Geoenvironmental Engineering**, v. 142, n. 5, p. 04016004, May 2016. ISSN 1090-0241. DOI: 10.1061/(ASCE)GT.1943-5606.0001452.

ZORNBERG, J.G.; SITAR, N.; MITCHELL, J.K. Limit Equilibrium as Basis for Design of Geosynthetic Reinforced Slopes. **Journal of Geotechnical and Geoenvironmental Engineering**, v. 124, n. 8, p. 684–698, Aug. 1998. ISSN 1090-0241. DOI: 10.1061/(ASCE)1090-0241(1998)124:8(684).

________. Performance of Geosynthetic Reinforced Slopes at Failure. **Journal of Geotechnical and Geoenvironmental Engineering**, v. 124, n. 8, p. 670–683, Aug. 1998. ISSN 1090-0241. DOI: 10.1061/(ASCE)1090-0241(1998)124:8(670).

A Analytical expressions for LID distribution

For linearly increasing distribution (LID), the expression for the energy dissipated by the geosynthetics along the log-spiral C-D and the crack B-C can be expressed as follow:

$$\begin{aligned}\dot{D}_{r(B-D)} &= \dot{D}_{r(B-C)} + \dot{D}_{r(C-D)} \\ &= \frac{2}{\left(\frac{H}{r_0}\right)} K_t \dot{\theta} r_0^2 \left\{ \frac{1}{3} \left(\exp\left[3 \tan\phi \left(\theta_h - \theta_0\right)\right] \sin^3\theta_h - \sin^3\theta_0 \right) + \right. \\ &\quad \left. - \frac{\sin\theta_0}{2} \left(\exp\left[2 \tan\phi \left(\theta_h - \theta_0\right)\right] \sin^2\theta_h - \sin^2\theta_0 \right) \right\} \\ &= K_t \dot{\theta} r_0^2 g_r \left(\theta_0, \theta_h, \theta_C, \phi\right)\end{aligned} \tag{A.1}$$

If $\sin\theta_0 + z_i/r_0 < 0$, the layers above the centre of rotation are not tensioned so no energy is dissipated in them. Thus, Eq. A.1 simplifies to:

$$\begin{aligned}\dot{D}_{r(B-D)} = \frac{2}{\left(\frac{H}{r_0}\right)} K_t \dot{\theta} r_0^2 \left\{ \frac{1}{3} \left(\exp\left[3 \tan\phi \left(\theta_h - \theta_0\right)\right] \sin^3\theta_h \right) + \right. \\ \left. - \frac{\sin\theta_0}{2} \left(\exp\left[2 \tan\phi \left(\theta_h - \theta_0\right)\right] \sin^2\theta_h \right) \right\} \end{aligned} \tag{A.2}$$

$$= K_t \dot{\theta} r_0^2 g_r \left(\theta_0, \theta_h, \phi\right) \tag{A.3}$$

B Analytical expressions for the external work rate calculation

The final expressions of the components of the external work rate are given in detail as follows:

$$f_1(\theta_0, \theta_h, \phi) = \frac{\left[e^{3(\theta_h - \theta_0)\tan\phi}\right]\left[3\tan\phi\cos\theta_h + \sin\theta_h\right] - 3\tan\phi\cos\theta_0 - \sin\theta_0}{3\left(1 + 9\tan^2\phi\right)} \tag{B.1}$$

$$f_2(\theta_0, \theta_h, \beta, \phi) = \frac{l_1}{6r_0}\sin\theta_0\left(2\cos\theta_0 - \frac{l_1}{r_0}\right) \tag{B.2}$$

$$\begin{aligned} f_3(\theta_0, \theta_h, \beta, \phi) = {} & \frac{e^{(\theta_h - \theta_0)\tan\phi}}{6}\left[\sin(\theta_h - \theta_0) - \frac{l_1}{r_0}\sin\theta_h\right] \\ & \left[\cos\theta_0 - \frac{l_1}{r_0} + \cos\theta_h\left(e^{(\theta_h - \theta_0)\tan\phi}\right)\right] \end{aligned} \tag{B.3}$$

$$f_4(\theta_0, \theta_C, \phi) = \frac{e^{3(\theta_C - \theta_0)\tan\phi} + \left(3\tan\phi\cos\theta_C + \sin\theta_C\right) - 3\tan\phi\cos\theta_0 - \sin\theta_0}{3\left(1 + 9\tan^2\phi\right)} \tag{B.4}$$

$$f_5(\theta_0, \theta_C, \phi) = \frac{l_2}{6r_0}\sin\theta_0\left(2\cos\theta_0 - \frac{l_2}{r_0}\right) \tag{B.5}$$

$$f_6(\theta_0, \theta_C, \phi) = \frac{e^{2(\theta_C - \theta_0)\tan\phi}\cos^2\theta_C}{3}\left(e^{(\theta_C - \theta_0)\tan\phi}\sin\theta_C - \sin\theta_0\right) \tag{B.6}$$

$$\begin{aligned} f_w(\theta_0, \theta_h, \theta_C, \phi) = {} & \frac{1}{r_0^3}\left(\int_{\theta_w}^{\theta_c} z_c r_{BC}^2 \tan\theta d\theta\right. \\ & \left. + \int_{\theta_C}^{\theta_{1-2}} z_1 r^2 \tan\phi d\theta + \int_{\theta_{1-2}}^{\theta_h} z_2 r^2 \tan\phi d\theta\right) \end{aligned} \tag{B.7}$$

where r is given in Eq. (2.4) and r_{BC} by the following expression:

$$r_{BC} = \frac{r_C\cos\theta_C}{\cos\theta} \tag{B.8}$$

z_c, z_1 and z_2 are given below:

$$z_c = r_0 \left\{ \exp\left[\tan\phi\left(\theta_C - \theta_0\right)\right] \cos\theta_C \tan\theta - \sin\theta_0 \right\} \tag{B.9}$$

$$z_1 = r_0 \left\{ \exp\left[\tan\phi\left(\theta - \theta_0\right)\right] \sin\theta - \sin\theta_0 \right\} \tag{B.10}$$

$$\begin{aligned} z_2 = r_0 \{ & \exp\left[\tan\phi\left(\theta - \theta_0\right)\right] \sin\theta \\ & - \left[\exp\left[\tan\phi\left(\theta_{1-2} - \theta_0\right)\right] \cos\theta_{1-2} - \exp\left[\tan\phi\left(\theta - \theta_0\right)\right] \cos\theta\right] \tan\beta - \sin\theta_0 \} \end{aligned} \tag{B.11}$$

The angle θ_{1-2} is determined from:.

$$\exp\left[\tan\phi\left(\theta_{1-2} - \theta_0\right)\right] \cos\theta_{1-2} - \cos\theta_0 + \frac{l_1}{r_0} = 0 \qquad \theta_{1-2} \in \left[\theta_0, \theta_h\right] \tag{B.12}$$

Note that the previous expression has two solutions and the one to be taken is the value ranging from θ_0 to θ_h.

The term related to the work rate of the facing contribution, for the conventional direction and for a force acting at $D = H/\lambda$ from the wall toe (generalization of the expression given by (LI, Z.; YANG, X.) (2018; 2019)) is given by:

$$\begin{aligned} f_7\left(\theta_0, \theta_h, \beta, \delta, \lambda, \phi\right) = & \sin\left(\beta + \delta\right) \left[\sin\theta_0 + \frac{\left(\lambda - 1\right)}{\lambda} \frac{H}{r_0}\right] \\ & - \cos\left(\beta + \delta\right) \left[\exp\left[\tan\phi\left(\theta_h - \theta_0\right)\right] \cos\theta_h + \frac{1}{\lambda} \frac{H}{r_0} \cot\beta\right] \end{aligned} \tag{B.13}$$

where H is the wall height and λ is a dimensionless term larger than 1.

For the modified direction the following expression applies (generalization of the expression given by Xie, Leshchinsky, and Yang (2016)):

$$\begin{aligned} f_7\left(\theta_0, \theta_h, \beta, \delta, \lambda, \phi\right) = & \sin\delta \left[\exp\left[\tan\phi\left(\theta_h - \theta_0\right)\right] \cos\theta_h + \frac{1}{\lambda} \frac{H}{r_0} \cot\beta\right] \\ & + \cos\delta \left[\exp\left[\tan\phi\left(\theta_h - \theta_0\right)\right] \sin\theta_h - \frac{1}{\lambda} \frac{H}{r_0}\right] \end{aligned} \tag{B.14}$$

C Analytical expressions for failure mechanisms emerging at the wall facing

When considering failure mechanisms emerging at the wall facing Eq. 3.17 and Eq. 3.21 need to be modified to account for the reduced height H' of the failure mechanism:

$$H' = H\left[1 - \frac{(i_{block} - 1)}{N_b}\right], i_{block} : 1 \to N_b$$
$$H' = H \times \Omega \tag{C.1}$$

where Ω is the height factor, i_{block} identifies the block immediately above the block-block interface intersected by the failure mechanism (Figure C.1) and N_b is the number of facing blocks.

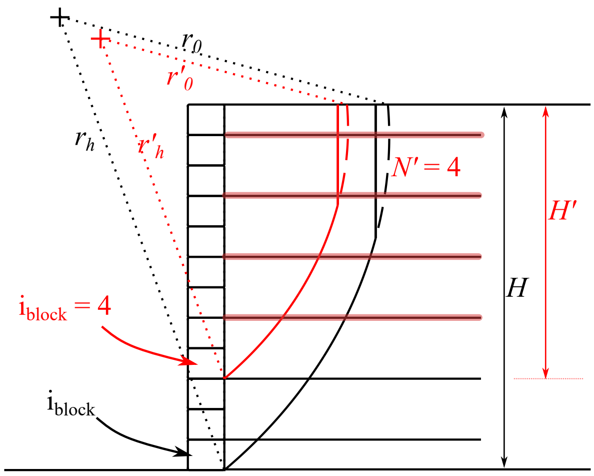

Figure C.1: Schematic of the failure surface emerging at the wall facing and notations.

For a partial wall height, only the weight of the column of blocks above the block-block interface considered contributes to the stability, therefore the reaction force acting on the facing element is given by P'_f:

$$\frac{P'_f}{\gamma H^2} = \frac{\Omega\,(\gamma_b/\gamma)\,(w_b/H)\tan\delta_{bb}}{\cos\delta_h - \sin\delta_h\tan\delta_{bb}} \tag{C.2}$$

where $\tan\delta_{bb}$ is the interface friction angle between two adjacent blocks.

The objective function given in Eq. , 3.17 becomes:

$$\frac{K_t}{\gamma H} = \frac{\Omega\left(f_1 - f_2 - f_3 - f_4 + f_5 + f_6 + r_u f_w\right)}{\left(\frac{H'}{r_0'}\right)\left(g_r\right)} - \frac{c}{\gamma H}\left(\frac{g_s}{g_r}\right) - \frac{1}{\Omega}\left(\frac{H'}{r_0'}\right)\frac{P_f'}{\gamma H^2}\frac{f_7}{\left(g_r\right)} \quad \text{(C.3)}$$

$$\frac{K_t}{\gamma H} = f(\theta_0, \theta_h, \theta_C, \beta, r_u, \phi, c/\gamma H, \delta, D, w_b/H, \delta_{base}, \delta_{bb}, \Omega)$$

The objective function given in Eq. 3.21, for a combined failure mechanism (rupture and pullout), becomes:

$$\begin{aligned}\frac{K_t}{\gamma H} = &\frac{\Omega\left(\frac{r_0'}{H'}\right)^2\left(f_1 - f_2 - f_3 - f_4 + f_5 + f_6 + r_u f_w\right) - \left(\frac{r_0'}{H'}\right)\left(\frac{c}{\gamma H}\right)\left(g_s\right)}{\frac{1}{N'}\sum_{rupture}\left(\sin\theta_0 + \frac{z_{(i)}}{r_0'}\right)} + \\ &+ \frac{-\frac{1}{\Omega}\frac{P_f'}{\gamma H^2} f_7 - 2 f_b \tan\phi\left(1 - r_u\right)\sum_{pullout}\left[\Omega\frac{z^*_{(i)}}{H'}\frac{L_{e(i)}}{H'}\left(\sin\theta_0 + \frac{z_{(i)}}{r_0'}\right)\right]}{\frac{1}{N'}\sum_{rupture}\left(\sin\theta_0 + \frac{z_{(i)}}{r_0'}\right)}\end{aligned} \quad \text{(C.4)}$$

$$\frac{K_t}{\gamma H} = f\left(\theta_0, \theta_h, \theta_C, \beta, r_u, \phi, c/\gamma H, \delta, D, w_b/H, \delta_{base}, \delta_{bb}, L/H, f_b, N', \Omega\right)$$

where N' is the number of reinforcement layers crossed above the intersection between the failure surface and the wall facing (Figure C.1). H' and r_o' are the geometric parameters related to the failure surface emerging at the wall facing as depicted in Figure C.1.

D Program Scripts (Matlab R2015a)

The codes developed and shown herein were based on the previous source codes from Abd (2017). The input data is a .mat file (whitout headline) in which each line represents one analysis to be conducted and the 20 columns the following parameters:

1. RES: Resolution (°) for the change in angles θ, θ_0 and θ_c;
2. f_b: bond coefficient between the soil and geosynthetic-reinforcement;
3. crack_constraint: 0 for no constraint for crack depth;
4. t: crack presence, 2 for intact slope and -1 for the most adverse pre-existing crack;
5. $^c/_{\gamma H}$: normalized cohesion;
6. β: facing batter (°);
7. γ: soil unit weight (kN/m);
8. ϕ': soil internal friction angle (°);
9. N: number of reinforcement layers (obs: function used $ff2n$ - Two-level full factorial design can return error for large N);
10. r_u :pore pressure coefficient pore pressure coefficient;
11. γ_b: facing block weight (kN/m);
12. w_b/H: normalized block width;
13. δ_{base}: interface friction angle between the wall facing and the foudation soil (°);
14. δ/ϕ': interface friction angle between the wall face and the retained soil over soil internal friction angle;
15. δ: interface friction angle between the wall face and the retained soil (°);
16. λ:dimensioneless term larger than 1 representing the position of the reaction force at the wall;
17. Force direction: 1 for conventional and 2 for modified;
18. L/H: normalized reinforcement length;
19. Dowdrag: 0 for no downdrag and 1 for consideration of downdrag force between soil and facing;
20. δ_{bb}:Interface friction angle between the wall facing blocks (°).

D.1 Main Program

```
% Main program
%Considers all reinfocements with same length (beta_prime=beta)
% ------------------------------------------------------------------------
function [Kreq_rup,Kreq_comb,LoH,SL,PL,d,dL,code_version,Xcir,Ycir,
    Xcir_L,Ycir_L,c_d_rup,c_d_comb,Flag_mode,face_loc_failure] =
    MainProgram_2020(study_case,data,RL,Reinf_length,flag_fixRht,fric_bb)
%clear
%clc
clear d dL Kreq_comb Kreq_rup LoH SL
LoH=Reinf_length;
disc_reinf = 0; %(0) Energy dissipated in reinf calculated continuously
    (integral) or (1) discretely
crack_constraint = data(study_case,3); %indicates if a maximum crack
    depth is considered (0 - no constraint; 1 - with constraint)
code_version='2021-With Face'
res=data(study_case,1); %angle resolution
%n1=max(size(cogh));
% Kh horizontal seismic coefficient
Kh_range=0;%:0.05:0.3;
n1=max(size(Kh_range));
% friction angle [deg]
phi_grad=data(study_case,8);
phi=phi_grad/180*pi;
b=tan(phi);
% slope inclination [deg]
beta_grad=data(study_case,6);
beta=beta_grad/180*pi;
n1=max(size(beta_grad));
% imaginary slope inclination for the below the toe failure
beta_prime_grad=beta_grad;
beta_prime=beta_prime_grad*pi/180;

fb=data(study_case,2);
t=data(study_case,4);
cogh = data(study_case,5);
N=data(study_case,9);
ru=data(study_case,10);

% unit weights
gamma=data(study_case,7);
gamma_w=10;
gammarat=gamma_w/gamma;
try
```

```
    qgh=data(study_case,20);
catch
    qgh = 0;
end

gamma_b = data(study_case,11); %block material unit weight
wbh = data(study_case,12); %wb/H - block width
fric_b_grad = data(study_case,13); %friction block/foundation
fric_b = fric_b_grad/180*pi;
delta_grad = data(study_case,15); %friction face/soil
delta = delta_grad /180*pi;
lambda = data(study_case,16);
flag_forcedir=data(study_case,17)
flag_downdrag=data(study_case,19)


Nb = N*2; %number of blocks - assumed
vec_fric_face = zeros (Nb,1); %vector with interface friction (base/face, block/block or geosynt./block at each block level)

if isempty(fric_bb)
    fric_bb = 38*pi()/180; %friction block/block
end
fric_gb = fric_bb ;%- 5*pi()/180; %friction geosynthetic/block - can be slightly reduced in comparisson with block/block interface
n_layers = 1:N;
if RL ~= 1 && RL ~= 2
    error('For uniform distribution: RF=1\nFor linear distribuition: RF=2\n');
else if RL==1
        layers_depth = (n_layers'-0.5)/N; %zi/H
else if RL==2
        layers_depth = 2/3*N*(sqrt((n_layers'/N).^3)-sqrt((n_layers'-1)/N).^3); %zi/H
    end
    end
end

%Assigning interface friction between elements of the face:
vec_fric_face (1) = fric_b; %at the wall base
i_g = 1;
for ii_block = Nb:-1:2
    h_norm = 1-(ii_block-1)/Nb;
    if abs(h_norm - layers_depth (i_g)) < 10^-5 %interface between geosynthetic and block
        vec_fric_face (ii_block) = fric_gb;
        i_g = i_g + 1;
```

```
    else
        vec_fric_face (ii_block) = fric_bb; %block/block interface
    end
end

vec_hi = (1-((1:Nb)-1)/Nb)'; %height of face considered normalized by total face height
if flag_forcedir == 1
    if flag_downdrag == 1
        vec_Pf_norm = vec_hi.*((gamma_b/gamma)*wbh*tan(vec_fric_face))./(cos(delta+beta-pi/2)-sin(delta+beta-pi/2)*tan(vec_fric_face));
    else
        vec_Pf_norm = vec_hi.*(gamma_b/gamma)*wbh*tan(vec_fric_face)/cos(delta+beta-pi/2);
    end
else
    if flag_downdrag == 1
        vec_Pf_norm = vec_hi.*((gamma_b/gamma)*wbh*tan(vec_fric_face))./(cos(delta)-sin(delta)*tan(vec_fric_face));
    else
        vec_Pf_norm = vec_hi.*((gamma_b/gamma)*wbh*tan(vec_fric_face))/cos(delta);
    end
end

if any(vec_Pf_norm) < 0
    fprintf('Force acting on the wall cannot be negative')
    return
end
if flag_fixRht==1
    RhT = data(study_case,18); %psi=Rh/NT
else
    RhT = [];
end

x_limits = [-60 70];
y_limits = [0 120];
z_limits = [-60 70];

% range of the angles
x_range_grad=x_limits(1):res:x_limits(2);
y_range_grad=y_limits(1):res:y_limits(2);
z_range_grad=z_limits(1):res:z_limits(2);
x_range=x_range_grad*pi/180;
y_range=y_range_grad*pi/180;
z_range=z_range_grad*pi/180;
n3=max(size(x_range));
```

```
n4=max(size(y_range));
n5=max(size(z_range));
d=0;

% Kreq_rup = -10;
close (figure(1))
figure(1)
hold on;
plot_wall_geometry
Kreq_face_vec = zeros (Nb,1);
Kreq_face_vec (:) = deal(NaN);
Kreq_toe = NaN;

if isempty(Reinf_length) %length is long enough -> all layers fail in
    tensile rupure
     Flag_mode=NaN;
     Kh = Kh_range;%seismic

     if cogh==0 || t==2
         [K_req_,K_req_toe_,i_block_,Z,F]=deal(zeros(n3,n4));

         No_crack_Kcall; %returns array K_req_ with Kreq for all angle
    combinations (without crack)
     else
         [K_req_,K_req_toe_,i_block_,Z,F]=deal(zeros(n3,n4,n5));

         With_crack_Kcall; %returns array K_req_ with Kreq for all angle
    combinations (with crack)
     end

     [Kreq, I]=max(K_req_(:)) %largest element and the respective linear
    index
     [Kreq_toe, I_toe]=max(K_req_toe_(:)) %largest element and the
    respective linear index
     face_loc_failure = i_block_(I)

     [I2,I3,I4] = ind2sub(size(K_req_),I); %determines the subscripts
    equivalents for the max element (k,l,j)

     beta_prime_=beta_prime;
     x_=x_range(I2);
     y_=y_range(I3);
     %z_=z_range(I4); z can change if the crack height constraint is
     %active
     if cogh ~=0 && t ~=2
         ZZ=Z(:);
         z_=ZZ(I);
```

```
        FF=F(:);
        flag=FF(I);
    else
        z_ = x_;
        flag = NaN;
    end
    x_grad=x_*180/pi
    y_grad=y_*180/pi
    z_grad=z_*180/pi
    %Verifies if the angles found are the limits of the ranges
    %evaluated
    if (I2==n3) || (I2==1)
        d=d+1
        Kreq=NaN;
        string='Increase x_range'
    end
    if (I3==n4) || (I3==1)
        d=d+1
        Kreq=NaN;
        string='Increase y_range'
    end
    if cogh ~= 0 && t ~=2 && ((I4==n5) || (I4==1))
        d=d+1
        Kreq=NaN;
        string='Increase z_range'
    end
    if flag>0 && cogh ~= 0 && t ~=2
        string='Active constraint'
    end

    if d>0
        fprintf('Check the range of the angles!\n');
        [Kreq_rup,Kreq_comb,Xcir, Ycir,SL,PL,Xcir_L,Ycir_L,dL,opt_LoH,
   opt_Kreq,c_d_rup,c_d_comb,face_loc_failure] = deal(NaN);
        beep;
        return
    end

%         if Kreq_face_vec(i_block) > Kreq_rup
    Kreq_rup = Kreq; %Kreq_face_vec(i_block);
    if Kreq_rup<0
        fprintf('no need for reinforcement!\n');
        [Xcir,Ycir,opt_LoH,opt_Kreq,c_d_rup] = deal(NaN);
        [Kreq_comb,SL,PL,Xcir_L,Ycir_L,dL,LoH,c_d_comb]=deal(NaN);
    else
        i_block = face_loc_failure;
        betaprime_grad=beta_prime_*180/pi;
```

```
        betaprime=beta_prime_;
        Hrx_=(exp(b*(y_-x_)))*sin(y_)-sin(x_)/(1-(i_block-1)/Nb); % H/rx
        dd=d;
        d_norm=(exp(b*(z_-x_)).*sin(z_)-sin(x_))./Hrx_; % cd/H -
    normalized crack depth
        Lrx=-exp(b.*(y_-x_)).*sin(betaprime+y_)./sin(betaprime)+sin(
    betaprime+x_)./sin(betaprime);
        lrx=-exp(b.*(z_-x_)).*cos(z_)+cos(x_);
        rx_norm=1./(exp(b.*(y_-x_)).*sin(y_)-sin(x_))*(1-(i_block-1)/Nb)
    ;
        hx_norm=(Lrx-lrx).*rx_norm;
        Xcir=-rx_norm.*exp(b.*(y_-x_)).*cos(y_)+(i_block-1)*1/Nb*cot(
    beta); %in relation to wall toe
        Ycir=rx_norm.*exp(b.*(y_-x_)).*sin(y_)+(i_block-1)*1/Nb; %in
    relation to wall toe
        [Kreq_comb,SL,PL,Xcir_L,Ycir_L,dL,LoH,c_d_comb]=deal(NaN);
        c_d_rup=d_norm; %crack depth for rupture mode of failure

        plot_spiral_tenscrack_betaprime
        plot_crack(1,beta,'r',d_norm,hx_norm,0.1,':');
        h2=plot(Xcir,Ycir,'r+');
        h3 = plot([Xcir;rx_norm*cos(x_)+Xcir],[Ycir;H_ini],'g:'); %rx
        h4 = plot([Xcir;(i_block-1)/Nb*cot(beta)],[Ycir;(i_block-1)/Nb],
    'g:'); %rv
        h5 = plot([Xcir;rx_norm*exp(b*(z_-x_))*cos(z_)+Xcir],[Ycir;H_ini
     - d_norm],'g:'); %rc
        pause(0.1)
    end
%           end
%       if isempty(RhT);
%           fname=sprintf('Beta%dfPhi%dcogh%4.2fRL%dt%dfb%3.1fConstraint%
    dRes%dN%d_wb%4.2flambda%ddeltab%ddeltafs%4.1fDowndrag%dPdirection%d.
    mat',beta_grad,phi_grad,cogh,RL,t,fb,crack_constraint,res,N,wbh,
    lambda,fric_b_grad,delta_grad,flag_downdrag,flag_forcedir);
%           save (fname); %saves results of case i before it goes to the
    next case
%       else
%           fname=sprintf('Beta%dfPhi%dcogh%4.2fRL%dt%dfb%3.1fConstraint%
    dRes%dN%dRhT%4.2fPdir%dlambda%ddeltab%ddeltafs%4.1fDowndrag%
    dPdirection%d.mat',beta_grad,phi_grad,cogh,RL,t,fb,crack_constraint,
    res,N,RhT,flag_forcedir,lambda,fric_b_grad,delta_grad,flag_downdrag,
    flag_forcedir);
%           save (fname); %saves results of case i before it goes to the
    next case
%       end

%       end
```

```
%      hold off
%      figure(2)
%      plot(Kreq_face_vec,(1:12)','-o')
%      set(gca, 'YDir','reverse')
%

else %Combined mechanism (rupture and pullout)
     dL=0;
     if cogh==0 || t==2
         [Local_Kreq_comb,i_block_comb,Local_Kreq_comb_toe,
    Local_Kreq_rup_disc,Local_Kreq_rup_cont,i_block_rup,z_local,
    Flag_local,Lrx_local,lrx_local,rx_norm_local,...
             x_grad_local,y_grad_local,Local_byp_layers,...
             Local_pul_layers,Xcir_L_local,Ycir_L_local,z_grad_local]=
    deal(zeros (n3,n4));
         crit_layers_mode=cell(n3,n4);
         crit_layers_mode(:)={NaN(N,1)};
         [c_d_comb, c_d_rup] =deal(0);
         %calculation of Kreq for all possible failure surfaces for the
    given
         %L/H
         No_crack_Klocal_call;
     else
         [Local_Kreq_comb,i_block_comb,Local_Kreq_comb_toe,
    Local_Kreq_rup_disc,Local_Kreq_rup_cont,i_block_rup, z_local,
    Flag_local,Lrx_local,lrx_local,rx_norm_local,...
             x_grad_local,y_grad_local,z_grad_local,Local_byp_layers,...
             Local_pul_layers,Xcir_L_local,Ycir_L_local] = deal(zeros (n3
    ,n4,n5));
         crit_layers_mode=cell(n3,n4,n5);
         crit_layers_mode(:)={NaN(N,1)};
         %calculation of Kreq for all possible failure surfaces for the
    given
         %L/H
         With_crack_Klocal_call;
     end
     %Arrange all data in a single array, filters out NaN values and sort
     rows according to L1H
     %Final_x_grad Final_y_grad Final_Lsurf_norm_local Final_Local_Kreq
    *100 Final_Xcir_L_local Final_Ycir_L_local Final_Local_byp_layers
    Final_Local_pul_layers Final_z_grad Flag];
     [Kreq_Comb_data,Final_crit_layers_mode] = SetData_Kplot(
    Local_Kreq_comb,x_grad_local,y_grad_local,z_grad_local,Lrx_local,
    lrx_local,rx_norm_local,Xcir_L_local,Ycir_L_local,Local_byp_layers,
    Local_pul_layers,Flag_local,crit_layers_mode);
     [Kreq_Rup_disc_data,~] = SetData_Kplot(Local_Kreq_rup_disc,
```

```
   x_grad_local,y_grad_local,z_grad_local,Lrx_local,lrx_local,
   rx_norm_local,Xcir_L_local,Ycir_L_local,[],[],[],[]);
    [Kreq_Rup_cont_data,~] = SetData_Kplot(Local_Kreq_rup_cont,
   x_grad_local,y_grad_local,z_grad_local,Lrx_local,lrx_local,
   rx_norm_local,Xcir_L_local,Ycir_L_local,[],[],[],[]);
    if disc_reinf == 1
        Kreq_Rup_data=Kreq_Rup_disc_data;
    else
        Kreq_Rup_data=Kreq_Rup_cont_data;
    end
%
    [Kreq_rup, I]=max(Kreq_Rup_data(:,4)); %largest element and the
   respective linear index

    Kreq_rup=Kreq_rup/100
    beta_prime_=beta_prime;
    x_grad=Kreq_Rup_data(I,1)
    y_grad=Kreq_Rup_data(I,2)
    z_grad=Kreq_Rup_data(I,7)

    x_=x_grad/180*pi;
    y_=y_grad/180*pi;
    z_=z_grad/180*pi;

    %Verifies if the angles found are the limits of the ranges
    %evaluated
    if x_== x_range(1) || x_== x_range(end)
        d=d+1
        Kreq_rup=NaN;
        string='Increase x_range'
    end
    if y_== y_range(1) || y_== y_range(end)
        d=d+1
        Kreq_rup=NaN;
        string='Increase y_range'
    end
    if cogh ~= 0 && t ~=2 && (z_== z_range(1) || z_== z_range(end))
        d=d+1
        Kreq_rup=NaN;
        string='Increase z_range'
    end
%     if flag>0 && cogh ~= 0 && t ~=2
%         string='Active constraint'
%     end

    if d>0
%         fprintf('Check the range of the angles!\n');
```

```
        [Kreq_rup,Kreq_comb,Xcir,Ycir,SL,PL,Xcir_L, Ycir_L,dL,opt_LoH,opt_Kreq,c_d_rup,c_d_comb] = deal(NaN);
        beep;
        error('Check the range of the angles!\n')

    else
        if Kreq_rup <0
            fprintf('no need for reinforcement!\n');
            [Xcir,Ycir,SL,PL,Xcir_L,Ycir_L,dL,opt_LoH,opt_Kreq,c_d_rup] = deal(NaN);
        else
        betaprime_grad=beta_prime_*180/pi;
        betaprime=beta_prime_;
        Hrx_=(exp(b*(y_-x_)))*sin(y_)-sin(x_); % H/rx
        dd=d;
        d_norm=(exp(b*(z_-x_)).*sin(z_)-sin(x_))./(exp(b.*(y_-x_)).*sin(y_)-sin(x_));
        Lrx=-exp(b.*(y_-x_)).*sin(betaprime+y_)./sin(betaprime)+sin(betaprime+x_)./sin(betaprime);
        lrx=-exp(b.*(z_-x_)).*cos(z_)+cos(x_);
        rx_norm=1./(exp(b.*(y_-x_)).*sin(y_)-sin(x_));
        hx_norm=(Lrx-lrx).*rx_norm;
        Xcir=-rx_norm.*exp(b.*(y_-x_)).*cos(y_);
        Ycir=rx_norm.*exp(b.*(y_-x_)).*sin(y_);
        c_d_rup=(1/Hrx_)*(exp(b*(z_-x_))*sin(z_)-sin(x_)); %crack depth for rupture mode of failure
%          [Kreq_comb,SL,PL,Xcir_L,Ycir_L,dL]=deal(NaN);
        end
    end

    if ~isempty(Kreq_Comb_data)
        [~, I_toeblock]=max(Local_Kreq_comb(:)); %largest element and the respective linear index
        [Kreq_toe, I_toe]=max(Local_Kreq_comb_toe(:)); %largest element and the respective linear index
        if Kreq_toe == 3 %reinforcement not sufficient already for toe failure
            face_loc_failure = 1;
        else
            face_loc_failure = i_block_comb(I_toeblock); %corrected 01/04/2021
        end
        [Kreq_comb, I]=max(Kreq_Comb_data(:,4)); %largest element and the respective linear index
        Kreq_comb=Kreq_comb/100
        beta_prime_=beta_prime;
        x_grad_L=Kreq_Comb_data(I,1)
```

```
        y_grad_L=Kreq_Comb_data(I,2)
        z_grad_L=Kreq_Comb_data(I,7)
        Flag_L = Kreq_Comb_data(I,10);
        SL = Kreq_Comb_data(I,8);
        PL = Kreq_Comb_data(I,9);
        mode_comb = cell2mat(Final_crit_layers_mode(I));
        Flag_mode = 0;
        ind_pul=find(mode_comb==1);
        ind_rup=find(mode_comb==0);
        if any(diff(ind_pul)>1) ||any(diff(ind_rup)>1)
          Flag_mode=1;
        end
        x_L=x_grad_L/180*pi;
        y_L=y_grad_L/180*pi;
        z_L= z_grad_L/180*pi;

        %Verifies if the angles found for the combined mechanism are the limits of the ranges
        %evaluated
        if x_L== x_range(1) ||x_L== x_range(end)
            dL=dL+1;
            Lrh_req=NaN;
            fprintf('Increase x_range\n');
        end
        if y_L== y_range(1) ||y_L== y_range(end)
            dL=dL+1;
            Lrh_req=NaN;
            fprintf('Increase y_range\n');
        end

        if cogh ~= 0 && t ~=2 && (z_L== z_range(1) ||z_L== z_range(end))
            dL=dL+1;
            Lrh_req=NaN;
            fprintf('Increase z_range\n');
        end
    else
        [Kreq_comb,SL,PL,Xcir_L,Ycir_L,dL,c_d_comb,Flag_mode,face_loc_failure]=deal(NaN);

        return
    end

    if dL>0
        if   Kreq_comb==10 %instability at top blocks (no amount of reinforcement will help)
             fprintf('Instability at the top blocks!');
             Flag_mode=NaN;
```

```
               [PL,Xcir_L,Ycir_L,opt_LoH,opt_Kreq,c_d_comb] = deal(NaN);
        else
%          fprintf('Check the range of the angles!\n');
        [SL,PL,Xcir_L, Ycir_L,opt_LoH,opt_Kreq,c_d_comb] = deal(NaN);
        LoH=Lrh_req;
        beep;
        error('Check the range of the angles!\n')
        end
    else
        %Combined mechanism - fixed L/H
        if  Kreq_comb == 3
            fprintf('Stability not possible for the given L/H\n');
                         face_factor = (1-(face_loc_failure-1)/Nb);
            figure(1)
            hold on
            g=(exp(b*(y_L-x_L)))*sin(y_L)-sin(x_L); % H/rx
            betaprime_grad_L=beta;
            betaprime_L=beta;
            Lrx_L=(-exp(b.*(y_L-x_L)).*sin(betaprime_L+y_L)./sin(betaprime_L)+sin(betaprime_L+x_L)./sin(betaprime_L)); %l1/rx
            lrx_L=(-exp(b.*(z_L-x_L)).*cos(z_L)+cos(x_L));%l2/rx
            rx_norm_L=1./(exp(b.*(y_L-x_L)).*sin(y_L)-sin(x_L))*face_factor; %rx/H
            hx_norm_L=(Lrx_L-lrx_L).*rx_norm_L;
            Xcir_L=-rx_norm_L.*exp(b.*(y_L-x_L)).*cos(y_L)+(face_loc_failure-1)*1/Nb*cot(beta);
            Ycir_L=rx_norm_L.*exp(b.*(y_L-x_L)).*sin(y_L)+(face_loc_failure-1)*1/Nb;
            Hrx_comb=((exp(b*(y_L-x_L)))*sin(y_L)-sin(x_L))/face_factor;
            d_norm_L=(exp(b*(z_L-x_L)).*sin(z_L)-sin(x_L))./Hrx_comb;%cd/H - normalized crack depth
            c_d_comb=d_norm_L;
            plot_spiral_tenscrack_betaprime_L
            plot_crack_L(1,beta,'r',d_norm_L,hx_norm_L,0.1,':');
            h2=plot(Xcir_L,Ycir_L,'r+');
            h3 = plot([Xcir_L;rx_norm_L*cos(x_L)+Xcir_L],[Ycir_L;H_ini],'g:'); %rx
            h4 = plot([Xcir_L;(face_loc_failure-1)/Nb*cot(beta)],[Ycir_L;(face_loc_failure-1)/Nb],'g:'); %rv
            h5 = plot([Xcir_L;rx_norm_L*exp(b*(z_L-x_L))*cos(z_L)+Xcir_L],[Ycir_L;H_ini - d_norm_L],'g:'); %rc
            pause(0.1)
            [PL,Xcir_L,Ycir_L,opt_LoH,opt_Kreq,c_d_comb] = deal(NaN);
        elseif Kreq_comb<0
             fprintf('No need for reinforcement(Kreq_comb = %d)\n',Kreq_comb);
             Flag_mode=NaN;
```

```
             [PL,Xcir_L,Ycir_L,opt_LoH,opt_Kreq,c_d_comb] = deal(NaN);

        else
            LoH
            face_factor = (1-(face_loc_failure-1)/Nb);
            figure(1)
            hold on
            betaprime_grad_L=beta;
            betaprime_L=beta;
            Lrx_L=(-exp(b.*(y_L-x_L)).*sin(betaprime_L+y_L)./sin(betaprime_L)+sin(betaprime_L+x_L)./sin(betaprime_L)); %l1/rx
            lrx_L=(-exp(b.*(z_L-x_L)).*cos(z_L)+cos(x_L));%l2/rx
            rx_norm_L=1./(exp(b.*(y_L-x_L)).*sin(y_L)-sin(x_L))*face_factor; %rx/H
            hx_norm_L=(Lrx_L-lrx_L).*rx_norm_L;
            Xcir_L=-rx_norm_L.*exp(b.*(y_L-x_L)).*cos(y_L)+(face_loc_failure-1)*1/Nb*cot(beta);
            Ycir_L=rx_norm_L.*exp(b.*(y_L-x_L)).*sin(y_L)+(face_loc_failure-1)*1/Nb;
            Hrx_comb=((exp(b*(y_L-x_L)))*sin(y_L)-sin(x_L))/face_factor;
            d_norm_L=(exp(b*(z_L-x_L)).*sin(z_L)-sin(x_L))./Hrx_comb;%cd/H - normalized crack depth
            c_d_comb=d_norm_L;
            plot_spiral_tenscrack_betaprime_L
            plot_crack_L(1,beta,'r',d_norm_L,hx_norm_L,0.1,':');
            h2=plot(Xcir_L,Ycir_L,'r+');
            h3 = plot([Xcir_L;rx_norm_L*cos(x_L)+Xcir_L],[Ycir_L;H_ini],'g:'); %rx
            h4 = plot([Xcir_L;(face_loc_failure-1)/Nb*cot(beta)],[Ycir_L;(face_loc_failure-1)/Nb],'g:'); %rv
            h5 = plot([Xcir_L;rx_norm_L*exp(b*(z_L-x_L))*cos(z_L)+Xcir_L],[Ycir_L;H_ini - d_norm_L],'g:'); %rc
            pause(0.1)
        end
    end
    if wbh ==0
        fname=sprintf('Beta%dfPhi%dcogh%4.2fLoH%3.1fRL%dt%dfb%3.1fConstraint%dRes%dN%d_NO_FACE_Surcharge%d.mat',beta_grad,phi_grad,cogh,LoH,RL,t,fb,crack_constraint,res,N,qgh)
%          save (fname); %saves results of case i before it goes to the next case
    else
        fname=sprintf('Beta%dfPhi%dcogh%4.2fLoH%3.1fRL%dt%dfb%3.1fConstraint%dRes%dN%d_wb%4.2flambda%ddeltab%ddeltafs%4.1fDowndrag%dPdirection%dSurcharge%d.mat',beta_grad,phi_grad,cogh,LoH,RL,t,fb,crack_constraint,res,N,wbh,lambda,fric_b_grad,delta_grad,flag_downdrag,flag_forcedir,qgh)
```

```
%          save (fname); %saves results of case i before it goes to the next case
    end
end

fname=sprintf('Beta%dfPhi%dcogh%4.2fLoH%3.1fRL%dt%dfb%3.1fConstraint%dRes%dN%d_wb%4.2flambda%ddeltab%ddeltafs%4.1fDowndrag%dPdirection%d.mat',beta_grad,phi_grad,cogh,LoH,RL,t,fb,crack_constraint,res,N,wbh,lambda,fric_b_grad,delta_grad,flag_downdrag,flag_forcedir)
if RL==1
    string = 'using Uniform Distribution of reinforcement'
else
    string = 'using Linearly Increasing Distribution of reinforcement'
end

end
```

D.2 Auxiliary functions and files

Read_data file:

```
 %Runs the main code a number of times until all the cases of an input file
%are read (column variables in the data input file: RES( ), fb, crack_constraint,t,cogh,
%beta,  gamma (kN/m),  phi,  N,  ru, gammab (kN/m), wb/H (m),fricb, delta/phi,delta,lambda,Force_direction,LoH,Downdrag

%clear

if exist ('data.mat','file')
    load ('data.mat')
    line_number=size(data,1)+1;
else
    filename=uigetfile('*.txt');
    fid = fopen (filename,'rt');
    if fid < 0
        fprintf('error opening file\n'); return;
    else
        % Read file as a set of strings, one per line:
        line_number = 1;
        headline = fgetl(fid);
        oneline{line_number}=fgetl(fid);
        while ischar(oneline{line_number})
            line_number = line_number + 1;
            oneline{line_number} = fgets(fid);

        end
```

```
        fclose(fid);
        %pre-allocation of data matrix
        data=zeros(line_number-1,19);%needs update (29-09-2020)
        for i=1 : line_number-1
            data(i,:) = sscanf(oneline{i}(1:end),'%f ');
        end
        save ('data.mat','data','line_number');
    end
end

%Calls the main program to run analyses
tic; %start the clock
if ~exist ('RL','var') || ~exist ('flag_fixRht','var')
    RL=input('RL (1 for UD and 2 for LID):'); %reinforcement distribuition
%      Flag_face = input('Face condition (with face (1); no face (0)):'); % with face (1); no face (0)
    flag_fixRht=input('Given Rh/NT? (0 for N and 1 for Y):');
    Kreq = zeros (line_number-1);

end

Current_analysis = zeros(line_number-1,19);

for ii=1:line_number-1 %runs analyses for all the case studies
    fprintf('Case %d...',ii);
    Reinf_length = data(ii,18);
    if Reinf_length >=10 %code for Long
        Reinf_length = [];
    end
    beta_grad=data(ii,6);
    phi_grad=data(ii,8);
    N=data(ii,9);
    if ~exist ('fric_bb','var')
        fric_bb = [];
    end
   [Kreq_rup,Kreq_comb,LoH,SL,PL,d,dL,code_version,Xcir,Ycir,Xcir_L,Ycir_L,c_d_rup,c_d_comb,Flag_mode,face_loc_failure] = MainProgram_2021(ii,data,RL,Reinf_length,flag_fixRht,fric_bb);

   Current_analysis (ii,:)= [beta_grad,phi_grad,RL,N,d,dL,LoH,Kreq_rup,Kreq_comb,face_loc_failure,SL,PL,Flag_mode, c_d_rup,c_d_comb,Xcir,Ycir,Xcir_L,Ycir_L];
   save('Current_analysis.mat','Current_analysis');

end

```

```
toc %stop the clok
beep;
```

```
function [Data_for_plot,Final_crit_layers_mode] = SetData_Kplot(Kreq,
    x_grad,y_grad,z_grad,Lrx,lrx,rxH,Xcir_L,Ycir_L,n_byp,n_pul,Flag,
    crit_layers_mode)

%L1_norm_local = Lrx.*rxH;
Final_Local_Kreq = (Kreq(~isnan(Kreq)))*100;
Final_x_grad = (x_grad(~isnan(Kreq)));
Final_y_grad = (y_grad(~isnan(Kreq)));
Final_z_grad = (z_grad(~isnan(Kreq)));
Final_Lrx_local = (Lrx(~isnan(Kreq)));
Final_lrx_local = (lrx(~isnan(Kreq)));
Final_rx_norm_local=(rxH(~isnan(Kreq)));
Final_L1_norm_local = Final_Lrx_local.*Final_rx_norm_local;
Final_L2_norm_local = Final_lrx_local.*Final_rx_norm_local;
Final_Lsurf_norm_local = Final_L1_norm_local-Final_L2_norm_local;
if ~isempty(crit_layers_mode)
    Final_crit_layers_mode =(crit_layers_mode(~isnan(Kreq)));
else
    Final_crit_layers_mode = [];
end
if ~isempty(Flag)
    Final_Flag = Flag(~isnan(Kreq));
else
    Final_Flag=[];
end
if isempty(n_byp) && isempty(n_pul)
    Final_Local_byp_layers= [];
    Final_Local_pul_layers = [];
else
    Final_Local_byp_layers= (n_byp(~isnan(Kreq)));
    Final_Local_pul_layers = (n_pul(~isnan(Kreq)));
end
Final_Xcir_L_local = Xcir_L(~isnan(Kreq));
Final_Ycir_L_local = Ycir_L(~isnan(Kreq));
aux_Data_for_plot = [Final_x_grad Final_y_grad Final_Lsurf_norm_local
    Final_Local_Kreq Final_Xcir_L_local Final_Ycir_L_local Final_z_grad
    Final_Local_byp_layers Final_Local_pul_layers Final_Flag];

% Data_for_plot = unique(Data_for_plot,'rows'); %filters repeated values
if ~isempty(aux_Data_for_plot)
    [Data_for_plot,I] = sortrows (aux_Data_for_plot,3); %sorts values
    according to L1/H in crescent order
    if ~isempty(Final_crit_layers_mode)
        Final_crit_layers_mode = Final_crit_layers_mode(I);
```

```
    end
else
    Data_for_plot=[];
end
end
```

```
Flag_plot = 0;
if Flag_plot == 1
    close
    plot_wall_geometry
end

parfor k=1:n3
    for l=1:n4
        for j=1:n5

            if (x_range(k)>y_range(l)-10e-6) || (x_range(k)>z_range(j)
   -10e-6) || (z_range(j)>y_range(l)-10e-6)
                K_req_(k,l,j)=NaN;
                i_block_(k,l,j)=NaN;
                K_req_toe_(k,l,j)=NaN;
                Z(k,l,j)=NaN;
                F(k,l,j)=NaN;
            else
                [X,Kreq_,Flag,iblock_,Kreq_toe_]=funxyz_n(x_range(k),
   y_range(l),z_range(j),b,beta,cogh,Kh,t,ru,gammarat,RL,
   crack_constraint,layers_depth,vec_Pf_norm,qgh, delta,lambda,
   flag_forcedir,RhT,Nb);
                K_req_(k,l,j)=Kreq_;
                i_block_(k,l,j)=iblock_;
                K_req_toe_(k,l,j)=Kreq_toe_;
                Z(k,l,j)=X; %consider crack constraint
                F(k,l,j)=Flag;
             end
        end
    end
end
```

```

Flag_plot = 0;
if Flag_plot == 1
    close (figure(1))
    figure(1)
    hold on;
    plot_wall_geometry
end
parfor k=1:n3 %use parfor
    for l=1:n4
```

```
        for j=1:n5
%                x_range_grad(k)
%                y_range_grad(l)
%                z_range_grad(j)
            if (x_range(k)>y_range(l)-10e-6) || (x_range(k)>z_range(j)
   -10e-6) || (z_range(j)>y_range(l)-10e-6)...
                    || (z_range(j)*180/pi==90 && x_range(k)*180/pi~=90)
                [Local_Kreq_comb(k,l,j),i_block_comb(k,l,j),
   Local_Kreq_comb_toe(k,l,j),Local_Kreq_rup_disc(k,l,j),
   Local_Kreq_rup_cont(k,l,j),Flag_local(k,l,j),Lrx_local(k,l,j),
   lrx_local(k,l,j),...
                    rx_norm_local(k,l,j),Local_byp_layers(k,l,j),
   Local_pul_layers(k,l,j),Xcir_L_local(k,l,j),...
                    Ycir_L_local(k,l,j)] = deal(NaN);
                x_grad_local(k,l,j)=x_range_grad (k);
                y_grad_local(k,l,j)=y_range_grad (l);
                z_grad_local(k,l,j) = z_range_grad(j);
            else
                %tic;
                [z_local_,Lrx_,lrx_,rx_norm_,Local_Kreq_,Local_Kreq_toe_
   ,i_block_comb_,Local_Kreq_rup_disc_,Local_Kreq_rup_cont_,i_block_rup_
   ,Flag_local_,byp_layers_,pul_layers_,count,crit_layers_mode_] =
   Req_strength_function (x_range(k),y_range(l),z_range(j),N,LoH,beta,b,
   cogh,t,ru,fb,crack_constraint,layers_depth,gammarat,code_version,RL,
   disc_reinf,vec_Pf_norm,qgh,delta,lambda,flag_forcedir,Nb,Flag_plot);
                %toc;
                Local_Kreq_rup_disc(k,l,j) = Local_Kreq_rup_disc_;
                Local_Kreq_rup_cont(k,l,j) = Local_Kreq_rup_cont_;
                i_block_rup(k,l,j)=i_block_rup_;
                Local_Kreq_comb(k,l,j) = Local_Kreq_;
                i_block_comb(k,l,j)=i_block_comb_;
                Local_Kreq_comb_toe(k,l,j)=Local_Kreq_toe_;
                x_grad_local(k,l,j)=x_range_grad (k);
                y_grad_local(k,l,j)=y_range_grad (l);
                z_local(k,l,j) = z_local_;
                z_grad_local(k,l,j)=z_local(k,l,j)*180/pi;
                Flag_local (k,l,j) = Flag_local_;
                Lrx_local(k,l,j) = Lrx_;
                lrx_local(k,l,j) = lrx_;
                rx_norm_local (k,l,j) = rx_norm_;
                Local_byp_layers(k,l,j)= byp_layers_;
                Local_pul_layers(k,l,j) = pul_layers_;
                Xcir_L_local(k,l,j)= -rx_norm_.*exp(b.*(y_range(l)-
   x_range(k))).*cos(y_range(l));
                Ycir_L_local(k,l,j)= rx_norm_.*exp(b.*(y_range(l)-
   x_range(k))).*sin(y_range(l));
                crit_layers_mode{k,l,j}=crit_layers_mode_;
```

```
%                   if Local_Kreq_comb(k,l,j) == 10 %instability at top
    blocks (no amount of reinforcement will help)
%                           continue
%                   end
                %fprintf('k=%4d, l= %4d, j = %4d\n',k,l,j);
            end
        end
    end
end
% end
```

```
%Loop to calculate Kreq when there is no crack

    parfor k=1:n3
        for l=1:n4
%              x_range_grad(k)
%              y_range_grad(l)
                if (x_range(k)>y_range(l)-10e-6)
                    K_req_(k,l)=NaN;
                    i_block_(k,l)=NaN;
                    K_req_toe_(k,l)=NaN;
                    F(k,l)=NaN;
                else
                    z_range = x_range(k);
                    [X,Kreq_,Flag,iblock_,Kreq_toe_]=funxyz_n(x_range(k)
    ,y_range(l),z_range,b,beta,cogh,Kh,t,ru,gammarat,RL,crack_constraint,
    layers_depth,vec_Pf_norm,qgh,delta,lambda,flag_forcedir,RhT,Nb);
                    K_req_(k,l)=Kreq_;
                    i_block_(k,l)=iblock_;
                    K_req_toe_(k,l)=Kreq_toe_;
                    F(k,l)=Flag;

                end
        end
    end
```

```
% for i=1:n1
%     Kh = Kh_range(i);
Flag_plot = 0;
if Flag_plot == 1
    close (figure(1))
    figure(1)
    hold on;
    plot_wall_geometry
end

parfor k=1:n3 %use parfor
    for l=1:n4
```

```
%          x_range_grad(k)
%          y_range_grad(l)
            if x_range(k)>y_range(l)-10e-6
                [Local_Kreq_comb(k,l),i_block_comb(k,l),Local_Kreq_comb_toe(k,l),Local_Kreq_rup_disc(k,l),Local_Kreq_rup_cont(k,l),Flag_local(k,l),Lrx_local(k,l),rx_norm_local(k,l),...
                    Local_byp_layers(k,l),Local_pul_layers(k,l),Xcir_L_local(k,l),...
                    Ycir_L_local(k,l)] = deal(NaN);
                x_grad_local(k,l)=x_range_grad (k);
                y_grad_local(k,l)=y_range_grad (l);
                z_grad_local(k,l)= x_grad_local(k,l);
                crit_layers_mode{k,l}=NaN(N,1);

            else
                %tic;
                z_range = x_range(k);
                [z_local_,Lrx_,lrx_,rx_norm_,Local_Kreq_,Local_Kreq_toe_,i_block_comb_,Local_Kreq_rup_disc_,Local_Kreq_rup_cont_,i_block_rup_,Flag_local_,byp_layers_,pul_layers_,count,crit_layers_mode_] = Req_strength_function (x_range(k),y_range(l),z_range,N,LoH,beta,b,cogh,t,ru,fb,crack_constraint,layers_depth,gammarat,code_version,RL,disc_reinf,vec_Pf_norm,qgh,delta,lambda,flag_forcedir,Nb,Flag_plot);
                %toc;
                Local_Kreq_rup_disc(k,l) = Local_Kreq_rup_disc_;
                Local_Kreq_rup_cont(k,l) = Local_Kreq_rup_cont_;
                i_block_rup(k,l)=i_block_rup_;
                Local_Kreq_comb(k,l) = Local_Kreq_;
                i_block_comb(k,l)=i_block_comb_;
                Local_Kreq_comb_toe(k,l)=Local_Kreq_toe_;
                x_grad_local(k,l)=x_range_grad (k);
                y_grad_local(k,l)=y_range_grad (l);
                z_local(k,l) = z_local_;
                z_grad_local(k,l)= x_grad_local(k,l);
                Flag_local (k,l) = Flag_local_;
                Lrx_local(k,l) = Lrx_;
                rx_norm_local (k,l) = rx_norm_;
                Local_byp_layers(k,l)= byp_layers_;
                Local_pul_layers(k,l) = pul_layers_;
                Xcir_L_local(k,l)= -rx_norm_.*exp(b.*(y_range(l)-x_range(k))).*cos(y_range (l));
                Ycir_L_local(k,l)= rx_norm_.*exp(b.*(y_range(l)-x_range(k))).*sin(y_range (l));
                crit_layers_mode{k,l}=crit_layers_mode_;
                %fprintf('k=%4d, l= %4d, j = %4d\n',k,l,j);
            end
    end
```

```
end
% end
```

```
function [z_local_,Lrx,lrx,rx_norm_,Local_Kreq_,Local_Kreq_toe_,i_block_comb_,Local_Kreq_rup_disc,Local_Kreq_rup_cont,i_block_rup_,Flag_local_,byp_layers_,pul_layers_,count,crit_layers_mode] = Req_strength_function (x,y,z,N,LoH,beta,b,cogh,t,ru,fb,crack_constraint,layers_depth,gammarat,code_version,RL,disc_reinf,vec_Pf_norm,qgh,delta,lambda,flag_forcedir,Nb,Flag_plot)
%surcharged added in 12/02/2021
%consideration of failure surface emerging at the face added in 25/03/2021
crit_layers_mode=NaN(N,1);
[Local_Kreq_rup_disc,Local_Kreq_rup_cont,i_block_rup_, Local_Kreq_,i_block_comb_,Local_Kreq_toe_,byp_layers_,pul_layers_]= deal(NaN);
count = 0; %counts number of cases evaluated
beta_prime = beta;
Hrx=(exp(b*(y-x)))*sin(y)-sin(x); % Hib/rxib
Lrx=-exp(b*(y-x))*sin(beta+y)/sin(beta)+sin(beta+x)/sin(beta);
%Lrx = 1/sin(y)*(sin(y-x)-Hrx*sin(beta+y)/sin(beta));
rx_norm_=1./(exp(b.*(y-x))*sin(y)-sin(x));
if Hrx< 0
    Local_Kreq_=NaN;
    Flag_local_ = NaN;
    z_local_ = z;
    lrx=NaN;
    return;
end
phi=atan(b);
%rx = H /(exp(b.*(y-x)).*sin(y)-sin(x));
if Lrx < 0
    Local_Kreq_=NaN;
    Flag_local_ = NaN;
    z_local_ = z;
    lrx=NaN;
    return
end
options = optimset('TolX',1e-10);

%eliminate cases in each log spiral crosses the top surface - 21/06/2020
theta=(x:0.01:y);
funY = (1-(rx_norm_.*exp(b*(y-x)).*sin(y)-rx_norm_.*exp(b*(theta-x)).*sin(theta)));

if any (funY<0)  %exists another root other than x
    Local_Kreq_=NaN;
    Flag_local_ = NaN;
```

```
    z_local_ = z;
    lrx=NaN;
    return
end

c_d=(1/Hrx)*(exp(b*(z-x))*sin(z)-sin(x));% current depth of the crack (h
    /Hib)
if crack_constraint == 1 %added 25/03/2020
    if ru==0
        m_d=3.83*cogh*tan(pi/4+phi/2) ; %maximum dry crack depth (hmax/H
    )
    else
        m_d=(2*cogh*tan(pi/4+phi/2))/(1-ru); %maximum wet crack depth (
    hmax/H)
    end
    %toc;

    if c_d > m_d
        %changes z because it imposes a constraint in crack depth
        F=1;
        if cogh==0
            z=x; %no crack for zero cohesion
            c_d = 0;
        else
            x0=x;
            %tic;
            fun = @(z)(1/Hrx)*(exp(b*(z-x))*sin(z)-sin(x))-m_d;
            [z] = fzero(fun,x0,options);%c_d-m_d = 0
            %toc;
            c_d = m_d;
        end
    else
        z=z;
        F=0;
    end
else
    z=z;
    F=0;
end

z_local_ = z;
Flag_local_ = F;

if cogh ~= 0
    % calculations of the dissipated enrgey function for the crack
    formation
        tan_theta_c = sin(x)/(exp(b*(z-x))*cos(z));
```

```
        theta_c = atan(tan_theta_c);

        if (theta_c>y-10e-6) || (theta_c<x-10e-6)
            Local_Kreq_=NaN;
            Flag_local_ = NaN;
            z_local_ = z;
            lrx=NaN;
            return
        end
        if t==2 %intact slope
            z=x;
            z_local_ = z; %05/03/2020
            gc=0;
            c_d=0;
        end
%         if z*180/pi == 90 %numerical problem for do integrals
    (01/02/2020)
%             z=89*pi/180;
%             Final_z = z;
%         end

        if t==0
            ft=0;
            int_ft=0;
            %closed form solution for the integral of fc(Eq. 10 of Abd
    and Utili, 2017)
            int_fc = int_fun_fc(z)-int_fun_fc(theta_c);
            fc=2*cos(phi)/(1-sin(phi));
            if sin(x) == 0 || theta_c==z; %06/05/2020
                Local_Kreq_=NaN;
                Flag_local_ = NaN;
                z_local_ = z;
                lrx=NaN;
                return
            else
                gc=(sin(x)/tan_theta_c)^2*(fc/2*int_fc+t*ft/(1-sin(phi))
    *int_ft);
            end

        elseif t==0.5
            %closed form solution for the integral of fc(Eq. 10 of Abd
    and Utili, 2017)
            int_fc = int_fun_fc(z)-int_fun_fc(theta_c);
            %closed form solution for the integral ft (Eq. 10 of Abd &
    Utili, 2017)
            int_ft = int_fun_ft(z,phi)-int_fun_ft(theta_c,phi);
            fc=2*cos(phi)/(1-sin(phi));
```

```
            ft=2*cos(phi)/(1+sin(phi)); %ok
            if sin(x) == 0 || theta_c==z; %06/05/2020
                Local_Kreq_=NaN;
                Flag_local_ = NaN;
                z_local_ = z;
                lrx=NaN;
                return
            else
                gc=(sin(x)/tan_theta_c)^2*(fc/2*int_fc+t*ft/(1-sin(phi))*int_ft);
            end
        %tic;
        elseif t==1
            %closed form solution for the integral of fc(Eq. 10 of Abd and Utili, 2017)
            %tic;
            int_fc = int_fun_fc(z)-int_fun_fc(theta_c);
            int_ft = int_fun_ft(z,phi)-int_fun_ft(theta_c,phi);
            fc=2*cos(phi)/(1-sin(phi));
            ft=2*cos(phi)/(1+sin(phi));
            %toc;
            if sin(x) == 0 || theta_c==z; %06/05/2020
                Local_Kreq_=NaN;
                Flag_local_ = NaN;
                z_local_ = z;
                lrx=NaN;
                return
            else
                gc=(sin(x)/tan_theta_c)^2*(fc/2*int_fc+t*ft/(1-sin(phi))*int_ft);
            end
        else %t=-1 - slope with most adverse pre existing crack - no crack formation
            gc=0;
        end
else
    gc=0;
    z=x; %no crack - cohesionless soil
    c_d = 0;
    z_local_ = z;
    Flag_local_ = F;
end
%toc;
lrx=cos(x)-exp(b*(z-x))*cos(z);
% calculation of the angle Th_1 (the angle made by the line between point
%P and the point of vertical projection of the crest point on the log-
```

```
    spiral surface
beta_grad=beta*180/pi;
if beta_grad==90 %02/02/2020
    Th_1=y;
else
    options = optimset('TolX',1e-10);
    x0=[x y];%02/01/2020
    [Th_1, ~, ~, output] = fzero(@(Th_1)exp(b*(Th_1-x))*cos(Th_1)-cos(x)
    +Lrx,x0,options);
end
if ((Th_1>y-10e-6)&& beta_grad<90) ||((Th_1>y+10e-6)&& beta_grad==90)||
    (Th_1<x)
    string='Th_1 not found';
    Local_Kreq_=NaN;
    return;
end

%Verification if tension crack is from the horizontal surface (right of
    the
%slope crest)
if ((1/Hrx)*exp(b*(z-x))*cos(z))<((1/Hrx)*exp(b*(Th_1-x))*cos(Th_1))
    Local_Kreq_=NaN;
    return
end

%tic;
g1=exp(2*b*(z-x))*(exp(2*b*(y-z))-1)/(2*b);  %Eq. 15 Abd & Utili (2017)

f1=(exp(3*b*(y-x))*(sin(y)+3*b*cos(y))-3*b*cos(x)-sin(x))/(3*(1+9*b^2));
f2=1/6*Lrx*sin(x)*(2*cos(x)-Lrx);
f3=1/6*exp(b*(y-x))*(sin(y-x)-Lrx*sin(y))*(cos(x)-Lrx+cos(y)*exp(b*(y-x)
    ));
%f4=1/2*Hrx^2*(cot(beta_prime)-cot(beta))*(cos(x)-Lrx-1/3*Hrx*(cot(
    beta_prime)+cot(beta))) ;% for below the toe failure
p1=(exp(3*b*(z-x))*(sin(z)+3*b*cos(z))-3*b*cos(x)-sin(x))/(3*(1+9*b^2));
p2=1/6*sin(x)*((cos(x))^2-exp(2*b*(z-x))*(cos(z))^2);
p3=1/3*exp(2*b*(z-x))*(cos(z))^2*(sin(z)*exp(b*(z-x))-sin(x));

%Contribuition of the facing element
if flag_forcedir ==1 %conventional (continum painel face)
    f7 = sin(beta+delta)*(sin(x) + (lambda-1)/lambda*Hrx) - cos(beta+
    delta)*...
        (exp(b*(y-x))*cos(y)+1/lambda*Hrx*cot(beta));
else %modified direction (block stacked face)
    f7= cos(delta)*(exp(b*(y-x))*sin(y)-Hrx/lambda)+...
                sin(delta)*(exp(b*(y-x))*cos(y)+Hrx/lambda*cot(beta));
end
```

```matlab

%Uniform distributed surcharge q (12/02/2021)
fq=0.5*(Lrx-lrx)*(2*cos(x)-(Lrx-lrx));

% Calculation of pu = ru*fw
if ru==0
    pu=0;
else
    if beta_prime<beta %case not tested
        x1=y; %(Th_1+y)/2;
        [Th_2, ~, ~, output2] = fzero(@(Th_2)exp(b*(Th_2-x))*cos(Th_2)-cos(x)+Lrx+Hrx*cot(beta),x1,options);
        if (Th_2>y-10e-6) || (Th_2<Th_1)
            Local_Kreq_=NaN;
            return;
        end
        u_3=@(Th)(exp(b.*(Th-x)).*sin(Th)-exp(b.*(y-x))*sin(y)).*b.*(exp(2.*b.*(Th-x)));
        u3=integral(u_3,Th_2,y);
    else
        u3=0;
    end

    % second: calculation of the angle th_w (which is the angle between the horizontal and the chord between the point p and the water level within the crack.
    d_= exp(b*(z-x))*sin(z)-sin(x); % the depth of the crack (h/rx)
    th_w=atan((exp(b*(z-x))*sin(z)-ru*(1/gammarat)*d_)/(exp(b*(z-x))*cos(z))); %need to check
    % third calculations of uc, u1 and u2
    u_c=@(Th)(exp(b.*(z-x)).*cos(z).*tan(Th)-sin(x)).*tan(Th).*(exp(2.*b.*(z-x)).*(cos(z)).^2)./(cos(Th)).^2;
    u_1=@(Th)(exp(b.*(Th-x)).*sin(Th)-sin(x)).*b.*(exp(2.*b.*(Th-x)));
    u_2=@(Th)(exp(b.*(Th-x)).*sin(Th)-(exp(b.*(Th_1-x)).*cos(Th_1)-exp(b.*(Th-x)).*cos(Th)).*tan(beta)-sin(x)).*b.*(exp(2.*b.*(Th-x)));
    % forth: integration of uc, u1 and u2
    %uc=integral(u_c,th_w,z);
    uc = int_fun_uc(z,x,z,b)-int_fun_uc(th_w,x,z,b);
    %u1=integral(u_1,z,Th_1);
    u1 = int_fun_u1(Th_1,b,x)-int_fun_u1(z,b,x);
    if beta_grad==90
        u2=0;
    else
        u2=integral(u_2,Th_1,y);
    end
    pu=ru*(uc+u1+u2+u3); %is it not been used to calculate Kreq?
end
```

```

sum_f = f1-f2-f3-p1+p2+p3+pu;


if f7<0
    error('f7 smaller than zero!')
%     return
end

%toc;
%tic
%profile on;
[vec_Local_Kreq_,vec_byp_layers_,vec_pul_layers_] = deal(NaN(Nb,1));
mtx_crit_layers_mode=deal(NaN(N,Nb));
layers_depth_to_H = layers_depth;
[vec_Kreq_rup_disc,vec_funK] = deal(NaN(Nb,1));

for toe_block = 1: Nb
%     fprintf('Current toe block: %d\n',toe_block);
    Pf_norm = vec_Pf_norm (toe_block);
    face_factor = 1-(toe_block-1)/Nb; %rxi/H = rxi/Hi*face_factor
    N_prime = length(layers_depth_to_H(face_factor-layers_depth_to_H
    >10^-6));   %zi/H < H'/H - number of reinforcement layers above the
    height of the toe_block considered
    layers_depth_prime = layers_depth_to_H(face_factor-layers_depth_to_H
    >10^-6 )/ face_factor; %normalized by current height considered H'
%     if N_prime==0
%         fprintf('top block\n')
%     end
    if exist ('Flag_plot','var') && Flag_plot ==1
        %see plot of logspirals evaluated while running
        H_ini = 1;
        betaprime=beta;
        color = 'r';
        linewidth = 0.1;
        linestyle = ':';
        rx_norm=1./(exp(b.*(y-x)).*sin(y)-sin(x))*face_factor;
        d_norm=(exp(b*(z-x)).*sin(z)-sin(x))./Hrx*face_factor; % cd/H -
    normalized crack depth
        hx_norm=(Lrx-lrx).*rx_norm;
        Xcir=-rx_norm.*exp(b.*(y-x)).*cos(y)+(1-face_factor)*cot(beta);
        Ycir=rx_norm.*exp(b.*(y-x)).*sin(y)+(1-face_factor);
        plot_spiral_tenscrack_betaprime

        h2=plot(Xcir,Ycir,'r+');
        h3 = plot([Xcir;rx_norm*cos(x)+Xcir],[Ycir;H_ini],'g:');
        h4 = plot([Xcir;(1-face_factor)*cot(beta)],[Ycir;(1-face_factor)
```

```
],'g:');
        h5 = plot([Xcir;(toe_block-1)/Nb*cot(beta)],[Ycir;(toe_block-1)/Nb],'g:'); %rv
        h6 = plot([Xcir;rx_norm*exp(b*(z-x))*cos(z)+Xcir],[Ycir;H_ini - d_norm],'g:'); %rc
        h7 = plot_crack(1,beta,'r',d_norm,hx_norm,0.1,':');
    end

    if face_factor^2*(1/Hrx)^2*sum_f + qgh*face_factor*fq/Hrx <0 %no need for face neither reinforcement
    %     fprintf('no need for reinforcement');
        [Local_Kreq_,byp_layers_,pul_layers_]=deal(NaN);
        crit_layers_mode=NaN(N_prime,1);
        vec_Local_Kreq_(toe_block) = Local_Kreq_;
        vec_byp_layers_(toe_block)=byp_layers_;%bypassed or not needed for stability
        vec_pul_layers_(toe_block)=pul_layers_;
        mtx_crit_layers_mode(1:N_prime,toe_block)=crit_layers_mode;
        continue
    end

    if (face_factor*1/Hrx)^2*sum_f-face_factor*1/Hrx*cogh*(gc+g1)-Pf_norm*f7+face_factor*1/Hrx*qgh*fq <0 %no reinforcement needed 21/06/2020; surcharge added in 12/02/2021
        crit_layers_mode=NaN(N_prime,1);
        [vec_byp_layers_(toe_block),vec_pul_layers_(toe_block)]=deal (NaN);%bypassed or not needed for stability
        mtx_crit_layers_mode(1:N_prime,toe_block)=crit_layers_mode;
        if isempty(layers_depth_prime)
            vec_Local_Kreq_(toe_block)=NaN;
            continue
        else
            Local_Kreq_=-10;
            vec_Local_Kreq_(toe_block)=Local_Kreq_;
        end
    elseif isempty(layers_depth_prime) %no reinforcement available to help on stability
        fprintf ('Block %d not stable!\n',toe_block)
        Local_Kreq_=10;
        Local_Kreq_rup_disc=10;
        Local_Kreq_rup_comb=10;
        i_block_comb_ = toe_block;
        [byp_layers_,pul_layers_,crit_layers_mode,i_block_rup_]=deal(NaN);
        return

    end
```

```

 %Calculus of theta_i and Lci for layers crossing the failure surface
 %Bypassed layers are ignored (no energy dissipation)
 %Compressed layers are ignored (no energy dissipation) - layers above center of rotation - sinx + z < 0
 %theta_i - angle related to the intersection of the failure surface with the i-layer
 %calculated according to Eq. 16, Michalowski (1997)

 theta0= (y-x)/2+x; %initial guess (half the angle between x and y)
 thetas = zeros(N_prime,1);
 for i = 1: N_prime
     [thetas(i)] = fzero(@(thetai) sin(thetai)*exp(b*(thetai-x))-(layers_depth_prime(i))*Hrx-sin(x),theta0,options);
     %theta_deg (i)=theta(i)*180/pi();
     %fprintf('x = %4.2f\n\ntheta_i = %4.2f (%4.1 f )\n\ny = %4.2f\n',x,theta(i,k),theta_i_deg,y);
 end

 if any(thetas(thetas > y+10e-6)) || any(thetas (thetas < x))
%          [Local_Kreq_rup_disc(toe_block),Local_Kreq_rup_cont(toe_block)] =deal(NaN);
     [vec_Kreq_rup_disc(toe_block),vec_funK(toe_block)]=deal(NaN);
     continue
 end

 layers_depth_slope_prime = layers_depth_prime;
 Th_2=y;
 aux = find(thetas > Th_1+10^-6);
 %depth of the i layer measured from slope face (depth/H) - FOR GENTLE SLOPES
 layers_depth_slope_prime (aux)=(1/Hrx)*(exp(b.*(thetas(aux)-x)).*sin(thetas(aux))-exp(b.*(y-x))...
 .*sin(y)+(exp(b.*(thetas(aux)-x)).* cos(thetas(aux))-exp(b.*(Th_2-x)).*cos(Th_2)).*tan(beta));

 if (x<0) && ((sin(x)+layers_depth_prime(1)*Hrx)<0)  %layers_depth already adjusted for face factor
     layers_depth_prime((sin(x)+layers_depth_prime*Hrx)<0)=0; %all layers above center of rotation must be disregarded for energy dissipation calc
     layers_depth_slope_prime ((sin(x)+layers_depth_prime*Hrx)<0)=0;
 end

 aux_Lcih = zeros (N_prime,1);
 theta_above_crack = thetas(layers_depth_prime< c_d);%zi/Hib < h/Hib
 aux_Lcih(find(layers_depth_prime < c_d)) = 1/Hrx*(exp(b*(
```

```
theta_above_crack-x))...
          .*cos(theta_above_crack)-exp(b*(z-x))*cos(z));

 %Calculus of the active length Laih(Lact_i/H) for all the layers -
 %normalized by H'
 aux_Laih = - (cos(y)+sin(y)*cot(beta))/Hrx * exp(b*(y-x)) + ...
 (cos(thetas)+sin(thetas)*cot(beta))/Hrx .* exp(b*(thetas-x))-
aux_Lcih;
 aux_Leih = LoH/face_factor - aux_Laih;

 rup_i = sin(x)+layers_depth_prime*Hrx;
 A_i = layers_depth_slope_prime.* (sin(x) + layers_depth_prime*Hrx);
%Normalized by current height H'
 B_i = layers_depth_slope_prime.* aux_Laih .* (sin(x) +
layers_depth_prime*Hrx); %Normalized by current height H'
 layers_mode = zeros(N_prime,1)-10;
 layers_mode(aux_Leih<0)=-1; %Bypassed
 layers_mode(layers_depth_prime == 0 & aux_Leih>0)=2; %compressed
layer
 %Rupture only mechanism - considers that the reinforcement length is
 long
 %enough
 sum_rup = sum(rup_i(layers_mode~=2));

 layers_depth_prime_withtoe = layers_depth_to_H(layers_depth_to_H -
face_factor <10^-6 )/ face_factor;
 rup_i_withtoe = sin(x)+layers_depth_prime_withtoe*Hrx;
 if RL == 1
    N_weighted = face_factor * N;
 elseif RL == 2
     N_weighted = face_factor^2 * N;
 end
 N_int =floor (N_weighted);
 N_remainder = N_weighted - N_int;
 sum_rup_weighted = sum(rup_i_withtoe(1:N_int))+rup_i_withtoe(end)*
N_remainder;

 g23_disc=Hrx/N_weighted*sum_rup_weighted; % equivalent to g23
calculated in funxyz_n

 vec_Kreq_rup_disc(toe_block) = (face_factor*(1/Hrx)^2*sum_f-1/Hrx*
cogh*(gc+g1)-Pf_norm*f7/face_factor+qgh*fq/Hrx)/(sum_rup_weighted/
N_weighted); %discrete calculus

 if RL==1
     % for uniformly distributed mode: (g23=g2+g4)
     if (x<0) && ((sin(x)+layers_depth_prime(1)*Hrx)<0)
```

```
            g23_int=(exp(2*b*(y-x))*(sin(y))^2)/2; %reinforcement layers above center of rotations are disregarded
        else
            g23_int=(exp(2*b*(y-x))*(sin(y))^2-(sin(x))^2)/2;
        end
    else
        % for linearly increasing density mode:
        if x<0 && ((sin(x)+layers_depth_prime(1)*Hrx)<0)
            g23_int=(2/Hrx)*((1/3)*(exp(3*b*(y-x))*(sin(y))^3)-(sin(x)/2)*(exp(2*b*(y-x))*(sin(y))^2));
            g23_micha = 1/3*(2*exp(2*b*(y-x))*(sin(y))^2-exp(2*b*(y-x))*sin(x)*sin(y));
        else
            g23_int=(2/Hrx)*((1/3)*(exp(3*b*(y-x))*(sin(y))^3-(sin(x))^3)-(sin(x)/2)*(exp(2*b*(y-x))*(sin(y))^2-(sin(x))^2));
            g23_li = 1/3*(sin(y)*exp(b*(y-x))-sin(x))*(2*sin(y)*exp(b*(y-x))+sin(x));
            g23_micha = 1/3*(2*exp(2*b*(y-x))*(sin(y))^2-exp(b*(y-x))*sin(x)*sin(y)-(sin(x))^2);
        end
    end
    vec_funK(toe_block) = face_factor*sum_f/(Hrx*g23_int)-cogh*((g1+gc)/g23_int)-(Pf_norm*Hrx*f7)/(face_factor*g23_int)+qgh*fq/g23_int;%Eq.20 (integral calculus)

%COMBINED MECHANISM (RUPTURE AND PULLOUT)
    if Local_Kreq_ ~= -10 %reinforcement needed
        %k - number of layers superpassed by the failure surface
        % k=length(aux_Leih(aux_Leih<0));
        %(Bypassed: -1;Pullout:1; Rupture: 0; %Compressed:2; Not mobilized:3);
        layers_mode(aux_Leih<0)=-1;
        layers_mode(layers_depth_prime == 0 & aux_Leih>0)=2; %compressed layer
        crit_layers_mode=layers_mode;
        crossed_thetas = thetas(layers_mode==-10);

        %Two-level full factorial design (last case: all layers being pulled
        %out)
        case_ind = ff2n(length(layers_mode(layers_mode==-10))); % exclueds compressed layers and/or bypassed
        [Local_Kreq_,byp_layers_,pul_layers_]=deal(NaN);
        t_layers_depth = (layers_depth_prime(layers_depth_prime >0 & aux_Leih>0));
        t_layers_depth_slope = (layers_depth_slope_prime(layers_depth_slope_prime >0 & aux_Leih>0));
```

```
    Laih=aux_Laih(layers_mode~=-1&layers_mode~=2); %crossed layers with pullout or rupture
    Leih =  LoH/face_factor - Laih; %anchorage length for crossed and tensioned layers
    Lcih = aux_Lcih (layers_mode~=-1 & layers_mode~=2);
    if any(crossed_thetas(crossed_thetas > y+10e-6)) || any(crossed_thetas(crossed_thetas > y+10e-6)) ||...
           any (Laih (Laih < -10^-6)) ||  any (Laih (Laih > LoH/face_factor))||...
          any (Leih <0)
          error('verify the lengths'); %go to next iteration of i
    end
    for i=1: size(case_ind,1)
          aux_A_i=A_i(layers_mode==-10); %crossed and not compressed
          aux_B_i=B_i(layers_mode==-10);
          aux_rup_i=rup_i(layers_mode==-10);
          A = sum (aux_A_i(case_ind(i,:)==1));
          B=sum(aux_B_i(case_ind(i,:)==1));
          sum_rup = sum(aux_rup_i(case_ind(i,:)==0));
          g23_comb=Hrx/N_prime*sum(rup_i); % equivalent to g23 calculated in funxyz_n

          if sum_rup~=0
              count = count+1;
              Kreq_temp = (face_factor*(1/Hrx)^2*sum_f-1/Hrx*cogh*(gc+g1)-Pf_norm*f7/face_factor+1/Hrx*qgh*fq-2*fb*b*(1-ru)*(A*face_factor*LoH/face_factor-B*face_factor))/(sum_rup/N_prime);
              Tr_norm = Kreq_temp/N_prime; %Tr/(gamma_H^2)
              Tp_norm = 2*layers_depth_slope_prime(layers_mode==-10)/face_factor.*Leih/face_factor*fb*b*(1-ru);
              aux_Tp_norm = Tp_norm(case_ind(i,:)==0); %layers failing by rupture
              %layers being pulled out shoud have Tpi<Tr and layers failing by
              %rupture should have Tpi>Tr, if these layers are subjected to
              %tension
              if  any(Tp_norm(case_ind(i,:)==1) >= Tr_norm) ...
                      || any(aux_Tp_norm<Tr_norm) || Kreq_temp < 0
                  continue %go to next iteration of i
              end
              if Kreq_temp > Local_Kreq_ ||(~isnan(Kreq_temp) && isnan(Local_Kreq_))%Update if the value for the case considered is larger
                  Local_Kreq_  = Kreq_temp;
                  byp_layers_ = sum(layers_mode==-1);
                  pul_layers_ = sum(case_ind(i,:)==1);
                  crit_layers_mode(layers_mode==-10)=case_ind(i,:)';
```

```
                if byp_layers_ + pul_layers_ > N_prime
                    error ('number of layers pulled out and superpassed is larger then N');
                end
            end
        elseif isnan(Local_Kreq_) %rest of the layers subject to pullout
            %layers only failing by pullout (Tr<=Tp)or bypassed
           %Numerator sum in Eq. 26 Abd&Utili (2017) - layers that fail by pullout (A*Lr/H - B)
            A = sum (aux_A_i(case_ind(i,:)==1));
            B=sum(aux_B_i(case_ind(i,:)==1));
           if A~=0
                %necessay length to balance energy equation
                aux_LoH_prime = (((face_factor*1/Hrx)^2*sum_f-face_factor*1/Hrx*cogh*(gc+g1)-Pf_norm*f7+face_factor*1/Hrx*qgh*fq)/(2*fb*b*(1-ru))+B*face_factor)/(A*face_factor); %necessary length from energy balance - normalized by H'
                energy_req = (face_factor*1/Hrx)^2*sum_f-face_factor*1/Hrx*cogh*(gc+g1)-Pf_norm*f7+face_factor*1/Hrx*qgh*fq;
                energy_avlb_i = 2*fb*b*(1-ru)*(A_i*face_factor*LoH/face_factor-B_i*face_factor);
                energy_avlb=sum(energy_avlb_i);
                min_LoH_prime=0;
                count2=1;
                if any(aux_LoH_prime - Laih <0) %initial assumption of number of layers pulled out is not true
                    fprintf ('check this case');
    %                  pul_cases = ff2n(N-length(layers_depth(layers_depth == 0)));
    %                  pul_cases(pul_cases==0)=-1;%bypassed
                    aux_LoH_sup = LoH/face_factor;
                    sorted_Laih=sort(Laih,'descend');
                    count_min = 1;
                    aux_LoH_inf = sorted_Laih(count_min);%this layer will not contribute anymore
                    aux_LoH_prime=aux_LoH_inf;
                    tol=energy_avlb-energy_req;
                    if Flag_plot == 1
                        figure(2)
                        hold on;
                        xlabel('L/H');
                        xlim([sorted_Laih(end) LoH/face_factor])
                        ylabel('tolerance=energy avlb - energy req');
                        plot([0 0.7],[0 0],'--k');
                    end
```

```
                     while abs(tol) > 10^-5
                         energy_avlb_i = 2*fb*b*(1-ru)*(A_i*
face_factor*aux_LoH_prime-B_i*face_factor);
                         energy_avlb=sum(energy_avlb_i(aux_LoH_prime-
Laih>0));
                         tol=energy_avlb-energy_req;
                         if Flag_plot == 1
                             figure(2)
                             hold on;
                             plot(aux_LoH_prime,tol,'Marker','x');
                             figure (1)
                             hold on;
                             if count_min > 1
                                 delete(hr)
                             end
                             hr = plot_line_reinforcement(H_ini,beta,
N,RL,'m',aux_LoH_prime);
                         end
                         if tol<-10^-6 %increase L/H
                             min_aux_LoH=aux_LoH_prime;
                             aux_LoH_inf=aux_LoH_prime;
                             aux_LoH_prime = (aux_LoH_sup +
aux_LoH_inf)/2;
                         elseif tol > 10^-6 %decrease L/H
                             count_min = count_min+1;
                             aux_LoH_sup = aux_LoH_prime;
                             if count_min <= length(sorted_Laih)
                                 if exist('min_aux_LoH','var')
                                     aux_LoH_inf = (aux_LoH_prime +
min_aux_LoH)/2;
                                 else
                                     aux_LoH_inf = sorted_Laih(
count_min);
                                 end
                                 aux_LoH_prime=aux_LoH_inf;
                             else
                                 aux_LoH_prime=(min_aux_LoH+
aux_LoH_prime)/2;
                             end
                         else
                             min_LoH_prime=aux_LoH_inf;
                         end
                     end
                 else
                     min_LoH_prime = aux_LoH_prime;
                 end
                 if min_LoH_prime > LoH/face_factor && all(
```

```
    min_LoH_prime - Laih >0)  %needs more than the length given
                        Kreq_temp=3; %high value means that length is not adequate
                        Local_Kreq_=Kreq_temp;
                        byp_layers_ = sum(layers_mode==-1);
                        pul_layers_ = NaN;
                        crit_layers_mode (:) = NaN;

                    elseif min_LoH_prime >0 %negative value means no reinforcement is needed
                        Tp_norm = 2*layers_depth_slope_prime(layers_depth_slope_prime >0)/face_factor.*(min_LoH_prime - aux_Laih(layers_depth_prime >0))/face_factor*fb*b*(1-ru); %minimum pullout force required for all layers, normalized by total height
                        Kreq_temp= max(Tp_norm)*N_prime;
                        if Kreq_temp>Local_Kreq_
                            Local_Kreq_ = Kreq_temp;%updates
                            byp_layers_=sum(layers_mode==-1);%bypassed or not needed for stability
                            pul_layers_=sum(Tp_norm>0);
                            case_ind(i,Tp_norm'>0)= 1;
                            case_ind (i,Tp_norm'<=0)= 3;
                            crit_layers_mode(layers_mode==-10)=case_ind;
                        end
                    end
                end
                count = count+1;
            end
        end
        vec_Local_Kreq_(toe_block) = Local_Kreq_;
        vec_byp_layers_(toe_block)=byp_layers_;%bypassed or not needed for stability
        vec_pul_layers_(toe_block)=pul_layers_;
        mtx_crit_layers_mode(1:N_prime,toe_block)=crit_layers_mode;
        if vec_Local_Kreq_(toe_block) ==3
            break
        end
    end
    if exist ('h11','var')
        delete([h11,h12,h2,h3,h4,h5,h6,h7])
    end
    if exist('hr','var')
        delete(hr)
    end
end

%FINAL RESULTS FOR RUPTURE ONLY
```

```
Kreq_rup_toe_disc = vec_Kreq_rup_disc(1);
[Kreq_rup,i_block_rup_disc_] = max(vec_Kreq_rup_disc);

Kreq_rup_toe_cont = vec_funK (1);
[funK,i_block_rup_cont_] = max(vec_funK);

if Kreq_rup>3 || Kreq_rup<-1
    Local_Kreq_rup_disc =NaN;
else
    Local_Kreq_rup_disc =Kreq_rup;
end
if funK>3 || funK<-1
    [Local_Kreq_rup_cont,i_block_rup_cont_] = deal(NaN);
else
    Local_Kreq_rup_cont = funK;
end
if disc_reinf == 0
    Local_Kreq_rup=Local_Kreq_rup_cont;
    i_block_rup_ = i_block_rup_cont_;
else
    Local_Kreq_rup = Local_Kreq_rup_disc;
    i_block_rup_ = i_block_rup_disc_;
end


%FINAL RESULTS FOR COMBINED MECHANISM
[Local_Kreq_,i_block_comb_] = max(vec_Local_Kreq_);
Local_Kreq_toe_ = vec_Local_Kreq_(1);
byp_layers_=vec_byp_layers_(i_block_comb_);%bypassed or not needed for
   stability
pul_layers_=vec_pul_layers_(i_block_comb_);
crit_layers_mode = mtx_crit_layers_mode (:,i_block_comb_);
layers_mode=crit_layers_mode;

if Local_Kreq_==-10 %no need for reinforcement
    Local_Kreq_=Local_Kreq_rup; %negative value - just to register
    [byp_layers_,pul_layers_,i_block_comb_,crit_layers_mode]=deal(NaN);
    return;
end

if Local_Kreq_>3 || Local_Kreq_<-1 %???
    [Local_Kreq_,byp_layers_,pul_layers_,i_block_comb_,crit_layers_mode
   ]=deal(NaN);
end

end
```

```
function int_fc = int_fun_fc (theta)

int_fc= 1/4*(-2*log(cos(theta/2)-sin(theta/2))+2*log(cos(theta/2)...
        +sin(theta/2))-2*(sec(theta))^2+1/(cos(theta/2)-sin(theta/2))^2 ...
        - 1/(cos(theta/2)+sin(theta/2))^2);

end
```

```
function int_ft = int_fun_ft (theta,phi)

int_ft=1/4*(2*sec(theta)^2+sin(phi)*(2*log(cos(theta/2)-sin(theta/2))...
        -2*log(cos(theta/2)+sin(theta/2))+1/(cos(theta/2)+sin(theta/2))^2 ...
        +1/(-1+sin(theta))));
end
```

```
function int_u1 = int_fun_u1 (Th,b,x)

int_u1= -((b*exp(2*b*Th-3*b*x)*(2*b*exp(b*Th)* cos(Th) - ...
    6*b^2*exp(b*Th)*sin(Th)+(1+9*b^2)*exp(b*x)*sin(x)))/(2*(b+9*b^3)));
end
```

```
function int_uc = int_fun_uc (Th,x,z,b)

int_uc= 1/6 *exp(2*b*(z-x))*(cos(z))^2 *(tan(Th))^2 *(-3 *sin(x)...
    + 2*exp(b*(z-x))* cos(z)*tan(Th));
end
```

D.3 Functions and files for plotting

```
function F=plot_line(height,slope,color,linewidth)

% plot straight line soil surface

xlim_right=1;
xlim_left=height*cot(slope);%-0.1;
axis_x=[xlim_left;xlim_right];
axis_y=[height;height];
F=plot (axis_x,axis_y,color,'LineWidth',linewidth);
end
```

```
function [hr] =  plot_line_reinforcement(H_ini,beta,N,RL,color,LoH)



% plot straight lines

```

```
Z=zeros(N,1);

for i=1:N
    if RL==1
         Z(i)=(i-0.5)*H_ini/N;
    else
        Z(i)=(2/3)*H_ini*N*(sqrt((i/N)^3)-sqrt(((i-1)/N)^3));
    end

    xlim_left=(H_ini-Z(i))*cot(beta);
    xlim_right=xlim_left+LoH*H_ini; %LoH; %Assumed value for
   reinforcement length
    axis_x=[xlim_left;xlim_right];
    axis_y=[H_ini-Z(i);H_ini-Z(i)];
    hr(i)=plot (axis_x,axis_y,color,'LineWidth',0.5);
end
end
```

```
function F=plot_line_slopesurface(height,slope,color,linewidth)

% plot straight line tan(alfa)

xlim_left = 0;
xlim_right=height*cot(slope);
axis_x=[xlim_left;xlim_right];
axis_y=[0;height];
plot (axis_x,axis_y,'Color',color,'LineWidth',linewidth,'LineStyle',':')
   ;
```

```
function F=plot_line_toe(height,slope,color,linewidth)

% plot straight line tan(alfa)

xlim_right=0;
xlim_left=-height/2-0.1;
axis_x=[xlim_left;xlim_right];
axis_y=axis_x*tan(slope);
plot (axis_x,axis_y,'Color',color,'LineWidth',linewidth);
```

plot_spiral_tenscrack_betaprime file:

```
j=1;
% theta0=x;
% thetam=z;
% thetah=y;
theta0=x_(j);
thetam=z_(j);
thetah=y_(j);
% theta0=x_range(k);
```

```
% thetam=y_range(l);
% thetah=x_range(k);
rzero=rx_norm(j);
% n_plot= numero di punti che uso per disegnare una spirale
n_plot=100;
% plot(Xcir(j),Ycir(j),'Marker','+','MarkerEdgeColor','c','MarkerSize
    ',10)
% imaginary spiral piece xx,yy
delta_theta=(thetam-theta0)/n_plot;
theta_theta_1=theta0:delta_theta:thetam;
rho=rzero*exp(b*(theta_theta_1-theta0));
% inizializzo gli assi
% asse_x=0;
% asse_y=0;
% cambio il sistema di coordinate
asse_x=rho.*cos(theta_theta_1);
asse_y=rho.*sin(theta_theta_1);
% Inverto l'asse y e traslo l'origine della spirale al piede del pendio
asse_y=-asse_y;
asse_x=asse_x+Xcir(j)-cot(betaprime(j))+cot(beta(j)); % equation for
    spiral passing below toe
asse_y=asse_y+Ycir(j);
% plotto
h12 = plot (asse_x,asse_y,'Color',[0.5 0.5 0.5],'LineWidth',linewidth,'
    LineStyle',linestyle);

% Secondo pezzo della spirale
delta_theta=(thetah-thetam)/n_plot;
theta_theta_2=thetam:delta_theta:thetah;
rho=rzero*exp(b*(theta_theta_2-theta0));
% inizializzo gli assi
% asse_x=0;
% asse_y=0;
% cambio il sistema di coordinate
asse_x=rho.*cos(theta_theta_2);
asse_y=rho.*sin(theta_theta_2);
% Inverto l'asse y e traslo l'origine della spirale al piede del pendio
asse_y=-asse_y;
asse_x=asse_x+Xcir(j)-cot(betaprime(j))+cot(beta(j)); % equation for
    spiral passing below toe
asse_y=asse_y+Ycir(j);
% plotto
h11 =plot (asse_x,asse_y,'Color',color,'LineWidth',linewidth,'LineStyle'
    ,linestyle);
```

plot_spiral_tenscrack_betaprime_L file:

```

```

```
theta0=x_L;
thetam=z_L;
thetah=y_L;
rzero=rx_norm_L;
% n_plot= numero di punti che uso per disegnare una spirale
n_plot=100;
% plot(Xcir_L(j),Ycir_L(j),'Marker','*','MarkerEdgeColor','g','
    MarkerSize',10)
% imaginary spiral piece xx,yy
delta_theta=(thetam-theta0)/n_plot;
theta_theta_1=theta0:delta_theta:thetam;
rho=rzero*exp(b*(theta_theta_1-theta0));
% inizializzo gli assi
% asse_x=0;
% asse_y=0;
% cambio il sistema di coordinate
asse_x=rho.*cos(theta_theta_1);
asse_y=rho.*sin(theta_theta_1);
% Inverto l'asse y e traslo l'origine della spirale al piede del pendio
asse_y=-asse_y;
asse_x=asse_x+Xcir_L-cot(betaprime_L)+cot(beta); % equation for spiral
    passing below toe
asse_y=asse_y+Ycir_L;
% plotto
if t==2
    h12=plot (asse_x,asse_y,'-','Color',color,'LineWidth',linewidth);
else
    h12=plot (asse_x,asse_y,'--','Color',color,'LineWidth',0.5);
end
% Secondo pezzo della spirale
delta_theta=(thetah-thetam)/n_plot;
theta_theta_2=thetam:delta_theta:thetah;
rho=rzero*exp(b*(theta_theta_2-theta0));
% inizializzo gli assi
% asse_x=0;
% asse_y=0;
% cambio il sistema di coordinate
asse_x=rho.*cos(theta_theta_2);
asse_y=rho.*sin(theta_theta_2);
% Inverto l'asse y e traslo l'origine della spirale al piede del pendio
asse_y=-asse_y;
asse_x=asse_x+Xcir_L-cot(betaprime_L)+cot(beta); % equation for spiral
    passing below toe
asse_y=asse_y+Ycir_L;
% plotto
h11=plot (asse_x,asse_y,'Color',color,'LineWidth',linewidth,'LineStyle',
    linestyle);
```

plot_wall_geometry file:

```
H_ini = 1;
j=1;
betaprime=beta;
color = 'r';
linewidth = 0.1;
linestyle = ':';
if isempty(LoH)
    LoH_plot = 1;
else
    LoH_plot = LoH;
end
hold on;
axis equal
plot_line(H_ini,beta,'k',0.1);
plot_line_toe(H_ini,0,'k',0.1);
plot_line_reinforcement(H_ini,beta,N,RL,'k',LoH_plot');
plot_block_facing (Nb,H_ini/Nb,wbh,beta,'k',0.1);
plot_line_slopesurface(H_ini,beta,'k',0.05);
```

E Results for LID distribution

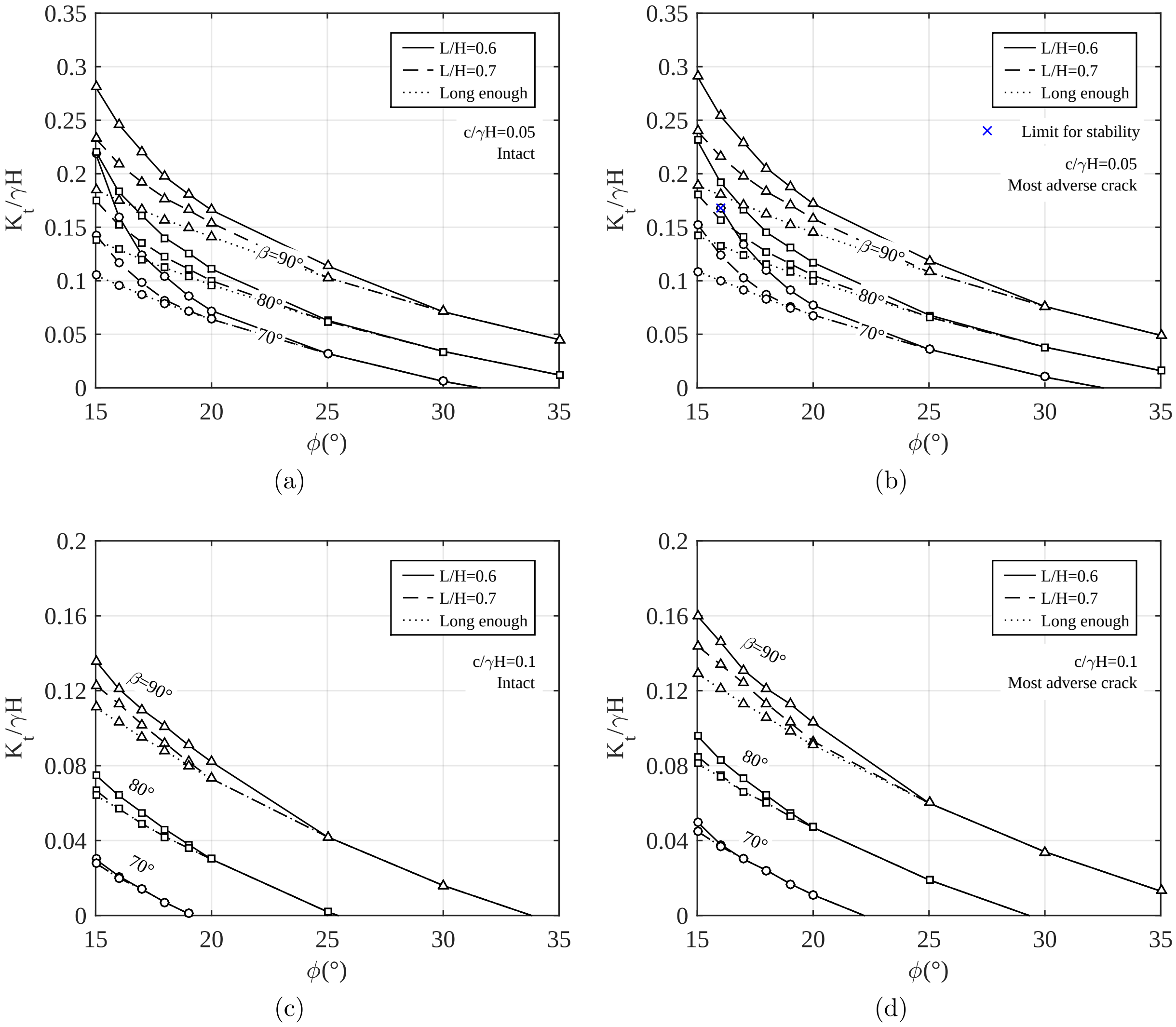

Figure D.1: Required reinforcement versus wall facing batter β for different L/H (sufficient length for rupture of all layers, $0.6H$ and $0.7H$) ($w_b/H = 0.1$, δ =$2/3\phi$, $\delta_{base} = 15°$, $\delta_{bb} = 38°$, $D = H/3$, modified force direction, LID reinforcement distribution). (a) & (c) are for a reinforced soil wall in intact soil and in the presence of tension cracks for $c/\gamma H = 0.05$, respectively; while (b) & (d) are for $c/\gamma H = 0.1$. The most adverse crack to stability is considered. The blue 'x' markers indicate the limit for stability, beyond which the prescribed reinforcement length is not sufficient to provide stability.

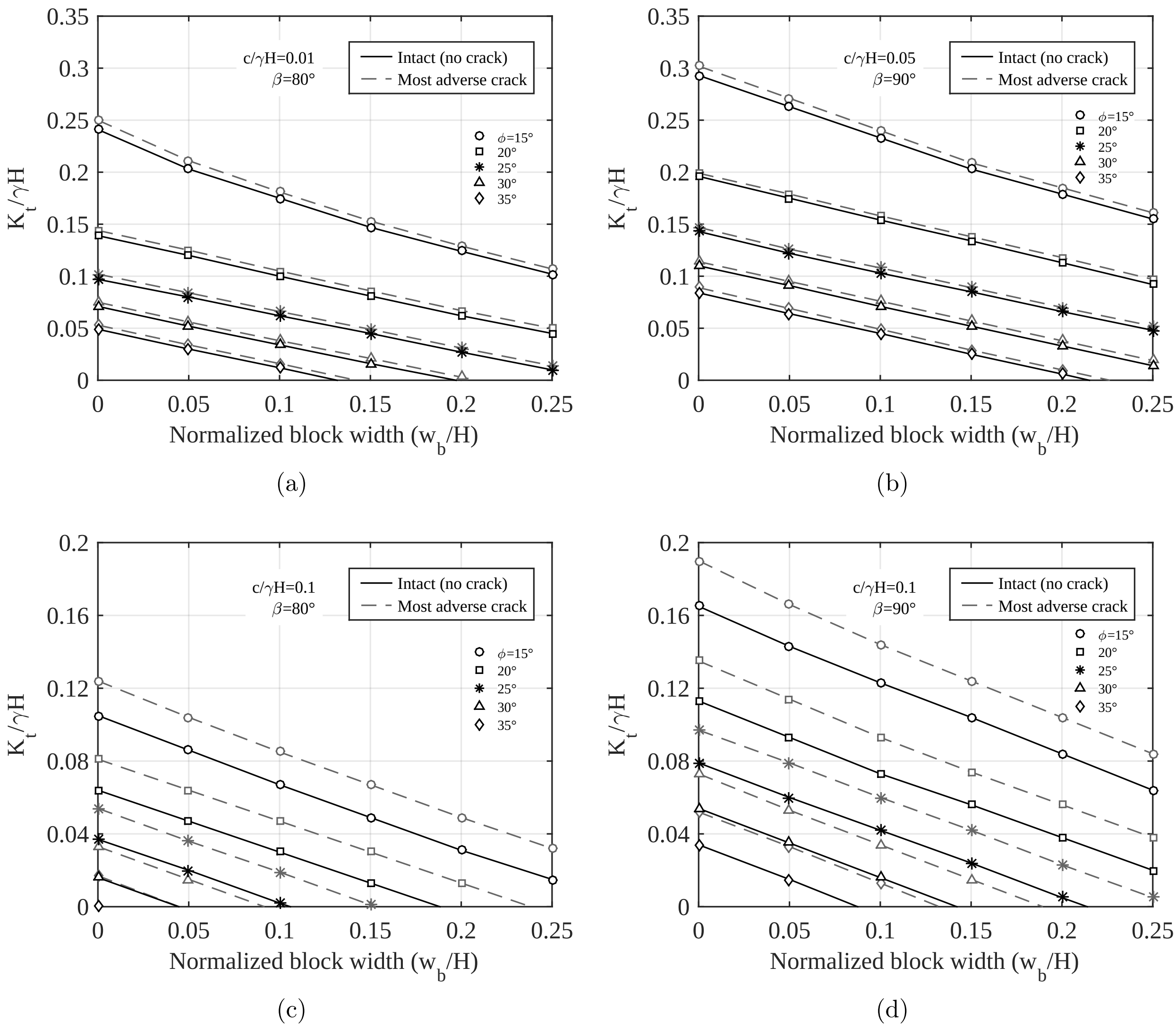

Figure D.2: Required reinforcement versus w_b/H for a reinforced soil wall in intact soil (black lines) and in the presence of tension cracks (grey lines). (a) & (b) are for $c/\gamma H = 0.05$ and $\beta = 80°$ and $\beta = 90°$, respectively; while (c) & (d) are for are for $c/\gamma H = 0.1$ and $\beta = 80°$ and $\beta = 90°$, respectively. ($\delta = 2/3\phi$, $\delta_{base} = 15°$, $\delta_{bb} = 38°$, $L/H = 0.7$, $D = H/3$, modified force direction, LID reinforcement distribution).

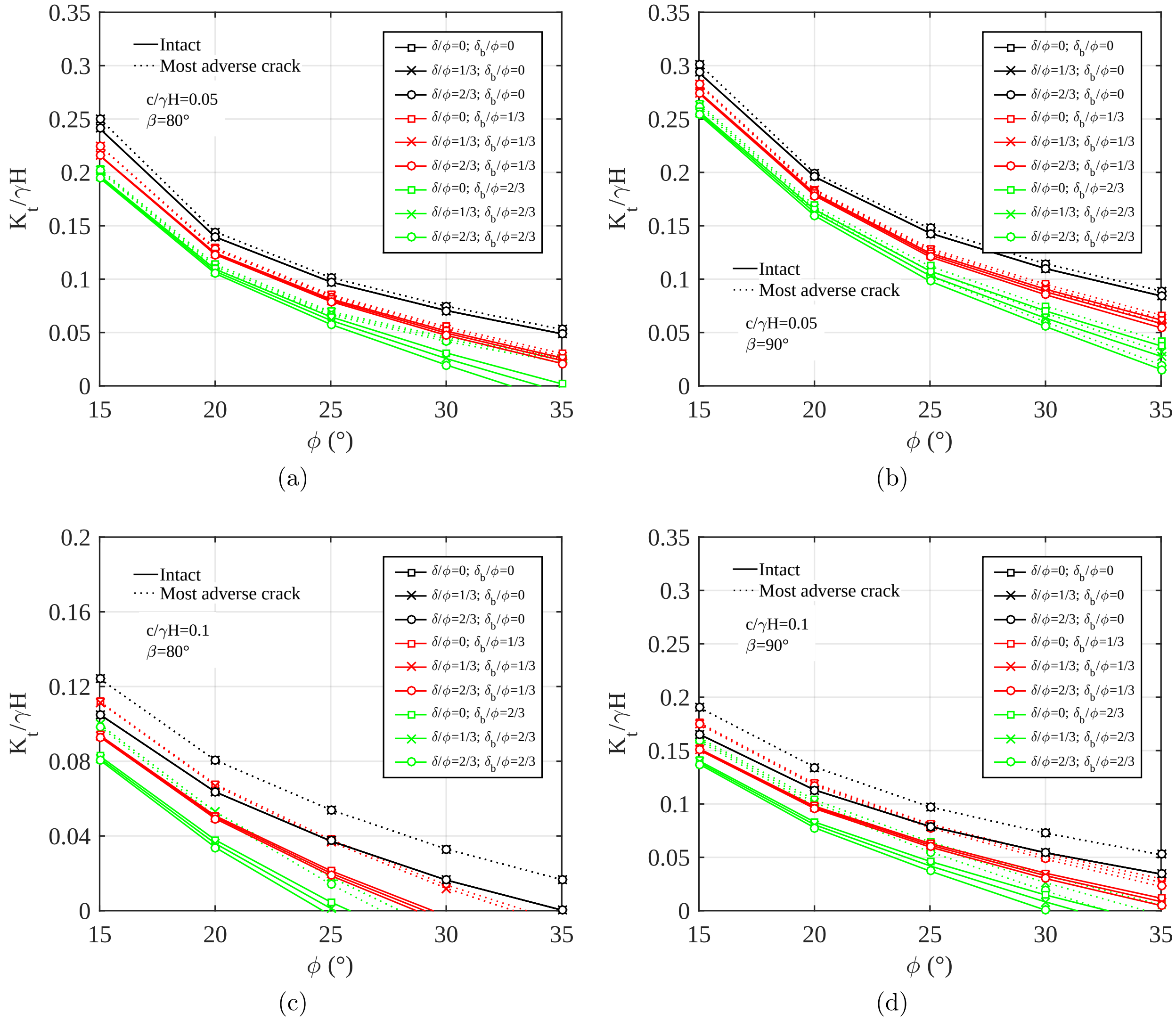

Figure D.3: Effect of facing-backfill δ and foundation-block δ_{base} interface friction for a reinforced soil wall in intact soil (black lines) and in the presence of tension cracks (grey lines). The most adverse crack to stability is considered. ($L/H = 0.7$, $\delta_{bb} = 38°$, $w_b/H = 0.1$, $D = H/3$, modified force direction, LID reinforcement distribution). (a) & (b) are for $c/\gamma H = 0.05$, $\beta = 80°$ and $\beta = 90°$, respectively; while (c) & (d) are for $c/\gamma H = 0.1$.

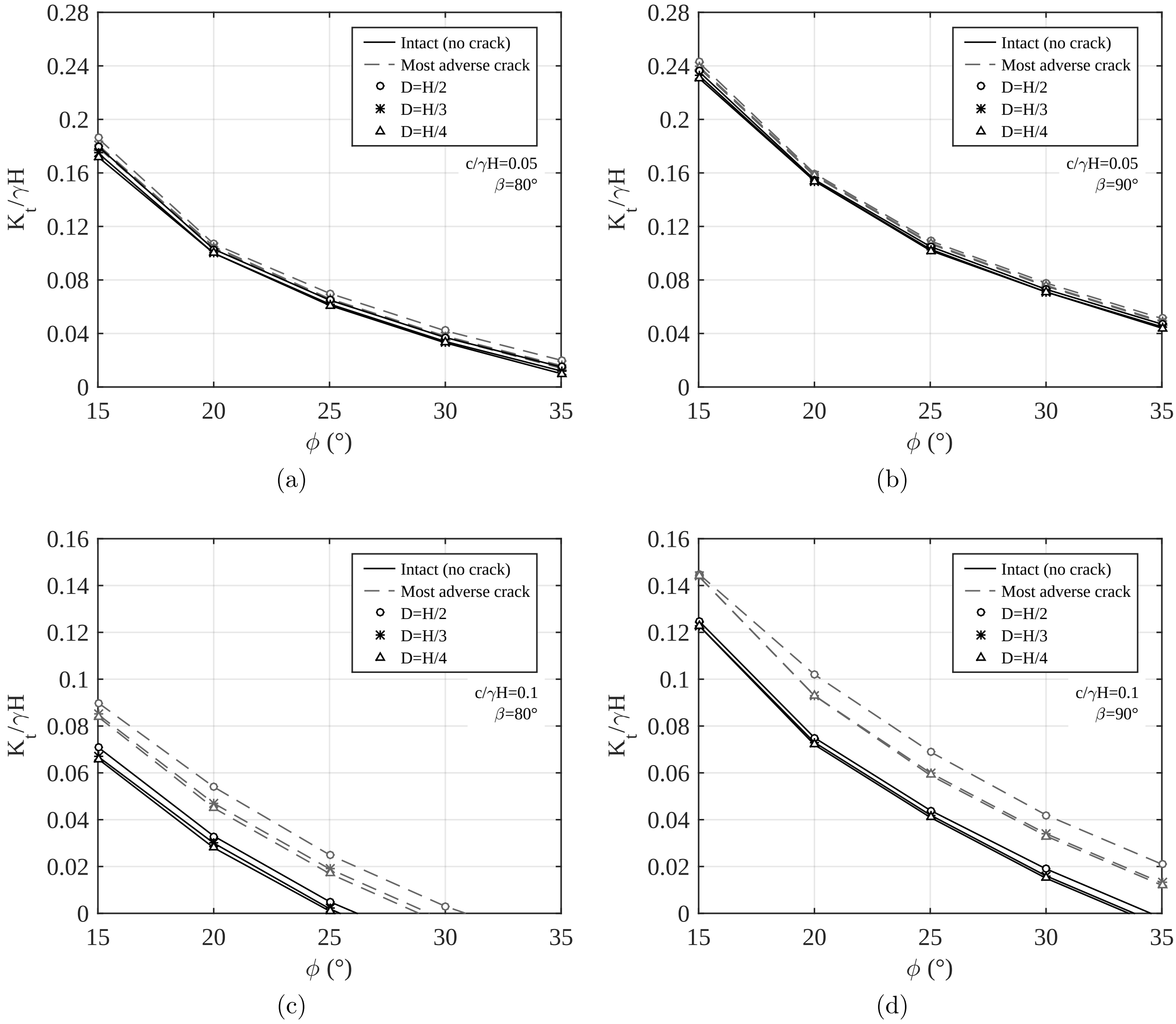

Figure D.4: Effect of location of reaction force acting at the facing (D) for a reinforced soil wall in intact soil (black lines) and in the presence of tension cracks (grey lines) ($\phi = 20°$, $\delta = 2/3\phi$, $\delta_{base} = 15°$, $\delta_{bb} = 38°$, $L/H = 0.7$, and $w_b/H = 0.1$, modified force direction, LID reinforcement distribution). (a) & (b) are for $c/\gamma H = 0.05$, $\beta = 80°$ and $\beta = 90°$, respectively, while (c) & (d) are for $c/\gamma H = 0.1$, $\beta = 80°$ and $\beta = 90°$. respectively.

F Script developed for data filtering of the physical test readings

```
from tkinter import *
from tkinter.filedialog import askopenfilename
import linecache
import math
import matplotlib.pyplot as plt
import numpy as np
import os
import matplotlib.ticker as ticker
from distutils.util import strtobool
import math


def data_processing(system, phase):
    #system (1 for System 5000 and 2 for System 8000)
    #phase (1 for construction and 2 for surcharge)


    #it iterates through the files of a folder
    if system == 1 and phase == 1:
        path = "D:\OneDrive - usp.br\ACADEMIC\DOUTORADO\Results\WallData
    \RawData\Construction\System5000"
    elif system == 1 and phase == 2:
        path = "D:\OneDrive - usp.br\ACADEMIC\DOUTORADO\Results\WallData
    \RawData\Surcharge\System5000"
    elif system == 2 and phase == 1:
        path = "D:\OneDrive - usp.br\ACADEMIC\DOUTORADO\Results\WallData
    \RawData\Construction\System8000"
    elif system == 2 and phase == 2:
        path = "D:\OneDrive - usp.br\ACADEMIC\DOUTORADO\Results\WallData
    \RawData\Surcharge\System8000"
    # os.chdir(path) #change the current working directory to specified
    path


    #To open a file chosen by the user:
    # Tk().withdraw()  # we don't want a full GUI, so keep the root
    window from appearing
    # input_filename = askopenfilename \
    #     (title="Select the .txt file with the analysis input data",
    #      filetypes=[('Text Files', '*.txt')])  # show an "Open" dialog
     box and return the path to the selected file
    # print(input_filename)
```

```python


# path for the a new text file with the filtered data
if system == 1 and phase == 1:
    folder_path = "D:\OneDrive - usp.br\ACADEMIC\DOUTORADO\Results\WallData\RawData\Construction\System5000\Filtered_data_System5000"
elif system == 1 and phase == 2:
    folder_path = "D:\OneDrive - usp.br\ACADEMIC\DOUTORADO\Results\WallData\RawData\Surcharge\System5000\Filtered_data_System5000"
elif system == 2 and phase == 1:
    folder_path = "D:\OneDrive - usp.br\ACADEMIC\DOUTORADO\Results\WallData\RawData\Construction\System8000\Filtered_data_System8000"
elif system == 2 and phase == 2:
    folder_path = "D:\OneDrive - usp.br\ACADEMIC\DOUTORADO\Results\WallData\RawData\Surcharge\System8000\Filtered_data_System8000"

# folder_path = "D:\OneDrive - usp.br\ACADEMIC\DOUTORADO\Results\WallData\RawData\Surcharge\System5000\Filtered_data_System5000"

history_file_path = folder_path + '\history_file.txt'
history_file = open(history_file_path, 'w') #clears the content of the file

history_file.write('system (1 for System 5000 and 2 for System 8000)\n')
history_file.write('phase (1 for construction and 2 for surcharge)\n\n')
history_file.write('System: {}\n'.format(system))
history_file.write('Phase: {}\n'.format(phase))
history_file.close()

for file in os.listdir(path):
    # Check whether file is in text format or not
    if file.endswith(".txt"):
        input_filename = f"{path}\{file}"
        print(input_filename)
    else:
        continue #goes to next file of the directory

    with open(input_filename, 'r') as InputFile:
        output_filename = input_filename.split("\\")[-1]
        file_path = folder_path + "\Filtered_" + output_filename
        outputfile = open(file_path, 'w')
        next(InputFile)
        outputfile.write("\n")
        analysis_name = InputFile.readline()
        outputfile.write(analysis_name)
```

```python

        history_file = open(history_file_path,'a')
        start_time = InputFile.readline()
        info = output_filename.split('.')[0] + ' ' + start_time.replace('Start Time:','')
        history_file.write(info)
        outputfile.write(start_time + '\n')
        next(InputFile)

        #selection of one instrument to use as reference for data filtering
        if system == 1 and phase == 2:
            sensor_id = 16  # refers to sensor column in the input data file (column 17 - TD06 at soil surface)
        elif system == 1:
            sensor_id = 3 #SPC-02
        elif system == 2 and phase ==1:
            sensor_id = 3
        else:
            sensor_id = 3
        step = 500 #default step for the filtered data, readings recorded in new file with this spacing
        initial_step = step
        tolerance = 0.021 # raw data with 2 decimals
        initial_data = 50  # number of initial readings to be stored
        flag_end = 0
        input_sensor_values = []
        input_ID = []
        input_times = []
        head_line = InputFile.readline()
        outputfile.write(head_line)


        for i in range(initial_data):
            line = InputFile.readline()
            if line == "":
                break
            content = line.strip().split()
            input_sensor_values.append(content[sensor_id])
            input_ID.append(content[0])
            input_times.append(content[1])


        # extracting the xth line
        last_line = 6 + initial_data  # refers to first line with data in the raw data file (system 5000)
        line_number = last_line + step
```

```
        particular_line = linecache.getline(input_filename, line_number)
        print(particular_line)
        if particular_line == "":
            flag_end = 1;

        while particular_line != "":  # up to the end of the file
            content = particular_line.strip().split()
            val1 = float(input_sensor_values[-1].replace(',', '.'))  # last value stored
            val2 = float(content[sensor_id].replace(',', '.'))
            # print(val2)
            diff = val2 - val1
            print('difference: ', diff)
            print(abs(diff))
            while abs(diff) > tolerance:
                step = int(step / 2)
                if step < 1:
                    break
                line_number = last_line + step
                particular_line = linecache.getline(input_filename, line_number)
                content = particular_line.strip().split()
                val1 = float(input_sensor_values[-1].replace(',', '.'))  # last value stored
                val2 = float(content[sensor_id].replace(',', '.'))
                diff = val2 - val1
                print('difference: ', diff)
            print('final step: ', step)
            input_sensor_values.append(content[sensor_id])
            input_ID.append(content[0])
            input_times.append(content[1])
            step = initial_step  # resets to larger step
            last_line = line_number
            line_number = last_line + step
            particular_line = linecache.getline(input_filename, line_number)

        # iteration over the last portion of the file
        if flag_end != 1:
            last_fileline = InputFile.readlines()[-1]  # last line of the file
            content_lastline = last_fileline.strip().split()
            last_ID = content_lastline[0]
            while step > 1:
                line_number = int(content_lastline[0]) + 5
                val1 = float(input_sensor_values[-1].replace(',', '.
```

```
'))  # last value stored
                val2 = float(content_lastline[sensor_id].replace(',', '.'))
                diff = val2 - val1

                content = content_lastline
                while abs(diff) > tolerance:
                    step = int((int(content[0]) - int(input_ID[-1])) / 2)
                    if step < 1:
                        break
                    line_number = last_line + step
                    particular_line = linecache.getline(input_filename, line_number)
                    content = particular_line.strip().split()
                    val1 = float(input_sensor_values[-1].replace(',', '.'))  # last value stored
                    val2 = float(content[sensor_id].replace(',', '.'))
                    diff = val2 - val1

                input_sensor_values.append(content[sensor_id])
                input_ID.append(content[0])
                input_times.append(content[1])
                last_line = line_number
                if input_ID[-1] == last_ID:
                    break

            if input_ID[-1] != last_ID:  # register the values of the last line of the file if not already registered
                input_sensor_values.append(content[sensor_id])
                input_ID.append(content[0])
                input_times.append(content[1])

        # writes the filtered values in a new file, replacing decimal character and sensors with negative numbers (inverted)
        n_lines = int(len(input_ID))
        for i in range(n_lines):
            # print(i)
            line_number = int(input_ID[i]) + 5
            # print(line_number)
            line = linecache.getline(input_filename, line_number)
            line = line.replace(',', '.')
            # print(line)
            content = line.strip().split()
            # print(float(content[16]))
            if system == 1 and phase == 2:
```

```
                    content[16] = str(-float(content[16])) #values registered with inverse sign during data acquisition
                    content[21] = str(-float(content[21])) #values registered with inverse sign during data acquisition
                line = ' '.join(content)
                # print(line)
                outputfile.write('{}\n'.format(line))

            outputfile.close()
            history_file.close()
            print ('Output file generated')
    print('Setted step: {}'.format(initial_step))
    print('Tolerance: {}'.format(tolerance))

def plot_results():  # plot filtered results for sensor_id
    Tk().withdraw()  # we don't want a full GUI, so keep the root window from appearing
    input_file = askopenfilename \
        (title="Select the .txt file with the filtered data for plotting",
         filetypes=[('Text Files', '*.txt')])  # show an "Open" dialog box and return the path to the selected file
    sensor_id = 4
    input_sensor_values = []
    input_times = []

    with open(input_file, 'r') as input_file:

        for line in range(5):
            next(input_file)
        i = 0
        for line in input_file:
            content = line.strip().split()
            input_sensor_values.append(float(content[sensor_id]))
            input_times.append(float(content[1]))
            i=i+1

    list_max = max(input_sensor_values)
    list_min = min(input_sensor_values)

    # fig, ax = plt.subplots()
    step_x = input_times[-1]/10
    x_ticks = np.arange(0, input_times[-1], step_x)
    plt.xticks(x_ticks)
    step = (max(input_sensor_values) - min(input_sensor_values))/10
    print(step)
    y_lim = max(list_max, 0.01)
```

```
    y_ticks = np.arange(list_min, y_lim, step)
    plt.yticks(y_ticks)
    plt.plot(input_times, input_sensor_values, linestyle=':', marker='.'
    , markersize='10',
             label='Sensor {} (Measured)'.format(sensor_id))

    plt.xlabel('Time (s)')
    plt.ylabel('sensor output')
    plt.tight_layout
    plt.legend()
    plt.grid()
    plt.show()


#call function for data processing
# system = input('Type 1 for System 5000 or 2 for System 8000: ')
# if system != '1' and system != '2':
#     raise ("You must Type 1 for System 5000 or 2 for System 8000:")
#
# phase = input('Type 1 for Construction or 2 for Surcharge: ')
# if system  != '1' and system != '2':
#     raise ("You must 'Type 1 for Construction or 2 for Surcharge: ")
# system = int(system)
# phase = int(phase)

#Given inputs alreadry known
system = 1
phase = 1
data_processing(system, phase)

#plotting results with filtered data
# plot_results()
```

G Automated Python Scripting for PLAXIS Analysis

The script developed is intended to conduct automated parametric analysis in which it is necessary to run a large amount of numerical analysis to evaluate the influence of key parameters on model performance. This is possible in PLAXIS 2D via a wrapper based on PYTHON programming language. For the initial tasks, primarily involving generating and running the reinforced soil walls PLAXIS models, customized scripts were written in Python coding language. Scripts for results data extraction are also presented.

The first required step was to generate the numerical model of the reinforced soil wall, given the input parameters of the current iteration.

G.1 Script to read input text files with model parameters

```
from tkinter import *
from tkinter.filedialog import askopenfilename
from distutils.util import strtobool
import math

def import_data_from_file (Flag_Input_from_File, structure_type):
    Tk().withdraw()  # we don't want a full GUI, so keep the root window from appearing
    input_filename = askopenfilename \
        (title = "Select the .txt file with the analysis input data", filetypes=[('Text Files', '*.txt')])  # show an "Open" dialog box and return the path to the selected file
    input_values = []
    input_ids = []
    new = True #indicates if it is a new set of parameters
    with open(input_filename, 'r') as InputFile:
        next(InputFile)
        next(InputFile)
        next(InputFile)
        for line in InputFile:
            print(line)
            content = line.strip().split(',')
            if len(content) == 1 and content != ['']:
                input_values.append("")
                input_ids.append("")
            elif len(content) > 1:
                input_ids.append(content[0])
                input_values.append(content[1])

        print(input_ids)
```

```
        print(input_values)

    for i in range(len(input_values)):
        if input_values[i] == 'True' or input_values[i] == 'False':
            input_values[i] = bool(strtobool(input_values[i]))
        else:
            try:
                input_values[i] = float(input_values[i])  # convert numeric input data from string to float
                if input_ids[i] == 'Number of blocks' or input_ids[i] == 'Number of reinforcement layers' or input_ids[i] == 'Surcharge type' or \
                        input_ids[i] == 'Staged construction flag' or input_ids[i] == 'flag_suction'\
                        or input_ids[i] == 'UsdaSoilType' or input_ids[i] == 'SoilModel':
                    input_values[i] = int(input_values[i])
            except:
                pass

    # Geometry and other settings
    i_idx = input_ids.index('') + 1
    f_idx = input_ids.index('', i_idx)
    # print(input_values[f_idx])
    geometric_set = list(zip(input_ids[i_idx:f_idx], input_values[i_idx:f_idx]))
    print(geometric_set)
    print(geometric_set[-1])

    i_idx = input_ids.index('',f_idx) + 1
    f_idx = input_ids.index('', i_idx)
    ModelType, ElementType = input_values[i_idx:f_idx]
    print(ModelType, ElementType)

    # Reinforced soil settings
    ModelName = input_values[input_ids.index('ModelName')]
    i_idx = input_ids.index('',f_idx) + 1
    f_idx = input_ids.index('', i_idx)
    soil_param = list(zip(input_ids[i_idx:f_idx], input_values[i_idx:f_idx]))
    print(soil_param)

    # geosynthetic settings
    i_idx = input_ids.index('', f_idx) + 1
    f_idx = input_ids.index('', i_idx)
    geosynthetic_param = list(zip(input_ids[i_idx:f_idx], input_values[i_idx:f_idx]))
```

```
    print(geosynthetic_param)

    if structure_type == 'slope':
        # Foundation soil settings
        i_idx = input_ids.index('', f_idx) + 1
        found_param = list(zip(input_ids[i_idx:], input_values[i_idx:]))
        print(found_param)

        return geometric_set, ModelType, ElementType, ModelName,
 soil_param, geosynthetic_param, found_param

    elif structure_type == 'wall':
        #Facing block settings
        i_idx = input_ids.index('', f_idx) + 1
        f_idx = input_ids.index('', i_idx)
        concrete_param = list(zip(input_ids[i_idx:f_idx], input_values[
 i_idx:f_idx]))
        print(concrete_param)

        #Soil/block interface settings
        i_idx = input_ids.index('', f_idx) + 1
        f_idx = input_ids.index('', i_idx)
        sb_interf_param = list(zip(input_ids[i_idx:f_idx], input_values[
 i_idx:f_idx]))
        print(sb_interf_param)

        #Block/block interface settings
        i_idx = input_ids.index('', f_idx) + 1
        f_idx = input_ids.index('', i_idx)
        bb_interf_param = list(zip(input_ids[i_idx:f_idx], input_values[
 i_idx:f_idx]))
        print(bb_interf_param)

        #Facing connectors settings
        i_idx = input_ids.index('', f_idx) + 1
        f_idx = input_ids.index('', i_idx)
        connect_param = list(zip(input_ids[i_idx:f_idx], input_values[
 i_idx:f_idx]))
        print(connect_param)

        #Anchor settings
        i_idx = input_ids.index('', f_idx) + 1
        toe_restrain_param = list(zip(input_ids[i_idx:], input_values[
 i_idx:]))
        print(toe_restrain_param)

        return geometric_set, ModelType, ElementType, ModelName,
```

```
    soil_param, geosynthetic_param, concrete_param, \
                sb_interf_param, bb_interf_param, connect_param,
    toe_restrain_param
    else:
        raise('Structure type must be slope or wall!')


def set_slope_model(Flag_Input_from_File=1):
    structure_type = 'slope'
    if Flag_Input_from_File:
        geometric_set, ModelType, ElementType, ModelName, soil_param,
    geosynthetic_param,found_param = import_data_from_file(
    Flag_Input_from_File, structure_type)
    else:  # if user want to set parameters inside the code
        beta_grad = 90
        c = 50  # cohesion
        gamma = 18
        H = 4
        comp_lift = 0.25
        geosynt_spacing = H
        if geosynt_spacing != H:
            n_gg = int(H / geosynt_spacing)
        else:
            n_gg = 0

        gg_length = 0.7 * H
        geosynthetic_type = 'Geogrid'
        xlim = 1.6 * H
        material_mode = 3  # 2 for MC and 3 for HS
        found_depth = H / 2
        found_width = 1.3 * xlim
        qy_init = 8  # compaction load, kPa
        mesh_coarsness = 1.33 * 0.06
        staged_construction_flag = 0  # 0 for no and 1 for yes
        surcharge_type = 1
        flag_suction = 1
        geometric_set = [('Facing batter (  )', beta_grad),
                         ('Structure height - H (m)', H),
                         ('Compaction lift (m)', comp_lift),
                         ('Reinforcement spacing', geosynt_spacing),
                         ('Number of reinforcement layers', n_gg),
                         ('Reinforcement length', gg_length),
                         ('Maximum horizontal coord', xlim),
                         ('Foundation depth', found_depth),
                         ('Foundation width', found_width),
                         ('Compaction load (kPa)', qy_init),
                         ('Surcharge type', surcharge_type),  # (Type1:
```

```
    load above; Type2: load above and below layer)
                        ('Mesh factor', mesh_coarsness),
                        ('Staged construction flag',
    staged_construction_flag),  # 0 for no and 1 for yes
                        ('Unsaturated condition',flag_suction)
                        ]

        ModelType = "PlaneStrain"
        ElementType = "6-Noded"

        # Reinforced soil settings
        # Material mode: 1-Linear elastic; 2-MC; 3-HS; 4-HS small;etc
        basic_param = [("MaterialName", "Campus II"),
                      ("DrainageType", "Drained"),
                      ("gammaUnsat", gamma),
                      ("gammaSat", gamma),
                      ("cref", c),
                      ("phi", 44),
                      ("psi", 11),
                      ("TensileStrength", 0),
                      ("InterfaceStrength", "Rigid"),
                      ("K0Determination", "Manual"),
                      ("K0PrimaryIsK0Secondary", True),
                      ("K0Primary", 0.5),
                      ('FlowDataModel', 3),
                      ('DefaultValuesAdvanced', True),
                      ('SoilTypeFlow', 3) #Fine
                      ]

        mc_param = basic_param + [("SoilModel", 2),
                                 ("Eref", 4000),
                                 ("nu", 0.3)]

        hs_param = basic_param + [("SoilModel", 3),
                                 ("E50ref", 56667),
                                 ("EoedRef", 56667),
                                 ("EurRef", 170000),
                                 ("powerm", 0.5),
                                 ("Rf", 0.9),
                                 ("Pref", 80),
                                 ("K0nc", 0.5),
                                 ("nu", 0.25)]

        if material_mode == 2:
            soil_param = mc_param
            ModelName = "MC"
        elif material_mode == 3:
```

```
            soil_param = hs_param
            ModelName = "HS"

        # Foundation soil
        found_param = [("MaterialName", "Foundation Soil"),
                       ("DrainageType", "Drained"),
                       ("gammaUnsat", 20),
                       ("gammaSat", 20),
                       ("SoilModel", 2),
                       ("Eref", 50000),
                       ("cref", 200),
                       ("phi", 35),
                       ("psi", 0),
                       ("nu", 0.3)]
        # Geosynthetic settings
        geosynthetic_param = [("MaterialName", geosynthetic_type),
                              ("Elasticity", "Elastic"),
                              ("IsIsotropic", True),
                              ("EA1", 97),
                              ("EA2", 97)]

    return geometric_set, ModelType, ElementType, ModelName, soil_param, geosynthetic_param, found_param

def set_wall_model(Flag_Input_from_File=1):
    structure_type = 'wall'
    if Flag_Input_from_File:
        geometric_set, ModelType, ElementType, ModelName, soil_param, geosynthetic_param, concrete_param, \
        sb_interf_param, bb_interf_param, connect_param, toe_restrain_param = import_data_from_file(Flag_Input_from_File, structure_type)

    else:  # if user want to set parameters inside the code
        # input
        wb = 0.3  # heel to toe
        hb = 0.15  # block height
        beta_grad = 82
        comp_lift = 0.25
        hor_setback = hb / (math.tan(math.radians(beta_grad)))
        # print(hor_setback)
        n_blocks = 24
        H = n_blocks * hb
        n_gg = 6
        len_connect = 0.1  # length of the connection element (connects reinforcement to face)
        gg_length = 2.22
```

```python
    xlim = 5.95
    ModelType = "PlaneStrain"
    ElementType = "6-Noded"
    surcharge_type = 1  # (Type1: load above; Type2: load above and below layer)
    qy_init = 8
    mesh_coarsness = 0.3
    staged_construction_flag = 1
    flag_suction = 1
    geometric_set = [('Facing batter (  )', beta_grad),
                     ('Block width (m)', wb),
                     ('Block height (m)', hb),
                     ('Number of blocks', n_blocks),
                     ('Structure height (m)', H),
                     ('Compaction lift(m)', comp_lift)
                     ('Number of reinforcement layers', n_gg),
                     ('Reinforcement length', gg_length),
                     ('Facing connector length', len_connect),
                     ('Maximum horizontal coord', xlim),
                     ('Compaction load (kPa)', qy_init),
                     ('Surcharge type', surcharge_type),  # (Type1: load above; Type2: load above and below layer)
                     ('Mesh factor', mesh_coarsness),
                     ('Staged construction flag', staged_construction_flag),  # 0 for no and 1 for yes
                     ('Unsaturated condition',flag_suction)
                     ]

    # Material mode: 1-Linear elastic; 2-MC; 3-HS; 4-HS small;etc
    basic_param = [("MaterialName", "Campus II"),
                   ("Colour", 964844),
                   ("DrainageType", "Drained"),
                   ("gammaUnsat", 16.8),
                   ("gammaSat", 16.8),
                   ("DilatancyCutOff", False),
                   ("cref", 1),
                   ("phi", 44),
                   ("psi", 11),
                   ("InterfaceStrength", "Rigid"),
                   ("K0Determination", "Manual"),
                   ("K0PrimaryIsK0Secondary", True),
                   ("K0Primary", 0.5)]

    mc_param = basic_param + [("SoilModel", 2),
                              ("Eref", 4000),
                              ("nu", 0.3)]

```

```
        hs_param = basic_param + [("SoilModel", 3),
                                  ("E50ref", 56667),
                                  ("EoedRef", 56667),
                                  ("EurRef", 170000),
                                  ("powerm", 0.5),
                                  ("Rf", 0.9),
                                  ("Pref", 80),
                                  ("K0nc", 0.5),
                                  ("nu", 0.25)]
        material_mode = 2
        if material_mode == 2:
            soil_param = mc_param
            ModelName = "MC"
        elif material_mode == 3:
            soil_param = hs_param
            ModelName = "HS"

        # geosynthetic material
        geosynthetic_type = "GEOGRID"
        geosynthetic_param = [("MaterialName", geosynthetic_type),
                              ("Elasticity", "Elastic"),
                              ("IsIsotropic", True),
                              ("EA1", 97)]

        #Facing blocks
        concrete_param = [("MaterialName", "Concrete"),
                          ("SoilModel", 1),
                          ("DrainageType", "Drained"),
                          ("gammaUnsat", 21.8),
                          ("gammaSat", 21.8),
                          ("nu", 0.15),
                          ("Eref", 100000)]

        # soil/block interface
        sb_interf_param = [("MaterialName", "Soil/block interface"),
                           ("SoilModel", 2),
                           ("Gref", 30000),
                           ("DrainageType", "Drained"),
                           ("gammaUnsat", 0),
                           ("gammaSat", 0),
                           ("cref", 1),
                           ("phi", 44),
                           ("psi", 11),
                           ("nu", 0.25),
                           ("K0Determination", "Manual"),
                           ("K0PrimaryIsK0Secondary", True),
                           ("K0Primary", 0.5)]
```

```

        # block/block interface
        bb_interf_param = [("MaterialName", "Block/block interface"),
                           ("SoilModel", 2),
                           ("Eref", 100000),
                           ("DrainageType", "Drained"),
                           ("gammaUnsat", 0),
                           ("gammaSat", 0),
                           ("cref", 46),
                           ("phi", 57),
                           ("psi", 0),
                           ("nu", 0.15)]

        # anchor material to represent toe restrain
        toe_restrain_param = [("MaterialName", "Toe restraint"),
                              ("Elasticity", "Elastic"),
                              ("EA", 4000)]

        # facing connectors material
        connect_param = [("MaterialName", "Facing connectors"),
                         ("Elasticity", "Elastic"),
                         ("EA", 1000)]

    return geometric_set, ModelType, ElementType, ModelName, soil_param, geosynthetic_param, concrete_param, \
              sb_interf_param, bb_interf_param, connect_param, toe_restrain_param

def save_analysis_data (structure_type, geometric_set, ModelType, ElementType,  ModelName, soil_param, geosynthetic_param,  found_param ="",
                        concrete_param = "", sb_interf_param = "", bb_interf_param = "", F_Time_Date = "", folder_path = "../Analyses/Slopes/",
                        connect_param = "", toe_restrain_param="", analysis_description=""):
# #Saves the input data in a text file for future reference
#
    if F_Time_Date == "":
        analysis_name = "/Inputs_for_" + structure_type.upper() + "_" + ModelName + "_" + analysis_description
    else: #saves all analysis parameters to text file indicating date of analysis (based on Engin, 2009)
        analysis_name = "/Inputs_for_" + structure_type.upper() + analysis_description + "_" + ModelName + "_at_" + F_Time_Date

    inputfile_path = folder_path + analysis_name + ".txt"
```

```
    inputfile = open(inputfile_path, 'w')
    inputfile.write("ANALYSIS NAME:\n")
    inputfile.write(analysis_name+'\n\n')
    inputfile.write("GEOMETRIC AND OTHER SETTINGS:\n\n")
    [inputfile.write('{},{:.2f}\n'.format(i, j)) for i, j in geometric_set]
    inputfile.write("\nMODEL AND ELEMENT PROPERTIES:\n\n")
    inputfile.write('{},{}\n'.format("ModelType", ModelType))
    inputfile.write('{},{}\n\n'.format("ElementType", ElementType))
    inputfile.write("REINFORCED SOIL PROPERTIES:\n\n")
    inputfile.write('{},{}\n'.format("ModelName", ModelName))
    [inputfile.write('{},{}\n'.format(i, j)) for i, j in soil_param]
    inputfile.write("\nGEOSYNTHETIC PROPERTIES:\n\n")
    [inputfile.write('{},{}\n'.format(i, j)) for i, j in geosynthetic_param]
    inputfile.write("\nFOUNDATION SOIL PROPERTIES:\n\n")
    if structure_type == 'slope':
        [inputfile.write('{},{}\n'.format(i, j)) for i, j in found_param]
    elif structure_type == 'wall':
        inputfile.write("\nBLOCK PROPERTIES:\n\n")
        [inputfile.write('{},{}\n'.format(i, j)) for i, j in concrete_param]
        inputfile.write("\nSOIL/BLOCK INTERFACE PROPERTIES:\n\n")
        [inputfile.write('{},{}\n'.format(i, j)) for i, j in sb_interf_param]
        inputfile.write("\nBLOCK/BLOCK INTERFACE PROPERTIES:\n\n")
        [inputfile.write('{},{}\n'.format(i, j)) for i, j in bb_interf_param]
        inputfile.write("\nFACING CONNECTORS PROPERTIES:\n\n")
        [inputfile.write('{},{}\n'.format(i, j)) for i, j in connect_param]
        inputfile.write("\nTOE RESTRAINT PROPERTIES:\n\n")
        [inputfile.write('{},{}\n'.format(i, j)) for i, j in toe_restrain_param]
    else:
        raise ('Strucutre type must be slope or wall')
    inputfile.close()
```

G.2 Main script

```
# Starting the server
import subprocess
import os
import sys
import math
import time
```

```
import psutil
from tkinter import Tk
from tkinter.filedialog import askdirectory
import os

from file_processing import *
from Record_Results import *
from Plotting_Results import *
from pathlib import Path


# #adds time counter and format time as day_date_month_year_time (from
    Engin, 2009)
start=time.time()
Time_Date=time.asctime(time.localtime(time.time()))
I_Time_Date=Time_Date.split()
I_Date = I_Time_Date[0]+"_"+I_Time_Date[2]+"_"+I_Time_Date[1]+"_"+
    I_Time_Date[4]
I_Time = I_Time_Date[3].replace(":", "_")
L_I_Time = len(I_Time)-3
I_Time = I_Time[0:L_I_Time]
F_Time_Date = I_Date+"_"+I_Time

#input
# Flag_Input_from_File = input('Do you want to load input data from file
    ? (1 for Yes and 0 for No):')
# print(Flag_Input_from_File )
# if int(Flag_Input_from_File) !=1 and int(Flag_Input_from_File) !=0:
#    print ('Please type 1 for Yes or 0 for No')
#    exit()

structure_type = 'wall'
Flag_Input_from_File = 1 # 1 means that the values will be imported from
     input file
vt = 0.1 #virtual thickness factor (between 0.01 and 1, default = 0.1)
#calls function to set materials and model properties and geometry
geometric_set, ModelType, ElementType, ModelName, soil_param,
    geosynthetic_param, concrete_param, \
                sb_interf_param, bb_interf_param, connect_param,
    toe_restrain_param = set_wall_model(Flag_Input_from_File)

#unpackin geometric parameters
beta_grad, wb, hb, n_blocks, H, comp_lift, n_gg, gg_length, len_connect,
     xlim, qy_init, surcharge_type,  \
        mesh_coarseness, staged_construction_flag, flag_suction,
    flag_mesh_update,gg_heights = [item[1] for item in geometric_set] #
    retrieves only the values
```

```

gg_heights = gg_heights.strip().split(' ')
for i in range(len(gg_heights)):
    gg_heights[i] = float(gg_heights[i])
# print(gg_heights)
# print(type(gg_heights[0]))

if gg_length > 0:
    flag_reinf = 1 #0 for unreinforced and 1 for reinforced
else:
    flag_reinf = 0
n_soil_layers = math.ceil(H / comp_lift) #scale up - integer
hor_setback = hb / (math.tan(math.radians(beta_grad)))

print('Number of facing blocks:{}\n'.format(n_blocks))
print('Number of compaction lifts:{}\n'.format(n_soil_layers))
#set model boundaries
Xmin = 0
Ymin = 0
Xmax = xlim
Ymax = H
flag_interface = 0 #if 0 interfaces are not activated, if 1 they are activated
flag_int_extension = 0
# launch PLAXIS
print("------------------Launching Plaxis...------------------------")
# print(sys.path)
sys.path.append('C:\\ProgramData\\Bentley\\Geotechnical\\PLAXIS Python Distribution V1\\python\\Lib\\site-packages')
sys.path.append('C:\ProgramData\Bentley\Geotechnical\PLAXIS Python Distribution v1.0.0')
from plxscripting.easy import *  # scripting library, *import all names that a module defines

inputport = 10000
outputport = 10001
plaxispw = r'1/WkZB%SCf2t^EN@'
plaxis_path = r'C:\Program Files\Bentley\Geotechnical\PLAXIS 2D CONNECT Edition V20'
plaxis_input = 'PLAXIS2DxInput.exe'

args = [os.path.join(plaxis_path, plaxis_input),
        "--AppServerPort={}".format(inputport),
        "--AppServerPassWord={}".format(plaxispw),
        "NO_CONTROLLERS"]
process_name="Plaxis2DXInput.exe"

```

```python
if process_name not in (p.name() for p in psutil.process_iter()): # checks if Plaxis is already opened and with server running
        inputprocess = subprocess.Popen(args)

# # then initialize the new_server with additional waiting time due to startup of PLAXIS
s_i, g_i = new_server('localhost', inputport, password=plaxispw, timeout=10.0)
s_i.new()

print("------------------Setting model and material properties...-----------------------")
# Set model and elements properties

g_i.setproperties("ModelType", ModelType, "ElementType", ElementType)
# Set model boundaries
g_i.SoilContour.initializerectangular(Xmin, Ymin, Xmax, Ymax)

# SOIL MENU
# soil
reinf_soil = g_i.soilmat()  # Create a soil material set
reinf_soil.setproperties(*soil_param[1:-3])
if flag_suction:
    reinf_soil.setproperties(soil_param[-3]) #set USDA data set
    reinf_soil.setproperties(soil_param[-2]) #set soil type
    reinf_soil.setproperties(soil_param[-1]) #set use defaults flow

#geosynthetic material
geosynthetic_mat = g_i.geogridmat()
geosynthetic_mat.setproperties(*geosynthetic_param)

# blocks
concrete = g_i.soilmat()
concrete.setproperties(*concrete_param)

if flag_interface:
    # soil/block interface
    sb_interf = g_i.soilmat()
    sb_interf.setproperties(*sb_interf_param[:-1]) #last parameter is Material mode (from adjacent soil or custom)

    # block/block interface
    bb_interf = g_i.soilmat()
    print(bb_interf_param)
    bb_interf.setproperties(*bb_interf_param)

#anchor material to represent toe restrain
```

```
toe_restrain_mat = g_i.anchormat()
print(toe_restrain_param)
toe_restrain_mat.setproperties(*toe_restrain_param)

#facing connectors material (ps: a zero length indicates that there is no facing connector)
connect_mat = g_i.anchormat()
connect_mat.setproperties(*connect_param)
connect_mat.setproperties("Colour",13790447)
# STRUCTURES MENU
print("------------------Setting geometry...-----------------------")
g_i.gotostructures()
poly_blocks, blocks, bb_pos_interfaces, bb_neg_interfaces, soil_layers, sb_interfaces, ext_bb_neg_interfaces, ext_sb_interfaces,list_points = {}, {}, {}, {}, {}, {}, {}, {}, {}
# creating soil layers
lines_compaction, lineloads_compaction = {}, {}
#adding soil layers
for i in range(n_blocks):
    xll = 0 + (i) * hb / math.tan(math.radians(beta_grad))
    yll = 0 + (i) * hb
    xur = xll + wb
    yur = yll + hb
    list_points["Point_Soil_{}_ll".format(str(i + 1))] = g_i.point(xll+wb, yll)
    list_points["Point_Soil_{}_ur".format(str(i + 1))] = g_i.point(xlim, yur)
    list_points["Point_Block_{}_ur".format(str(i + 1))] = g_i.point(xur, yur)
    list_points["Point_Soil_{}_ll".format(str(i + 1))].rename("Point_Soil_{}_ll".format(str(i + 1)))
    list_points["Point_Soil_{}_ur".format(str(i + 1))].rename("Point_Soil_{}_ur".format(str(i + 1)))
    list_points["Point_Block_{}_ur".format(str(i + 1))].rename("Point_Block_{}_ur".format(str(i + 1)))
    g_i.rectangle(g_i.Points[-3], g_i.Points[-2])
    soil_layers["Soil_Layer_{}".format(str(i + 1))] = g_i.Soils[-1]
    g_i.Soils[-1].Material = reinf_soil
    # adding surcharge
    lines_compaction["Soil_Layer_{}".format(str(i + 1))], lineloads_compaction["Soil_Layer_{}".format(str(i + 1))] = g_i.lineload(g_i.Points[-1], g_i.Points[-2], "qy_start", -qy_init)[-2:]
    #print(lines_compaction["Soil_Layer_{}".format(str(i + 1))].Name)

#adding blocks and interfaces
lines_sb_interf = []
for i in range(n_blocks):
```

```python
    xll = 0 + (i) * hb/math.tan(math.radians(beta_grad))
    yll = 0 + (i) * hb
    xur = xll + wb
    yur = yll + hb
    list_points["Point_Block_{}_ll".format(str(i + 1))] = g_i.point(xll, yll)
    list_points["Point_Block_{}_ll".format(str(i + 1))].rename("Point_Block_{}_ll".format(str(i + 1)))
    poly_blocks["Block_{}".format(str(i + 1))], blocks["Block_{}".format(str(i + 1))] = g_i.rectangle(list_points["Point_Block_{}_ll".format(str(i + 1))], list_points["Point_Block_{}_ur".format(str(i + 1))])[-2:] #returns soil object and polygon object
    poly_blocks["Block_{}".format(str(i + 1))].rename("Pol_Block_{}".format(str(i + 1)))
    blocks["Block_{}".format(str(i + 1))].rename("Block_{}".format(str(i + 1)))
    # print(blocks["Block_{}".format(str(i + 1))])
    # print(poly_blocks["Block_{}".format(str(i + 1))])
    g_i.Soils[-1].Material = concrete

    if flag_interface:
        # adding soil/block and block/block interfaces
        sb_interf_material_mode = sb_interf_param[-1][-1]
        line_sb_interf = g_i.line(list_points["Point_Soil_{}_ll".format(str(i + 1))], list_points["Point_Block_{}_ur".format(str(i + 1))])
        line_sb_interf.rename ("Line_Soil_block_interface_{}".format(str(i + 1)))
        # print(line_sb_interf)
        # print(line_sb_interf.Name)
        lines_sb_interf.append(line_sb_interf)
        if sb_interf_material_mode == "Custom":
            sb_interfaces["Block_{0}".format(str(i + 1))] = g_i.neginterface(line_sb_interf, "MaterialMode", sb_interf_material_mode, "Material", sb_interf,"VirtualThicknessFactor", vt)
        elif sb_interf_material_mode == "From adjacent soil":
            sb_interfaces["Block_{0}".format(str(i + 1))] = g_i.neginterface(line_sb_interf, "MaterialMode", sb_interf_material_mode, "VirtualThicknessFactor", vt)
            #print(sb_interfaces["Block_{0}".format(str(i + 1))].Name)
        else:
            raise('Invalid interface material mode')


        if i < n_blocks-1:
            # adding block/block interfaces
            #g_i.line(xll, yur, xur+hor_setback/2, yur)
            #bb_interfaces["Block_{0}&{1}".format(str(i + 1), str(i + 2)
```

```
)] = g_i.Lines[i]
            list_points["Point_Block_{}_ul".format(str(i + 1))] = g_i.point(xll, yur)
            list_points["Point_Block_{}_ul".format(str(i + 1))].rename("Point_Block_{}_ul".format(str(i + 1)))
            line_bb_interf = g_i.line(list_points["Point_Block_{}_ul".format(str(i+1))], list_points["Point_Block_{}_ur".format(str(i+1))])
            line_bb_interf.rename("Line_Interface_Block_{0}_{1}".format(str(i + 1), str(i + 2)))
            bb_pos_interfaces["Block_{0}&{1}".format(str(i + 1), str(i + 2))]= g_i.posinterface(line_bb_interf,"MaterialMode", "Custom", "Material", bb_interf,"VirtualThicknessFactor", vt)
            bb_neg_interfaces["Block_{0}&{1}".format(str(i + 1), str(i + 2))]= g_i.neginterface(line_bb_interf,"MaterialMode", "Custom", "Material", bb_interf,"VirtualThicknessFactor", vt)

#Extend interfaces for allow for flexibility to the model
if flag_interface and flag_int_extension:
    lines_ext_sb_interf = []
    for i in range(n_blocks):
        xll = 0 + (i) * hb/math.tan(math.radians(beta_grad))
        yll = 0 + (i) * hb
        xur = xll + wb
        yur = yll + hb

        # Extend interfaces between soil and blocks slightly below block heel
        if i > 0:
            line_ext_sb_interf = g_i.line((xur, 0.98*yll), list_points["Point_Soil_{}_ll".format(str(i + 1))])[-1]
            lines_ext_sb_interf.append(line_ext_sb_interf)
            ext_sb_interfaces["Block_{0}".format(str(i + 1))] = g_i.neginterface(line_ext_sb_interf, "MaterialMode", "From adjacent soil","VirtualThicknessFactor", vt)
        # Extension of interfaces for flexibility (parameters from adjacent soil, Rint=1)
        if i < n_blocks-1:
            ext_bb_neg_interfaces["Block_{0}&{1}".format(str(i + 1), str(i + 2))]= g_i.neginterface(list_points["Point_Block_{}_ur".format(str(i + 1))], (xur+0.5*hor_setback, yur),"MaterialMode", "From adjacent soil", "Material", bb_interf,"VirtualThicknessFactor", vt)[-1]

#adding geosynthetic objects and face connectors
geosynthetics = {}
lines_gg = {}
geosynthetics_inserted = {}
```

```
lines_gg_inserted = {}
#gg_heights = [(gg_layer-0.5)*H/n_gg for gg_layer in list(range(1, n_gg+1))]
connectors = {}
lines_connect = {}

#adding point at the upperleft point of the wall to post-processing
upperleft_point = g_i.point((H-hb)/math.tan(beta_grad*math.pi/180), H)
upperleft_point.rename('upperleft_point')

print(gg_heights)
# if flag_interface:
#     for i in range(n_blocks-1):
#         print("Point_Block_{}_ul: ".format(str(i + 1)), list_points["Point_Block_{}_ul".format(str(i + 1))].y)

for i in range(n_blocks-1):
    # print(list_points["Point_Block_{}_ul".format(str(i + 1))].y)
    # print(abs(list_points["Point_Block_{}_ul".format(str(i + 1))].y - gg_heights[-1]))
    if flag_interface and (list_points["Point_Block_{}_ul".format(str(i + 1))].y - gg_heights[-1]) < 10e-5:
        topGG_point = list_points["Point_Block_{}_ul".format(str(i + 1))]
        break
    else:
        topGG_point = g_i.point(gg_heights[-1]/math.tan(beta_grad*math.pi/180)-hor_setback, gg_heights[-1])
        break

topGG_point.rename('topGG_point')

left_gg_coords = []

for i_gg in range(n_gg):
    #retrieves points from model correspondent to the left coordinate of the reinforcement
    for i_block in range(n_blocks - 1):
        print(list_points["Point_Block_{}_ur".format(str(i_block + 1))].y)
        if abs(list_points["Point_Block_{}_ur".format(str(i_block + 1))].y - gg_heights[i_gg]) < 10e-5:
            # left_gg_coords.append(list_points["Point_Block_{}_ur".format(str(i_block + 1))])
            left_gg_coords.append(list_points["Point_Soil_{}_ll".format(str(i_block + 2))])
            break
```

```
    # print(left_gg_coords[-1])
    # print(left_gg_coords[-1].Name)
    if len_connect == 0:
        # lines_gg["Line_GG_{}".format(str(i_gg + 1))], geosynthetics["GG_{}".format(str(i_gg + 1))] = g_i.geogrid(left_gg_coords[-1], (left_gg_coords[-1].x + gg_length, left_gg_coords[-1].y), "Material", geosynthetic_mat)[-2:]
        lines_gg["Line_GG_{}".format(str(i_gg + 1))], geosynthetics["GG_{}".format(str(i_gg + 1))] = \
            g_i.geogrid(left_gg_coords[-1], (left_gg_coords[-1].x + gg_length, left_gg_coords[-1].y), "Material", geosynthetic_mat)[-2:]
        lines_gg["Line_GG_{}".format(str(i_gg + 1))].rename("Line_GG_{}".format(str(i_gg + 1)))
        geosynthetics["GG_{}".format(str(i_gg + 1))].rename("GG_{}".format(str(i_gg + 1)))
        # # Geogrids inserted into the blocks to simulate mechanical connector (Guler et al, 2007)
        # lines_gg_inserted["Line_GG_{}_inserted".format(str(i_gg + 1))], geosynthetics_inserted["GG_{}_inserted".format(str(i_gg + 1))] = \
        #     g_i.geogrid(list_points["Point_Block_{}_ll".format(str(i_block + 1))], left_gg_coords[-1], "Material", geosynthetic_mat)[-2:]
        #Geogrids inserted between blocks
        # geosynthetics_inserted["GG_{}_inserted".format(str(i_gg + 1))] = \
        #     g_i.geogrid(list_points["Point_Block_{}_ll".format(str(i_block + 2))], left_gg_coords[-1], "Material", geosynthetic_mat)[-1]
        # # print(geosynthetics_inserted["GG_{}_inserted".format(str(i_gg + 1))])
        # geosynthetics_inserted["GG_{}_inserted".format(str(i_gg + 1))].rename("GG_{}_inserted".format(str(i_gg + 1)))

    else:
        list_points["Point_Connector_{}_right".format(str(i_gg + 1))] = g_i.point((left_gg_coords[-1].x + len_connect, left_gg_coords[-1].y))
        list_points["Point_Connector_{}_right".format(str(i_gg + 1))].rename("Point_Connector_{}_right".format(str(i_gg + 1)))
        lines_connect["Line_Connection_{}".format(str(i_gg + 1))], connectors["Connection_{}".format(str(i_gg + 1))] = \
        g_i.n2nanchor(left_gg_coords[-1], list_points["Point_Connector_{}_right".format(str(i_gg + 1))], "Material",connect_mat)[-2:]
        lines_connect["Line_Connection_{}".format(str(i_gg + 1))].rename("Line_Connection_{}".format(str(i_gg + 1)))
        lines_gg["Line_GG_{}".format(str(i_gg + 1))], geosynthetics["GG_{}".format(str(i_gg + 1))] =\
            g_i.geogrid(list_points["Point_Connector_{}_right".format(str(i_gg + 1))], (list_points["Point_Connector_{}_right".format(str(
```

```
    i_gg + 1))].x + gg_length, list_points["Point_Connector_{}_right".
    format(str(i_gg + 1))].y), "Material", geosynthetic_mat)[-2:]
        lines_gg["Line_GG_{}".format(str(i_gg + 1))].rename("Line_GG_{}"
    .format(str(i_gg + 1)))
        geosynthetics["GG_{}".format(str(i_gg + 1))].rename("GG_{}".
    format(str(i_gg + 1)))

#adding fixed end anchor to represent toe restrain
# x_toe = g_i.Pol_Block_1[0].x
# y_toe = g_i.Pol_Block_1[0].y
g_i.fixedendanchor(list_points["Point_Block_1_ll"])
g_i.FixedEndAnchor_1.Material = toe_restrain_mat
g_i.FixedEndAnchor_1.Direction_x = -1


#Boundary conditions - prescribed displacements
list_points["Point_Soil_1_lr"] = g_i.point(xlim, 0)
list_points["Point_Soil_1_lr"].rename("Point_Soil_1_lr")
right_bound = g_i.line(list_points["Point_Soil_1_lr"], list_points["
    Point_Soil_{}_ur".format(n_soil_layers)])
disp_right_bound = g_i.linedispl(right_bound,"Displacement_x", "Fixed",
    "Displacement_y", "Free")
foundation_line=g_i.line(list_points["Point_Soil_1_ll"], list_points["
    Point_Soil_1_lr"])
disp_found_bound = g_i.linedispl(foundation_line,"Displacement_x", "
    Fixed", "Displacement_y", "Fixed")
block_base_line = g_i.line(list_points["Point_Block_1_ll"], list_points[
    "Point_Soil_1_ll"])
disp_block_base_bound = g_i.linedispl(block_base_line,"Displacement_x",
    "Free", "Displacement_y", "Fixed")
# heel_point = g_i.point(wb, 0)
# heel_point.rename("heel_point")
heel_point_bound = g_i.pointdispl(list_points["Point_Soil_1_ll"],"
    Displacement_x", "Free", "Displacement_y", "Fixed")


#Boundary conditions - groundwater flow BCs
g_i.gwfbc(list_points["Point_Block_1_ll"], list_points["Point_Soil_1_lr"
    ]) # Bottom of the domain
g_i.gwfbc(right_bound) # right of the domain
g_i.GWFlowBC_1.Behaviour = "Closed" # Make the gwfbc on the base of the
    foundation impermeable
# [print(gwbc.Name) for gwbc in g_i.GroundwaterFlowBCs]

# #MESH MENU
print("------------------Defining mesh...-----------------------")
#print(lines_gg["GG_1"].Name)
```

```
#print(geosynthetics["GG_1"])

g_i.gotomesh()
#refine geosynthetics and connections
# print('List of lines:\n')
# for item in g_i.Lines:
#     print(item.Name)
# for i in range(len(lines_gg)):
#     ggname = str(lines_gg["Line_GG_{}".format(str(i + 1))].Name)
#     # ggname = ggname + '_1'  # object name of line generated for mesh
for line in g_i.Lines:
    # print(str(line.Name))
    # print(type(line.Name))
    if "GG" in str(line.Name):
        print(str(line.Name))
        line.CoarsenessFactor = 0.06
        # break

for i in range(len(lines_connect)): #NEEDS CHECKING
    cname = lines_connect["Line_Connection_{}".format(str(i + 1))].Name
    cname = cname + '_1'  # object name of line generated for mesh
    for line in g_i.Lines:
        # print(str(line.Name))
        # print(type(line.Name))
        if cname in str(line.Name):
            #print(str(line.Name))
            line.CoarsenessFactor = 0.03125
            break

if flag_interface:
    #Refine mesh around soil/block interface
    for i in range(len(lines_sb_interf)):
        #print(str(lines_sb_interf[i].Name))
        # print(type(line.Name))
        line_meshname = lines_sb_interf[i].Name + '_1'  # object name of
    line generated for mesh
        for line in g_i.Lines:
            if line_meshname in str(line.Name):
                # print(str(line.Name))
                line.CoarsenessFactor = 0.03125
                break
    if flag_int_extension:
        for i in range(len(lines_ext_sb_interf)):
            #print(str(lines_ext_sb_interf[i].Name))
            # print(type(line.Name))
            line_meshname_ext = lines_ext_sb_interf[i].Name + '_1'  #
   object name of line generated for mesh
```

```
            for line in g_i.Lines:
                if line_meshname_ext in str(line.Name):
                    # print(str(line.Name))
                    line.CoarsenessFactor = 0.03125
                    break


#refine mesh for the first block (toe reactions)
bname = poly_blocks["Block_1"].Name
bname = bname + '_1' #object name of polygon generated for mesh
# print(geosynthetics["GG_1"].info())

for item in g_i.Polygons:
    if item.Name == bname:
        item.CoarsenessFactor = 0.03125
        break

mesh = g_i.mesh(mesh_coarseness, True)
print(mesh)
if flag_interface:
    g_i.BlockblockInterface.Eref=g_i.Concrete.Eref.value
    g_i.BlockblockInterface.nu = g_i.Concrete.nu.value


s_o, g_o = new_server('localhost', outputport, password=plaxispw)
#Adjustment of block/block interface shear according to virtual
    thickness
# g_i.viewmesh()
# virtual_thick = list(g_o.getresults(g_o.Interfaces[-1], g_o.
    ResultTypes.Interface.VirtualInterfaceThickness, "node"))[-1]
# print( 'virutual thickness: ', virtual_thick)
# print(float(g_i.BlockblockInterface.Gref.value))
# s_o.close()
# Gblock_updated = round(1500*virtual_thick*1000/10.5) #G=1500 kPa and
    10.5 mm is the value of virtual thickness used by Damians (2013), for
     a different value, G must be adjusted
# print(Gblock_updated)
#
# g_i.BlockblockInterface.Gref.set(Gblock_updated)
#g_i.viewmesh()

#selecting nodes for plotting results - facing displacements
face_points = {}
g_i.selectmeshpoints()
face_points["FacePoint_Toe"] = g_o.addcurvepoint("node", (0, 0)) #toe
    displacement
face_points["FacePoint_Toe"].rename("FacePoint_Toe")
```

```
face_points["FacePoint_Top"] = g_o.addcurvepoint("node", (H/math.tan(
    math.radians(beta_grad)), H-hb/2)) #top displacement at the center of
     the top block
face_points["FacePoint_Top"].rename("FacePoint_Top")

#points in the center of the left face of the block row imediatly above
    the geogrid layer

for i in range(n_gg):
    face_points["FacePoint_GG_{}".format(str(i+1))] = g_o.addcurvepoint(
    "node", ((gg_heights[i]-hb)/math.tan(math.radians(beta_grad)),
    gg_heights[i]-hb/2))
    face_points["FacePoint_GG_{}".format(str(i+1))].rename("
    FacePoint_GG_{}".format(str(i+1)))
#     # print(face_points["FacePoint_GG_{}".format(str(i+1))])
# # time.sleep(5) %delays execution by 5s

# #points in the upper left corner of the block row imediatly above the
    geogrid layer
# for i in range(n_gg):
#     face_points["FacePoint_GG_{}".format(str(i+1))] = g_o.
    addcurvepoint("node", ((gg_heights[i]-hb)/math.tan(math.radians(
    beta_grad)), gg_heights[i]))
#     face_points["FacePoint_GG_{}".format(str(i+1))].rename("
    FacePoint_GG_{}".format(str(i+1)))
g_o.update()

if flag_suction:
    # #FLOW CONDITIONS MENU
    print("------------------Setting flow conditions
    ...-----------------------")
    g_i.gotoflow()
    waterlevel_s = g_i.waterlevel((0, 0), (xlim, 0))

# #STAGES MENU
print("------------------Setting construction phases
    ...-----------------------")
g_i.gotostages() # Move to STAGED CONSTRUCTION tab
# Phase_1 (Installation)
phases = {}
previous_toplineloads = []
previous_bottomlineloads = []
count_gg = 0
UseDefaultIterationParams = False
MaxUnloadingSteps = 100
MaxSteps = 3000
MaxIterations = 80
```

```
DesiredMinIterations = 8
DesiredMaxIterations = 20

for i in range(n_soil_layers):
     #print("Phase:", i+1)
     if i == 0:
          phases["SoilLayer_{}".format(str(i+1))] = g_i.phase(g_i.
    InitialPhase) # Add first Phase
          # print(phases["SoilLayer_{}".format(str(i + 1))])
          # print(g_i.Phase_1)
          phases["SoilLayer_{}".format(str(i+1))].Identification = "
    SoilLayer_{}".format(str(i + 1))
          current_phase = phases["SoilLayer_{}".format(str(i+1))]
          g_i.setcurrentphase(current_phase)  # Make Phase_1 current

          #SET ITERATION PARAMETERS FOR INITIAL PHASE
          current_phase.Deform.UseUpdatedMesh = flag_mesh_update
          current_phase.Deform.UseDefaultIterationParams =
    UseDefaultIterationParams
          current_phase.Deform.MaxUnloadingSteps = MaxUnloadingSteps
          current_phase.Deform.MaxSteps = MaxSteps
          current_phase.Deform.MaxIterations = MaxIterations
          current_phase.Deform.DesiredMinIterations = DesiredMinIterations
          current_phase.Deform.DesiredMaxIterations = DesiredMaxIterations
          previous_phase = current_phase

          # Activating line displacements and toe restraint (boundary
    conditions)
          g_i.Deformations.deactivate(current_phase) #deactivates default
    boundary conditions
          g_i.LineDisplacements.activate(current_phase)
          g_i.PointDisplacements.activate(current_phase)
          g_i.FixedEndAnchor_1.activate(current_phase)
          g_i.GroundwaterFlowBCs.activate(g_i.InitialPhase)
          if flag_suction:
               g_i.InitialPhase.Deform.IgnoreSuction = False

     else:
          phases["SoilLayer_{}".format(str(i+1))] = g_i.phase(
    previous_phase) # Add next Phase from previous one
          phases["SoilLayer_{}".format(str(i + 1))].Identification = "
    SoilLayer_{}".format(str(i + 1))
          current_phase = phases["SoilLayer_{}".format(str(i+1))]
          g_i.setcurrentphase(current_phase)  # Make phase current
          previous_phase = current_phase
          #current_phase.MaxStepsStored = 10

```

```
        # SET ITERATION PARAMETERS FOR REST OF PHASES
        current_phase.Deform.UseUpdatedMesh = flag_mesh_update
        current_phase.Deform.UseDefaultIterationParams = UseDefaultIterationParams
        current_phase.Deform.MaxUnloadingSteps = MaxUnloadingSteps
        current_phase.Deform.MaxIterations = MaxIterations
        current_phase.Deform.DesiredMinIterations = DesiredMinIterations
        current_phase.Deform.DesiredMaxIterations = DesiredMaxIterations
        current_phase.Deform.MaxSteps = MaxSteps
        if flag_suction:
            #Activating consideration of suction
            current_phase.Deform.IgnoreSuction = False

    # Activating facing block,soil layer and interfaces for the current phase
    current_blockname1 = str(blocks["Block_{}".format(str(i + 1))].Name)+"_1"
    current_blockname2 = str(blocks["Block_{}".format(str(i + 1))].Name)+"_2"
    current_soilname = str(soil_layers["Soil_Layer_{}".format(str(i + 1))].Name)+"_1"
    #soilname = soilname + '_1'  # object name of polygon generated for mesh
    current_soilcluesters = [soil_item for soil_item in g_i.Soils if (current_blockname1 == str(soil_item.Name) or \
                                                                       current_blockname2 == str(soil_item.Name) or current_soilname == str(soil_item.Name))]
    [current_soil.activate(current_phase) for current_soil in current_soilcluesters]
    if flag_interface == 1:
        current_sb_interface_name = str(sb_interfaces["Block_{0}".format(str(i + 1))].Name)

        # print('soil/block interface:', current_sb_interface_name)
        if i > 0:
            current_bb_neg_interface_name = str(bb_neg_interfaces["Block_{0}&{1}".format(str(i), str(i + 1))].Name) # between current block (i+1) and previous one (i)
            current_bb_pos_interface_name = str(bb_pos_interfaces["Block_{0}&{1}".format(str(i), str(i + 1))].Name) # between current block (i+1) and previous one (i)
            if flag_int_extension:
                current_ext_sb_interface_name = str(ext_sb_interfaces["Block_{0}".format(str(i + 1))].Name)
                current_ext_bb_neg_interface_name = str(ext_bb_neg_interfaces["Block_{0}&{1}".format(str(i), str(i + 1))].
```

```
Name)  # extension from between current block (i+1) and previous one (i)

            current_ext_sb_interfaces = [interface for interface in g_i.Interfaces if current_ext_sb_interface_name
                                          in str(interface.Name) and str(interface.Name).split("_")[1] == str(2*n_blocks+i+(i-1))]
            [current_ext_sb_interface.activate(current_phase) for current_ext_sb_interface in current_ext_sb_interfaces]
        # print('neg blockl/block interface:', current_bb_neg_interface_name)
        # print('pos block/block interface:', current_bb_pos_interface_name)
    else:
        current_bb_neg_interface_name = ""
        current_bb_pos_interface_name = ""
        if flag_int_extension:
            current_ext_bb_neg_interface_name = ""

    #Soil/block interface
    current_sb_interfaces = [interface for interface in g_i.Interfaces if current_sb_interface_name
                             in str(interface.Name) and str(interface.Name).split("_")[1] == str(2*i+1)]

    [current_sb_interface.activate(current_phase) for current_sb_interface in current_sb_interfaces]


    #Block/block interfaces (positive and negative)
    if 0 < i < n_blocks:
        current_bb_interfaces = [interface for interface in g_i.Interfaces if ((current_bb_neg_interface_name in
                                 str(interface.Name) and str(interface.Name).split("_")[1] == str(2 * i))
                                 or (current_bb_pos_interface_name in str(interface.Name) and str(interface.Name).split("_")[1] == str(i)))]
        [current_bb_interface.activate(current_phase) for current_bb_interface in current_bb_interfaces]

        # print(str(2*n_blocks+i+(i-2)))
        if flag_int_extension:
            current_ext_bb_neg_interfaces = [interface for interface in g_i.Interfaces if ((current_ext_bb_neg_interface_name in
                                              str(interface.Name) and str(interface.Name).split("_")[1] == str(2*n_blocks+i+(i-2))))]
```

```
                [current_ext_bb_neg_interface.activate(current_phase) for current_ext_bb_neg_interface in current_ext_bb_neg_interfaces]

    #Activating compaction loading
    current_toplineload_name = str(lineloads_compaction["Soil_Layer_{}".format(str(i + 1))].Name)
    if surcharge_type == 2 and i>0:
        current_bottomlineload_name = str(lineloads_compaction["Soil_Layer_{}".format(str(i))].Name)
    # print(current_toplineload_name)

    if surcharge_type == 1: #deactivating compaction load of previous layer
        [previous_topline.deactivate(current_phase) for previous_topline in previous_toplineloads if i>0]
        previous_toplineloads = []
    elif surcharge_type == 2: #reverse sign of compaction load of previous layer
        [previous_bottomline.deactivate(current_phase) for previous_bottomline in previous_bottomlineloads if i > 1]
        for previous_topline in previous_toplineloads:
            if i>0:
                previous_topline.qy_start[previous_phase] = 8
        previous_bottomlineloads = []
        previous_toplineloads = []
        # [previous_line.qy_start[previous_phase] == 8 for previous_line in previous_toplineloads if i > 0]
        # raise('needs implementation')
    else:
        raise('Surcharge type must be 1 for Type 1 or 2 for Type 2')
    for line in g_i.LineLoads:
        #print(lineload.Name)
        if current_toplineload_name in str(line.Name) and str(line.Name).split("_")[1] == str(i+1):
            # print('previous line loads:', previous_toplineloads)
            # print(line.Name)
            line.activate(current_phase)
            previous_toplineloads.append(line)
            # print(line)
    if surcharge_type == 2:
        for line in g_i.LineLoads:
            #print(lineload.Name)
            if i>0 and current_bottomlineload_name in str(line.Name) and str(line.Name).split("_")[1] == str(i):
                # print('previous line loads:', previous_bottomlineloads)
                # print(line.Name)
```

```
            line.activate(current_phase)
            previous_bottomlineloads.append(line)
            # print(line)

 #Activating geosynthetics and facing connectors - after compaction of its corresponding layer
 current_height = (i+1)*comp_lift
 # [print(geosynthetic.Name) for geosynthetic in g_i.geogrids]
 delta_heights = [current_height-layer_height for layer_height in gg_heights] #compares current soil lift height with geogrid heights
 # print(delta_heights)
 # print(any(delta_height < 10**-6 for delta_height in delta_heights))
 if flag_reinf == 1 and any(abs(delta_height-comp_lift) < 10**-6 for delta_height in delta_heights):
     current_geosynthetic_name = str(geosynthetics["GG_{}".format(str(count_gg + 1))].Name)

     current_geosynthetics = [geosynthetic for geosynthetic in g_i.geogrids if current_geosynthetic_name in str(geosynthetic.Name) if str(geosynthetic.Name).split("_")[1] == str(count_gg+1)]
     # print(current_geosynthetic[-1].Name)
     # print(current_geosynthetics)
     [geosynthetic.activate(current_phase) for geosynthetic in current_geosynthetics]

     if len_connect > 0:
         current_connector_name = str(connectors["Connection_{}".format(str(count_gg + 1))].Name)
         current_connector = [connector for connector in g_i.NodeToNodeAnchors if current_connector_name in str(connector.Name) if
                            str(connector.Name).split("_")[1] == str(count_gg + 1)]
         current_connector[-1].activate(current_phase)
     # else:
     #     current_geosynthetic_inserted_name = str(geosynthetics_inserted["GG_{}_inserted".format(str(count_gg + 1))].Name)
     #
     #     current_geosynthetic_inserted = [geosynthetic for geosynthetic in g_i.geogrids if
     #                              current_geosynthetic_inserted_name in str(geosynthetic.Name) if
     #                              str(geosynthetic.Name).split("_")[1] == str(count_gg + 1)]
     #     print(current_geosynthetic_inserted[-1].Name)
     #     current_geosynthetic_inserted[-1].activate(current_phase)
```

```
        count_gg += 1

# Adds end of construction phase
phases["EOC"] = g_i.phase(previous_phase) # Add next Phase from previous one
phases["EOC"].Identification = "End of Construction"
current_phase = phases["EOC"]
g_i.setcurrentphase(current_phase)  # Make phase current
previous_phase = current_phase
[previous_line.deactivate(current_phase) for previous_line in previous_toplineloads] #deactivates compaction load

# #Saves the project if asked by the user - needs debugging to find problem in the path
# OptionToSave = input('Do you want to save the calculated project? (0 for No and 1 for Yes)')
# if OptionToSave:
#     analysis_description = "-"+ input('Optional analysis description (press enter if no additional description is desired: ')
#     analysis_name = "Inputs_for_" + structure_type.upper() + analysis_description + "-" + ModelName + "_at_" + F_Time_Date
#     print(analysis_name)
#     parent_dir = r'../Analyses/Walls/Plaxis_Projects/'
#     #Create a folder to save project files
#     folder_name = analysis_name
#     folder_path = os.path.join(parent_dir, folder_name)
#     save_path = folder_path + "/" + analysis_name
#     g_i.save(save_path)

g_i.calculate()
# g_i.view(g_i.Phases[-1])
print('mesh:', mesh_coarseness)
g_i.view(g_i.Phases[-1]) #opens output in the last phase

face_point_top = g_o.curvePoints[1]
height_face_point_top = H-hb/2
print(height_face_point_top)
face_point_toe = g_o.curvePoints[0]
height_face_point_toe = 0
print(height_face_point_toe)


print("------------------Recording results for EOC ...-----------------------")
# Tk().withdraw()  # we don't want a full GUI, so keep the root window from appearing
# parent_dir = askdirectory(title='Select Folder to save the numerical
```

```
    results')  # shows dialog box and return the path
parent_dir = r"D:\OneDrive - usp.br\ACADEMIC\DOUTORADO\Results\NumericalAnalysis\Analyses\Yara_PhD\Numerical_Results"
# print(parent_dir)
filename = 'Results_GGlayers_Disp.txt'
path = os.path.join(parent_dir, filename)
record_toe_facedisp(s_o, g_o, s_i, g_i, path, face_point_toe,
    height_face_point_toe, mesh_coarseness)

for i in range (n_gg):
    layer_point = g_o.curvePoints[i+2]
    # print(layer_point)
    h_layer = gg_heights[i]
    record_facedisp(s_o, g_o, s_i, g_i, path, layer_point, h_layer,
    mesh_coarseness) #records face displacements in a .txt file

record_top_facedisp(s_o, g_o, s_i, g_i, path, face_point_top,
    height_face_point_top, mesh_coarseness)

filename = 'Results_ToeReactions_file.txt'
path = os.path.join(parent_dir, filename)
record_toe_reactions(s_o, g_o, s_i, g_i, wb,path, mesh_coarseness) #
    records toe reaction in a .txt file
s_o.close()
# plot_disp_profile()


## and to make sure PLAXIS is closed after the run:
## Popen process .terminate()  this is a hard stop! nice closure of the
    project is recommended
# s_i.close()
# inputprocess.terminate()
```

G.3 Script to evaluate mesh convergence

```


"""Conduct analyses with different meshs to evaluate mesh convergence
    with reference to the displacement of left uppermost point in the
    model"""
import subprocess
import os
import sys
import psutil
from tkinter import *
from tkinter.filedialog import askopenfilename
import math
```

```
from file_processing import *
from Record_Results import *


# __author__ = "Yara B. Franco"
# __email__ = "yarabf@usp.br"
# __date__ = "2021"

sys.path.append('C:\\ProgramData\\Bentley\\Geotechnical\\PLAXIS Python Distribution V1\\python\\Lib\\site-packages')
sys.path.append('C:\ProgramData\Bentley\Geotechnical\PLAXIS Python Distribution v1.0.0')
from plxscripting.easy import *  # scripting library, *import all names that a module defines

inputport = 10000
outputport = 10001
plaxispw = r'1/WkZB%SCf2t^EN@'
plaxis_path = r'C:\Program Files\Bentley\Geotechnical\PLAXIS 2D CONNECT Edition V20'
plaxis_input = 'PLAXIS2DxInput.exe'

args = [os.path.join(plaxis_path, plaxis_input),
        "--AppServerPort={}".format(inputport),
        "--AppServerPassWord={}".format(plaxispw)]
process_name = "Plaxis2DXInput.exe"

if process_name not in (p.name() for p in psutil.process_iter()):  # checks if Plaxis is already running
    # # initialize the new_server with additional waiting time due to startup of PLAXIS
    inputprocess = subprocess.Popen(args)
    s_i, g_i = new_server('localhost', inputport, password=plaxispw, timeout=5.0)
    user_input = input("Do you want to open a Plaxis project to conduct a mesh analysis? (1 for Yes and 0 for No):")
    if user_input:
        Tk().withdraw()  # we don't want a full GUI, so keep the root window from appearing
        filename = askopenfilename \
            (title="Select the PLAXIS project to open", filetypes=[
                ('PLAXIS 2D Project', '*.p2dx')])  # show an "Open" dialog box and return the path to the selected file
        parent_dir = r'../Analyses/Walls/Plaxis_Projects/'
        open_path = os.path.join(parent_dir, filename)
        print(open_path)
```

```
        # s_i.new()
        # s_i.open(
        #     r'D:/OneDrive - usp.br/ACADEMIC/DOUTORADO/Results/NumericalAnalysis/Analyses/Walls/Plaxis_Projects/WALL-RMC_Wall6-15-noded_mesh0.3_MC_NoInterface.p2dx')
        s_i.open(open_path)
    elif user_input == 0:
        exit()
    else:
        raise ('You should select 1 for Yes or 0 for No')
else:
    s_i, g_i = new_server('localhost', inputport, password=plaxispw, timeout=5.0)

# # s_o.open(open_path)
#Get geometric parameters
# g_i.gotostructures()
# H = max(g_i.Points.y.value)
# print(g_i.upperleft_point.x.value)
# print(g_i.upperleft_point.y.value)

# g_i.gotostages()
# s_o, g_o = new_server('localhost', outputport, password=plaxispw)
# g_i.view(g_i.Phases[-1]) #opens output in the last phase
# curvepoint = g_o.FacePoint_Top
# # print(curvepoint.x.value)
# calls function to set materials and model properties and geometry
geometric_set, ModelType, ElementType, ModelName, soil_param, geosynthetic_param, concrete_param, \
sb_interf_param, bb_interf_param, connect_param, toe_restrain_param = set_wall_model()

# unpackin geometric parameters
beta_grad, wb, hb, n_blocks, H, comp_lift, n_gg, gg_length, len_connect, xlim, qy_init, surcharge_type, \
mesh_coarseness, staged_construction_flag, flag_suction, flag_mesh_update = [item[1] for item in
                geometric_set]  # retrieves only the values



# wb = g_i.heel_point.x
mesh_coarseness_i = 0.3
mesh_coarseness_f = 0.02
# Gblock = [39881,32105,24328,16551,8774,1994] #values calculated for virtual thickness factor 0.1 and wall 6
```

```
n_mesh = 4
mesh_coarseness = mesh_coarseness_i

gg_heights = [(gg_layer - 0.5) * H / n_gg for gg_layer in list(range(1, n_gg + 1))]

path = 'D:/OneDrive - usp.br/ACADEMIC/DOUTORADO/Results/NumericalAnalysis/Analyses/Walls'
file1_path = path + '/Results_GGlayers_Disp.txt'
file2_path = path+ '/Results_ToeReactions.txt'
os.remove(file1_path)
os.remove(file2_path)

for i in range(1, n_mesh+1):
    print('mesh factor:', mesh_coarseness)
    g_i.gotomesh()
    mesh = g_i.mesh(mesh_coarseness, True)
    print(mesh)
    s_o, g_o = new_server('localhost', outputport, password=plaxispw)
    # g_i.viewmesh()
    # virtual_thick = list(
    # g_o.getresults(g_o.Interfaces[-1], g_o.ResultTypes.Interface.VirtualInterfaceThickness,"node"))[-1]
    # print('virutual thickness: ', virtual_thick)
    # # print(float(g_i.BlockblockInterface.Gref.value))
    # Gblock_updated = round(
    #     1500 * virtual_thick * 1000 / 10.5)  # G=1500 kPa and 10.5 mm is the value of virtual thickness used by Damians (2013), for a different value, G must be adjusted
    # print('updated G for block/block interface:', Gblock_updated)
    # s_o.close()
    # g_i.BlockblockInterface.Gref.set(Gblock_updated)

    #selecting nodes for plotting results - facing displacements
    face_points = {}
    g_i.selectmeshpoints()
    face_points["FacePoint_Toe"] = g_o.addcurvepoint("node", (0, 0))  # toe displacement
    face_points["FacePoint_Toe"].rename("FacePoint_Toe")
    face_points["FacePoint_Top"] = g_o.addcurvepoint("node",(H / math.tan(math.radians(beta_grad)), H))  # top displacement
    face_points["FacePoint_Top"].rename("FacePoint_Top")
    for i_gg in range(n_gg):
        face_points["FacePoint_GG_{}".format(str(i_gg + 1))] = g_o.addcurvepoint("node", (
        (gg_heights[i_gg] - hb) / math.tan(math.radians(beta_grad)), gg_heights[i_gg]))
```

```python
        face_points["FacePoint_GG_{}".format(str(i_gg + 1))].rename("FacePoint_GG_{}".format(str(i_gg + 1)))
        # print(face_points["FacePoint_GG_{}".format(str(i+1))])
    # time.sleep(5) %delays execution by 5s
    g_o.update()
    g_i.gotostages()
    g_i.calculate()
    print('mesh:', mesh_coarseness)
    g_i.view(g_i.Phases[-1])  # opens output in the last phase

    face_point_top = g_o.curvePoints[1]
    for ii_gg in range(n_gg):
        layer_point = g_o.curvePoints[ii_gg + 2]
        # print(layer_point)
        h_layer = gg_heights[ii_gg]
        record_facedisp(s_o, g_o, s_i, g_i, layer_point, h_layer, mesh_coarseness)
    record_top_facedisp(s_o, g_o, s_i, g_i, face_point_top, mesh_coarseness)
    record_toe_reactions(s_o, g_o, s_i, g_i, wb, mesh_coarseness)

    mesh_coarseness = mesh_coarseness_i - i*(mesh_coarseness_i - mesh_coarseness_f)/(n_mesh-1)
    s_o.close()
```

G.4 Script to record relevant results from the analysis

```python
"""Script with functions to record general results from Plaxis analysis"""

#Displays results for curve points that have been previously selected
def record_toe_facedisp (s_o,g_o,s_i, g_i,path, curvepoint, point_height, mesh_coarseness="-"): #point at the top block of the wall
    top_ux = g_o.getcurveresults(curvepoint, g_i.Phases[-1], g_o.ResultTypes.Soil.Ux)*1000 #value in mm
    print('top_ux:', top_ux)
    NodeNo = str(g_o.GeneralInfo.NodeCount)
    ElemNo = str(g_o.GeneralInfo.SoilElementCount)
    Element_Type = str(g_o.GeneralInfo.NodesPerSoilElement)
    print(NodeNo)
    print(ElemNo)
    # print(Element_Type)
    # s_o.close()
    print(type(top_ux))
    print(type(point_height))
    point_height=float(point_height)
    with open(path,'a+') as results_file:
```

```
        # Move read cursor to the start of file.
        results_file.seek(0)
        # If file is not empty then append '\n'
        data = results_file.read(100)
        if len(data) == 0:
            results_file.write('ELEMENT_TYPE\tMESH COARSNESS\tNodeNo\tElemNo\tHeight (m)\tUX (mm)\n')
            results_file.write(('{}\t{}\t{}\t{}\t{:.2f}\t{:.4f}'.format(Element_Type, mesh_coarseness, NodeNo, ElemNo,point_height, top_ux)))
        else:
            results_file.write("\n")
            # Append text at the end of file
            results_file.write(('{}\t{}\t{}\t{}\t{:.2f}\t{:.4f}'.format(Element_Type, mesh_coarseness, NodeNo, ElemNo,point_height, top_ux)))

def record_top_facedisp (s_o,g_o,s_i, g_i,path, curvepoint, point_height, mesh_coarseness="-"): #point at the top block of the wall
    top_ux = g_o.getcurveresults(curvepoint, g_i.Phases[-1], g_o.ResultTypes.Soil.Ux)*1000 #value in mm
    print('top_ux:', top_ux)
    NodeNo = str(g_o.GeneralInfo.NodeCount)
    ElemNo = str(g_o.GeneralInfo.SoilElementCount)
    Element_Type = str(g_o.GeneralInfo.NodesPerSoilElement)
    print(NodeNo)
    print(ElemNo)
    # print(Element_Type)
    # s_o.close()
    with open(path,'a+') as results_file:
        # Move read cursor to the start of file.
        results_file.seek(0)
        # If file is not empty then append '\n'
        data = results_file.read(100)
        if len(data) == 0:
            results_file.write('ELEMENT_TYPE\tMESH COARSNESS\tNodeNo\tElemNo\tHeight (m)\tUX(mm)\n')
            results_file.write(('{}\t{}\t{}\t{}\t{:.2f}\t{:.4f}'.format(Element_Type, mesh_coarseness, NodeNo, ElemNo,point_height, top_ux)))
        else:
            results_file.write("\n")
            # Append text at the end of file
            results_file.write(('{}\t{}\t{}\t{}\t{:.2f}\t{:.4f}'.format(Element_Type, mesh_coarseness, NodeNo, ElemNo, point_height, top_ux)))

def record_facedisp(s_o, g_o, s_i, g_i, path, FacePoint_GG_layer, point_height, mesh_coarseness="-"):

```

```
    layerGG_ux = g_o.getcurveresults(FacePoint_GG_layer, g_o.Phases[-1], g_o.ResultTypes.Soil.Ux)*1000 #value in mm
    print('current_gg_ux:', layerGG_ux)
    NodeNo = str(g_o.GeneralInfo.NodeCount)
    ElemNo = str(g_o.GeneralInfo.SoilElementCount)
    Element_Type = str(g_o.GeneralInfo.NodesPerSoilElement)


    with open(path,'a+') as results_file:
        # Move read cursor to the start of file.
        results_file.seek(0)
        # If file is not empty then append '\n'
        data = results_file.read(100)
        if len(data) == 0:
            results_file.write('ELEMENT_TYPE\tMESH COARSNESS\tNodeNo\tElemNo\tHeight (m)\tUX(mm)\n')
            results_file.write(
                ('{}\t{}\t{}\t{}\t{:.2f}\t{:.4f}'.format(Element_Type, mesh_coarseness, NodeNo, ElemNo, point_height,layerGG_ux)))
        else:
            results_file.write("\n")
            # Append text at the end of file
            results_file.write(
                ('{}\t{}\t{}\t{}\t{:.2f}\t{:.4f}'.format(Element_Type, mesh_coarseness, NodeNo, ElemNo, point_height,layerGG_ux)))

#
def record_toe_reactions(s_o, g_o, s_i, g_i, wb, path, mesh_coarseness=""):
    import numpy as np
    from tkinter import Tk
    from tkinter.filedialog import askdirectory
    import os
    from numpy import trapz

    g_i.gotostages()
    n_phases =len(g_i.Phases)-1
    NodeNo = str(g_o.GeneralInfo.NodeCount)
    ElemNo = str(g_o.GeneralInfo.SoilElementCount)
    Element_Type = str(g_o.GeneralInfo.NodesPerSoilElement)

    with open(path,'a+') as Results_ToeReactions_file:
        # Move read cursor to the start of file.
        Results_ToeReactions_file.seek(0)
        # If file is not empty then append '\n'
        data = Results_ToeReactions_file.read(100)
```

```
        for i in range(n_phases):
            if len(data) == 0 and i == 0:
                Results_ToeReactions_file.write('ELEMENT_TYPE\tMESH COARSNESS\tNodeNo\tElemNo\tPHASE\tRx(kN)\tRy(kN)\n')
            elif i == 0:
                Results_ToeReactions_file.write('\n\nELEMENT_TYPE\tMESH COARSNESS\tNodeNo\tElemNo\tPHASE\tRx(kN)\tRy(kN)\n')
            Rx = list(g_o.getresults(g_o.FixedEndAnchors[0], g_i.Phases[i+1], g_o.ResultTypes.FixedEndAnchor.AnchorForce2D,"node"))
            # print("Phase {}: Rx = {}".format(i+1,Rx[0]))
            xcoords_blocktoe = list(g_o.getresults(g_o.Block_1, g_o.Phases[i+1], g_o.ResultTypes.Soil.X, 'node'))
            ycoords_blocktoe = list(g_o.getresults(g_o.Block_1, g_o.Phases[i + 1], g_o.ResultTypes.Soil.Y, 'node'))
            sigmayys_blocktoe = list(g_o.getresults(g_o.Block_1, g_o.Phases[i+1], g_o.ResultTypes.Soil.SigyyE, 'node',True)) #with smoothing
            vert_stresses_blocktoe = zip(xcoords_blocktoe, ycoords_blocktoe,sigmayys_blocktoe)
            vert_stresses_blocktoe = [line for line in vert_stresses_blocktoe if line[1]<10**-6] #only bottom line of toe block
            vert_stresses_blocktoe = list(set(vert_stresses_blocktoe)) # remove duplicates
            vert_stresses_blocktoe = sorted(vert_stresses_blocktoe)  # sort by x coord
            # [print(line) for line in vert_stresses_blocktoe]
            xcoords_blocktoe = [line[0] for line in vert_stresses_blocktoe]
            sigmayys_blocktoe = [line[2] for line in vert_stresses_blocktoe]
            Ry = np.trapz(sigmayys_blocktoe, x=xcoords_blocktoe)
            # print("Phase {}: Ry = {}".format(i+1, Ry))
            # Append text at the end of file
            if i == n_phases-1:
                Results_ToeReactions_file.write(('{}\t{}\t{}\t{}\t{}\t{:.4f}\t{:.4f}'.format(Element_Type, mesh_coarseness, NodeNo, ElemNo, i+1, Rx[0], Ry)))
            else:
                Results_ToeReactions_file.write(('{}\t{}\t{}\t{}\t{}\t{:.4f}\t{:.4f}\n'.format(Element_Type, mesh_coarseness,
                                  NodeNo, ElemNo, i + 1, Rx[0],
                                  Ry)))
        print('end of loop')
# #Testing functions
```

```
# import sys
# sys.path.append('C:\\ProgramData\\Bentley\\Geotechnical\\PLAXIS Python
    Distribution V1\\python\\Lib\\site-packages')
# sys.path.append('C:\ProgramData\Bentley\Geotechnical\PLAXIS Python
   Distribution v1.0.0')
# from plxscripting.easy import *  # scripting library, *import all
   names that a module defines
#
# inputport = 10000
# outputport = 10001
# plaxispw = r'1/WkZB%SCf2t^EN@'
# plaxis_path = r'C:\Program Files\Bentley\Geotechnical\PLAXIS 2D
   CONNECT Edition V20'
# plaxis_input = 'PLAXIS2DxInput.exe'
# s_i, g_i = new_server('localhost', inputport, password=plaxispw,
   timeout=5.0)
# s_o, g_o = new_server('localhost', outputport, password=plaxispw)
#
# record_toe_reactions(s_o, g_o, s_i, g_i,wb=0.3)
```

G.5 Script to plot relevant results from the analysis

```
def plot_facedisp ():
    import matplotlib.pyplot as plt
    import numpy as np
    from tkinter.filedialog import askopenfilename
    from tkinter.filedialog import askdirectory
    import os

    # with open(r'D:\OneDrive - usp.br\ACADEMIC\DOUTORADO\Results\
   NumericalAnalysis\Analyses\Walls\Results_TopFaceDisp.txt','r') as
   result_file:
    file_path = askopenfilename(title='Select file to retrieve numerical
    results for displacements', filetypes=[('Text Files', '*.txt')]) #
   shows dialog box and return the path
    print(file_path)
    with open(file_path,'r') as result_file:
        meshs = []
        hor_disps = []
        gg_heights = []
        next(result_file)
        for line in result_file:
            print('line:', line)
            meshs.append(float(line.split('\t')[1]))
            gg_heights.append(float(line.split('\t')[-2]))
            hor_disps.append(float(line.split('\t')[-1])*-1)
    plt.subplot(2, 1, 1)
```

```
    series_idx = 0
    colors = ['k','b','y','r','m','g','k']
    unique_gg_heights = sorted(set(gg_heights))
    print(unique_gg_heights)
    n_gg = len(unique_gg_heights)
    # print(n_gg)
    data_mesh=[]
    data_ux = []
    for i in range(n_gg):
        for j in range(len(meshs)):
            if gg_heights[j] == unique_gg_heights[i]:
                data_mesh.append(meshs[j])
                data_ux.append(hor_disps[j])
        # print(data_mesh)
        # print(data_ux)
        plt.plot(data_mesh, data_ux, c=colors[i], marker='.', markersize='10', label='Layer {} (Numerical)'.format(i+1))
        data_mesh = []
        data_ux = []
    file_path = askopenfilename(title='Select file to retrieve experimental results for displacements',filetypes=[('Text Files', '*.txt')]) # shows dialog box and return the path
    # print(file_path)
    with open(file_path,'r') as measured_data_file:
        next(measured_data_file)
        count = 0
        measured_gg_heights = []
        measured_face_ux = []
        for line in measured_data_file:
            measured_gg_heights.append(float(line.split(' ')[0]))
            measured_face_ux.append(float(line.split(' ')[-1])*-1)
            plt.plot([0.4, 0.01], [measured_face_ux[-1], measured_face_ux[-1]], c=colors[count], linestyle=':',label='Layer {} (Measured)'.format(count+1))  # Measurement data - target
            count += 1


    plt.xticks(np.arange(0.05, 0.2, step=0.05))
    plt.xlabel('mesh factor')
    plt.ylabel('Horizontal facing displacement (mm)')
    plt.gca().invert_xaxis()
    plt.tight_layout
    # plt.legend()
    plt.grid()
    plt.show()

def plot_toereactions():
```

```python
import matplotlib.pyplot as plt
import numpy as np
from tkinter.filedialog import askopenfilename
from tkinter.filedialog import askdirectory
import os

file_path = askopenfilename(title='Select file to retrieve experimental results for toe reactions',
                            filetypes=[('Text Files', '*.txt')])  # shows dialog box and return the path
print(file_path)
with open(file_path,'r') as result_file:
    next(result_file)
    Rxs = []
    Rys = []
    phases = []
    for line in result_file:
        print(line.split('\t')[0])
        phases.append(int(line.split('\t')[0]))
        try:
            Rxs.append(float(line.split('\t')[1]))
        except:
            Rxs.append("")
        Rys.append(float(line.split('\t')[2]))
print(phases)
print(Rxs)
print(Rys)
plt.subplot(2,1,2)
plt.plot(phases, Rxs, c='k', marker='+', markersize='5', linestyle='-',
              label='Rx (measured)')
plt.plot(phases, Rys, c='grey', marker='x', markersize='5', linestyle='-',
              label='Ry (measured)')
plt.xlabel('phase')
plt.ylabel('Toe load (kN/m)')
# plt.yticks(np.arange(0, 40, step=5))
# plt.show()
file_path = askopenfilename(title='Select file to retrieve numerical results for toe reactions',
                            filetypes=[('Text Files', '*.txt')])
with open(file_path,'r') as result_file:
    meshs = []
    Rxs = []
    Rys = []
    phases = []
    linestyles = ['-','--','-.',':','--','-','--','-.',':']
```

```
        i=0
        next(result_file)
        for line in result_file:
            print(line)
            if line == "\n":
                print(phases)
                print(Rxs)
                print(meshs[-1])
                plt.plot(phases, Rxs,c='k', marker='.', markersize = '10', linestyle=':', label='Rx (mesh={:.3f}'.format(meshs[-1]))
                plt.plot(phases, Rys,c='grey', marker='.', markersize='10',fillstyle = 'none', linestyle=':', label='Ry (mesh={:.3f}'.format(meshs[-1]))

                meshs = []
                Rxs = []
                Rys = []
                phases = []
                i+=1
                next(result_file) #skips header
            else:
                meshs.append(float(line.split('\t')[1]))
                phases.append(int(line.split('\t')[-3]))
                Rxs.append(float(line.split('\t')[-2])*-1)
                Rys.append(float(line.split('\t')[-1])*-1)
        if result_file.read() == "": #end of file
            print(phases)
            print(Rxs)
            print(meshs[0])
            plt.plot(phases, Rxs, c='k', marker='.', markersize='10', linestyle=':',
                     label='Rx (mesh={:.2f})'.format(meshs[-1]))
            plt.plot(phases, Rys, c='grey', marker='.', markersize='10', fillstyle='none', linestyle=':',
                     label='Ry (mesh={:.2f})'.format(meshs[-1]))
    plt.legend()
    plt.tight_layout
    plt.grid()
    plt.show()

    # plt.plot(meshs, hor_disps, marker='.', markersize='10')
    # plt.xlabel('mesh factor')
    # plt.ylabel('Horizontal facing displacement at the top (mm)')
    # plt.gca().invert_xaxis()
    # plt.show()

def plot_disp_profile(): #plots experimental results
```

```

import matplotlib.pyplot as plt
from tkinter.filedialog import askopenfilename
import numpy as np

# Tk().withdraw()  # we don't want a full GUI, so keep the root window from appearing
input_filename = askopenfilename \
    (title="Select the .txt file with the numerical results displacements to plot",
     filetypes=[('Text Files', '*.txt')])  # show an "Open" dialog box and return the
with open(input_filename, 'r') as numerical_result_file:
    meshs = []
    hor_disps = []
    gg_heights = []
    next(numerical_result_file)
    for line in numerical_result_file:
        # print('line:', line)
        meshs.append(float(line.split('\t')[1]))
        gg_heights.append(float(line.split('\t')[-2]))
        hor_disps.append(float(line.split('\t')[-1])*-1)

    colors = ['k', 'b', 'y', 'r', 'm', 'g']
    unique_gg_heights = sorted(set(gg_heights))
    print(unique_gg_heights)
    n_gg = len(unique_gg_heights)
    count = 1
    for i in range(len(meshs)):
        if count < n_gg:
            count +=1
        else:
            plt.plot(hor_disps[i-n_gg+1:i+1], gg_heights[i-n_gg+1:i+1], marker='.', markersize='10',
                     label='Predicted (mesh = {})'.format(meshs[i]))
            count = 1
    print(len(meshs))
    # plt.plot(hor_disps[-n_gg:], gg_heights[-n_gg:], c='k', marker='.', markersize='10', label='Predicted (mesh = {})'.format(meshs[-1]))
    data_mesh = []
    data_ux = []

    input_filename = askopenfilename \
        (title="Select the .txt file with the experimental results displacements to plot",
         filetypes=[('Text Files', '*.txt')])  # show an "Open"
```

```
    dialog box and return the
        with open(input_filename, 'r') as measured_data_file:
            next(measured_data_file)
            measured_gg_heights = []
            measured_face_ux = []
            for line in measured_data_file:
                measured_gg_heights.append(float(line.split(' ')[0]))
                measured_face_ux.append(float(line.split(' ')[-1]))

        plt.plot(measured_face_ux, measured_gg_heights, c='xkcd:grey',
    linestyle=':', marker='s',
                              label='Measured')  # Measurement data - target
        plt.legend()
        plt.tight_layout
        plt.grid()
        plt.ylabel('height (m)')
        plt.xlabel('Horizontal facing displacement at the top (mm)')
        # analysis_id = input('Analysis ID:')
        # plt.title(analysis_id)
        plt.show()


#
# plot_facedisp()
# plot_toereactions()
# plot_disp_profile()
```

H Input file template for automated PLAXIS Analysis

ANALYSIS NAME:
Inputs_for_RSW_MC_at_Tue_5_Jan_2021_10_51
GEOMETRIC SETTINGS:
Facing batter (°),82.00
Block width (m),0.30
Block height (m),0.15
Number of blocks,24.00
Structure height (m),3.60
Compaction lift (m),0.50
Number of reinforcement layers,6.00
Reinforcement length,2.22
Facing connector length,0.10
Maximum horizontal coord,5.95
Compaction load (kPa),0.00
Surcharge type,1
Mesh factor,0.03
Staged construction flag,1
flag_suction,0
MODEL AND ELEMENT PROPERTIES:
ModelType,PlaneStrain
ElementType,6-Noded
SOIL PROPERTIES:
ModelName,MC
MaterialName,Campus II
DrainageType,Drained
gammaUnsat,16.8
gammaSat,16.8
DilatancyCutOff,False
cref,1
phi,44
psi,11
InterfaceStrength,Rigid
K0Determination,Manual
K0PrimaryIsK0Secondary,True
K0Primary,0.5

SoilModel,2
Eref,4000
nu,0.3
DataSetFlow,usda
UsdaSoilType,clay
UseDefaultsFlow,From data set
GEOSYNTHETIC PROPERTIES:
MaterialName,GEOGRID
Elasticity,Elastic
IsIsotropic,True
EA1,97
EA2,97
BLOCK PROPERTIES:
MaterialName,Concrete
SoilModel,1
DrainageType,Drained
gammaUnsat,21.8
gammaSat,21.8
nu,0.15
Eref,100000
SOIL/BLOCK INTERFACE PROPERTIES:
MaterialName,Concrete
SoilModel,1
Gref, 30000
DrainageType,Drained
gammaUnsat,0
gammaSat,0
cref,1
phi,44
psi,11
nu,0.25
K0Determination,Manual
K0PrimaryIsK0Secondary,True
K0Primary,0.5
BLOCK/BLOCK INTERFACE PROPERTIES:
MaterialName,Block/block interface
SoilModel,2
Eref,100000
DrainageType,Drained

gammaUnsat,0
gammaSat,0
cref,46
phi,57
psi,0
nu,0.15
FACING CONNECTORS PROPERTIES:
MaterialName,Facing connectors
Elasticity,Elastic
EA,1000
TOE RESTRAINT PROPERTIES:
MaterialName,Toe restraint
Elasticity,Elastic
EA,4000